REFERENCE ONLY

UNIVERSITY OF LONDON THESIS

Degree PhD Year 2005 Name of Author KANUNGO, S

COPYRIGHT

This is a thesis accepted for a Higher Degree of the University of London. It is an unpublished typescript and the copyright is held by the author. All persons consulting the thesis must read and abide by the Copyright Declaration below.

COPYRIGHT DECLARATION

I recognise that the copyright of the above-described thesis rests with the author and that no quotation from it or information derived from it may be published without the prior written consent of the author.

LOANS

Theses may not be lent to individuals, but the Senate House Library may lend a copy to approved libraries within the United Kingdom, for consultation solely on the premises of those libraries. Application should be made to: Inter-Library Loans, Senate House Library, Senate House, Malet Street, London WC1E 7HU.

REPRODUCTION

University of London theses may not be reproduced without explicit written permission from the Senate House Library. Enquiries should be addressed to the Theses Section of the Library. Regulations concerning reproduction vary according to the date of acceptance of the thesis and are listed below as guidelines.

A. Before 1962. Permission granted only upon the prior written consent of the author. (The Senate House Library will provide addresses where possible).

B. 1962 - 1974. In many cases the author has agreed to permit copying upon completion of a Copyright Declaration.

C. 1975 - 1988. Most theses may be copied upon completion of a Copyright Declaration.

D. 1989 onwards. Most theses may be copied.

This thesis comes within category D.

☑ This copy has been deposited in the Library of UCL

☐ This copy has been deposited in the Senate House Library, Senate House, Malet Street, London WC1E 7HU.

BIOSTRATIGRAPHY AND PALAEOCEANOGRAPHY OF MID-CRETACEOUS CALCAREOUS NANNOFOSSILS: STUDIES FROM THE CAUVERY BASIN, SE INDIA; THE ~~GAULT CLAY FORMATION~~, SE ENGLAND; ~~ODP LEG 171B, WESTERN~~ NORTH ATLANTIC AND ~~ODP LEG 198, NORTHWEST~~ PACIFIC OCEANS

Sudeep Kanungo

Dept. of Earth Sciences
University College London

Thesis submitted for the degree of Doctor of Philosophy
University of London
January 2005

ProQuest LLC
789 East Eisenhower Parkway
P.O. Box 1346
Ann Arbor, MI 48106-1346

To my parents
and
Naina...

'There are no eternal facts as there are no absolute truths.'

- Friedrich Nietzsche

Abstract

The applications of mid-Cretaceous (Aptian-Cenomanian) nannofossils in biostratigraphy and palaeoceanography have been advanced based on four specific studies from India, UK, the Atlantic and Pacific Oceans. A biostratigraphic study on outcrop samples from two new sections in the Cauvery Basin (SE India) has significantly improved stratigraphic resolution in the basin using the recent zonation schemes of Bown et al. (1998) and Burnett (1998). In addition to highlighting problems associated with a few marker species for the Cenomanian, the Albian/Cenomanian and Cenomanian/Turonian boundaries have been examined with respect to their nannofossil proxies. Qualitative comparisons of coeval assemblages from India with those from three other palaeogeographical settings (England, France and the Pacific) have confirmed the overall cosmopolitan nature of Albian nannofloras, in which provinces such as the Tethyan, Boreal and Austral cannot be clearly differentiated.

A palaeoclimatic study of a short section in the Gault Clay (S. England) suggests a major warming event starting at the mid-/Late Albian boundary in the Weald of the Anglo-Paris Basin. The cold-water species, *Repagulum parvidentatum*, gives strong evidence for this warming event by showing a rapid decline in its percentage abundance, which precisely coincides with a light oxygen isotope peak and the influx of Tethyan ammonites. A sharp productivity rise based on the well-known fertility index, *Zeugrhabdotus noeliae*, is found to be concomitant with the warming event.

A palaeoceanographic study of the Early Albian OAE1b event in the western North Atlantic (Leg 171B), based on its nannofossil productivity record and geochemical data, supports the increased productivity model as a plausible mechanism for this anoxic event. A similar study on the Pacific Ocean (Leg 198, Shatsky Rise) shows a marked temporal variation in the abundance distribution of productivity-related taxa (e.g., *Biscutum constans*, *Zeugrhabdotus noeliae*) in relation to the OAE1a (Early Aptian) and OAE1b (Early Albian) events. Possible explanations for this variation have been proposed, in light of the heightened submarine volcanism in the Pacific during the mid-Cretaceous. *Watznaueria* is found to be the most abundant taxon in all mid-Cretaceous assemblages and its dominance is considered to be independent of preservation, indicating its broad palaeoecological tolerance rather than resistance to dissolution.

On the basis of taxonomic observations, four new species have been erected: *Calculites karaiensis*, *Loxolithus bicyclus*, *Manivitella fibrosa* and *Tranolithus simplex*.

Acknowledgements

Several people need to be thanked for their invaluable support in making this thesis possible. Firstly, I would like to thank Prof. Alan Lord, for inspiring me to take on this challenge and assisting me in obtaining financial support for this PhD. I express sincere gratitude to my supervisor, Dr. Paul Bown, for his excellent guidance, healthy criticism and good-natured supervision (Paul is admittedly my real 'guru'!); Dr. Jackie Lees for her scientific insights, enthusiastic motivation and for being there in the time of need; and Dr. Tony Hurford for his support in official matters pertaining to the college. I also owe sincere thanks to Prof. Andy Gale and Dr. Jeremy Young, my supervisors at the Natural History Museum; especially to Andy for providing me with sample materials to kick-start the doctoral project. Dr. A. Nederbragt gave useful advice on diversity analysis. I wish to acknowledge Dr. Sally Radford for suggesting me to pursue higher studies at UCL, and referring me to Prof. Alan Lord in that regard.

I remain grateful to the UCL Graduate School (Thomas Witherden-Batt Scholarship and other supplementary funds) and the Overseas Research Scholarship for funding the PhD. From the Graduate School, I particularly thank Anne Macdonald for her benevolent support.

I wish to thank Jim Davy and Daniel Howard from the Micropalaeontology Unit in UCL for maintaining and sharing excellent camaraderie. A very special note of thanks is due to my friends, who have stood by me through difficult times during the write-up period, and have made my stay in UCL a very memorable experience. In that respect, a BIG 'thank-you' to Ian Bailey, Lena Broadley, Heather Cheshire, Gerd van den Daele, Jayne Dunn, David Eccles, Rupert Green and Sev Kender. Ian Bailey and Heather Cheshire deserve special mention for proofreading parts of this thesis, helping me organise ideas, and for their patience during the final months, when I consistently plagued them with a barrage of queries! Ian, David and Sev helped a good deal with the graphics and formatting.

Finally, I acknowledge my family for their constant encouragement, enthusiasm and moral support, and from whom I have drawn my strength during these years of doctoral research.

CONTENTS

Chapter 1	**Introduction**	**12**
	1.1 Objectives	12
	1.2 Study areas	13
	1.2.1 Cauvery Basin, SE India	13
	1.2.2 Gault Clay Formation, SE England	13
	1.2.3 ODP Leg 171B, Blake Nose, western North Atlantic	13
	1.2.4 ODP Leg 198, Shatsky Rise, northwest Pacific	13
	1.3 An overview of the mid-Cretaceous world	15
	1.4 Calcareous nannofossils – an introduction	18
	1.5 Thesis overview	20
Chapter 2	**Previous studies**	**21**
	2.1 Previous work on mid-Cretaceous nannofossil biostratigraphy	21
	2.2 Mid-Cretaceous palaeobiogeography and palaeoceanography	26
	2.2.1 Palaeobiogeography and palaeoceanography	26
	2.2.2 Relevant papers on mid-Cretaceous palaeobiogeography and palaeoceanography	27
	2.3 Multispecies palaeoproductivity and palaeotemperature indices	39
Chapter 3	**Materials and Methods**	**41**
	3.1 Acquisition of samples	41
	3.2 Slide preparation	41
	3.3 Laboratory Techniques	42
	3.4 Abundance estimation	42
	3.5 Preservation estimation	43
	3.6 Observation and counting strategy	43
	3.6.1 Biostratigraphy	43
	3.6.2 Counting technique	43
	3.6.3 Relative abundance vs. absolute abundance	44
	3.6.4 Palaeobiogeography	45
	3.7 Diversity analysis	45
Chapter 4	**Cauvery Basin, SE India**	**46**
	4.1 Aims	47
	4.2 Introduction	47
	4.3 Geological history of the Cauvery Basin	49
	4.4 Previous nannofossil work	49

4.5 Methods 50
4.6 Biostratigraphy of the Karai Formation 51
4.6.1 Lithostratigraphic details 51
4.6.2 Sample details – Karai Formation, Section 1 and Section 2 52
4.6.3 Results 52
4.6.3.1 Preservation, abundance and diversity 52
4.6.3.2 Biostratigraphy 53
4.6.4 Discussion 57
4.6.4.1 Testing the reliability of markers in Section 1 57
4.6.4.2 Testing the reliability of markers in Section 2 60
4.6.4.3 Nannofossil proxies for stage boundaries 60
4.6.4.3.1 The Albian/Cenomanian boundary 60
4.6.4.3.2 The Cenomanian/Turonian boundary 62
4.7 Conclusions 64

Chapter 5 Gault Clay Formation, SE England 65
5.1 Aims 65
5.2 Geological history of southern England 66
5.3 The Gault Clay Formation 67
5.4 Previous work 67
5.5 Methods 68
5.6 Details of the study section 69
5.7 Results 71
5.7.1 Preservation, abundance and diversity 71
5.7.2 Biostratigraphy 72
5.7.3 Palaeoenvironmental analysis 74
5.7.3.1 Oxygen isotope ($\delta^{18}O$) data 74
5.7.3.2 Quantitative nannofossil data 75
5.7.3.3 Productivity Index and Nutrient Index 78
5.8 Discussion 79
5.8.1 Macropalaeontological evidence for the Late Albian warming 79
5.8.2 Nannofossil evidence for the Late Albian warming 79
5.8.3 Nannofossil evidence from previous studies 82
5.8.4 Other significant taxa in the nannofossil assemblages 83
5.8.5 Productivity Index 84
5.8.6 Nutrient Index and its modification 85
5.9 Palaeoclimatic summary 87
5.10 Conclusions 87

Chapter 6 **ODP Leg 171B, Blake Nose, western North Atlantic** **89**
6.1 Aims 89
6.2 Introduction 90
6.3 The Blake Nose setting and the OAE1b 91
6.4 Previous work 92
6.5 Methods 93
6.6 Results 93
6.6.1 Preservation, abundance and diversity 93
6.6.2 Biostratigraphy 94
6.6.3 Geochemical data 97
6.6.4 Quantitative nannofossil data 97
6.6.4.1 Diversity Indices 97
6.6.4.2 % abundance trends 99
6.6.4.3 Absolute abundance 102
6.6.4.4 Multispecies nutrient indices 102
6.7 Discussion 102
6.7.1 Correlation of the Blake Nose section and missing time 102
6.7.2 Preservation 103
6.7.3 Comparison of relative and absolute abundance methods 104
6.7.4 The Blake Nose palaeoenvironment during the OAE1b 107
6.8 Conclusions 111

Chapter 7 **ODP Leg 198, Shatsky Rise, northwest Pacific Ocean** **113**
7.1 Aims 113
7.2 Introduction 113
7.3 Previous work 115
7.4 Study sections 115
7.5 Methods 117
7.6 Results 117
7.6.1 Preservation, abundance and diversity 117
7.6.1.1 Section 1207B 117
7.6.1.2 Section 1213A-B 118
7.6.2 Biostratigraphy 118
7.6.3 % abundance and diversity indices 118
7.6.3.1 Section 1207B 118
7.6.3.2 Section 1213A-B 121
7.7 Discussion 124
7.7.1 'Near absence' of productivity indicators during OAE1a 124
7.7.2 Productivity indicators during OAE1b 125
7.7.3 Palaeoecological interpretation of abundant taxa 126

7.7.4 Global rise of *B. constans* in the Late Albian 128
7.7.5 Diversity indices 131
7.8 Conclusions 133

Chapter 8 **Palaeobiogeography** **135**
8.1 Introduction 135
8.2 Results 136
8.3 Discussion 136
8.3.1 Comparison of assemblages between India, Europe and Pacific 136
8.4 Conclusions 143

Chapter 9 **Taxonomy** **144**
9.1 Taxonomic list of identified species 144
9.2 Systematic Palaeontology 151
Light Microscope Plates (1-30) 165

Chapter 10 **Conclusions** **195**
10.1 Cauvery Basin stratigraphy 195
9.1.1 Biostratigraphy 195
9.1.2 Palaeobiogeographic differences 196
10.2 Palaeoceanography 197
9.2.1 Palaeoclimate interpretation 197
9.2.2 Proxy testing 198
9.2.3 Nannofossil productivity record for the OAE1a and OAE1b 199
10.3 Taxonomy 200
10.4 Recommendations for future work 200

References **202**
Appendix 1 Cauvery Basin data 224
Appendix 2 Gault Clay data 236
Appendix 3 ODP Leg 171B, Blake Nose data 242
Appendix 4 ODP Leg 198, Shatsky Rise data 246

LIST OF FIGURES AND TABLES

Chapter 1 Introduction

Fig. 1.1 Palaeogeographic reconstruction of the Albian 14

Fig. 1.2 Time interval covered in this study 16

Table 1.1 Depositional conditions in productivity and preservation models 17

Chapter 2 Previous studies

Fig. 2.1 Compilation of mid-Cretaceous nannofossil datums 25

Fig. 2.2 Dissolution index vs. *W. barnesiae*. From Roth & Bowdler (1981) 28

Fig. 2.3 Distribution of *B. constans*. From Roth & Bowdler (1981) 29

Fig. 2.4 Distribution of *Z. noeliae*. From Roth & Bowdler (1981) 29

Fig. 2.5 Distribution of *W. barnesiae*. From Roth & Bowdler (1981) 30

Fig. 2.6 Distibution of neritic taxa. From Roth & Bowdler (1981) 30

Fig. 2.7 Distribution of *S. primitivum*. From Mutterlose (1992b) 36

Table 2.1 Dissolution ranking of species. From Roth & Bowdler (1981) 27

Table 2.2 Nannofossil palaeoecological indices used by Premoli-Silva et al. (1989) 34

Table 2.3 Summary of nannofossil indices with the principal publications 37

Chapter 3 Materials and Methods

Table 3.1 List of samples used in the study 41

Table 3.2 Semi-quantitative abundance estimation scale 42

Table 3.3 Total calcareous nannofossil abundance scale 42

Table 3.4 Preservation estimation scale 43

Chapter 4 Cauvery Basin, SE India

Fig. 4.1 Location of Cauvery Basin on a map of India 48

Fig. 4.2 Palaeolatitudinal position of India during the Albian 48

Fig. 4.3 Biostratigraphy of Karai Formation, Section 1 54

Fig. 4.4 Age-depth plot of Karai Formation, Section 1 55

Fig. 4.5 Biostratigraphy of Karai Formation, Section 2 56

Fig. 4.6 Age-depth plot of Karai Formation, Section 2 57

Fig. 4.7 Compilation of Cenomanian/Turonian boundary events 63

Table 4.1 Cretaceous stratigraphy of the Cauvery Basin 51

Table 4.2 Nannofossil events at Albian/Cenomanian boundary 61

Chapter 5 Gault Clay Formation, SE England

Fig. 5.1 Palaeogeographic location of Gault in the Weald 66

Fig. 5.2 Location map of the Copt Point section 69

Fig. 5.3 Photograph of the Copt Point section 69

Fig. 5.4 Sample and Bed details along with the ammonite zones 71

Fig. 5.5 Nannofossil biostratigraphy of the study section 73

Fig.5.6 Oxygen isotope ($\delta^{18}O$) trend of the section 74

Fig. 5.7 Correlation of nannofossil fertility indices with the $\delta^{18}O$ trend 76

Fig. 5.8 Correlation of *R. parvidentatum* and *S. primitivum* with the $\delta^{18}O$ trend 77

Fig. 5.9 Correlation of *R. asper*, *T. orionatus* and *F. oblongus* with the $\delta^{18}O$ trend 78

Fig. 5.10 Plots of other taxa (*P. columnata*, *R. crenulata* and *L. carniolensis*) 78

Fig. 5.11 Biogeographic distribution of R. *parvidentatum* 81

Fig. 5.12 Comparison of the Productivity Index, Nutrient Index and its modification proposed 86

Chapter 6 ODP Leg 171B, Blake Nose, western North Atlantic

Fig. 6.1 Location of Site 1049 in the Atlantic 92

Fig. 6.2 Geochemical and diversity data 98

Fig. 6.3 % abundance trends of major nannofossil taxa 100

Fig. 6.4 Correlation of the Blake Nose and Vocontian Basin OAE1b succession 103

Fig. 6.5 % and absolute abundance trends of *B. constans*, *D. ignotus* and *Z. noeliae* 105

Fig. 6.6 % abundance and absolute abundance of *Watznaueria* spp. and *Nannoconus* spp. 106

Fig. 6.7 Summary diagram showing changes in productivity through the study section 110

Table 6.1 Nannofossil distribution and biostratigraphy of the Blake Nose section 95

Chapter 7 ODP Leg 198, Shatsky Rise, northwest Pacific

Fig. 7.1 Location of Shatsky Rise, Site 1207 and 1213 in the Pacific 116

Fig. 7.2 % abundance trends of major nannofossil taxa at Site 1207 119

Fig. 7.3 Nutrient Index and diversity indices at Site 1207 120

Fig. 7.4 % abundance trends of major nannofossil taxa at Site 1213 122

Fig. 7.5 Nutrient Index and diversity indices at Site 1213 123

Fig. 7.6 Comparative % abundance of *B. constans* during the Late Albian 130

Table 7.1 %abundance data for *B. constans* in the Late Albian 129

Table 7.2 Comparison of diversity indices between the four study sections 132

Chapter 8. Palaeobiogeography

Fig. 8.1 Palaeobiogeographic distribution at the *T. orionatus* datum-level 138

Fig. 8.2 Palaeobiogeographic distribution at the *E. turriseiffelii* datum-level 139

Fig. 8.3 Palaeobiogeographic distribution at the *C. kennedyi* datum-level 140

Table 8.1 Palaeobiogeographic summary of selected taxa 142

Chapter 1. Introduction

1.1 Objectives

This thesis describes a number of biostratigraphic and palaeoceanographic studies from the Aptian-Cenomanian interval of India, UK, the Atlantic and Pacific Oceans. The objectives were to improve the stratigraphic resolution in the Cauvery Basin (SE India) and enhance the understanding of mid-Cretaceous palaeoceanography and palaeoecology. The principal approach has been to investigate the mid-Cretaceous interval on different sampling scales, i.e., low and high-stratigraphic resolution, on sections representing disparate palaeolatitudes and environmental settings.

The overall objectives of the study were two fold:

a) **Biostratigraphy**: Test the recent zonation schemes of Bown et al. (1998) and Burnett (1998), and examine their applicability on two new measured sections of the Karai Formation in Cauvery Basin, SE India. Previous work on nannofossil biostratigraphy in the Cauvery Basin is limited, e.g., Kale & Phansalkar (1992a, b); Kale et al. (2000), and the nannofossil biostratigraphy of these new sections (Gale et al. 2002) has not been fully evaluated.

b) **Palaeoceanography**:

- **Palaeobiogeography**: Examine the palaeobiogeographic affinities of the Cauvery Basin nannofossil assemblages during the mid-Cretaceous. Test the hypothesis that Albian nannofloras were cosmopolitan, by qualitative and quantitative comparisons of the Cauvery Basin nannofossil assemblages with coeval assemblages from European and Pacific areas.

- **Nannofossil palaeoecology and palaeoceanographic applications**: Test and compare nannofossil productivity indicators (e.g., *Biscutum constans*, *Zeugrhabdotus noeliae* and *Discorhabdus ignotus*) and palaeotemperature proxies (e.g., *Repagulum parvidentatum*, *Seribiscutum primivitum* and *Rhagodiscus asper*) on continental and oceanic settings. Test the significance of the recently proposed Nannofossil Nutrient Index of Herrle (2002) and the Nannofossil Productivity Index of Gale et al. (2000). Examine palaeoproductivity changes through the oceanic anoxic events, OAE1a (Early Aptian) and OAE1b (Early Albian) in the Atlantic and Pacific sections. Address the role of nannofossil productivity during these events in order to get a better understanding of their causal mechanisms.

1.2 Study areas

The study areas are briefly introduced here. Figure 1.1 shows the location of these areas in a palaeogeographic reconstruction of the Albian (~100 Ma). Detailed descriptions of the study areas are given in the respective chapters.

1.2.1 Cauvery Basin, SE India

The Cauvery Basin is a passive-margin sedimentary basin situated on the Coromandel Coast of SE India, in the state of Tamil Nadu. The growth of the basin is associated with the rifting of India from Antarctica-Australia in the Early Cretaceous (Veevers et al. 1991). The basin contains one of the best developed and stratigraphically continuous Cretaceous sequences in India. The Karai Formation, the subject of this study, represents a shelf setting.

1.2.2 Gault Clay Formation, Folkestone, SE England

The Gault Clay Formation in the Weald of the Anglo-Paris Basin represents the Middle and Upper Albian substages. The Gault Clay directly underlies the Chalk Group and represents a shallow epicontinental-sea environment. The section at Copt Point (Folkestone, SE England), which was sampled for a palaeoclimatic investigation, is regarded as a reference section for the Gault Clay Formation (Owen 1975).

1.2.3 Blake Nose, ODP Leg 171B, western Atlantic

In 1997, the Ocean Drilling Program (ODP) completed Leg 171B in the Blake-Bahama Basin in the western North Atlantic Ocean. Site 1049 is located on the eastern margin of the Blake Nose, a spur of the Blake Plateau, at the same location that was previously drilled by the Deep Sea Drilling Project (DSDP) Site 390. Located at a depth of 2671 m below sea level, the site represents mid-bathyal water depths (Norris, Kroon, Klaus et al. 1998b). A ~6 m long section from Site 1049, containing the OAE1b black shale interval was examined for this study.

1.2.4 Shatsky Rise, ODP Leg 198, northwest Pacific

Shatsky Rise is a medium-sized large igneous province (LIP), in the northwest Pacific Ocean. During Leg 198 of the ODP to Shatsky Rise in 2001, mid-Cretaceous chert-rich successions were cored at five sites, yielding a good record of calcareous nannofossils. The two sites, 1207 and 1213, from which material was available for this study, are located on the Northern and Southern Highs of the province. Both sites are located in lower bathyal water depths (>3000 m) and represent a mid-oceanic palaeoequatorial setting during the mid-Cretaceous (Bralower, Premoli-Silva, Malone et al. 2002).

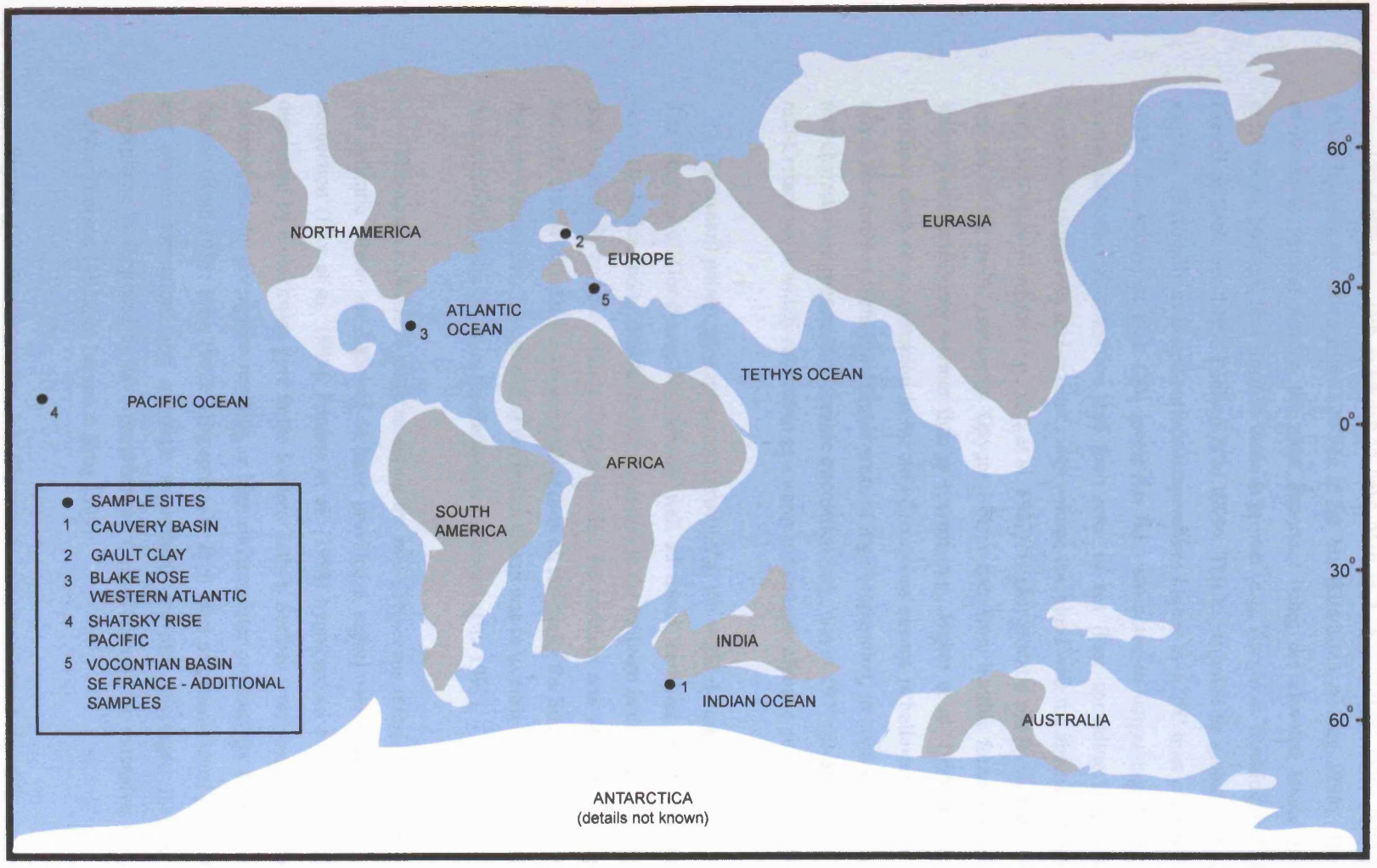

Figure 1.1 Palaeogeographic reconstruction of the Albian showing the location of the study sections. Reconstruction modified after Barron (1987). The distribution of land and sea shown on this figure is approximate.

1.3 An overview of the mid-Cretaceous world

The Earth's climate is known to have been in a 'greenhouse' mode during the mid-Cretaceous, which broadly extended from 120 Ma to 90 Ma (Gradstein & Ogg 1996). The greenhouse mode is attributed to several factors, the most important being the elevated levels of atmospheric CO_2, in proportions, perhaps, four times to those at present (e.g., Barron & Washington 1985; Huber et al. 1995; Fassell & Bralower 1999; Poulsen et al.1999). This contributed to global and polar warmth, with an estimate of globally averaged surface temperatures higher by 6.2°C than present day (e.g., Barron et al. 1995). The source of high CO_2 levels has been attributed to outgassing during periods of extensive submarine/subaerial volcanism and high rates of sea floor spreading (e.g., Larson 1991a, b). The consequent increase in mid-oceanic ridge volume combined with the absence of polar icecaps, resulted in very high sealevel stands (e.g., Haq et al. 1987). Higher eustatic sea levels led to shallow epicontinental seas on all the major continents. Oxygen isotope data from benthic foraminifera indicate that the deep water was significantly warmer than at present (e.g., Huber et al. 1995; Wilson & Norris 2001). In addition, deep-water formation in the mid-Cretaceous oceans is believed to have been largely salinity-driven and derived from low-latitude areas of high evaporation, in contrast to 'thermohaline' circulation that characterises present-day oceanic circulation (e.g., Savin 1977; Brass et al. 1982; Gale 2000). The mid-Cretaceous is widely referred to as a warm and equable climatic period in Earth's history.

The overall palaeogeographic reconstruction of the world during the Albian is shown in Figure 1.1. The breakup of Gondwana was already well advanced, resulting in five separate continents (South America, Africa, India, Antarctica and Australia) in the southern hemisphere. A large open eastern Tethys and a relatively narrow western Tethys divided the northern and southern hemisphere continents. The Atlantic Ocean was much narrower than at present, especially the South Atlantic, which opened rapidly in the Late Cretaceous. The growth of the Indian Ocean was in its early stages after the rifting of India from Antarctica-Australia began in the Hauterivian (Veevers et al. 1991).

The ocean circulation patterns during the mid-Cretaceous remain poorly understood. The Tethyan and Atlantic Ocean are believed to have provided a stable, westward flowing circumglobal oceanic connection (Hay et al. 1999). Poulsen et al. (1998) hypothesised a complex palaeocirculation model dominated by a clockwise gyre in the western Tethys. Surface water currents in the form of gyres and a palaeoequatorial divergence resulting in high surface-water productivity have been hypothesized for the Pacific (Roth 1981; Erba 1992b). Exceptionally high rates of oceanic crust production (mid-ocean ridge and plateau formation) and a mantle superplume are also envisaged for the Pacific. The mantle superplume is supposed to have provided the thermal energy for extensive volcanism on the Pacific seafloor (Larson 1991a, b; Larson & Erba 1999).

Figure 1.2 illustrates the mid-Cretaceous stages covered in this study. The climatic and oceanographic conditions of the mid-Cretaceous appear to have been favourable for the deposition of organic-rich sediments on short time scales (several hundred kyrs), named Oceanic Anoxic Events

(OAEs) by Schlanger & Jenkyns (1976). Two of these OAEs, the Early Aptian OAE1a, and the Cenomanian/Turonian boundary OAE2, are known to have been global, and are expressed as C_{org}-rich black shales in all marine depositional settings regardless of facies type, palaeolatitude or palaeowater depth (Leckie et al. 2002).

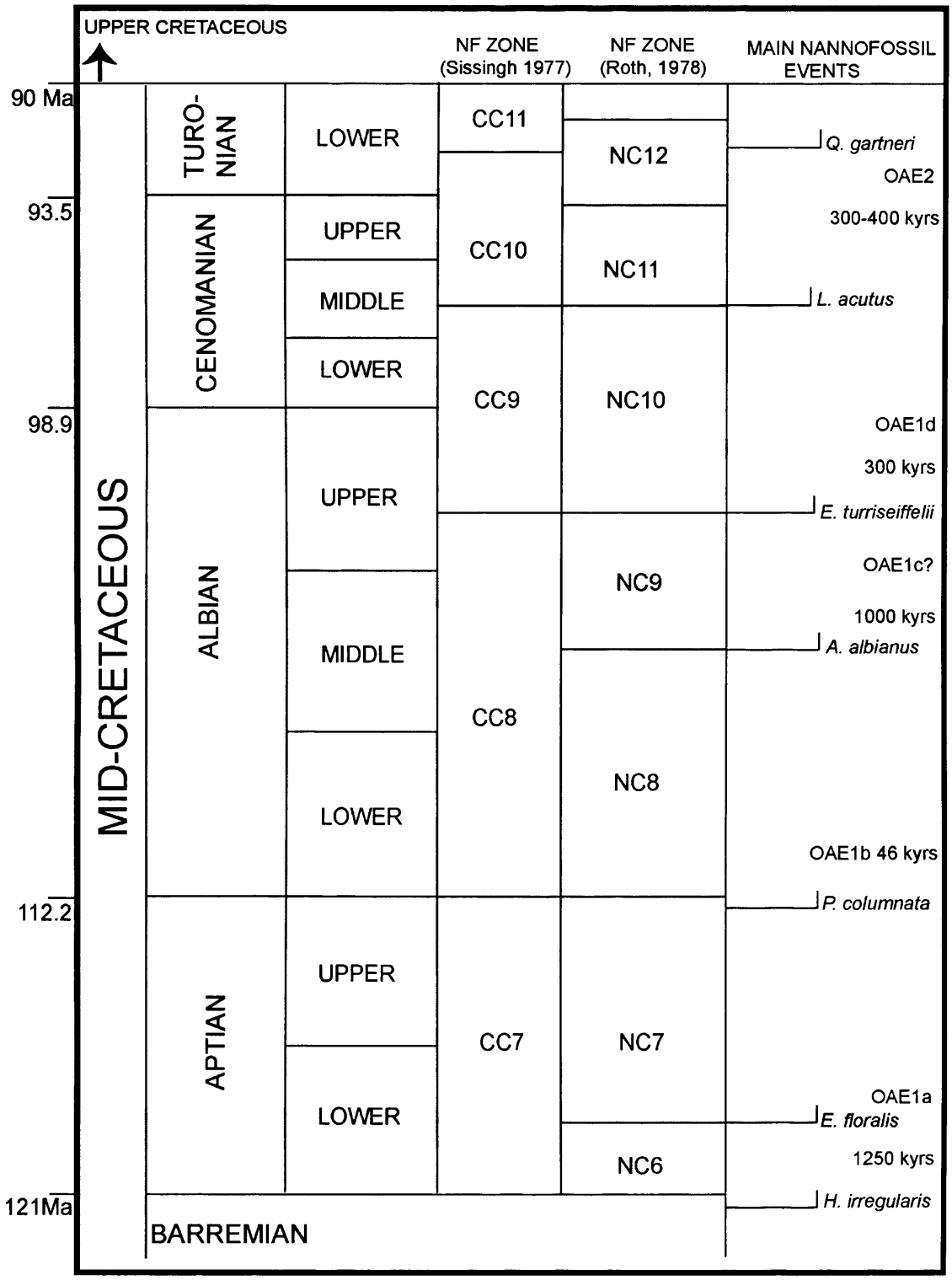

Figure 1.2. Time interval covered in this study along with the position of the mid-Cretaceous OAE's. OAE positions and duration are taken from Erba (2004).

The OAE1 event is further divided into subevents, i.e., the Early Albian OAE1b, the mid-Albian OAE1c and the Late Albian OAE1d, which are thought to be of regional significance only (Figure 1.2). The carbon isotope record shows large positive excursions associated with the OAEs, which are thought to reflect the rapid burial of organic matter during episodes of enhanced productivity (Weissert 1989; Arthur et al. 1990; Erba 1994; Erbacher et al. 1996; Weissert et al. 1998; Jenkyns 1999, 2003; Larson & Erba 1999; Leckie et al. 2002). In addition, significant decreases in the $^{87}Sr/^{86}Sr$ isotope record are observed, at least for the global OAEs, suggesting a link between these events and major volcanic/tectonic episodes (Bralower et al. 1997; Jones & Jenkyns 2001; Leckie et al. 2002). Due to the biogenic nature of pelagic sediments, evolutionary changes within planktonic communities in the form of extinctions and/or appearances are thought to be associated with the global OAEs (e.g. Bralower et al. 1993; Erba 1994; Premoli Silva et al. 1999; Leckie et al. 2002).

It is well known that black shales accumulated beneath dysoxic or anoxic waters. However, whether the oxygen deficiency is the cause of organic matter preservation or merely a symptom of it remains a contentious issue. Two models of black shale deposition – the preservation and the productivity models – are widely cited in literature. The **preservation model** (e.g., Demaison & Moore 1980; Wignall 1991) is based on the theory that organic carbon mineralisation is less efficient in anoxic conditions than in oxic conditions and that black shales accumulate as a result of enhanced preservation. The **productivity model** (e.g., Berger 1979; Calvert 1987) considers that organic-rich sediments are essentially formed by a high flux of organic carbon to the sea floor, irrespective of benthic oxygen levels. In the productivity model, bottom-water anoxia may arise, but this is considered to be the result of a high oxygen demand unrelated to the amount of organic carbon that is preserved. The preservation and productivity models are essentially incompatible as they consider contrasting sets of conditions for the deposition of black shales. Table 1.1 summarises the differences in the two models.

Depositional conditions	**Preservation Model**	**Productivity Model**
Water column	Stratified, lower water column overturned slowly	Well mixed
Primary productivity	Low-moderate 1-100 g/cm^2/yr	High 200-600 g/cm^2/yr
Sediment accumulation rate	Low 100-10 cm/1000 yrs	Usually high 1-10 m/1000 yrs

Table 1.1 Depositional conditions implicit in the preservation and productivity models. From Wignall (1994).

High surface water productivity is usually associated with a high flux of organic matter to the sea floor (e.g., Bralower & Thierstein 1984, 1987). This correlation is however not necessarily direct, as the burial efficiency of carbon is also controlled by variations of oxygen level and sedimentation rate. Nevertheless, a quantitative measure of surface water productivity is important in understanding the mechanisms involved in the formation of black shales. Concentrations of nutrients such as phosphates

and nitrates are poor productivity measures as they undergo intense recycling in the water column and only an insignificant fraction goes into the sediments. Therefore fluctuations in biogenic silica or calcite are commonly used as proxies for primary organic carbon deposition. For Mesozoic oceans, where calcareous nannoplankton were the dominant phytoplankton, especially in areas of high nutrient abundance, nannofossils provide the best proxy for organic matter influx. Silica deposition through radiolarian sourced-cherts is also used as a measure of productivity, e.g., in the Pacific Ocean and its margins (Murchey & Jones 1992).

Recent studies have attempted to combine the two models – black shale deposition may be characterised by both high productivity and the sluggish circulation associated with a stratified water column. Phosphates are supposed to be the key nutrients, as they are regenerated and released to the upper water column under anoxic bottom waters, thereby facilitating higher productivity. For a detailed synthesis on black shales and their causal mechanisms see Wignall (1994).

1.4 Calcareous nannofossils – an introduction

Calcareous nannofossils are a group of organically precipitated calcite bodies that share a common size of less than 30 microns (<30 μm). The vast majority of them are however, 5-15 μm in length. Nannofossils are fossilised remains or probable remains of living haptophyte algae, more specifically the coccolith-bearing sub-group known as coccolithophores. These unicellular, photosynthetic algae are capable of secreting calcareous scales (coccoliths) that form a cell-wall covering called the coccosphere. The coccosphere usually disintegrates after the death of the alga, and gets transported to the sea-floor sediments, where the individual coccoliths or the entire coccosphere are preserved. Apart from coccolithophores, the polyphyletic grouping includes the numerous *incertae sedis* nannoliths that have dubious biological affinities and more rarely, calcareous dinoflagellates, juvenile foraminifera and ascidian spicules. The term nannoflora is often used interchangeably with nannofossils and/or nannoplankton reflecting the 'floral' or autotrophic origins of the vast majority of these fossil forms, although this is debatable in view of the heterogeneous group that they constitute. Coccolithophore biology, ecology, mode of formation, life cycles and functions are described in Winter & Siesser (1994). A comprehensive summary is given in Bown & Young (1998a). However, a few salient points are mentioned in the following paragraphs.

On the basis of morphology and mode of formation, coccoliths can be classified into two broad categories, heterococcoliths and holococcoliths. Heterococcoliths are far more common in the fossil record compared to holococcoliths, whose record is sporadic. Heterococcoliths and holococcoliths are linked with each other through life cycle stages, a fact that becomes evident from the morphological transitions observed in modern coccolithophores. A good example is *Coccolithus pelagicus*, a living species that produces both holococcolith and heterococcolith phases in separate life cycle stages.

The ecology of fossilised coccoliths is believed to be broadly analogous with their living counterparts, the coccolithophorid algae. Extant coccolithophores have a widespread marine distribution (both shelf and oceanic) in latitudes less than 70°, attaining highest diversities in warm, stratified, oligotrophic, mid-ocean environments. The majority of coccolithophores are ecological specialists (k-selected) adapted to warm, low-nutrient conditions, whereas only a very few species have higher levels of environmental tolerance characteristic of opportunistic strategies. A good example is the living species *Emiliania huxleyi*, which shows very broad ecological tolerances and is dominantly abundant in marine environments from low to high latitudes. Such r-selected, growth-maximising species display wider temperature tolerances and respond to nutrification events. Indeed surface-water nutrient concentration appears to be the primary factor controlling coccolithophore abundance and diversity, whereas temperature exerts a major secondary influence. The role of salinity as a limiting factor controlling coccolith productivity is not clearly understood, as the majority of coccolithophores are known to have wide salinity tolerances. Brand (1994) and Winter et al. (1994) are two recent synthesis papers on coccolithophore ecology.

The primary utility of nannofossils has traditionally been in biostratigraphy. Because of their planktonic origin, stratigraphic continuity, rapid evolution, small size and superabundance, they lend themselves to high-resolution zonation schemes from the Late Triassic (when they first appeared in the rock record) to the Recent. They have been widely used as biostratigraphic tools both in academia and industry for over 20 years now. Nannofossils are now being increasingly used as palaeoceanographic proxies because of their important role in global climate change. Because nannoplankton contribute to biological processes such as photosynthesis and biomineralisation, the increases in their abundance and/or crises affect the inorganic and organic carbon cycle and adsorption of atmospheric CO_2 in the oceans (Burnett et al. 2000). By analogy with living calcareous nannoplankton, the morphology, size and distribution of Mesozoic nannofossils can be used as sensitive indicators of past surface water-mass conditions, mainly those related to fertility and temperature. Other applications of nannofossil studies are in the areas of palaeobiogeography and cyclostratigraphy (e.g., Burnett et al. 2000; Erba et al. 1992).

The mid-Cretaceous marks a particularly important episode in the history of nannofossils, as there was a significant breakdown of biogeographic differentiation at this time (e.g., Mutterlose 1992b; Bown 2001). It was therefore, a time of high-diversity and cosmopolitan nannofloras. From a palaeoceanographic viewpoint, nannofossils assumed a pivotal role in the Cretaceous, as they were the most important rock-forming group among the phytoplankton. Therefore, their role in primary productivity is crucial in understanding the causal mechanisms of OAEs. Elevated phytoplankton productivity is cited as a major component of mid-Cretaceous OAEs, especially OAE1a and OAE2 (e.g., Arthur et al. 1990; Leckie et al. 2002).

1.5 Thesis overview

The layout of this thesis is as follows. The principal chapters (Chapters 4–7) are distinguished on the basis of their specific studies. Each of these chapters is presented as a self-contained unit.

Chapter 1 is introductory and sets the scene. **Chapter 2** provides a background to mid-Cretaceous nannofossil biostratigraphy and palaeoceanography, highlighting the previous work done in these fields, by means of a comprehensive literature review. **Chapter 3** describes the methodology of the research. This chapter provides a list of the sample material, followed by notes on preparation, observation and data-generation techniques.

Chapter 4 is based on a study of the Cauvery Basin in SE India. It chiefly addresses the biostratigraphy of the Albian-Cenomanian interval, based on sample material from two new sections in the basin. **Chapter 5** is a palaeoclimatic/palaeoceanographic study of the Gault Clay Formation at Folkestone, England, using a combination of macrofossils, nannofossils and geochemical data. **Chapter 6** is a palaeoceanographic investigation of the Early Albian OAE1b. It is based on sample material from Blake Nose in the western North Atlantic (ODP Leg 171B). **Chapter 7** is a palaeoceanographic study focussing on productivity changes during OAE1a and OAE1b in the equatorial Pacific at Shatsky Rise (ODP Leg 198).

Chapter 8 is a palaeobiogeographic study based on qualitative and quantitative comparisons of assemblages from the Cauvery Basin, Shatsky Rise and some European sections. **Chapter 9** deals with the systematic palaeontology of the studied nannofossils. This includes a taxonomic list of all identified species followed by critical notes on some of the important species. The light microscope (LM) plates are presented in this chapter. The final chapter, **Chapter 10**, is a summation of the overall conclusions in light of the aims and objectives of this study. Some ideas for future work are presented at the end of this chapter.

Chapter 2. Previous studies

2.1 Previous work on mid-Cretaceous nannofossil biostratigraphy

In stratigraphic terms, the 'mid-Cretaceous' refers to an informal division broadly ranging from the Aptian (~120 Ma) to the Turonian (~90 Ma) (Gradstein & Ogg 1996). Almost all Cretaceous nannofossil zonation schemes are composed of two parts, the Lower Cretaceous, covering the Berriasian to Albian stages, and the Upper Cretaceous, comprising the Cenomanian to Maastrichtian stages. As a result, mid-Cretaceous nannofossil biostratigraphy is essentially derived out of these two divisions, i.e., the Lower Cretaceous and the Upper Cretaceous. Although its definition is informal and thereby flexible, the term 'mid-Cretaceous' is widely used in stratigraphic and micropalaeontological studies.

The definition of Cretaceous stage boundaries are based on Global Boundary Stratotype Sections and Points (GSSP's) which serve as standard reference sections for the base and/or top of a boundary. The boundaries are defined on a number of criteria including lithostratigraphic, palaeontological, geochemical and magnetostratigraphic criteria. The mid-Cretaceous stages (Aptian to Turonian) are traditionally defined using ammonites, although more recently other micro- and macrofossils such as planktonic foraminifera, ostracods, dinoflagellate cysts, nannofossils and/or inoceramid bivalves are being increasingly used. However, all stratigraphic boundaries do not have GSSP's due to difficulties in finding accessible sections without hiatuses. For example, the base of the Aptian does not have a GSSP but only a working definition, which is the base of the magnetic polarity chronozone M0r. Similarly, the base of the Albian does not have a GSSP but a working definition based on the first occurrence of the ammonite *Leymeriella* (*L.*) *tardefurcata*. An alternative marker for the Aptian/Albian boundary is the lowest (first) occurrence of the nannofossil *Prediscosphaera columnata* (= *P. cretacea* of earlier studies). The GSSP for the base of the Cenomanian is at the Mont Risou section in the Haute-Alpes (SE France). It is based on the lowest occurrence of the planktonic foraminifer *Rotalipora globotruncanoides*. The Cenomanian/Turonian boundary has its GSSP in Pueblo, Colorado (western USA) based on the lowest occurrence of the ammonite *Watinoceras devonense*. Further information on stage boundary definitions can be obtained from Gradstein et al. (2004).

Initial nannofossil studies on the Cretaceous were mostly taxonomic in content (e.g., Stradner 1963; Stover 1966; Hill 1976). The early biostratigraphic studies that aimed to provide a zonation for a part or the entire Cretaceous were Cepek & Hay (1969, 1970), Manivit (1971), Worsley (1971), Thierstein (1971, 1973, 1974, 1976), Manivit et al. (1977), Hay (1977) and Verbeek (1977). Thierstein (1971, 1973) produced a biostratigraphic zonation for the Lower Cretaceous (Berriasian-Albian) based on low-latitude sample material from western Tethys (SE France) and the proto-Atlantic Ocean. He recognised two important Albian marker species, *Prediscosphaera cretacea* (= *P. columnata*) and *Eiffellithus turriseffelii*, that are used to this day. Manivit et al. (1977) produced a biozonation exclusively for the mid-Cretaceous interval, where they proposed some important events, e.g., LO of *Hayesites albiensis* (Upper Albian) and LO of *Cruciellipsis chiasta* (= *Helenea chiastia*) in the Upper Cenomanian.

The FO is the first occurrence of a taxon at a type locality that may or may not be its first appearance datum (FAD), in part due to diachroneity. Similary, the LO is the last occurrence of a taxon at a type locality that may or not be its last appearance datum (LAD). The FAD/LAD serve as reference levels for the evolutionary inception or extinction of a taxon.

Verbeek (1977) proposed a Middle and Upper Cretaceous biozonation, based on samples from Tunisia, southern Spain and France. He was one of the first to attempt (with Wonders in 1977) a correlation of nannofossil and planktonic foraminiferal bioevents for the Albian to Turonian interval. Thierstein (1976) produced the first integrated Mesozoic biostratigraphy, in which nannofossil bioevents were correlated with the absolute time scale, and with foraminiferal and calpionellid datum levels. The FO's of *P. albianus* (= *Axopodorhabdus albianus*) and *Lithraphidites alatus* (= *L. acutus*) were used as zonal events in the mid-Albian and basal Cenomanian in his study. Although these initial zonations were pioneering attempts, they are practically redundant now due to the low resolution of the zones and the poor taxonomic concepts of the marker species.

The next phase of zonation scheme development came in the late seventies and proved to be more robust. The important studies amongst these include the zonation scheme of Sissingh (1977) and Roth (1978). Sissingh (1977) proposed a total of twenty-six zones for the entire Cretaceous, out of which four covered the mid-Cretaceous interval. Based on material from SE France and Tunisia, most of his mid-Cretaceous zonal markers were adopted from Thierstein (1971), whereas one was newly proposed, the FO of *Microrhabdulus decoratus* for the Upper Cenomanian.

Perch-Nielsen (1979) reviewed and summarised the zonation of other workers such as Thierstein (1976) and Sissingh (1977). She did not propose any modifications to their zones, but suggested a few events to constrain the Albian/Cenomanian (e.g., LO's *Braarudosphaera stenorhetha*, *B. regularis*, etc.) and the Cenomanian/Turonian boundary (FO of *Quadrum gartneri*), in light of information she had acquired from the North Sea region. Additionally, she reviewed evolutionary lineages of stratigraphically important genera such as *Eiffellithus*, *Eprolithus* and *Lithraphidites*.

Perch-Nielsen (1983) significantly improved the resolution of Sissingh's (1977) zonation by proposing several additional markers in the Aptian-Albian interval. She used alphanumeric codes for Sissingh's zones, by prefixing the letters 'CC' to each of his zones. The focus of her work was on recognising Cretaceous stage boundaries in low- to mid-latitude sections by means of nannofossils. The notable events she proposed for the Aptian were the FO's of *Rucinolithus irregularis* (= *Hayesites irregularis*) and *Braarudosphaera africana*, and the LO of *Micrantholithus obtusus*. However, she misplaced the LO of *Eprolithus antiquus* in the Aptian. For the Albian, the FO's of *Tranolithus phacelosus* (= *T. orionatus*) and *Corollithion signum* were used to subdivide Zone CC8 (*P. columnata*, Early Albian). The FO of *Corollithion* cf. *C. completum* (= *C. kennedyi*) was used as an event for the Lower Cenomanian for the first time.

Perch-Nielsen (1985) gave a comprehensive synthesis of Mesozoic nannofossils covering biostratigraphy, palaeoecology and taxonomy. This paper incorporated the modifications proposed by Perch-Nielsen (1983), and described all Mesozoic species and genera, accompanied by SEM and LM illustrations. Evolutionary lineages were also discussed for all stratigraphically significant Mesozoic genera.

The DSDP greatly advanced biostratigraphy by extending the availability of sample material from oceanic sections. Studies by Wise and other workers (e.g., Wise & Wind 1977; Wise 1983) confirmed certain high-latitude taxa from the southwest Atlantic Ocean such as *Seribiscutum primitivum*, *Repagulum parvidentatum* and *Sollasites falklandensis*. It was also realised that forms confined to high-latitudes often showed a bipolar distribution.

Roth (1978) proposed a Cretaceous zonation scheme based on DSDP material from the northwest Atlantic Ocean. He attempted to correlate the European land stages with oceanic stages and calibrated these stages against radiometric dates. A total of twenty-three zones (NC1-NC23) covered the Cretaceous. The mid-Cretaceous part of his scheme (Aptian-Cenomanian) included a total of six zones from NC6 to NC12. The LO of *Lithraphidites acutus* was recognised in the Upper Cenomanian, an event which had not featured in previous schemes. Zone NC11 of the Cenomanian was defined by the total range of *L. acutus*. Roth (1983) used a few additional events such as the FO's of *Eprolithus floralis* in the basal Aptian, and *T. orionatus* in the basal Albian, to improve the resolution of the zones of Roth (1978). This was based on information from DSDP Site 534 in the western Atlantic.

Bralower et al. (1993) conducted a literature review of 39 sections recovered by the DSDP/ODP, and analysed several Aptian-Albian sections (both land and core material). The biostratigraphic investigation in their study resulted in the modification of the NC zones of Roth (1978), including correlation with planktonic foraminiferal zones. The resolution of the Aptian-Albian nannofossil zones was significantly improved in their study. The most notable changes in the Aptian were the subdivision of Zone NC7 (Late Aptian) based on the LO of *M. hoschulzii* and the FO of *P. achlyostaurion* (= *R. achylostaurion*). For the Albian, the FO of *Eiffellithus* cf. *E. eximius* (= *E. monechiae*) was used to define the base of the Subzone NC9B. Bralower et al. (1995) used the same set of mid-Cretaceous zonal events as Bralower et al. (1993), to propose an integrated Cretaceous nannofossil and planktonic foraminiferal biostratigraphic scheme. Bralower et al. (1997) investigated mid-Cretaceous seawater Sr-isotope stratigraphy and correlated it with the planktonic foraminiferal and nannofossil biostratigraphy.

The zonations of Bown et al. (1998) and Burnett (1998) are recent additions to the Cretaceous bisotratigraphic schemes. The Aptian-Albian interval is included under the Lower Cretaceous 'BC' zones of Bown et al. (1998), whereas the Cenomanian is included within the Upper Cretaceous 'UC' zonation of Burnett (1998). The nannofossil events in both these zonation schemes are calibrated against macrofossil (ammonite) zones. SEM and LM illustrations of all Mesozoic taxa are provided along with the zonations.

The Aptian zones by Bown et al. (1998) are based on different zonal events for the Boreal and Tethyan regions. For example, the FO of *R. achlyostaurion* is a conspicuous event in the Tethyan scheme, but is not used in the Boreal scheme. Similarly, the LO's of *C. rothii* and *R. angustiforata* are present only in the Tethyan zonation. Such differences indicate that there was provincialism within the Aptian. The majority of the marker species are common to the Tethyan and Boreal regions, but the stratigraphic order of their occurrence differs in the two regions. The Indian Ocean events are more comparable to the Tethyan events.

The Albian events in Bown et al. (1998) are based on a succession of cosmopolitan marker species from *P. columnata* to *E. turriseiffelii*. There are only a few taxa that show endemic distribution, especially in the Boreal region (Crux 1991). Examples include *Braloweria boletiformis* and *Tegulalithus tessellatus*, which are used as additional events only for the Boreal region (England and the North Sea Basin). Burnett (1998) formulated the Cenomanian zonation based on two regions: Europe and the Indian Ocean. The primary marker species used for both regions are the same. However, there are several secondary markers that are recognised mainly in the European region. Further discussion on her zonation scheme follows in Chapter 4.

Figure 2.1 is a compilation of the mid-Cretaceous nannofossil datums taken from zonation schemes discussed in this section. In summary, Cretaceous nannofossil biostratigraphy began on sample material from low-latitude sections in the Tethyan region. With the steady refinement of taxonomic concepts, increase in biostratigraphic resolution and the availability of oceanic material from sections worldwide, Cretaceous nannofossil zones have achieved a resolution that is now comparable to that of cephalopods. The nannofossil zones are however, far more widely applicable than the ammonite zones. The mid-Cretaceous interval is particularly known for its cosmopolitan marker species that are relatively straightforward in their application and are correlatable over wide regions.

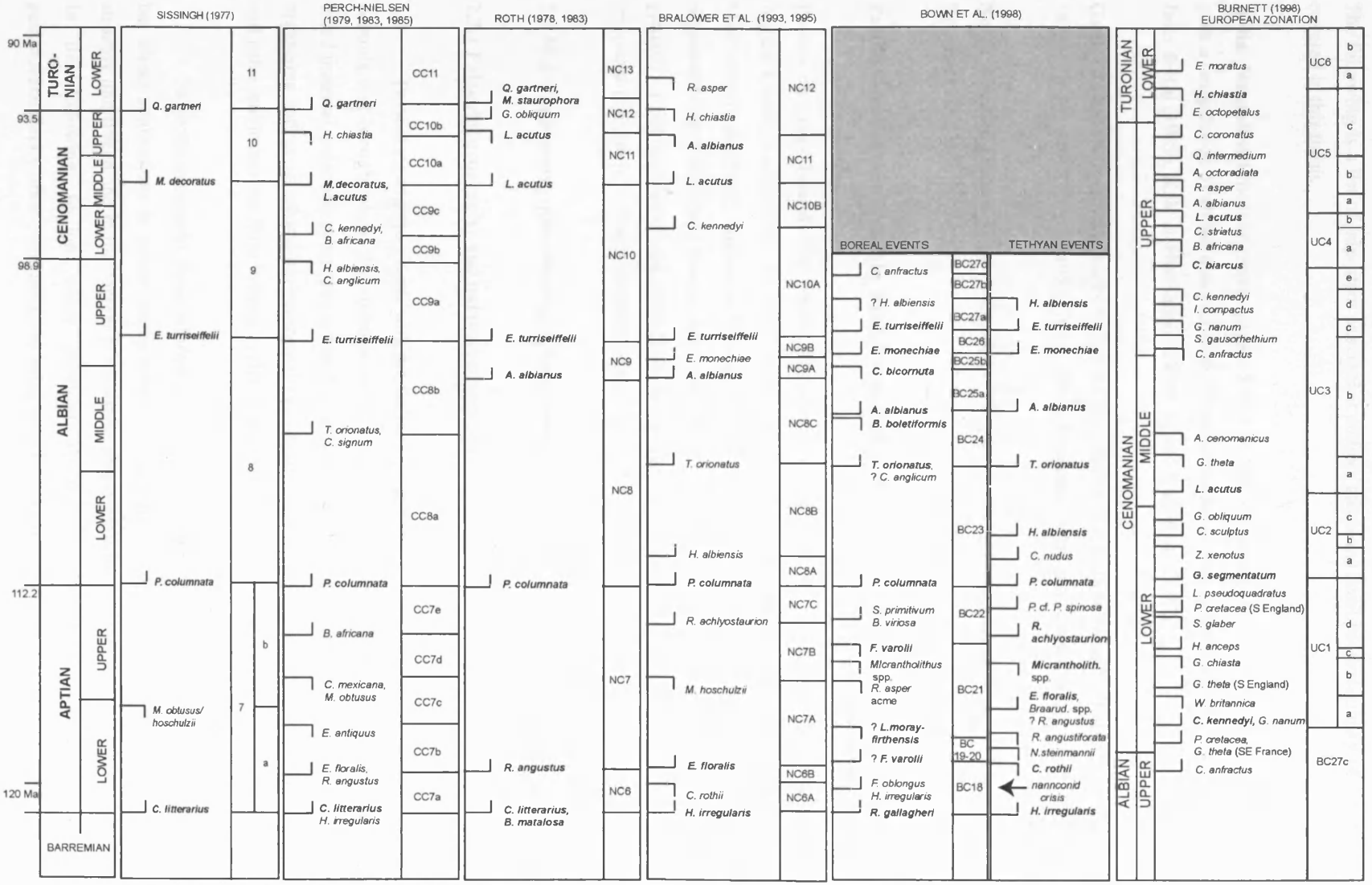

Figure 2.1 Compilation of mid-Cretaceous nannofossil datum-levels. Sequence of events in each study is more important. First Occurrence Last Occurrence

The following is a list of important papers that address the nannofossil biostratigraphy of the study areas covered in this thesis.

India: Nannofossil biostratigraphy papers based on land sections in India are relatively few. Rai (2002) gave a compilation of all the nannofossil publications on India. Papers that address the Cauvery Basin are Jafar & Rai (1989), Kale & Phansalkar (1992a, b) and Kale et al. (2000).

Gault Clay: The significant works on Gault Clay nannofossils include those by Black (1971, 1972, 1973, 1975), Taylor (1982), Crux (1982, 1989, 1991), Jeremiah (1996) and Bown (2001).

North Atlantic Ocean: Wind & Cepek (1979), Roth (1983), Covington & Wise (1987), Applegate & Bergen (1989), etc.

Pacific Ocean (around Shatsky Rise): Cepek (1981), Roth (1981), Erba & Covington (1992), etc.

Papers on stage boundaries: Papers that specifically address the nannofossil biostratigraphy of the Aptian/Albian boundary are Kennedy et al. (2000), Herrle & Mutterlose (2003) and more recently, Mutterlose et al. (2003). Burnett *in* Gale et al. (1996) discussed the Albian/Cenomanian boundary at the proposed Global Stratotype Section and Point (GSSP), Mt. Risou section in southern France. There are a plethora of publications on the nannofossil biostratigraphy of the Cenomanian/Turonian boundary. The important ones include Bralower (1988), Jarvis et al. (1988), Lamolda et al. (1994) and Paul et al. (1999).

2.2 Mid-Cretaceous palaeobiogeography/palaeoceanography

2.2.1 Palaeobiogeography and palaeoceanography

Palaeobiogeography deals with the distribution patterns of fossil organisms through time and the controls that brought about this distribution (Cecca 2002). Due to inherent limitations in dealing with fossil material, palaeobiogeography is based on assumptions that are made by analogies with present-day organisms and geographical/environmental conditions. This involves reconstructing palaeogeographies and palaeoenvironments from indirect evidence and relating it to fossil distributions.

Palaeobiogeography feeds information into the understanding of ocean phenomena and therefore has direct applications in palaeoceanography – the scientific study of past oceans. The two fields are strongly interlinked and in the context of Mesozoic nannofossil studies, they can be overlapping in scope. In the following section where previous literature is discussed, palaeobiogeography and palaeoceanography often come across as being used interchangeably.

2.2.2 Relevant papers on mid-Cretaceous palaeobiogeography and palaeoceanography

Initial studies on mid-Cretaceous palaeoceanography were qualitative and limited to comments on preservational aspects and diversity changes (Roth and Berger 1975; Roth 1978) or assigning taxa to different palaeobiogeographic realms (e.g., Thierstein 1971, 1973, 1976; Taylor 1978; Perch-Nielsen 1979).

One of the first quantitative studies on mid-Cretaceous palaeobiogeography and palaeoceanography was carried out by Roth and Bowdler (1981). This study proved to be a benchmark as it set the foundation for nannofossil-based palaeoceanographic studies. A total of eighteen sites (nine continental margin sites, six oceanic sites and three on shallow rises and plateaux) from the Atlantic Ocean were studied to understand the role of surface water fertility, temperature and calcite dissolution on the distribution of nannofossil assemblages. The time interval covered in this study ranged from the Late Barremian (Zone NC5) to Early Cenomanian (Zone NC11). Zones NC5 to NC9 (Barremian to Late Albian) were classified as the Lower Middle Cretaceous, whilst Zone NC10 and younger were included under the Upper Middle Cretaceous. The main contributions of this work are summarised under three headings, which are:

a) Preservation: Nannofossil preservation was not particularly good (no preservation category was explicitly mentioned) and was severely affected by dissolution, except in the lowermost Middle Cretaceous. Roth & Bowdler (1981) obtained dissolution rankings for all statistically significant taxa and formulated a dissolution index based on it (Table 2.1). A plot of the dissolution index versus the abundance of *Watznaueria barnesiae* showed that the dissolution index gave a measure of preservation that was equivalent to the relative abundance of *W. barnesiae* in a sample (Figure 2.2). Samples containing more than 40% *W. barnesiae* were regarded as dissolution-affected and eliminated from biogeographic studies.

Rank	Species Name
1 (most resistant)	*Watznaueria barnesiae*
2	*Cretarhabdus* sp.
3	*Zygodiscus diplogrammus*
4	*Zygodiscus elegans*
5	*Parhabdolithus splendens*
6	*Watznaueria supracretacea*
7	*Biscutum constans*
8	*Manivitella pemmatoidea*
9	*Lithraphidites carniolensis*
10	*Zygodiscus erectus*
11	*Eiffellithus turriseiffelii*
12	*Prediscosphaera cretacea*
13	*Discorhabdus ignotus*
14	*Vagalapilla stradneri*
15 (most susceptible)	*Parhabdolithus angustus*

Table 2.1: Dissolution ranking for species from Zones NC8 to NC11.

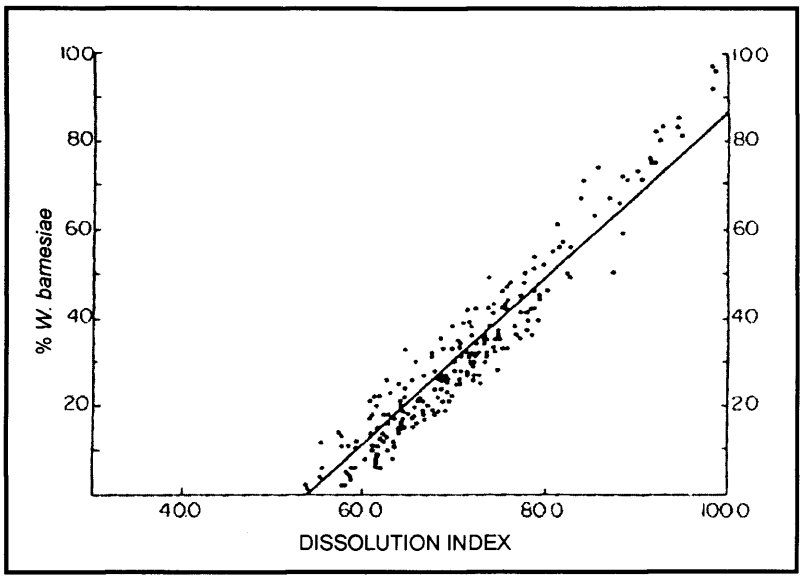

Figure 2.2 Dissolution index vs. relative index of *W. barnesiae*.
From Roth & Bowdler (1981).

b) Biogeographic patterns of major species: The biogeographic patterns of the major taxa were plotted in a series of reconstruction maps for sets of nannofossil zones such as NC10-11, NC8-9, NC7 and NC6 (Figure 2.3 to 2.6). The palaeoecology of the following taxa was inferred on the basis of their distribution in the Atlantic Ocean sites.

Watznaueria barnesiae: Interpreted as an oceanic species based on the observation of an increase in relative abundance of the species with depth. No latitudinal gradient was observed. It was found to be less abundant in well-preserved assemblages from continental sites unless the assemblages had been enriched by dissolution. This trend was observed for all the zones.

Biscutum constans: Most abundant along continental margins and in epicontinental deposits. No latitudinal or depth trend, i.e., change in relative abundance with respect to shelf/oceanic setting of the site, was observed for this species.

Zygodiscus erectus (=***Zeugrhabdotus noeliae***): Distribution pattern similar to *B. constans*, with highest concentration along the continental margins and in epicontinental basins, and lowest concentrations in the western basins of the North Atlantic. In the South Atlantic, the species was most abundant at Site 363, a plateau site characterised by upwelling of deep Angola Basin-water. No latitudinal or shelf/oceanic trend was observed for this species.

Parhabdolithus splendens, ***P. asper*** (= ***Rhagodiscus splendens***, ***R. asper***): Highest abundances were observed in oceanic samples. Neither water depth nor latitude was an important factor in its distribution.

Broinsonia **spp.**: Interpreted as a species common in waters of higher fertility and unstable 'nearshore' environments and epicontinental seas.

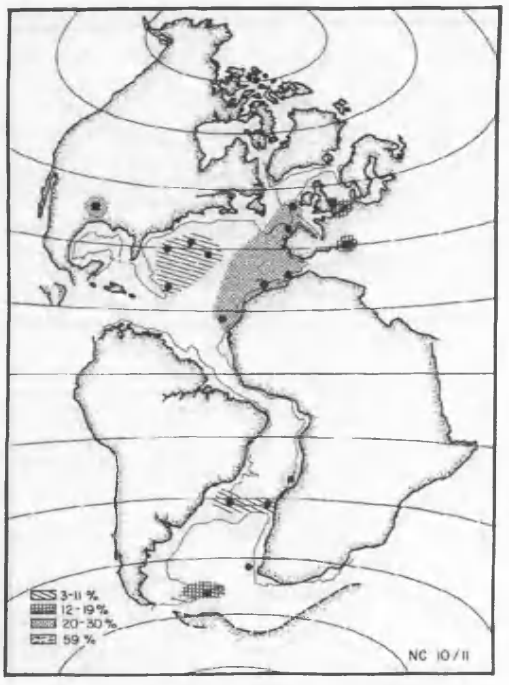

Figure 2.3a Biogeographic distribution of *B. constans* in the Atlantic Ocean, Zones NC10 to NC11.

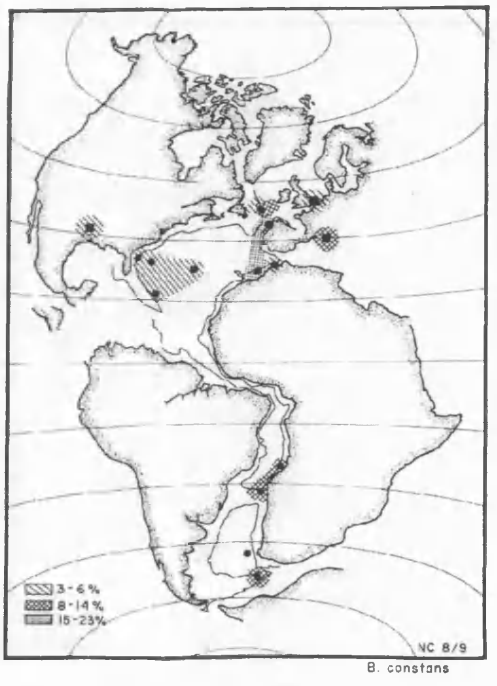

Figure 2.3b Biogeographic distribution of *B. constans* in the Atlantic Ocean, Zones NC8 to NC9.

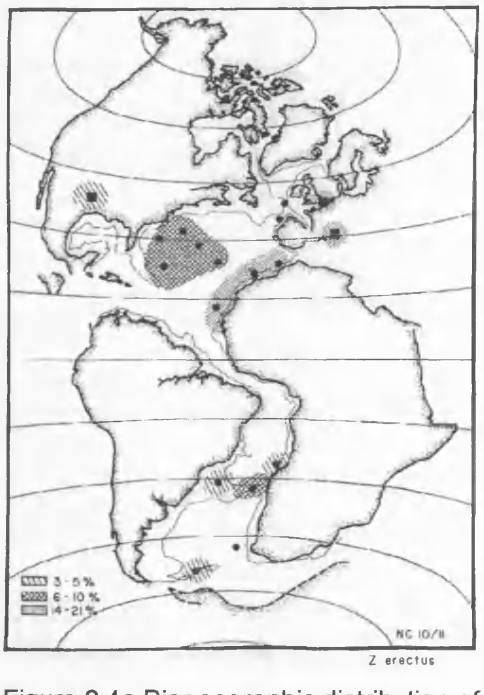

Figure 2.4a Biogeographic distribution of *Z. noeliae* (= *Z. erectus*) in the Atlantic Ocean, Zones NC10 to NC11.

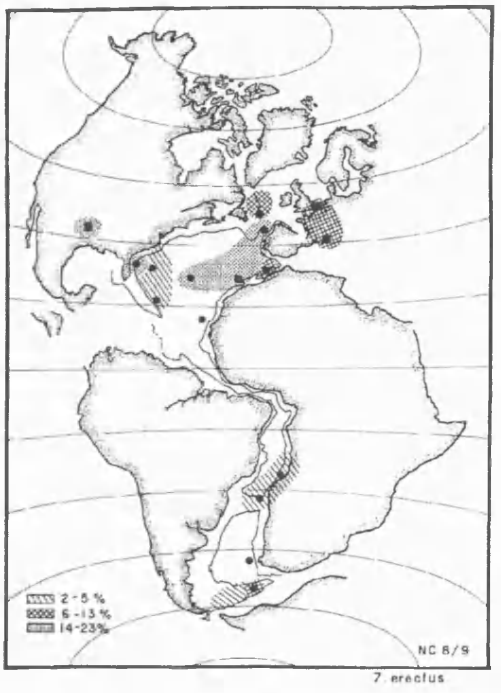

Figure 2.4b Biogeographic distribution of *Z. noeliae* (= *Z. erectus*) in the Atlantic Ocean, Zones NC8 to NC9.

Figures 2.3 and 2.4. From Roth & Bowdler (1981)

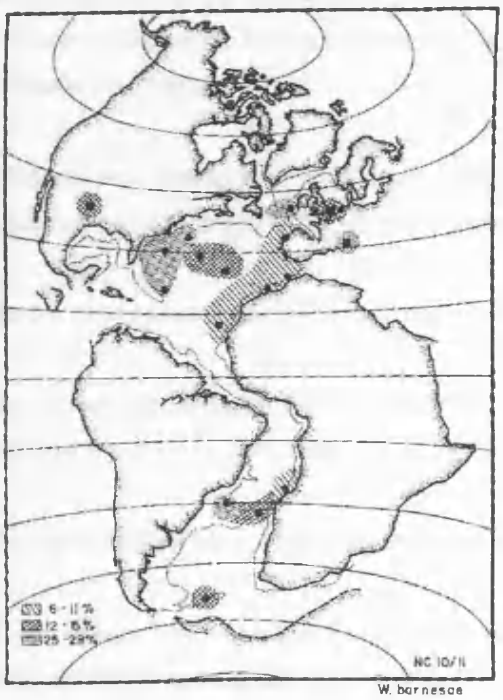

Figure 2.5a Biogeographic distribution of *W. barnesiae* in the Atlantic Ocean, Zones NC10 to NC11.

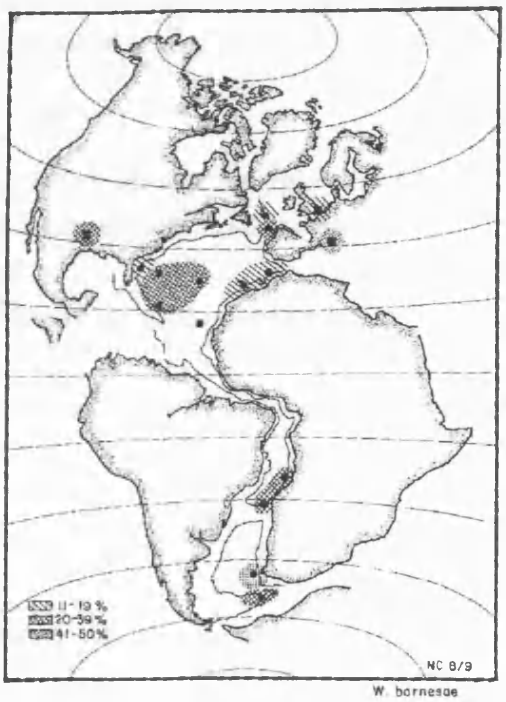

Figure 2.5b Biogeographic distribution of *W. barnesiae* in the Atlantic Ocean, Zones NC8 to NC9.

Figure 2.6a Biogeographic distribution of neritic taxa (*Braarudosphaera*, *Broinsonia* and *Nannoconus*) in the Atlantic Ocean, Zones NC10 to NC11.

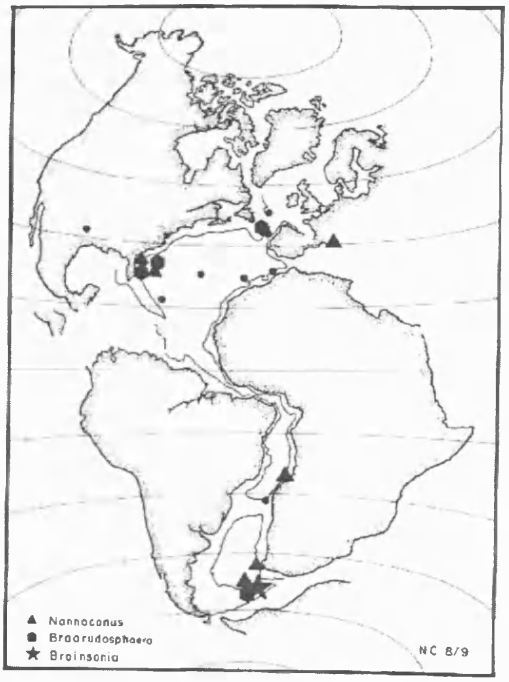

Figure 2.6b Biogeographic distribution of neritic taxa (*Braarudosphaera*, *Broinsonia* and *Nannoconus*) in the Atlantic Ocean, Zones NC8 to NC9.

Figures 2.5 and 2.6. From Roth & Bowdler (1981)

Braarudosphaera* spp.** (including ***Micrantholithus): Limited to continental margin sites characterised by sediment redeposition from shallower sources. Interpreted as an indicator of higher fertility and other unstable conditions.

Nannoconus: Indicator of continental margin, shallow plateau and epicontinental sea conditions. Preservation was thought to play an important role in the distribution of this genus.

Seribiscutum primitivum: Excellent indicator of high-latitudes in the mid-Cretaceous.

***Zygodiscus diplogrammus* (=*Zeugrhabdotus diplogrammus*)**: Showed a preference for continental margins and epicontinental seas.

Sollasites falklandensis*, *Octocyclus magnus: Showed a preference for high-latitudes.

***Cretarhabdus* spp.**, ***Retecapsa* spp.**, ***Prediscosphaera* spp.**: Interpreted as cosmopolitan species with wide environmental tolerances.

On the basis of the bigeographic distribution of these taxa, mid-Cretaceous nannofossils were divided into three distinct assemblages:

High-latitude assemblages: Recorded from the Falkland Plateau and marked by monspecific assemblages of *Corollition* sp. and *Zeugrhabdotus elegans* during the lower Middle Cretaceous, (Barremian-Upper Albian) indicative of blooms during upwelling periods. Upper Middle Cretaceous assemblages (Upper Albian-Lower Turonian) from the same region consisted of abundant *W. barnesiae* and *S. primitivum* with reduced *B. constans* and *Z. noeliae*. Samples from the Boreal region, such as Gault Clay, were variable in composition, indicating unstable environmental conditions. The Gault Clay contained *S. primitivum* in proportions around five to ten times less abundant than on Falkland Plateau.

Continental-margin assemblages: Characterised by relatively rare *W. barnesiae*, and common *B. constans* and species of *Zeugrhabdotus*, although these two taxa alternated in abundances in some samples. *Nannoconus* was more abundant in shallow plateaus with low terrigenous input, and in epicontinental seas. *Braarudosphaera*, *Micrantholithus* and *Broinsonia* were thought to have preferences for continental margin regions and epicontinental seas.

Oceanic assemblages: Higher abundances of *W. barnesiae*, *R. splendens*, *R. asper* and *Lithraphidites carniolensis*.

c) Palaeoceanography: The main palaeoceanographic implications of nannofossil distribution in the Atlantic Ocean were:

1. Nannofossil preservation was understood to be a more sensitive indicator of calcite dissolution than the total calcium carbonate content of sediments because it is not affected by dilution with detrital material. Preservational changes were considered to be a proxy record of increased dissolved CO_2 in bottom and interstitial waters.

2. The poor preservation of the coccoliths in the Atlantic, during the Early/Middle Albian when organic-rich sediments were common, was attributed to the intensive dissolution of carbonate during oxidation of organic matter and the concurrent production of CO_2 that resulted in low carbonate contents and poor preservation of coccoliths. During the Late Albian/Cenomanian, more vigorous deep circulation and increased temperature gradients (shown by *S. primitivum*) allowed better mixing of deep waters (reduced stability), and less CO_2 in deep waters resulted in better preservation of coccoliths in the sediments. The preservation patterns of coccoliths were used to deduce large-scale palaeoceanographic changes in the Atlantic Ocean.

3. Mid-Cretaceous nannofossils were used as a proxy record of temperature and nutrient concentration in the surface waters of the Atlantic Ocean. The bipolar distribution of cold-water species, e.g., *S. primitivum* to latitudes greater than 40° (Falkland Plateau) suggested that temperature gradients between low and high latitudes were smaller during the mid-Cretaceous than today. The tropical belt, ranging from 40°N to 40°S, was characterised by weak latitudinal but strong neritic-oceanic gradients. Continental-margin assemblages enriched with *B. constans* and *Z. noeliae* were understood to be indicative of higher nutrient concentration caused by upwelling along the eastern margin of the North and South Atlantic Oceans. Western-margin assemblages were thought to represent low terrigenous input and lower nutrient concentrations, and this was expressed by the presence of *Nannoconus* and the reduced abundance of *Z. noeliae*.

4. The preservation of organic matter in sediments was thought to be the result of rapid burial, especially on the continental margin sites, and/or low concentrations of oxygen in warm and saline bottom waters derived largely from evaporite basins. An overall negative correlation between calcium carbonate and organic carbon content was noted for the organic-rich sediments. The mid-Cretaceous was thought to have had lower dissolved-oxygen concentrations that led them towards anoxia when accompanied by topographic isolation. Brine influx was thought to be preferred mechanism for increasing the stability of the water column during the mid-Cretaceous.

Roth & Krumbach (1986) continued the investigation on the Middle Cretaceous by extending their study to the Indian Ocean. Their results were similar to those of Roth & Bowdler (1981). In general, preservation in the Indian Ocean samples was comparable with the Atlantic Ocean as the majority of the samples showed 'slight to moderate dissolution effects'. *W. barnesiae* was still upheld as the most dissolution resistant taxon followed by *Zeugrhabdotus*. *B. constans* featured at the bottom of their dissolution-ranking list as the taxon most susceptible to dissolution. They suggested that samples containing more than 40% *Watznaueria* were too highly dissolved to reflect original species composition

and should be avoided in biogeographic studies. Results on biogeography were based on multivariate statistical analysis (Q-mode factor analysis) applied on three time slices (Zones NC10/11, NC8/9, NC7). The three primary factors were interpreted as (i) high latitude, (ii) surface-water fertility and (iii) neritic factor, based on the mathematical loadings given to species whose ecological preferences were known. Ecological preferences of most taxa were the same as interpreted by Roth & Bowdler (1981) with the addition of two species, *Eprolithus floralis* as high-latitude, and *Eiffellithus turriseiffelii* as neritic. The exact palaeoecology of *R. asper/R. splendens* was thought to be 'elusive' especially for the time slice NC8/9 (early-mid Albian).

The implication of these two landmark papers was that temperature and surface-water fertility were proposed as the primary controls on Cretaceous nannofossil palaeobiogeography, with nutrient availability playing a key role in the neritic-oceanic differentiation of the assemblages. The ecological affinities of several abundant species were tentatively established and it became possible to put constraints on palaeoceanographic models (surface water currents, location of upwelling regions, haline-driven deep water circulation) using quantitative studies of nannofossil preservation, biogeographic distribution and abundance patterns. For the Atlantic and Indian Oceans, a wide tropical to subtropical zone was proposed, which was flanked by Boreal and Austral Zones.

Other significant studies by Roth (e.g., Roth 1981, 1983, 1986, 1987, 1989) had similar palaeoceangraphic themes; some were time and region-specific (e.g., Roth 1981, equatorial Pacific) whilst others were more general and covered the entire Jurassic and Cretaceous intervals (e.g., Roth 1989). Wise (1983) suggested another high-latitude taxon, *Repagulum parvidentatum*, from the Southern Ocean, although its distribution was not clear at that time. It was confirmed in later studies (e.g., Wise 1988; Crux 1991) to have a bipolar distribution similar to *S. primitivum*.

Watkins (1986, 1989) advanced palaeoceanographic studies significantly by using diversity indices (Shannon's diversity and evenness) as a measure of the stability and energy flux within the photic zone and the communities living therein. He used diversity indices on quantitative nannofossil counts from the interbedded calcareous shales and chalks of the Greenhorn Limestone (Cenomanian-Turonian) in the Western Interior Basin (USA). Samples showed variable preservation, but were generally affected by intensive diagenesis. Results showed that chalk assemblages had relatively higher diversity and evenness, interpreted as indicating oligotrophic surface-waters. Marlstones showed lower diversity and evenness, as well as higher percentages of *B. constans* and *Zeugrhabdotus* spp. This was indicative of uneven nutrient distribution and niche space, suggesting mesotrophic surface waters with concomitant higher phytoplankton productivity during marlstone deposition. The higher surface fertility resulted in sediment anoxia during marlstone deposition, leading to high rates of organic carbon burial. Reduced phytoplankton production during chalk deposition, allowed oxygenation of the sea floor and establishment of diverse benthic invertebrate communities. *W. barnesiae* did not show any correlation with diversity values, suggesting that it did not have a direct relationship with diagenesis as suggested by Roth & Bowdler (1981).

Premoli Silva et al. (1989) used a set of physico-chemical and palaeoecological indices for palaeoceanographic interpretations. Their results were summarised in a table that is reproduced here (Table 2.2). An important observation is the inclusion of *D. rotatorius* (= *D. ignotus*) in the high-fertility group, which was previously limited to *B. constans* and *Zeugrhabdotus* spp.

CHEMICO-PHYSICAL INDICES	**MICARB CONTENT**	**CALCAREOUS NANNFOSSILS Total abundance**	**Diversity** (no. of species)	***W. barnesiae* %**
DIAGENESIS	high	medium-high	low-moderate	high
PRIMARY DISSOLUTION	absent	low	low	high

PALAEOECOLOGICAL INDICES	**TYPE OF FERTILITY**	**PALAEOCEANOGRAPHY**
A= *B. constans* *D. rotatorius* (= *D. ignotus*) *Zeugrhabdotus* spp.	high fertility	vigorous upwelling
B= *P. asper* (= *R. asper*) *L. carniolensis*	moderate fertility	warmer waters
C= Nannoconids	carbonate productivity	surface water high fertility ? higher salinity?
D= *L. floralis* (= *E. floralis*)	-	high latitudes and cooler waters

Table 2.2 Chemico-physical and nannofossil palaeoecological indices used by Premoli Silva et al. (1989).

Erba (1987; 1992a, b; 1994) and Erba et al. (1989, 1992) demonstrated the utility of nannofossil species as productivity indices in palaecoeanographic interpretations. Her research interest was chiefly the black shale deposition (OAE1a and OAE2) and its links with nannofossil productivity during the mid-Cretaceous. Her initial studies on the Fucoidi Marls in the Umbria-Marche Basin of Italy (e.g., Erba 1987, 1992a) demonstrated the use of (i) *B. constans*, *Z. noeliae* and *D. rotatorius* (= *D. ignotus*) as high productivity indicators associated with upwelling, that showed an inverse correlation with *W. barnesiae*, excluding the closed-sum effect, (ii) *R. asper* and *L. carniolensis* as indicators of primary productivity, and *R. asper* as a warm-water species, (iii) nannoconids as indicators of carbonate productivity associated with black shales, (iv) *E. floralis* as a cool water species. In a study of the Albian Gault Clay (Erba et al. 1989, 1992), fluctuations in the abundance of *B. constans* and *W. barnesiae*, regarded as fertility and non-fertility indices, were shown to be Milankovitch cyclicity-driven, with periodicities of ~41 kyr (obliquity cycle) and 100 kyr (short eccentricity cycle). *R. parvidentatum* and *R. asper* were used as cold- and warm-water indicators and provided evidence for orbitally driven cycles suggesting that cyclic variations of surface water temperature were perhaps, also significant in the Gault Clay.

Erba (1992b) put significant constraints on the fertility levels shown by *B. constans* and *Z. noeliae*, in light of observations from the equatorial Pacific, Sites 800, 801 and 802. According to her, *B. constans* was sensitive to high-fertility in a mesotrophic environment, whereas *Z. noeliae* was an index of high fertility under eutrophic conditons. This was based on the observation that *Z. noeliae* was really abundant only in the upwelling belt, whereas *B. constans* increased in abundance at the margins of the high-fertility areas in the zone of equatorial divergence. This fertility-partitioning was a significant development, although Fisher and Hay (1999) contradicted Erba's hypothesis by suggesting the reverse, i.e., *Z. noeliae* may be representative of lower fertility conditions than *B. constans*. The hypothesis by Fisher & Hay (1999) was based on comparisons of Pearson's correlation coefficients, calculated on relative abundance data from samples in the Western Interior Seaway, USA.

Erba (1994) in a paper on the 'nannoconid crisis' related to the Early Aptian OAE1a event, hypothesised *Nannoconus* to be a lower photic zone dweller (like the extant species *Florisphaera profunda*) that bloomed depending on the depth of the nutricline. The nannoconid to coccolith proportion in sediments was dependant on the nutricline/thermocline dynamics at different frequencies. Thus fertility of the upper photic zone was correlated to turnover of nutrients due to volcanic activity and the input of nutrients from the continents into the oceans. Recent studies by Erba (e.g., Erba & Tremolada 2004; Erba 2004) on mid-Cretaceous black shales have reiterated a similar hypothesis by integrating geochemical with microfossil data.

Bralower and co-workers (Bralower &Thierstein 1984, 1987; Bralower et al. 1993, 1994, 1997, 1999) investigated mid-Cretaceous black shales (mainly Aptian-Albian) from numerous sections located at different latitudes. Based on integrated planktonic foraminiferal and nannofossil biostratigraphy, they divided the Aptian-Albian OAE into three individual anoxic episodes, OAE1a (Early Aptian), OAE1b (Early Albian) and OAE1c (early Late Albian). The distribution of the Albian OAEs was found to be patchy compared to the Early Aptian OAE1a. None of these anoxic events were associated with major biotic extinctions, but were marked by changes in the community structure of planktonic foraminifera. Nannofossil taxa did not show radical changes in response to OAEs, but showed nearshore affinities at some sites, or were replaced by other phytoplankton at other sites. Sea level transgressions and climatic consequences of volcanism were understood to be likely factors that conditioned the oceans to be prone to dysoxia/anoxia through feedback mechanisms (Bralower et al. 1993, 1994). In a study of mid-Cretaceous Sr-isotope stratigraphy (Bralower et al. 1997), the Aptian-Albian stages were found to be characterised by a marked decrease in $^{87}Sr/^{86}Sr$ values, which was related to the release of volcanic Sr due to increased seafloor spreading that produced the Ontong Java, Manihiki and Kerguelen Plateaux.

Mutterlose (1989; 1992a, b; 1996) discussed the palaeoceanographic significance of taxa such as *Nannoconus* and *Rhagodiscus asper* in his papers. He used high abundances of *Rhagodiscus asper* as an indicator for warm waters in his study of Aptian sections from northwest Germany and the North Sea. By high abundances, he meant percentages in the range of >30% from the Upper Aptian at some of the sections in northwest Germany. He also observed that in the Gott Section (northwest Germany), *R. asper*

outnumbered *W. barnesiae* and *Biscutum* in some Upper Aptian samples. Thus, *R. asper* was stated to 'play the role *W. barnesiae* usually does' in some selected samples. He used the abundances of *Nannoconus* and *R. asper* along with other fossil groups (ammonites, belemnites and planktonic foraminifera) to propose an influx of warm water floras and faunas from the western Tethys into the NW European region during the mid-Aptian. In his subsequent studies (e.g., Mutterlose & Ruffell 1999; Mutterlose & Kessels 2000; Bischoff & Mutterlose 1998; Habermann & Mutterlose 1998), *R. asper* was used as a warm-water species in palaeoceanographic studies.

Mutterlose (1996) showed that in certain parts of the Lower Cretaceous, *Biscutum* spp. (indicative of high fertility/cool upwelling water) and *R. asper* have a negative correlation. On the basis of this inverse correlation he inferred that *R. asper* had warm-water affinities. Such indirect linkages make this interpretation dubious. Similarly, *W. barnesiae* was used as an indicator of low surface water fertility even though no correlation was noted between the abundances of *B. constans* and *W. barnesiae*. However, the high-latitude distribution of *S. primitivum* was shown clearly by Mutterlose (1992b) and is reproduced here (Figure 2.7).

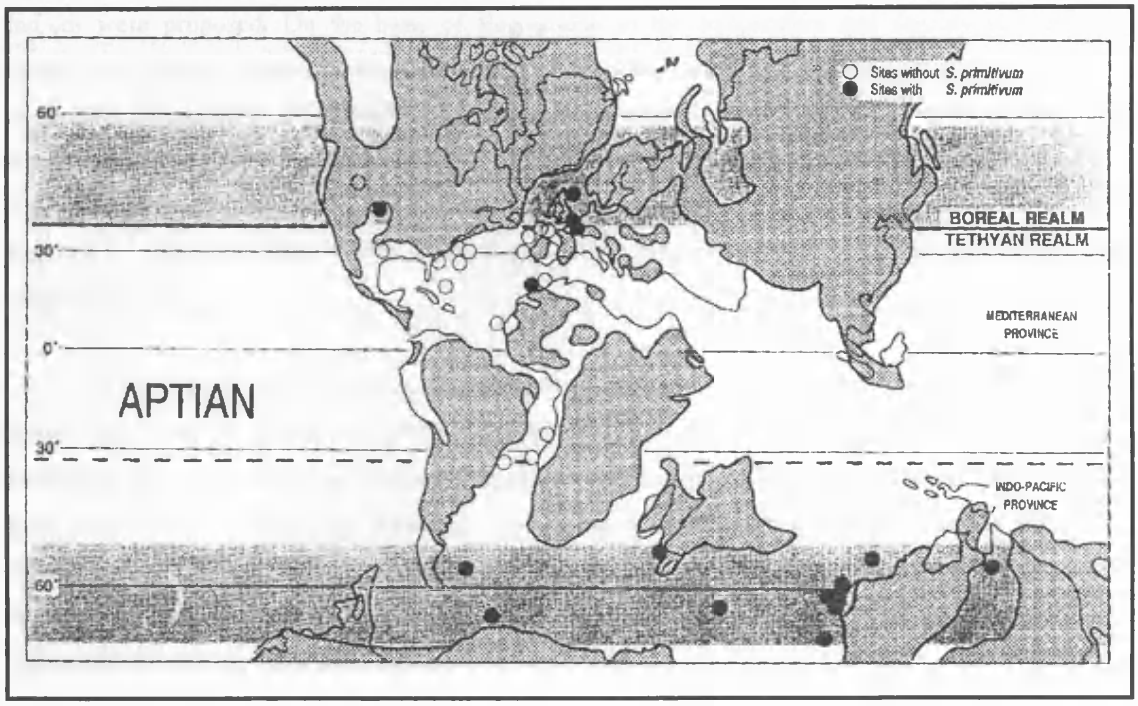

Figure 2.7. Palaeogeographic reconstruction showing the bipolar distribution of *Seribiscutum primitivum*. From Mutterlose (1992b).

Williams & Bralower (1995) conducted detailed nannofossil assemblage studies on three sections from the margins of the Early Cretaceous North Sea Basin. Both absolute (numbers of nannofossils per gram) and relative (% of the assemblage) abundance data were used to study the relationships between nannofossil taxa. They suggested a higher cut-off point (70%) for *W. barnesiae* as a dissolution index than previously proposed (40%) by Roth & Krumbach (1986). They based this suggestion on the observation that there was no link in the studied sections between species richness and

the abundance of *W. barnesiae*. The lack of correlation between *W. barnesiae* percentages and parameters such as $CaCO_3$, TOC, species richness and total nannofossil abundances indicated that either diagenesis had not generally altered nannofossil assemblages, or that *W. barnesiae* and/or species richness were poor proxies for preservational effects. Additionally, it was suggested that *W. barnesiae* represented lower fertility conditions, an observation which is thought to be an oversimplification as it is based on the usually observed inverse correlation between *B. constans* and *W. barnesiae*. *Rhagodiscus asper* was suggested to be related to lower fertility conditions associated with warmer surface waters in the basin.

The palaeobiogeography of the Lower Cretaceous (Berriasian-Barremian) and the palaeoecology of important taxa such as *Watznaueria*, *Nannoconus*, *Biscutum* and *Zeugrhabdotus*, were critically examined by Street (1998) in her Ph.D. thesis. A comprehensive summary of nannoplankton biogeography is given in her thesis.

Herrle (2002) used nannofossils and oxygen/carbon isotopes to reconstruct palaeoceanographic changes in the Vocontian Basin and the Atlantic Ocean during the Aptian to Early Albian in relation to black shale formation. Based on the composition of nannofossil assemblages, nutrient and temperature indices were proposed. On the basis of fluctuations in the temperature and fertility records using nannofossil indices, climatic variations involving monsoonal circulation and changes in the intensity of deep-water formation at low latitudes were inferred. The supraregional Early Albian OAE1b black shale was postulated to have been deposited under extremely warm and humid conditions during times of very strong monsoonal circulation/winds and diminished basin ventilation. A series of papers (Herrle 2003; Herrle et al. 2003) have been written on this theme by integrating geochemical with nannofossil and other microfossil data.

These are some of the principal publications that have established the use of nannofossils as proxies for recording palaeoceanographic conditions of Cretaceous surface waters. Variation in their abundance and composition is understood to reflect changes in palaeoclimate, nutrient supply, detrital input, surface-water salinity, etc. There are about ten to twelve taxa that typically make up 90% of the nannofossil assemblages in the mid-Cretaceous and may be used for palaeoceanographic interpretations. A summary of these taxa along with the principal publications associated with them is given in a chronological order in Table 2.3 below.

Species name	**Palaeoecological affinity**	**Principal publications**
B. constans	high productivity	Roth (1981); Roth and Bowdler (1981); Windley (1995); Roth and Krumbach(1986); Erba (1987); Watkins (1989); Premoli Silva et al. (1989); Erba (1992a, b); Erba et al. (1992); Fisher and Hay (1999); Gale et al. (2000); Street and Bown (2000).
D. ignotus (= *rotatorius*)	high productivity	Premoli Silva et al. (1989); Erba (1992a); Coccioni et al. (1992); Herrle (2002); Herrle et al. (2003).
Eprolithus floralis	1. high-latitude	1.Roth & Krumbach (1986); Wise

	2. increased fertility	(1988); Premoli Silva et al. (1989); Erba (1992a); 2.Premoli Silva et al. (1999)
L. carniolensis	1. oceanic/low productivity 2. neritic (referring to *L. bollii* and *L. alatus*, not *L. carniolensis*)	1.Thierstein (1976); Roth and Bowdler (1981); Watkins (1989), Eshet & Almogi-Labin (1996); 2. Applegate et al. (1989).
Nannoconus	1. low-latitude (tropical) neritic taxon, living in shallow plateaux and epicontinental seas 2. Tethyan, warm water 3. meroplanktonic, calcareous dinoflagellate affinities, shallow-water, Tethyan 4. deep-photic zone, oligotrophic 5. cosmopolitan	1.Roth & Bowdler (1981); Roth & Krumbach (1986); Street & Bown (2000) 2.Mutterlose (1989, 1992a, b); Street & Bown (2000) 3.Busson & Noël (1991) 4.Erba (1994) 5. Deres & Achéritéguy (1980); Perch-Nielsen (1985)
P. columnata	cosmopolitan	1. Roth and Bowdler (1981); Crux (1991), Mutterlose (1992b).
R. parvidentatum	high-latitude	Wise (1983); Wise (1988); Crux (1991); Erba et al. (1992); Bown et al. (1998); Street and Bown (2000), Lees (2002); Herrle (2002).
R. crenulata	cosmopolitan	Roth and Bowdler (1981); Lees (2002).
R. asper	1. warm water 2. lower fertility associated with warmer waters	1.Roth and Krumbach (1986); Erba (1987); Mutterlose (1987, 1989); Premoli Silva et al. (1989); Crux (1989, 1991); Erba et al. (1992); Bischoff and Mutterlose (1998); Mutterlose and Kessels (2000); Herrle (2002). 2.Williams & Bralower (1995)
S. primitivum	high-latitude	Thierstein (1974); Wise and Wind (1977); Roth and Bowdler (1981); Roth and Krumbach (1986); Crux (1991); Mutterlose (1992b); Street and Bown (2000); Lees (2002); Herrle (2002).
T. orionatus	possibly high-latitude	Wind (1979); Roth (1983); Crux (1991); Lees (2002).
Watznaueria spp. (mainly *barnesiae* + *fossacincta*)	1. not highest latitude 2. high-latitude 3. low-latitude 4. cosmopolitan 5. oceanic 6. low productivity 7. dissolution resistant (proxy for preservation, 40% cut-off) 8. poor proxy for preservation (70% cut-off, instead of 40%) 9. r-selected	1.Bukry (1973); Thierstein (1981); Shafik (1990); Huber and Watkins (1992); Watkins et al. (1996). 2.Roth and Bowdler (1981) 3.Thierstein (1981). 4.Mutterlose (1992b). 5.Roth and Bowdler (1981); Roth and Krumbach (1986). 6. Roth and Krumbach (1986); Erba et al. (1992); Williams & Bralower (1995); Fisher and Hay (1999). 7.Hill (1975); Thierstein (1980); Roth (1981); Roth and Bowdler (1981); Roth and Krumbach (1986); Erba (1992a). 8.Williams and Bralower (1995) 9.Thierstein (1981); Thomsen (1989); Street & Bown (2000); Lees et al. (2004)
Z. noeliae (=*erectus*)	high productivity	Roth (1981); Roth and Bowdler (1981); Roth and Krumbach (1986); Watkins (1989); Premoli Silva et al. (1989); Erba (1987); Erba (1992a, b); Erba et al. (1992); Windley (1995); Williams and Bralower (1995); Fisher and Hay (1999); Street and Bown (2000), Herrle (2002).

Table 2.3 Summary of the palaeoecological interpretations made on important mid-Cretaceous taxa along with the published sources.

2.3 Multispecies palaeoproductivity and palaeotemperature indices

The use of multispecies indices as a quantitative measure to reconstruct spatial and temporal development of palaeoproductivity and palaeotemperatures is relatively recent in origin. Gale et al. (2000) proposed a Productivity Index in their study of the Cenomanian-Turonian biodiversity changes at Eastbourne, SE England. A simple ratio based on the three important (and often dominant) species, *Biscutum* spp., *Zeugrhabdotus* spp., and *Watznaueria* spp., was used to calculate the Productivity Index.

$$\text{P (Productivity Index)} = \left[\frac{\%Zeug.spp. + \%Bisc.spp.}{\%Watz.spp.}\right]$$

According to them, the rationale behind using these taxa was that *Zeugrhabdotus* and *Biscutum* were better able to exploit eutrophic conditions than *Watznaueria* and so an index based on the relative abundance of these taxa would record productivity change. The limitations of this index were (i) the abundance of *Watznaueria*, a robust taxon, increases with deteriorating preservation, and (ii) the closed-sum effects of interpreting percentage data. In view of these limitations, they suggested that this index works best on relatively well-preserved samples when the reciprocal relationship between these two sets of taxa can be shown as genuine rather than a closed-sum artefact.

Herrle (2002) used positive and negative loadings of the assemblages given by R-mode Principal Components Analysis to formulate a Nutrient Index (NI). This was based on samples from the Vocontian Basin in SE France. The NI, expressed as a %, was defined as:

$$\text{NI (Nutrient Index)} = \left[\frac{(\%D.ign. + \%Zeug.spp)}{(\%Watz.spp.) + (\%D.ign. + \%Zeug.spp.)}\right] * 100$$

It is worth speculating why *B. constans* did not feature in the grouping of productivity-related taxa, despite its presence in the assemblages. Its exclusion from the nutrient index was not clearly explained by Herrle (2002).

The Temperature Index (TI) proposed by Herrle (2002) was defined as:

$$\text{TI} = \left[\frac{(Be + S + Rp + Ss + Zt)}{(Ra + Zd) + (Be + S + Rp + Ss + Zt)}\right] * 100$$

where Be = *Biscutum* aff. *ellipticum*, S = *Seribiscutum* spp., Rp = *Repagulum parvidentatum*, Ss = *Staurolithites stradneri*, Zt = *Zeugrhabdotus trivectis*, Ra = *Rhagodiscus asper*, Zd = *Zeugrhabdotus diplogrammus*.

The TI is questionable as the palaeotemperature affinities of most of these taxa, with the exception of *R. parvidentatum* and *S. primitivum* are dubious. The cold water affinities of *Biscutum* aff. *ellipticum*, a large-sized variety of *B. constans*, and *S. stradneri* are largely unproven. *Z. trivectis* is very rare in the mid-Cretaceous and is therefore not appropriate in an index. The warm-water affinity of *R. asper* is debatable (see Chapter 5), whereas that of *Z. diplogrammus* is conjectural. For these reasons, the TI is not considered in this study.

In summary, studies on mid-Cretaceous palaeobiogeography and palaeoecology in the last two decades have established the potential of nannofossils as proxies for two important palaeoceanographic parameters, i.e., nutrient concentration and temperature. Additionally, variations in nannofossil abundance and composition reflect changes in palaeoclimate, detrital input and surface-water salinity. Both single species and multispecies nutrient indices are now available as quantifiers of surface-water fertility and temperature for the mid-Cretaceous. However, a rigorous testing of these nannofossil indices is necessary in order to verify their applicability and understand their limitations. Further discussion on single species and multispecies nutrient indices follows in Chapters 5 and 6.

Chapter 3. Materials and Methods

3.1 Acquisition of samples

The sample material for this study includes outcrop and core samples, covering the Aptian to Cenomanian interval of the mid-Cretaceous. The outcrop samples from the Cauvery Basin (SE India) were provided by A. S. Gale and were collected during field seasons in 2001 and 2002. Core samples from ODP Legs 198 and 171B were provided by P. R. Bown. In total, six sections were studied in detail – three outcrop (two from India and one from England) and three cores (two from the Pacific and one from the Atlantic). In addition, a number of extra samples were analysed for palaeobiogeographic analysis. These include mostly outcrop and some borehole samples from England and France. Details of the samples studied are summarised in Table 3.1.

Sample Type	Location	Details	Number of samples
Principal samples			
Outcrop	**SE India**, Cauvery Basin	Karai Formation, Section 1	146
		Karai Formation, Section 2	67
Outcrop	**SE England**, Folkestone	Gault Clay Formation	41
Core	Leg 171B, Blake-Bahama Basin, **North Atlantic Ocean**	Hole 1049C	34
Core	Leg 198, Shatsky Rise, **northwest Pacific Ocean**	Holes 1207B, 1213A/B	37
Additional samples			
Borehole	S England, Hampshire	Selborne, Sel 1& 2	8
Outcrop	S England, Kent	Warren section	3
Outcrop	SE France, Vocontian Basin	Mt. Risou section	2
Outcrop	SE France, Vocontian Basin	Col de Palluel section	14
Core	Leg 198, Shatsky Rise, northwest Pacific Ocean	Hole 1214A	5

Table 3.1 Details of sample material used in this study.

The study sections encompass mid-Cretaceous palaeolatitudes ranging from ~60° S (Cauvery Basin, India) to ~ 45° N (Gault Clay Formation, England). Sampling strategy was largely determined by the thickness of the section, the preservational state of the nannofossils (preliminary studies were conducted to check preservation) and over and above all, the purpose of the investigation being conducted. Sample descripitions are given in the respective chapters. The study sections were broadly coeval (Aptian to Turonian), although some sections had a longer stratigraphic range (Karai Formation and Shatsky Rise) than others (Gault Clay and Blake Nose). The Aptian to Cenomanian stages have been studied in greater detail compared to the Turonian. The only Turonian material considered in this study is the Karai Formation of Cauvery Basin, which ranges as far as the EarlyTuronian.

3.2 Slide Preparation

Smear slides were used throughout this study. Slide preparation (Bown & Young 1998b) was kept simple in order to retain the original sediment composition. Techniques such as centrifuge separation

and ultrasonic cleaning were deliberately avoided as they can potentially alter the original composition of the nannofossil assemblage in a sample. The most important consideration while preparing smear slides was to avoid contamination, so appropriate measures were taken, e.g., using distilled water, disposal materials, cleaning all glassware in dilute HCl, etc.

3.3 Laboratory Techniques

An Olympus BH-2 oil-immersion-objective light microscope (LM) was used to generate all the nannofossil data. A magnification of ca. x1000 was employed to observe the nannofossils under cross-polarised illumination (XPL). Taxa exhibiting low birefringence were also viewed under phase-contrast illumination. All slides were initially logged for an hour or more, before performing the counts. Abundance and preservation estimation strategies are explained separately in the next section.

Scanning Electron Microscopy (SEM) was largely abandoned after initial attempts on selected Gault Clay and Cauvery Basin samples. Excessive amounts of clay hampered the preparation of clean SEM stubs. Results obtained were not satisfactory (clay largely obscured the specimens). Since taxonomy was not a principal objective of the project, alternative methods for preparing cleaner SEM stubs (to reduce the clay) were not pursued.

LM photography was done on all the principal study sections except Shatsky Rise, using the NIH-Image digital capture technique (see Bown & Young 1998b). The plates are presented in Chapter 8.

3.4 Abundance estimation

Estimation of the semi-quantitative abundance of species in the assemblage were recorded as per the scale in Table 3.2.

Abundant (A)	>10 specimens per field of view
Common (C)	1-10 specimens per field of view
Few/Frequent (F)	1 specimen per 2-10 fields of view
Rare (R)	1 specimen in >10 fields of view
Very Rare (VR)	only 1 or 2 specimens observed during logging

Table 3.2 Semi-quantitative abundance estimation scale used in this study.

An estimate of the total calcareous nannofossil abundance compared to other biogenic particles and inorganic components in a sample was recorded as per the scale in Table 3.3.

High (H)	Each field of view has > 20-30 nannofossils
Moderate (M)	Each field of view has up to 10 nannofossils
Low (L)	Each field of view has < 3 nannofossils
Barren (B)	No nannofossils in a field of view

Table 3.3 Total calcareous nannofossil abundance scale.

3.5 Preservation estimation

As preservation constitutes an important attribute of nannofossil studies, an accurate estimation of the preservational state of an assemblage is crucial to conveying the integrity of any dataset. Preservation can be hard to quantify, as it can vary between different categories within the same sample, such as good to moderate or moderate to poor. Additionally, etching and overgrowth may be observed in the same sample making preservation estimation more difficult. Roth (1983) presented a list of preservation categories with alphanumeric codes assigned to each of the categories. The categories ranged from heavily etched (E3) to pristine samples showing excellent preservation (X), further extending to heavily overgrown samples (O3). Thus heavy etching and heavy overgrowth constituted the two end-members of his preservation scale. Although Roth's preservation categories are useful, a relatively straightforward qualitative classificatory scheme was used in this study based on the standard categories given in Table 3.4.

Very Good (VG)	No evidence of etching or overgrowth, no alteration of morphological features (pristine), specimens are very easily identified.
Good (G)	Some specimens are slightly etched or overgrown, but easily identifiable.
Moderate (M)	Specimens are identifiable although there is moderate overgrowth and/or etching (extended elements, slightly serrated outlines, delicate structures partially obscured, etc.).
Poor (P)	Overgrowth and etching is considerable, making identification difficult (delicate structures completely obscured, material fragmented with mostly solution-resistant taxa left)

Table 3.4 Preservation categories used in this study.

3.6 Observation and counting strategy

3.6.1 Biostratigraphy

The approach to biostratigraphy in this study has been semi-quantitative, using the standard categories given in Table 3.2. Dating was achieved based on first and last occurrences (FO & LO) of marker species logged in a section, using established Cretaceous zonation schemes. The zonation schemes used in this study have been discussed in Chapter 2, section 2.1.

3.6.2 Counting technique

Quantitative data for palaeoceanographic studies was gathered by counting a standard number of nannofossils and converting them into percentages (relative abundance method). For each slide, 300+ nannofossils (usually between 300 & 400) were counted in randomly chosen fields of view of approximately equal density. The number of fields of view counted was recorded to give an estimation of the overall nannofossil abundance in a sample, in terms of the number of specimens per field of view.

3.6.3 Relative abundance vs. absolute abundance

The pros and cons of relative abundance against absolute abundance data were considered before opting for the former method. The closed-sum effect is an inherent shortcoming of the relative abundance method. This implies that there is interdependency in the percentage figures between the various taxa, such that an increase in the percentage of one taxon may cause an apparent decline in taxa which did not actually decrease in absolute abundance. In other words, fluctuations in the percentage of a dominant species may affect the abundance of other species. This often comes into play while interpreting the percentage abundance fluctuations of *W. barnesiae*, *B. constans* and *Z. noeliae*, as they constitute the three dominant taxa in most mid-Cretaceous assemblages.

The absolute abundance method of counting, expressed as specimens per unit area of the slide (e.g., specimens per 20 fields of view) or specimens per unit weight of the sediment (per gram) does not suffer from the closed-sum effect. The former method (specimens per fixed fields of view) is relatively straightforward as it is based on the assumption that the grain density is roughly constant in each slide and is therefore representative of the sample (Backman & Shackleton 1983). Elaborate procedures involving weighing a known amount of sediment followed by evaporative settling on a cover slip have also been prescribed (Wei 1988, Beaufort 1991). Rutledge (1995) argued that the absolute abundance method does not in reality give absolute figures because it does not account for the dilution factor by detrital material. Thus absolute abundance figures may be largely influenced by variations in the supply of terrigenous clastics or clay, rather than giving a true representation of variations in phytoplankton productivity. This is especially relevant in the context of Cretaceous sediments that are rhythmically bedded or largely influenced by terrigenous supply.

Another limitation of the absolute abundance method is that small taxa such as *B. constans*, *D. ignotus*, *R. parvidentatum*, etc. can get eliminated from the count data especially in fields of view dominated by large and bright nannofossils such as *Nannoconus*. This was observed in the Blake Nose section and is discussed in Chapter 6.

The relative abundance method was favoured mainly because of the time constraints of finishing the project. The relative abundance method is faster, readily reproducible, and an easily comparable form of data between different workers. I also believe that after considerable practice, it is possible to get consistent sediment density in a smear slide using roughly equal amounts of sediment.

However, the absolute abundance method based on counting fixed numbers of fields of view, i.e., specimens per unit area of slide, was tested on one of the study areas (Blake Nose section) in order to verify whether it agrees or conflicts with the relative abundance data. Nannofossils were counted in 20 fields of view in samples from the Blake Nose section and compared with the percentage abundance data. These counts were performed on the same slides through which percentage abundance data was generated.

3.6.4 Palaeobiogeography

In order to obtain mid-Cretaceous palaeobiogeographic trends, quantitative data (300+ specimen counts) were generated from three time slices in the Albian-Cenomanian interval, in accordance with the methodology used by Street and Bown (2000). The three time-slices chosen were the FO's of *Tranolithus orionatus* (Middle Albian), *Eiffellithus turriseiffelii* (Upper Albian) and *Corollithion kennedyi* (Lower Cenomanian). Samples were chosen from different palaeobiogeographical provinces for this purpose. Details are given in Chapter 8, section 8.1.

3.7 Diversity analysis

Diversity indices are particularly useful in palaeoceanographic investigations and were therefore applied to the percentage abundance data in the Blake Nose and Shatsky Rise sections. The three diversity indices used were: Species richness or simple diversity (S), Equitability (E) and Shannon's Diversity (H). Species richness is the simplest measure of diversity, representing the number of taxa in an assemblage. It was measured by counting the number of species logged in each sample. Equitability or evenness is a measure of dominance within an assemblage and takes into account the distribution of individuals between taxa. It was calculated using the modified Hill's ratio (Ludwig & Reynolds 1988). Shannon's Diversity Index, which incorporates species richness and evenness into a single value, measures the uncertainty of any randomly picked individual belonging to one particular species in the assemblage (Shannon & Weaver 1949). These indices are reviewed in Watkins (1989), Fisher & Hay (1999) and Street & Bown (2000).

Chapter 4. Cauvery Basin, SE India

Abstract

A suite of samples from the Cauvery Basin, SE India, belonging to the mudrock-claystone dominated Karai Formation were analysed for biostratigraphy. The nannofossil biostratigraphy of the Karai Formation is established in two sections, Section 1 and Section 2, located in the Karai and Garudamangalam villages in the Tiruchirapalli district of Tamil Nadu, SE India. The study applied the zonation scheme of Sissingh (1977) with modifications by Perch-Nielsen (1983, 1985), supported by that of Bown et al. (1998) for the Albian, and Burnett (1998) for the Cenomanian. The Karai Formation, Section 1 is dated as Early Albian (Zone BC23) to Early Turonian (Subzone UC6b), whereas Section 2 ranges from the Late Albian (Subzone BC27a) to the earliest Turonian (Subzone UC6a inferred). The aim of testing the zonation schemes of Bown et al. (1998) and Burnett (1998) on samples from India revealed that while the former scheme is applicable in full, the latter has zonal markers that are unusable in this region, and is therefore not fully applicable. Two zones, UC2 and UC4 are not applicable because of problems with their respective marker species, *Gartnerago segmentatum* and *Cylindralithus biarcus*. A hiatus is recognised in both sections comprising Zone UC5 (uppermost Cenomanian), making the Cenomanian/Turonian boundary interval incomplete. Simultaneous last occurrences of *Lithraphidites acutus* and *Helenea chiastia* within the same sample is observed in both sections. The Albian/Cenomanian boundary is identified in both sections using the FO of *Corollithion kennedyi*, supported by additional datum-levels such as the FO of *Gartnerago* cf. *G. nanum*, FO of *Gartnerago chiasta*, LO of *Hayesites albiensis* and LO of *Staurolithites glaber*. The FO of *G.* cf. *G. nanum* is a useful event in constraining the Albian/Cenomanian boundary. Some secondary marker species previously recorded in the Indian Ocean such as *Helicolithus anceps* and *Quadrum intermedium* are absent in the Cauvery Basin. Their absence is more likely due to their rarity rather than stratigraphic problems.

4.1 Aims

The aims of this study were as follows:

1. To evaluate the nannofossil biostratigraphy of the Karai Formation (Sections 1 and 2), using established zonation schemes;
2. To verify the applicability of the zonation schemes of Bown et al. (1998) and Burnett (1998) on the sections;
3. To test the hypothesis that Albian-Cenomanian nannofloras were cosmopolitan;
4. To study the palaeobiogeographic affinities of the Cauvery Basin nannofossil assemblages.

4.2 Introduction

The Cauvery Basin is the southernmost of a series of pericratonic, passive-margin sedimentary basins located along the Coromandel Coast of India, in the state of Tamil Nadu (Figure 4.1). The basin has a large areal extent (~ 25, 000 km^2) and extends towards the east into the offshore area (17, 500 km^2), between latitude 12° 15' N near Pondicherry and 8° 15' N to the south of Ramanathapuram (Tewari et al. 1996b). The basin contains one of the best developed and most comprehensively studied Cretaceous sequences in India and is well known for its palaeofaunal and palaeofloral diversity, and lithological associations.

The evolution of the Cauvery Basin, a pre-rift basin existing along the continental margin of southeast India, is intimately linked with the rifting of India from Antarctica-Australia that began during the Early Cretaceous (Powell et al. 1988; Veevers et al. 1991). This rifting was significant for the subsequent development of the eastern Indian Ocean during the early part of the Cretaceous (Holmes and Watkins 1992). Palaeogeographic reconstructions indicate palaeolatitudes of ~ 60°S for SE India (Figure 4.2) during the mid-Albian (106 Ma) based on Ocean Drilling Stratigraphic Network (ODSN) reconstructions.

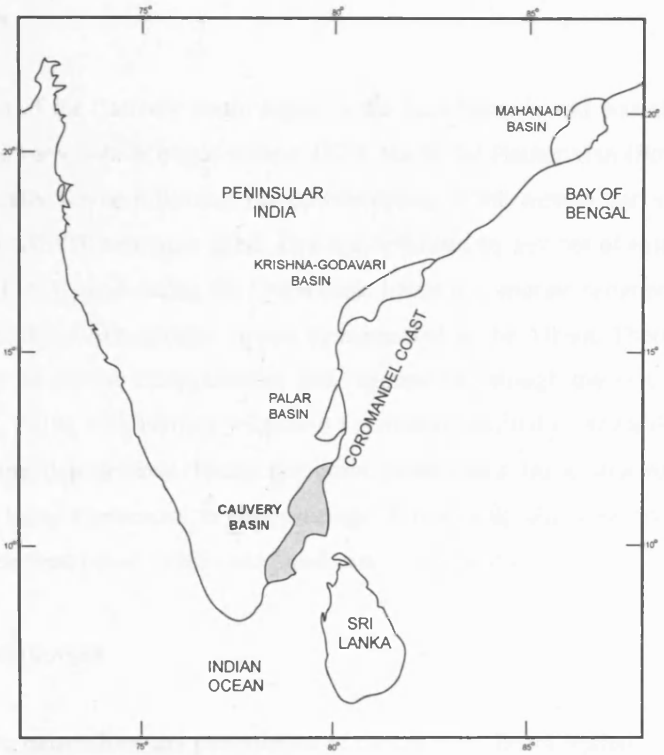

Figure 4.1 Peninsular India showing onshore parts of the east-coast sedimentary basins. Modified after Powell et al. (1988).

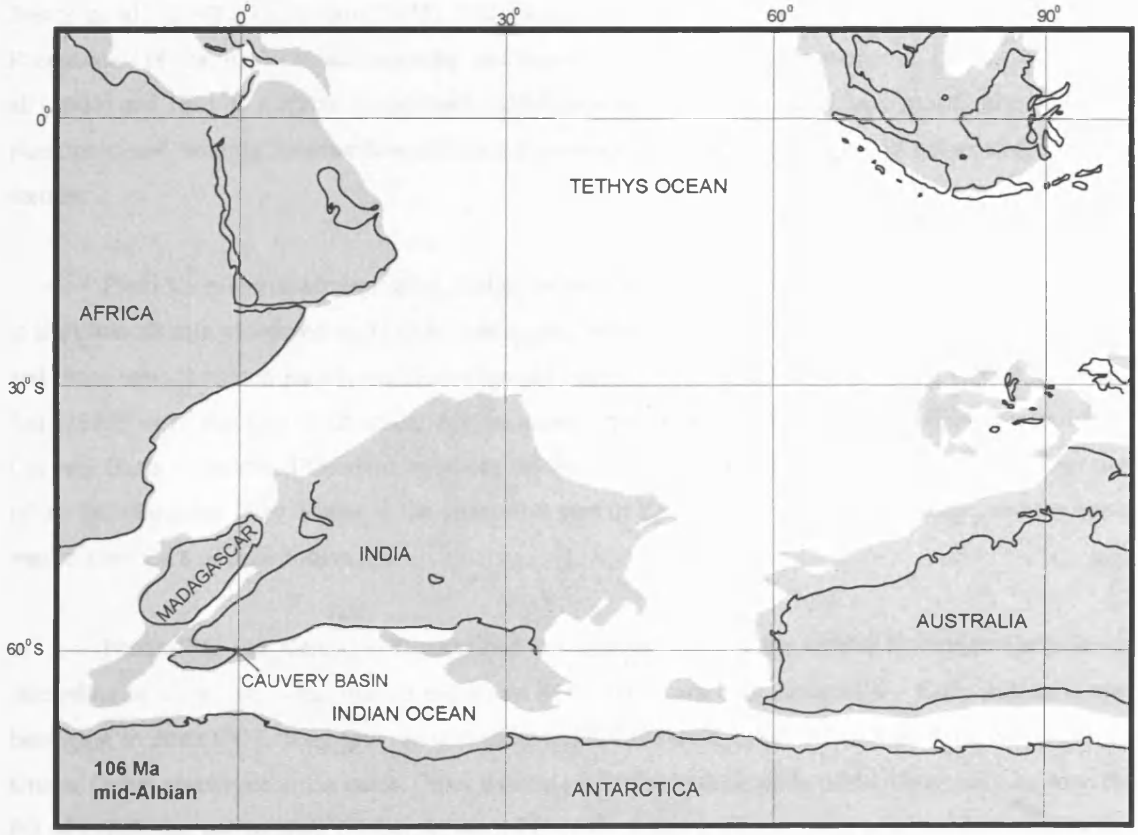

Figure 4.2 Palaeolatitudinal position of the Cauvery Basin during the Albian (www.odsn.de).

4.3 Geological history

The evolution of the Cauvery Basin began in the Late Jurassic and was closely linked with the break-up of East Gondwana, which began around 132.5 Ma in the Hauterivian (Powell et al. 1988). The basin became tectonically active following the downwarping of the eastern part of the Indian cratonic shield, mainly along a NE-SW basement trend. This was followed by a series of extensional block faulted movements along a NE-SW trend during the Cretaceous. Initial non-marine sedimentation was succeeded by marine deposits resulting from a major marine transgression in the Albian. Thereafter, deposition was controlled by a series of marine transgressions and regressions through the rest of the Mesozoic and Cenozoic (Sastri et al. 1977). The Tertiary witnessed a continued basinal tilt towards the east, resulting in an easterly shift of the depocentres. Today the basin preserves a thick succession of well-exposed sedimentary rocks of Early Cretaceous to Holocene age. For a comprehensive review of the geological history of the basin, see Sastri et al. (1981) and Sundaram et al. (2001).

4.4 Previous nannofossil work

Studies on the palaeoflora and palaeofauna of the Cauvery Basin started mainly in the 1970's by a group of scientists working jointly for the Geological Survey and the Oil and Natural Gas Commission (ONGC) of India. Important papers that address the micro- and macropalaeontology of the basin include Sastry et al. (1968), Govindan (1972), Narayanan (1977), Ayyasami and Banerji (1984), Kale and Phansalkar (1992a, b), Venkatachalapathy and Ragothaman (1995a, b), Tewari et al. (1996a, b), Kale et al. (2000) and Hart et al. (2001). Micropalaeontological studies on the basin have mostly been based on planktonic and benthic foraminifera covering biostratigraphy, palaeoecology and palaeoenvironmental themes.

Previous micropalaeontological studies on the Cauvery Basin have not given adequate attention to the nannofossils preserved in its rich sedimentary infill. Only five papers have been published so far and these have focussed mainly on biostratigraphy, using the 'CC' zones of Sissingh (1977). Jafar and Rai (1989) were the first to describe Albian nannofloras from the Dalmiapuram Grey Shales of the Cauvery Basin, considered to be the basal part of the Uttatur Group. Their study assigned the lower part of the Dalmiapuram Grey Shales to the uppermost part of Zone CC7 of Early Albian age, and the upper part to Zone CC8 of mid-Albian age.

Phansalkar and Kale (1989) described the exposed base of the Uttatur Group as diachronous. According to them, the oldest marine sediments in the basin are Late Aptian (?) – Early Albian in age, belonging to Zone CC7. They also recognised Zone CC8 (Middle-Upper Albian) in the basal part of the Uttatur Group elsewhere in the basin. Other datums identified in their study of the Uttatur Shales were the FO of *Eiffellithus turriseiffelii* (Upper Albian), LO of *Hayesites albiensis* (below the Albian/Cenomanian boundary), FO of *Microrhabdulus decoratus* (Middle Cenomanian), FO of *Ahmuellerella octoradiata*

(Upper Cenomanian), FO of *Quadrum gartneri* (Upper Cenomanian) and the LO of *Axopodorhabdus albianus* (Lower Turonian).

Kale and Phansalkar (1992a) gave a more comprehensive review of the nannofloras from the Uttatur Group. Five standard nannofloral zones of Sissingh (1977), from Zone CC7 to CC11, were recognised in the assemblages. Consequently, the base of the Uttatur Group was placed in the Upper Aptian (?) - Lower Albian based on the presence of *Prediscosphaera columnata*, *Axopodorhabdus albianus* and *Cribrosphaerella ehrenbergii*. The upper boundary of the Uttatur Group was placed in the Middle Turonian.

Kale and Phansalkar (1992b) made some palaeobiogeographic remarks on the Uttatur nannofossil assemblages in addition to biostratigraphy. A high latitude palaeobiogeographic position was inferred on the basis of the high abundance of taxa such as *Seribiscutum primitivum*, *Rhagodiscus asper*, *R. splendens* and *Biscutum* spp. They suggested that the high abundance of *Nannoconus* spp. in the Dalmiapuram Grey Shales and in the eastern Indian Ocean indicated a probable gateway between the Cauvery Basin and the eastern Indian Ocean. According to them, the condensed nature of the Middle Cenomanian section and the frequent Cenomanian-Turonian hiatuses recorded in the Indian Ocean implied a regressive phase around that time. The nannofloras of the Uttatur Group showed a decreasing dominance of high latitude taxa by the Turonian, confirming a shift in the palaeolatitudinal position of the Indian plate from high to more temperate latitudes (Kale and Phansalkar 1992b).

Kale et al. (2000) discussed palaeobiogeographic and palaeoecological aspects of the nannofloral distribution from the Uttatur Group. They noted a latitudinal shift of the Cauvery Basin from Austral (Late Aptian to Late Albian) to temperate settings (Early Turonian) based on a decrease in the abundance of families Biscutaceae and Rhagodiscaceae. They suggested that the nannofloras of the Uttatur Group reflected open marine conditions. According to them, the Late Aptian - Middle Albian recorded a major transgressive episode resulting in the change of environment from an epicontinental basin setting towards an open marine setting for the basins in southern India. Nannoconids were reported to be an important constituent of the assemblages. A correlation of the nannofossil zones from the Cauvery Basin with those from the Indian Ocean was presented in their study (Fig. 5, pp. 220).

Bralower et al. (1993) correlated the Dalmiapuram Grey Shales with the early Late Albian Oceanic Anoxic Event, OAE1c, falling within the Nannofossil Subzone NC9B. They used biostratigraphical data from Kale and Phansalkar (1992b) for their study. Previous work on the nannofossil biostratigraphy and palaeobiogeography of the Cauvery Basin is limited to these papers.

4.5 Methods

The methods used to investigate the biostratigraphy and palaeobiogeography are described in Chapter 3, sections 3.6.1 and 3.6.4. Notes on the estimation of preservation are made in that chapter.

4.6 Biostratigraphy of the Karai Formation

4.6.1 Lithostratigraphic details

The Karai Formation, named by Sundaram and Rao (1986), is traditionally included in the Uttatur Group of the Cretaceous succession in the Ariyalur region. The Karai Formation comprises the oldest marine strata in the Cauvery Basin and was dated as Late Albian-Middle Turonian by Sundaram and Rao (1986). The Uttatur Group rests on the Archaean basement and/or the Gondwana Group in this region. The Cretaceous succession comprises the Gondwana Group (Lower Cretaceous) overlain by the Uttatur, Trichinopoly and the Ariyalur groups (Upper Cretaceous) in that order (Table 4.1). Numerous workers have contributed to the lithostratigraphic classification of the basin and as a result, differences exist in the nomenclature of the individual lithological units within the various litho-groups. For a detailed review of the lithostratigraphy of the basin, see Sundaram and Rao (1986), Acharyya and Lahiri (1991), Tewari et al. (1996a) and Sundaram et al. (2001).

Age	**Group/Formation, Lithology**	**Max. thickness (m) at outcrop**
Palaeocene	Niniyur-Pondicherry Formation	
Maastrichtian-Campanian	**Ariyalur Group**: Kallamedu Sandstone at top, but mainly claystone and fossiliferous limestone.	950
Coniacian-mid-Turonian	**Trichinopoly Group**: calcareous sandstone, sandy conglomerate, shelly limestone and claystone.	800
Early Turonian-Late Albian	**Uttatur Group**: gypsiferous claystone, fossiliferous limestone, conglomerate, black carbonaceous shale at base.	850
mid-Albian	**Dalmiapuram Formation/Karai Shale (included by some authors in the Uttatur Group)**: reefoidal algal limestone and black carbonaceous shale, unconsolidated marls, calcareous clays.	400 +
Aptian-Hauterivian	**Sivaganga Formation** (Upper Gondwana): gritty and pebbly sandstone.	350
Archaean-Precambrian	Granite, gneiss, metamorphic rocks.	

Table 4.1 Cretaceous stratigraphy of the Cauvery Basin (from Acharyya and Lahiri, 1991).

4.6.2 Sample details-Karai Formation, Section 1 and Section 2

The Karai Formation is a mudrock-claystone facies included in the Uttatur Group. Two new sections of the Karai Formation were sampled in the Karai and Garudamangalam villages in the Tiruchirapalli District of Tamil Nadu for this study (Gale, personal communication). The sections are referred to as Section 1 (at Karai) and Section 2 (at Garudamangalam) in this chapter. Both the sections are new and have not been examined before. Samples were collected by Prof. A. S. Gale and Dr. B. Hathway during several field seasons (2000-2002). Field descriptions and logs are from their work. The nannofossil biostratigraphy is part of a broad multidisciplinary sequence stratigraphic study involving ammonite stratigraphy (Gale et al. 2002). Precise locality maps showing where samples were collected can be obtained from A. S. Gale.

Section 1 exceeds 450 m in thickness and comprises yellow to brown, glauconitic, weathered mudstones. The gently dipping unit is exposed in almost flat badlands on the northern side of the Karai-Kulakkalnattam road, 60 km NNE of Tiruchirapalli. The succession also has silty, fine-grained sandstones with carbonate concretions, minor lenticular shell beds and pedogenically altered marine sands/silts (palaeosols). Rare bundles of macroscopic calcareous rhizocretions are present in the succession. The entire succession is bioturbated to some degree and is richly fossiliferous with a diverse ammonite fauna. Black shales or organic-rich sediments are not encountered within this formation.

The sample material is composed of mudrocks with occasional sandy and silt-rich horizons. Samples were collected at regular 4.5 m intervals throughout the Albian-Cenomanian interval. The Cenomanian/Turonian boundary (C/T) was sampled at 0.1 to 0.5 m intervals, to enable a high-resolution biostratigraphy of the boundary. A few extra samples from the C/T boundary interval were collected in a separate field season in 2002. A total of 146 samples from Section 1 were analysed for this study.

Karai Formation, Section 2, was measured in the village of Garudamangalam. Section 2, is ~190 m in thickness and comprises a suite of 67 samples. Continuous exposures are hard to find in this village. Therefore three separate sections were measured. The log in Fig. 4.5 represents the composite section. Samples were collected at 3.5 m intervals from the Late Albian-Turonian interval. The lithology is similar to Karai Section 1, comprising fine to medium-grained, brown to yellow coloured mudrocks with occasional sandstones in between. The succession is bioturbated and has a rich ammonite fauna. Black shales are not encountered in this section either.

4.6.3 Results

4.6.3.1 Preservation, abundance and diversity

Section 1: Out of the 146 samples that were analysed, 4 were barren and the rest yielded rich nannofloras. Nannofossil preservation varies from poor (P) to good (G), but is generally in the good to moderate (G-

M) category, with etching evident in some samples. The assemblage diversity is high, with ~ 150 species identified in the sample set. Similar to preservation patterns, nannofossil abundance varies from low (L) to high (H), but is generally moderate. Preservation is better in the Albian than the Cenomanian. The range-chart for Section 1 is presented in Appendix 1.

Section 2: Out of the 67 samples that were analysed, 4 were barren and the rest yielded rich nannofossils. Preservation is mostly moderate (M) and occasionally good (G). Assemblage diversity is comparable to Section 1 with an overall 140 species in the sample set. Nannofossil abundance varies from low to high, but is generally moderate. The range-chart for Section 2 is presented in Appendix 1.

4.6.3.2 Biostratigraphy

The biostratigraphy of the Karai Formation is established using the zonation scheme of Sissingh (1977) with modifications by Perch-Nielsen (1983, 1985), supported by that of Bown et al. (1998), and Burnett (1998). The zonation of Roth (1978, 1983) with modifications by Bralower et al. (1993, 1995) is applied to the sections for comparative purposes.

Section 1: A summary diagram of the biostratigraphy of Section 1 is shown in Figure 4.3. An age-depth plot of this section is shown in Figure 4.4. Zones CC8a-CC10 of Perch-Nielsen (1985), and Zones BC23-UC6b of Bown et al. (1998) and Burnett (1998) are recognised from this section, giving an Early Albian to Early Turonian age. Zone CC10 of Perch-Nielsen (1985) could not be subdivided into Subzones CC10a and CC10b because of the simultaneous last occurrence of *H. chiastia* along with other marker species in the Upper Cenomanian. Zones NC8A to NC12 are recognised from Bralower et al. (1993, 1995). The following zonal/subzonal events are identified from Bown et al. (1998) and Burnett (1998). They are listed in order from older to younger events along with the sample and corresponding zone number.

Presence of *Prediscosphaera columnata*, KA 0, Zone BC23, (at the base of the section)
FO *Tranolithus orionatus*, KA 22.5, Zone BC24 base
FCO *Axopodorhabdus albianus*, KA 54, Zone BC25 base
FO *Eiffellithus monechiae*, KA 175.5, Zone BC26 base
FO *Eiffellithus turriseiffelii*, KA 184.5, Subzone BC27a/UC0a base
LO *Hayesites albiensis*, KA 278.5, Subzone BC27a/UC0a top
FO *Corollithion kennedyi*, KA 301, Zone UC1 base
FO *Gartnerago segmentatum* (small), KA 328, Zone UC2 base
LO *Z. xenotus*, KA 391, Subzone UC2a top
FO *Lithraphidites acutus*, KA 404.5, Subzone UC3a base
LO *Staurolithites gausorhethium*, KA 433, Subzone UC3b top
LO *C. kennedyi*, KWB2-2, Subzone UC3d top
LO's *Helenea chiastia*, *A. albianus*, *L. acutus*, KA 448.2

FO *Eprolithus octopetalus*, KA 448.9, Subzone UC6a base

FO *Eprolithus moratus*, KA 451.9, Subzone UC6b base

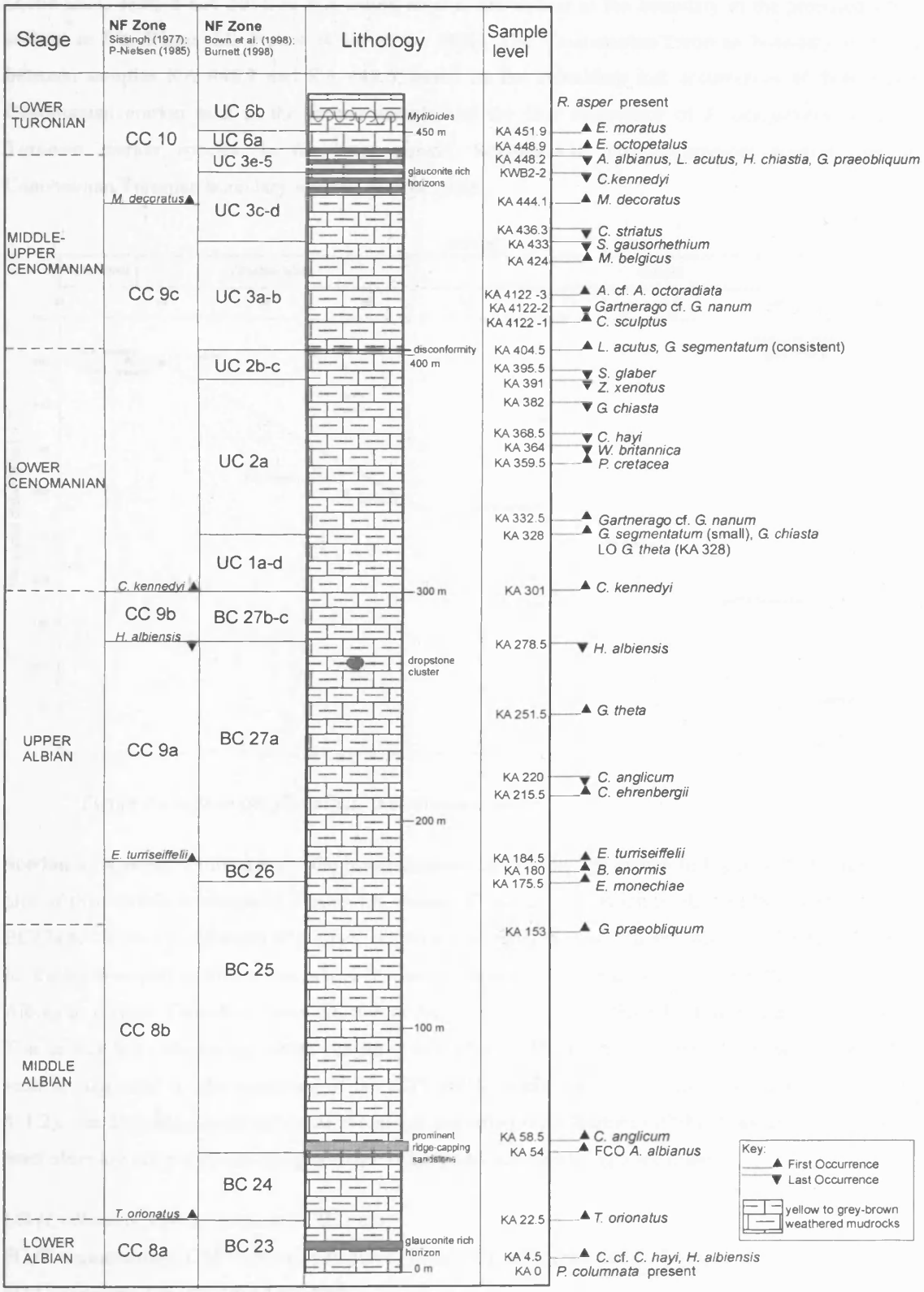

Figure 4.3 Schematic log data showing biostratigraphy of Karai Formation, Section 1 (Gale, *pers.comm.*).

Based on the observations, the Albian/Cenomanian and the Cenomanian/Turonian boundaries have been demarcated. The Albian/Cenomanian boundary is identified based on the FO of *C. kennedyi* (Zone UC1, sample KA 301), as this datum-level is the closest to the boundary in the proposed GSSP section at Mt. Risou, SE France (Gale et al. 1996). The Cenomanian/Turonian boundary is placed between samples KA 448.2 and KA 448.9, based on the coincident last occurrences of three Upper Cenomanian marker taxa in the former sample and the first occurrence of *E. octopetalus*, an Early Turonian marker species, in the latter sample. Simultaneous last occurrences suggest that the Cenomanian/Turonian boundary interval is incomplete.

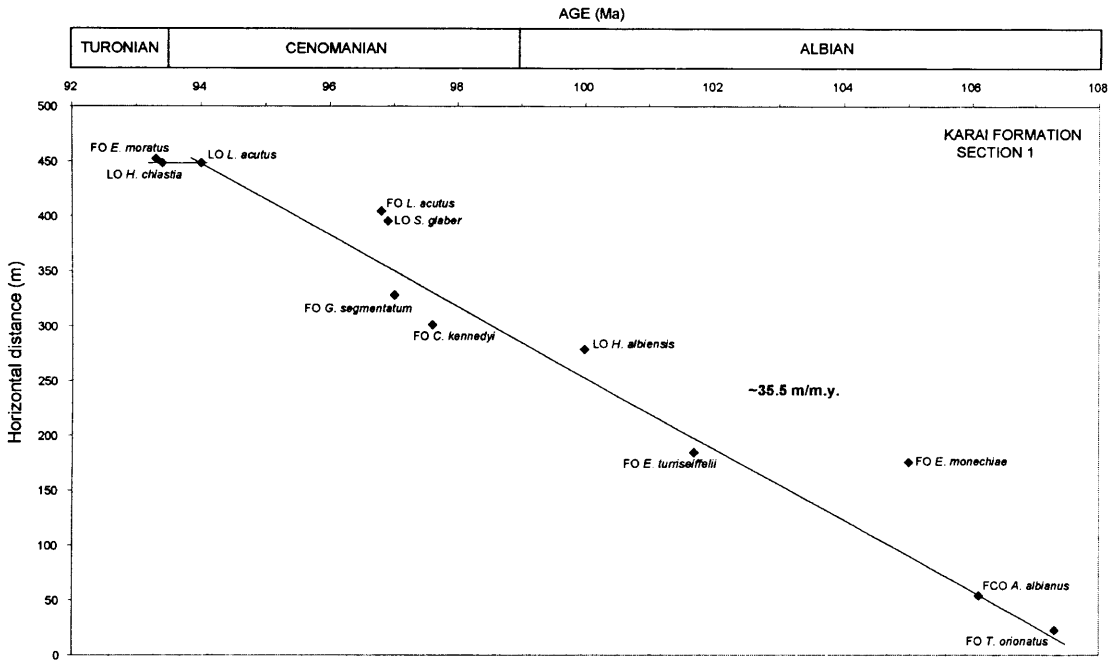

Figure 4.4 Age-depth plot of Karai Formation, Section 1.

Section 2: A summary diagram of the biostratigraphy of Section 2 is shown in Figure 4.5. An age-depth plot of this section is shown in Figure 4.6. Zones CC9a-CC10 of Perch-Nielsen (1985), and Subzones BC27a to UC3e-5 (combined) of Burnett (1998) are recognised from this section. Zone UC6a is inferred for the topmost part of the section, above the last occurrence of *H. chiastia*. The age of the section is Late Albian to earliest Turonian. Zones NC10A to NC12 are recognised from Bralower et al. (1993, 1995). This section has a shorter age range compared to Section 1. The Upper Cenomanian is incomplete in this section, suggested by the clustering of the LO's of *H. chiastia* and *L. acutus* in the same sample (GA 811.2). The following zonal/subzonal events are identified from Burnett (1998). They are listed in order from older to younger events along with the sample and corresponding zone number.

LO *H. albiensis*, GM 3, Subzone BC27a top

FO *G. segmentatum*, GM 7, not used to define Zone UC2, as it preceded *C. kennedyi*

FO *C. kennedyi*, GR 15, Zone UC1 base

FO *L. acutus*, GA 64, Subzone UC3a base

LO *S. gausorhethium*, GA 68, Subzone UC3b top

LO *C. kennedyi*, GAS 5, Subzone UC3d top

LO *A. albianus*, GA 88, could not be used as a zonal subevent

LO's *H. chiastia*, *L. acutus*, GA 811.2

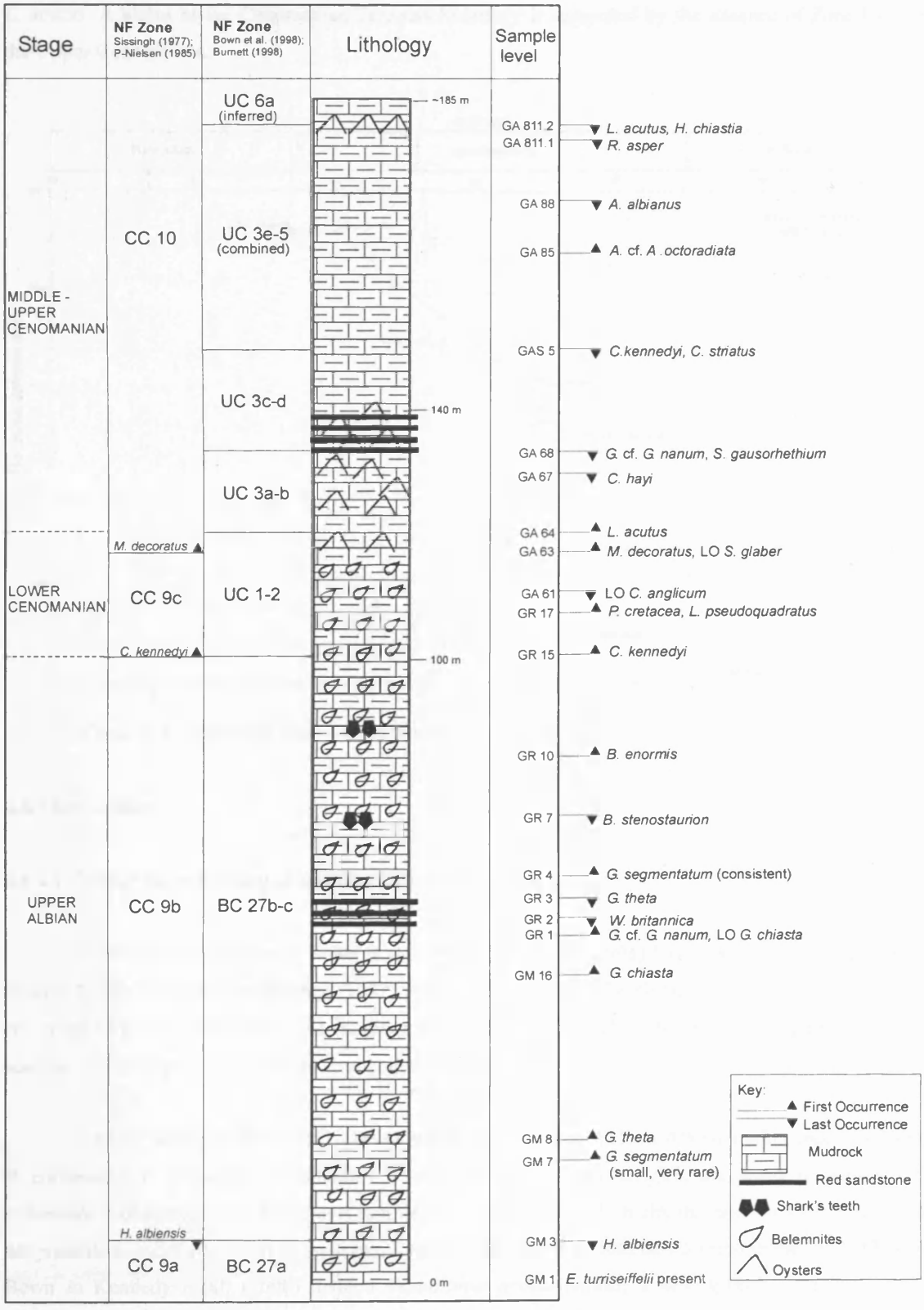

Figure 4.5 Schematic log data showing biostratigraphy of Karai Formation, Section 2 (Gale, *pers. comm.*)

The Albian/Cenomanian boundary is placed in sample GR 15, based on the FO of *C. kennedyi*. The additional boundary events, e.g., FO of *G.* cf. *G. nanum*, FO/LO of *G. chiasta*, FO of *G. theta*, etc. are found stratigraphically lower in the section, prior to the FO of *C. kennedyi*. No definitive Early Turonian markers such as *Q. gartneri* or *E. octopetalus* are observed above the coincident LO's of *H. chiastia* and *L. acutus*. A hiatus at the Cenomanian/Turonian boundary is suggested by the absence of Zone UC5 in the Upper Cenomanian.

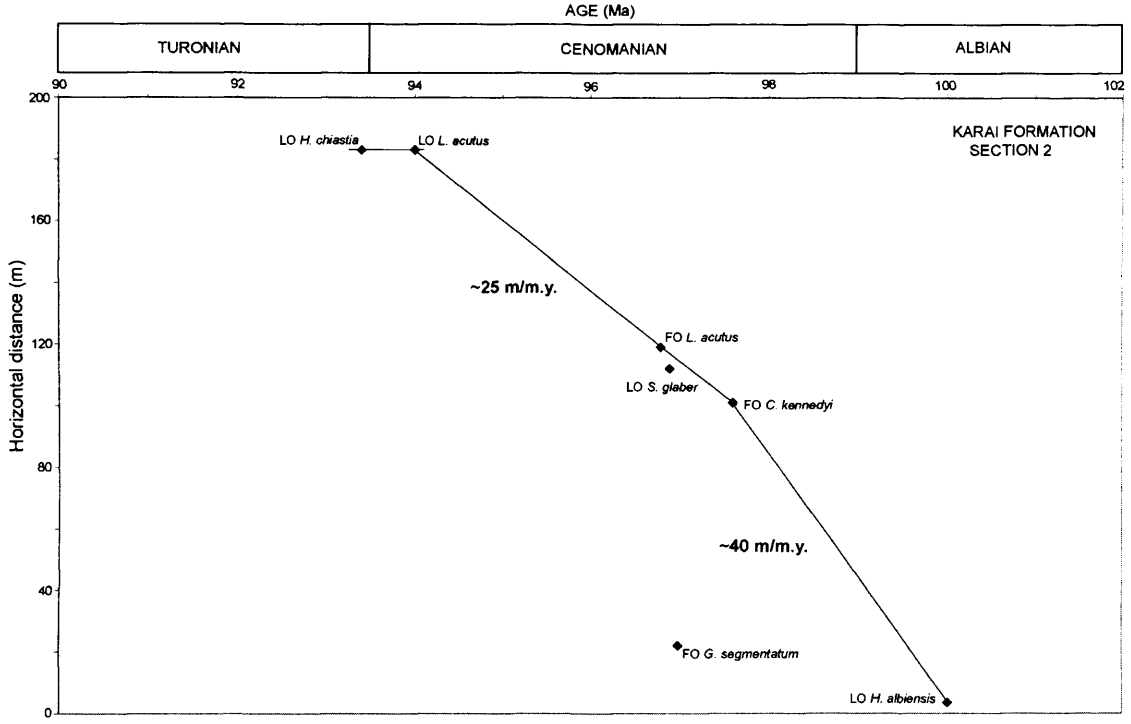

Figure 4.6. Age-depth plot of Karai Formation, Section 2.

4.6.4 Discussion

4.6.4.1 Testing the reliability of markers in Section 1 (Figure 4.3)

The zonation schemes of Bown et al. (1998) and Burnett (1998) have been thoroughly tested on Section 1. The CC zones of Sissingh (1977) with modifications by Perch-Nielsen (1983, 1985), and the NC zones of Roth (1978, 1983) with modifications by Bralower et al. (1993, 1995) are applicable to the section, even though they are low in stratigraphic resolution.

The BC Zones of Bown et al. (1998), which employ cosmopolitan Albian marker species such as *P. columnata*, *T. orionatus*, *A. albianus*, *E. monechiae* and *E. turriseiffelii* are easily recognised. *P. columnata* is observed in the lowermost sample of the section (KA 0) in circular and elliptical forms. It is not possible to ascertain which of these two forms appeared first as both co-occurred in the sample KA 0. Bown *in* Kennedy et al. (2000) defined *Tranolithus praeorionatus*, a new species thought to be a precursor to *T. orionatus*. This species is not identified in Section 1. Following the proposal by Bown

(2001), the zonal event FO *A. albianus* has been revised to the first consistent occurrence (FCO) of *A. albianus*. This amendment was proposed on the basis of the observation that *A. albianus* is inconsistent and rare at the base of its range. This is observed in this study too.

Two subzones are not identified in Section 1, i.e., Subzone BC25b (LO of *Ceratolithina bicornuta*) and Subzone BC27c (FO of *Calculites anfractus*). Other secondary markers used in the BC zonation of Bown et al. (1998), such as *Ceratolithina hamata*, *Owenia hillii*, *Braloweria boletiformis* and *Tegulalithus tessellatus* are absent in Section 1. Almost all of these taxa are thought to be restricted to NW Europe (Crux 1991; Bown 2001). Therefore their absence in the Cauvery Basin is not surprising.

A synthesis of the published ranges of Albian marker taxa is given in Bown (2001). Using this as a standard, the ranges of important Albian taxa logged in the Karai Formation have been compared with their published ranges. The FO of *C. hayi* is found in Subzone CC8a (Lower Albian, sample KA 4.5) in Section 1, whereas its earliest first appearance is reported from Subzone CC9b. This suggests that *C. hayi* may have appeared early in the Austral latitudes (Early Albian) and then migrated into the Boreal and Tethyan regions during the Late Albian.

The first and last occurrence of *S. falklandensis* are biostratigraphical events in the Indian Ocean (Fig. 5.2, Bown et al. 1998). This species is reported to be common in the Falkland Plateau (DSDP Sites 327 and 330) where its presence defines the *S. falklandensis* Subzone in the Early Albian (Wise and Wind 1977). However, *S. falklandensis* is very rare in the Karai Formation. It is identified in only one sample, and is therefore, not usable as a biostratigraphic marker or as a conclusive palaeobiogeographic indicator of Austral latitudes. The distinguishing features of the taxon, i.e., its large size (~10 μm), recurved outer cross bars and prominent sutures where the crossbars join the shields, are observed in the specimens. The identification of this species is definite (Plate 9, Chapter 8).

Hayesites albiensis shows a consistent occurrence throughout the Albian, terminating in the Upper Albian Zone BC27, which is in agreement with previous studies (Bown 2001). A large gap is noted in its occurrence near its extinction in the Upper Albian. Similarly, breaks are observed in the ranges of *G. theta*, *G. praeobliquum* and *S. gausorhethium* as they approach their extinction. The species *H. irregularis* shows a sporadic distribution in the Albian.

In summary, the Albian BC23-27 Zones of Bown et al. (1998) based on cosmopolitan marker species such as *P. columnata*, *A. albianus* and *E. turriseiffelii* are straightforward in their application. Most of the secondary events in this zonation scheme, which are thought to be restricted mainly to NW Europe, e.g., LO's of *C. bicornuta* and *B. boletiformis* are however absent in the Karai Formation, Section 1.

The Cenomanian UC zonation of Burnett (1998) was aimed at improving the resolution of Upper Cretaceous biostratigraphy by replacing a number of problematic markers from the CC and NC

zonation schemes of Sissingh (1977) and Roth (1978) respectively. The zonation of Burnett (1998) is based on two regions, Europe and the Indian Ocean. The zonations for the two regions employ the same primary markers, although they differ in the secondary markers. For the Cenomanian, the number of secondary events used for Europe is higher than that for the Indian Ocean. In this study, both these schemes have been taken into account while testing the applicability of the UC zones.

Zones UC1 (FO *C. kennedyi*), UC2 (FO *G. segmentatum*), UC3 (FO *L. acutus*) and Subzone UC6b (FO *E. moratus*) are recognised from Section 1. The unidentified zones are UC4 (FO *C. biarcus*) and UC5 (LO *L. acutus*). Some of the subzonal events are absent (e.g. FO *C. anfractus*, LO *I. compactus*), while others are present (FO *P. cretacea*, LO *W. britannica*), but not in the stratigraphic positions reported in Burnett (1998).

Starting from the base of the Cenomanian, the problematic markers are discussed here in stratigraphic order. *Calculites anfractus* is absent, as a result of which Subzone BC27c/UC0c is not identified. The holococcolith species, *C. anfractus*, is reported from Europe and is generally known to be sporadic in occurrence. This undermines its utility as a nannofossil proxy for the Albian/Cenomanian boundary, proposed by Burnett *in* Gale et al. (1996). Similarly, *H. anceps* is absent in the Karai Formation, probably due to its rare distribution.

G. segmentatum is present in small sizes of ~ 5 μm at the base of its range (see Plate 13, Chapter 8). More typical sizes (>8 μm) and the consistent occurrence of this species are noted stratigraphically higher after a gap of nearly 15 samples (~ 100 m). Small sizes are rarely observed after its regular occurrence.

Cylindralithus biarcus is very rare and sporadic in the Upper Cenomanian. It is not conclusively identified in most samples. As a result, Zone UC4 is not recognised in Section 1. Due to taxonomic problems associated with this species, it has been recombined into the genus *Rotelapillus* (Lees and Bown, *in press*). The reliability of *C. biarcus* as a zone marker is considered dubious. Lees (2002) reported *C. biarcus* from Northern Europe and the Indian Ocean.

The Upper Cenomanian in Section 1 is problematic with regards to its biostratigraphy. The simultaneous LO's of important marker taxa such as *A. albianus*, *H. chiastia* and *L. acutus* in the same sample indicates the absence of Zone UC5. The LO of *L. acutus* is used to define the base of Zone UC5, whereas the LO of *H. chiastia* defines the base of Zone UC6 (Burnett 1998). Moreover, the LO of *H. chiastia* is the closest nannofossil proxy for the C/T boundary (see section 4.8.3.2), so it's grouped LO with other taxa suggests that the boundary interval is incomplete. *R. asper* is present in good numbers in the topmost sample of the section within the Lower Turonian. Previous studies have placed its LO variably in the Upper Cenomanian (Subzone UC5b) or the Lower Turonian (Figure 4.7).

In summary, the UC zonation of Burnett (1998) for the Cenomanian is not fully applicable to the Karai Formation, Section 1. Two markers are found to be problematic. The FO of *G. segmentatum* occurs considerably lower in its stratigraphic position compared to Burnett (1998). Zone UC4 is unusable because *C. biarcus* is very rare. Zone UC5 is missing due to a stratigraphical break in the section manifested by the simultaneous LO's of three important Upper Cenomanian marker taxa. Two subzonal marker species recorded in the Indian Ocean, *H. anceps* and *Q. intermedium*, are absent in the Cauvery Basin, possibly due to their rare distribution.

4.6.4.2 Testing the reliability of markers in Section 2 (Figure 4.5)

Similar problems are encountered with the zonation of Burnett (1998) for the Cenomanian, which is not fully applicable to Section 2 either. Zones UC1 (FO *C. kennedyi*) and UC3 (FO *L. acutus*) are recognised in this section. Zones UC2 (FO *G. segmentatum*) and UC4 (FO *C. biarcus*) are not recognised due to problems with their markers. The FO of *G. segmentatum* is stratigraphically lower in this section with respect to the FO of *C. kennedyi*, which is a reliable datum-level for the Early Cenomanian. Hence the species shows diachroneity in relation to the FO of *C. kennedyi* in the two sections. Similar to Karai Formation, Section 1, it is found in small sizes (~ 5 μm) at the base of its range in the Late Albian with consistent occurrence after a gap of several samples. Age-depth plots (Figs. 4.4 and 4.6) show that the FO of *G. segmentatum* is diachronous in the two sections with respect to the FO of *C. kennedyi*, and is therefore unreliable as a marker species. The early appearance of this species in the Late Albian suggests that it may have evolved earlier in the Austral latitudes before migrating to the Boreal regions. A similar observation has been made for *C. hayi* in this study.

Zone UC4 is not recognised because *C. biarcus* is absent in this section. The clustered LO's of marker species *L. acutus* and *H. chiastia*, within the same sample (GA 811.2), resulted in the absence of Zone UC5 in Section 2.

The ranges of certain taxa such as *C. hayi*, *C. anglicum* and *W. britannica* are noted to be discontinuous in this section, especially when they approach their extinction. *Z. xenotus* is probably reworked into the Upper Cenomanian and Lower Turonian sediments (samples GA 810 and GA 816). *Z. kerguelenensis* (Watkins *in* Wise et al. 1992), a species described from the Kerguelen Plateau in the Southern Ocean, is sporadically distributed in this section. It is mostly observed in side view with a prominent stem, making its appearance very distinctive (Plate 3, Chapter 8). Secondary markers such as *C. anfractus*, *H. anceps* and *Q. intermedium* are also absent in Section 2.

4.6.4.3. Nannofossil proxies for stage boundaries

4.6.4.3.1. Albian/Cenomanian Boundary

The nannofossil proxies that were used to define the Albian/Cenomanian boundary at the proposed GSSP section in SE France (Mt. Risou) were the FO of *Calculites anfractus* below the

boundary, and the LO of *Staurolithites glaber* above the boundary (Burnett *in* Gale et al. 1996). Of these two species, *C. anfractus* is absent in the Karai Formation, Section 1. *Staurolithites glaber* is frequently observed, and its LO is noted in sample KA 395.5 above the boundary. However, the LO of *S. glaber* is preceded by other definitive Lower Cenomanian markers. The closest proxy in Section 1 for the base of the Cenomanian is *C. kennedyi*. The FO of *Gartnerago* cf. *G. nanum* is also useful in constraining the boundary. *Gartnerago* cf. *G. nanum* has a short stratigraphic range in Section 1 from the Early Cenomanian (close to the FO of *C. kennedyi*) to the mid-Cenomanian (Zone UC3). Thus, the Albian/Cenomanian boundary is tentatively identified using the FO of *C. kennedyi* (sample KA 301), supported by the FO of *G. chiasta* (sample KA 328), FO of *G.* cf. *G. nanum* (sample KA 332.5) and the LO of *H. albiensis* (sample KA 278.5). Precise demarcation of the boundary will depend in part on the ammonite biostratigraphy for both sections.

The closest nannofossil proxy for the base of the Cenomanian in Section 2 is *C. kennedyi*. The Albian/Cenomanian boundary is slightly difficult to identify in this section as some of the additional events such as the FO/LO of *G. chiasta*, FO of *G.* cf. *G. nanum* and the FO of *G. theta* occur stratigraphically lower in the Upper Albian, prior to the FO of *C. kennedyi*. Therefore the Albian/Cenomanian boundary is tentatively identified in Section 2 using the FO of *C. kennedyi*, supported by the LO of *S. glaber* above it. The stratigraphic order of important nannofossil events around the boundary in the Karai Formation are compared with the Mt. Risou section in Table 4.2.

Karai Formation Section 1	**Karai Formation, Section 2**	**Mt. Risou, SE France**
LO *S. glaber*	LO *S. glaber*	LO's *B. africana*, *W. britannica*, *C. anglicum*
LO *Z. xenotus*	LO *C. anglicum*	FO *C. kennedyi*
LO *G. chiasta*	FO *P. cretacea*	FO's *G. praeobliquum*, *P. cretacea*
LO *C. hayi*	FO *C. kennedyi* **(Alb./Cen. boundary)**	FO *R. planus*
LO *W. britannica*	LO *B. stenostaurion*	FO *G. theta*
FO *P. cretacea*	LO *G. theta*	LO *S. glaber*
FO *G.* cf. *G. nanum*	LO *W. britannica*	**Alb./Cen. boundary**
FO's *G. segmentatum*, *G. chiasta*; LO *G. theta*	LO *G. chiasta*, FO *G.* cf. *G. nanum*	FO *C. anfractus*
FO *C. kennedyi* **(Alb./Cen boundary)**	FO *G. chiasta*	LO *Arkhangelskiella*? sp.
LO *H. albiensis*	LO *B. africana*	FO *G. chiasta*, LO *C. anglicum*
FO *G. theta*	FO *G. theta*	FO *Arkhangelskiella*? sp.
LO *C. anglicum*	FO *G. segmentatum*	LO *H. albiensis*
	LO *H. albiensis*	

Table 4.2. Stratigraphic order of events around the Albian/Cenomanian boundary in the Cauvery Basin compared with the Mt. Risou section, SE France (Burnett *in* Gale et al. 1996).

A comparison of nannofossil events around the Albian/Cenomanian boundary at the Mt. Risou section in France with the Karai Formation shows that most of the events are common to both regions. However, there are inconsistencies in the order of events in the three sections (Table 4.2). Burnett *in* Gale et al. (1996) reported the FO and LO of *Arkhangelskiella* sp.? (= *Broinsonia*? *stenostaurion*) in the Upper Albian. The FO of this species has been identified in the Upper Aptian (Bown *in* Kennedy et al. 2000; Herrle and Mutterlose 2003), therefore it was misplaced near the Albian/Cenomanian boundary. In summary, based on the study the FO of *C. kennedyi* is a reliable nannofossil proxy for the Albian/Cenomanian boundary in continental settings. The FO's of *G. chiasta*, *G. theta* and *G.* cf. *G. nanum*, and the LO's of *S. glaber*, *W. britannica* and *H. albiensis* are additional events that can be used to constrain the boundary. *Gartnerago* cf. *G. nanum* shows potential as a new marker species with respect to its first and last occurrence in the Early-mid Cenomanian. However, *C. anfractus* is a poor choice of marker for the Albian/Cenomanian boundary as suggested by Burnett *in* Gale (1996).

4.6.4.3.2. Cenomanian/Turonian Boundary

Although there is still some confusion over the true sequence of nannofossil first and last occurrences around the C/T boundary, the most commonly used nannofossil proxies for defining the boundary are the LO of *Helenea chiastia* and the FO of *Quadrum gartneri* (Bralower 1988; Perch-Nielsen 1985; Burnett 1998; Burnett and Whitham 1999). Figure 4.7 summarises the stratigraphic order of last occurrence events around the C/T boundary based on important papers in the last 15 years. The figure shows that the principal last occurrence events in the Upper Cenomanian include those of *C. kennedyi*, *C. striatus*, *L. acutus*, *A. albianus*, *R. asper* and *H. chiastia*. The order of these events is inconsistent in different sections, although it is clear that the LO of *H. chiastia*, the youngest among these events, is the most commonly used proxy for the C/T boundary (Burnett and Whitham 1999). Most of the above-mentioned events are reliable in tracing the boundary except the LO of *R. asper*, which is diachronous. Different workers have variably recorded the LO of *R. asper* either in the Upper Cenomanian or in the Lower Turonian. In the Cauvery Basin, the taxon persists up to the top of Karai Section 1 into the Lower Turonian. In Karai Section 2, the taxon has its LO in the Upper Cenomanian (Zone UC3e-5) below the coincident LO's of *H. chiastia* and *L. acutus*.

In Karai Section 1, the LO of *H. chiastia* is recognised in sample KA 448.2, along with the LO's of *A. albianus* and *L. acutus*. *Q. gartneri* is not found in any of the samples. The C/T boundary is bracketed by the coincident last occurrences of *H. chiastia, L. acutus* and *A. albianus* (sample KA 448.2) and the FO of *E. octopetalus* (sample KA 448.9). Zone UC5 (LO *L. acutus*) is absent as a result of the coincident last occurrences, making the boundary interval incomplete.

The coincident last occurrences of *H. chiastia* and *L. acutus* indicate that the C/T boundary interval in Karai Section 2 is also incomplete. No Early Turonian taxa (e.g. *E. octopetalus*, *E. moratus*, *Q. gartneri*) are observed above the LO of *H. chiastia* in Section 2.

STAGE	Rock Canyon (Colorado, USA) **Bralower (1988)**	*S Ferriby Quarry (N. England) + Shakespeare Cliff (S. England) **Bralower (1988)**	Shakespeare Cliff (S. England) **Jarvis et al. (1988)**	Ganuza (N. Spain) and Shakespeare Cliff (England) **Lamolda et al. (1994, 1997)**	N. Europe and Indian Ocean **Burnett (1998); Lees (2002)**	Western Interior Seaway (USA) @ Escalante # Portland & Bounds **Bralower & Bergen (1998)**	N. Italy (southern Alps) **Luciani & Cobianchi (1999)**	Eastbourne (S. England) **Paul et al. (1999)**	Cauvery Basin (SE India) Karai Fm., Section 1 * Karai Fm., Section 2 & **This study**
TURONIAN	*R. asper*	* *A. albianus* * *H. chiastia, R.asper*			*H. chiastia*	# & *R. asper*			* *R. asper* present
W. devonense ammonite									hiatus
CENOMANIAN	*H. chiastia* *L. acutus, C. striatus* *A. albianus, C. kennedyi*	+ *R. asper, H. chiastia* + *A. albianus, C. striatus* *+ *C. kennedyi*	*H. chiastia* *R. asper* *C. striatus* *L. acutus, A. albianus*	*H. chiastia* *L. acutus* *A. albianus* *C. kennedyi*	*R. asper* *A. albianus* *L. acutus* *C. striatus* *C. kennedyi*	@ # & *H. chiastia* @ *R. asper* @ # *C. striatus* & @ *L.acutus* & # *A. albianus* & # *C. kennedyi* & *C. striatus* *C. kennedyi* reworked in Bounds section	*H. chiastia, C. kennedyi* *A. albianus* *R. asper* *L. acutus* *C. striatus*	*H. chiastia* *R. asper* *L. acutus* *A. albianus* *C. konnedyi*	* Concurrent *H. chiastia, A. albianus, L. acutus* *C. kennedyi* & Concurrent *H. chiastia L. acutus* *R. asper* *A. albianus* *C. kennedyi, C. stnatus*

Figure 4.7 Compilation of C/T boundary nannofossil events. The events are not calibrated against ammonite or radiometric dates. The focus is on the relative sequence of events in each study. ▼— = Last Occurrence.

4.8 Conclusions

1. Using the zonation scheme of Sissingh (1977) with modifications by Perch-Nielsen (1983, 1985), supported by that of Bown et al. (1998) for the Albian and Burnett (1998) for the Cenomanian, the age of Karai Formation, Section 1 is concluded to be Early Albian to Early Turonian. The age of Karai Formation, Section 2 is Late Albian to earliest Turonian.

2. The zonation schemes of Sissingh (1977) with modifications by Perch-Nielsen (1983, 1985), and of Roth (1978, 1983) with modifications by Bralower et al. (1993, 1995) are applicable to both sections even though they are low in stratigraphic resolution. The BC zones of Bown et al. (1998) for the Albian are easily applicable to Karai Formation, Section 1, with the exception of some subzonal markers (e. g. *C. bicornuta*) that are not identified in the basin. The UC zones of Burnett (1998) for the Cenomanian are not fully applicable to either of the two sections.

3. Zones UC2 and UC4 could not be applied confidently due to problematic markers. *G. segmentatum* (Zone UC2) is diachronous with respect to the FO of *C. kennedyi* in the two sections of the Karai Formation. Its FO is stratigraphically lower than the FO of *C. kennedyi* in Karai Formation, Section 2. *C. biarcus* (Zone UC4) is very rare and sporadic in Karai Formation, Section 1 and absent in Karai Formation, Section 2. It is therefore not practical as a marker species. Some of the secondary marker species such as *H. anceps* and *Q. intermedium*, which have been identified in the Indian Ocean, are absent in the Cauvery Basin, probably due to their rarity rather than stratigraphic problems.

4. The Albian/Cenomanian boundary is identified in both sections using the FO of *C. kennedyi*, supported by additional events such as the FO of *Gartnerago* cf. *G. nanum*, FO of *G. chiasta* and LO of *S. glaber*. The Cenomanian/Turonian boundary interval is incomplete in both sections, indicated by the simultaneous last occurrences of marker taxa such as *H. chiastia* and *L. acutus* in the same sample, resulting in the absence of Zone UC5 (LO *L. acutus*) of the Upper Cenomanian.

5. *Gartnerago* cf. *G. nanum* shows potential as a new marker species with respect to its first and last occurrence. It has a short stratigraphic range from the Early Cenomanian (close to the FO of *C.kennedyi*) to the mid-Cenomanian (Zone UC3) in the Cauvery Basin. It occurs frequently in both sections of the Karai Formation, thereby showing biostratigraphic utility.

6. The early appearance of *C. hayi* in the Early Albian and *G. segmentatum* in the Late Albian within the Cauvery Basin suggests that these two species may have originated in the Austral latitudes before migrating to other regions. The reported first occurrences of these two species are in the Late Albian and Early Cenomanian respectively (Bown 2001; Burnett 1998).

Chapter 5. The Gault Clay Formation, Folkestone, SE England

Abstract

The aim of this study was to investigate a palaeoclimatic/palaeotemperature shift at the mid-/Late Albian boundary in a 10 m-long section from the Gault Clay Formation, Folkestone, SE England. The nannofossil biostratigraphy of the section was established using the zonation scheme of Bown et al. (1998). Zone BC24 to Subzone BC25b (mid- to early Late Albian) are recognised in the rich and uniformly well-preserved samples ('good' to 'very good' preservation). The primary evidence for a warming event that commenced at the mid-/Late Albian boundary comes from ammonite data reporting the invasion of Tethyan ammonite genera at the base of Bed VIII in the Gault Clay (Spath 1923-43, Owen 1975). Additional evidence is obtained from oxygen isotope ($\delta^{18}O$) data measured on bulk Gault Clay material that is correlated with quantitative nannofossil data. $\delta^{18}O$ values show a dramatic lightening between 4.75 and 5.5 m in the section, reaching a minimum value of –3.818 ppt at 5.5 m. Although oxygen isotope values have not been directly converted into temperatures, it is believed that at least a component of the oxygen isotope values are controlled by palaeotemperatures. If this is correct, then the Lower Gault sediments (*E. lautus* Ammonite Zone) record a significant and progressive temperature fall. The light oxygen peak between 4.75 and 5.5 m records a rapid and probably short-lived warming event at or close to the base of the Upper Albian *D. cristatum* Ammonite Subzone. Following this, temperatures stayed consistently higher than those in the Middle Albian.

Nannofossil data provide support to this palaeotemperature shift. A significant decline in the % abundance of the cold-water nannofossil species *Repagulum parvidentatum* (from 11 to 1%) in Bed VIII coincides with the lightening of $\delta^{18}O$ values. Thus the striking coincidence of the influx of Tethyan ammonites, the light $\delta^{18}O$ peak and the decline in *R. parvidentatum* indicates a significant warming event at the mid-/Late Albian boundary in the Gault Clay. A productivity increase based on high percentages of *Z. noeliae* (~ 40%) is found to be concomitant with this warming event suggesting that surface waters were nutrient-rich, and the warming may have driven increased precipitation and run-off, delivering more nutrients into the basin. Stronger winds may have led to increased storminess, enhancing mixing in the waters. In terms of nannofossil palaeotemperature proxies, *R. parvidentatum* is proved here to be an excellent cold-water indicator. The warm-water affinity of *Rhagodiscus asper* is dubious in this section. The semi-quantitative abundance pattern of *Flabellites oblongus* suggests that it may have been adapted to warm waters during the mid-Cretaceous.

5.1 Aims

The aims of this study were as follows:

1. To investigate a palaeoclimatic/palaeotemperature shift in the Gault Clay section, first suggested by ammonite data, at the Middle/Upper Albian boundary using geochemical, nannofossil and macrofossil data;

2. To evaluate the nannofossil biostratigraphy of the section in the first instance, using established zonation schemes.

5.2 Geological history of southern England

During the Cretaceous, southern England was located in the Weald of the Anglo-Paris Basin (Figure 5.1). The Anglo-Paris Basin was orientated along a NW-SE axis with occasional links to the North Sea through the Bedfordshire Straits (Tyson & Funnell 1987). The Weald is the ancient name for a tract of sand and clay rocks between the North and South Downs in southeastern England. The term 'Wealden' is used for these rocks and thus for their contained fossils. The northern boundary of the Weald Basin is faulted against the London Platform (Hughes 1975).

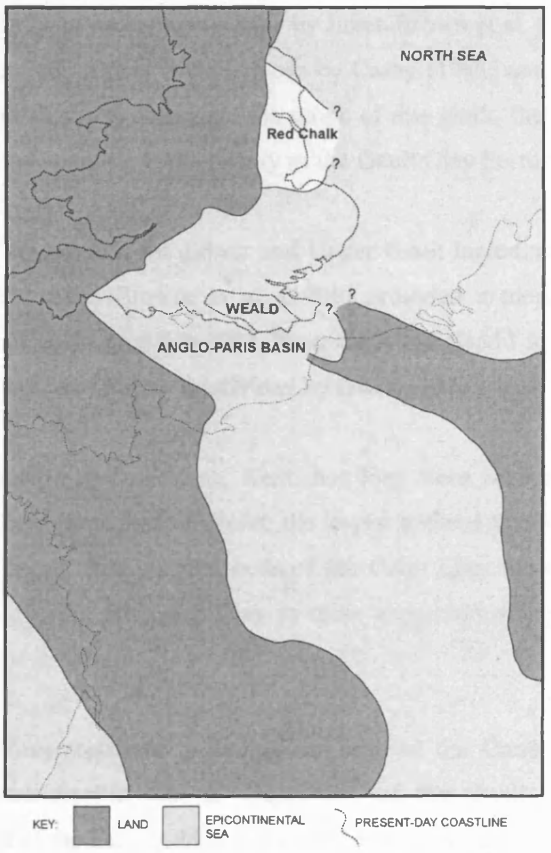

Figure 5.1 Palaeogeographic setting of the Gault Clay in the Weald of the Anglo-Paris Basin. Modified from Owen (1975).

The first important marine trangression across large parts of the Anglo-Paris Basin took place in the Early Aptian (*obsoletus* ammonite subzone). This trangression resulted in temporary links with the East Midlands Shelf via the Bedfordshire Straits and possibly shallow-water connections with the proto-Atlantic Ocean along the line of the present day English Channel (Tyson & Funnell 1987). Tectonic activity in the middle part of the Early Albian led to the development of a widespread unconformity in the *tardefurcata* ammonite zone (Casey 1961). After this, a predominantly trangressive phase continued into the *mammillatum* ammonite zone (Early Albian). Continuation of the transgression through the mid-

Albian led to the retreat of the landmasses in the Late Albian. Thus a northwest European mid- and Late Albian epicontinental sea extended from south-east England across to the North Sea, Denmark, northern Germany, Poland and into Russia (Tyson & Funnell 1987). Owen (1971, 1975) reported that the trangression reached its peak in the *intermedius* ammonite subzone (mid-Albian) and continued into the *cristatum* ammonite subzone (early Late Albian).

5.3 The Gault Clay Formation

The Middle and Upper Albian substages are represented in the Gault Clay Formation of southern England. The Gault Clay has been studied for more than a century now. Numerous workers have studied the stratigraphy and palaeontology of the Gault clays, particularly on the outcrops in the Folkestone area, where the most continuous record of the strata exists. Research on the Folkestone Gault Clay can be traced back to the pioneering work on its stratigraphy by Jukes-Brown et al. (1900) and Spath (1923-43). Important works in the twentieth century include those by Casey (1961) and Owen (1971, 1975). Since detailed discussion on the stratigraphy is beyond the scope of this work, the reader is directed to Owen (1971), which provides a good synopsis of the history of the Gault Clay Formation.

Price (1874, 1875) recognised the Lower and Upper Gault including the eleven beds that were proposed by earlier workers. Jukes-Browne et al. (1900) provided a more detailed subdivision that resulted in the redefinition of units, from I to XIII. These divisions (Bed I to XIII) of Jukes-Browne are still in use today although they were further subdivided by Owen (1971).

The Copt Point section at Folkestone, Kent, has long been regarded as a suitable reference section for the Gault Clay Formation. At Copt Point, the lowest beds of the Gault Clay rest on sediments of the Lower Greensand Group. The topmost beds of the Gault Clay are not clearly exposed in this section. The Chalk Group overlies the Gault Clay in other exposures along the coast of SE England (Owen 1975).

There are various interpretations regarding the base of the Gault Clay Formation based on lithostratigraphic and biostratigraphic criteria. Deposition of the Gault Clay is believed to have commenced towards the end of the Early Albian in the most basinal areas, but not until the middle part of the mid-Albian in the more marginal localities. The base of the Lower Gault, by definition, lies in the phosphatic nodule bed called the 'Sulphur Band'. The base of the Upper Gault lies in the phosphatic nodule bed that overlies an erosion surface, at the base of Bed VIII. Details of the Lower Gault at the Copt Point section are given in Owen (1971).

5.4 Previous nannofossil work

Nannofossil studies on the Gault Clay can be traced back to the monographs of Maurice Black in the early seventies (Black 1972, 1973, 1975). The classic work by Black constitutes one of the earliest

works on Albian coccoliths, preceded only by a few other workers such as Stradner (1963), Manivit (1965) and Stover (1966). These monographs include notes on the stratigraphy of the Gault Clay, preparation techniques and a detailed morphological description of its nannofossils. The taxonomic descriptions in these monographs covered all the major families of Cretaceous nannofossils. Around 14 genera and 28 species were described out of which many were new. Several subspecies were also described. In fact, such a detailed study on the Gault Clay nannofossils has not been repeated since. The transmission electron micrographs in these monographs remain unsurpassed to this day.

In the eighties, nannofossil studies on the Gault Clay were made by Taylor (1982) and Crux (1982, 1989). Crux (1991) described diverse and abundant Middle and Upper Albian nannofossil assemblages from the Gault Clay exposed at Munday's Hill in Bedfordshire, England. Apart from studying the stratigraphic distribution, he compared his results with other areas in order to trace the palaeoceanographic variations in northwest Europe during the mid- and Late Albian. A nannofloral province for northwest European localities was defined on the basis of endemic species such as *Braloweria boletiformis*, *Ceratolithina hamata* and *Gaarderella granulifera* in his study. The abundance patterns of the high latitude taxa, *R. parvidentatum* and *S. primitivum*, were studied to infer cool and warm pulses during the mid-Late Albian in England.

Erba et al. (1992) undertook quantitative analysis on core material from the Gault Clay in southern England (near Folkestone and Sevenoaks) to understand their palaeoceanographic significance. Their study was the first to document Milankovitch frequency cycles in the Gault Clay based on the abundance patterns of some nannofossil indices related to fertility and temperature.

Jeremiah (1996) studied the Gault Clay at various outcrops in southern England including Copt Point, East Anglia, Bedfordshire and Buckinghamshire. His study established a biostratigraphic zonation scheme for the Albian and Lower Cenomanian for academic and industrial purposes. The nannofossil zones were mostly based on LAD's and acme datums, and were correlated with the ammonite zones. Bown (2001) recently investigated the biostratigraphy of the Gault Clay from BGS borehole samples in Hampshire.

5.5 Methods

The methods used for biostratigraphy and quantitative analyses were straightforward. Semi-quantitative (relative abundance based) biostratigraphy and 300 specimen % abundance counts (Bown & Young 1998) were the principal methods of analysis in this study. These methods have been discussed in Chapter 3, sections 3.6.1 and 3.6.2. Methods of estimating the preservation of the nannofossils are also discussed in that chapter.

5.6 Details of the study section

Location: Coastal outcrop exposed in a sea-cliff off the English Channel at Copt Point, 1 km east of Folkestone harbour, Kent, UK (Figure 5.2).

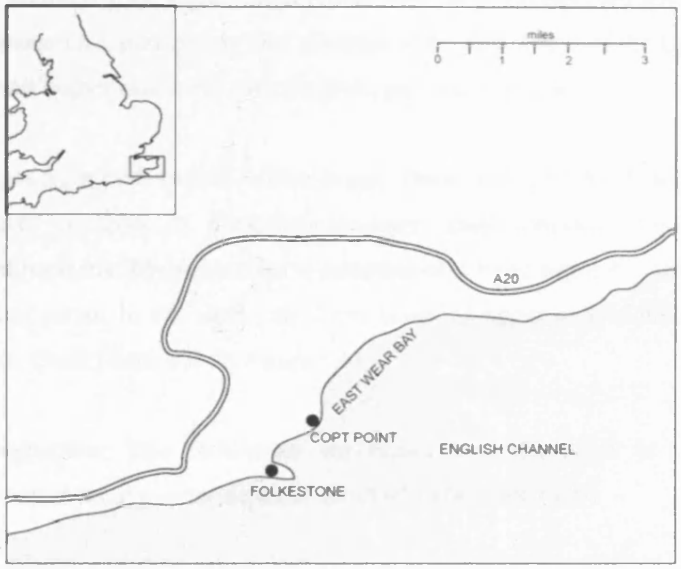

Figure 5.2 Location of Copt Point section near Folkestone (gaultammonite.co.uk)

Thickness: The overall thickness of the section is about 25 m, out of which 10 m was sampled for this study (Bed II to Bed X). Figure 5.3 is a photograph of the study section measured at Copt Point.

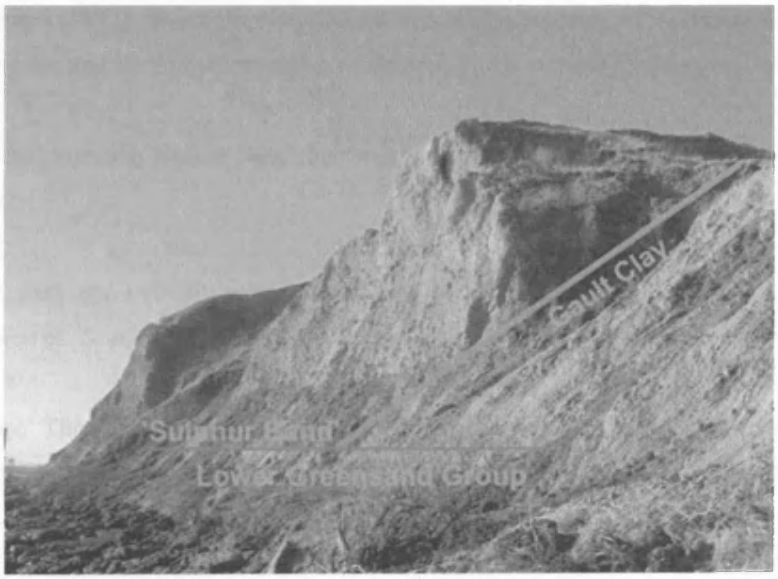

Figure 5.3 Photo of the Copt Point Section (Folkestone) sampled for this study.

Time frame: The 10m-long section encompasses ~ 2Ma, based on dates of the biostratigraphic datums by Bralower, Premoli Silva, Malone et al. (2002).

Sampling: Samples were collected under the guidance of Prof. A. S. Gale in two field seasons. A total of 41 samples were collected for the study. The section was sampled from Bed II (lowest sample) to Bed X

(topmost sample). The sample spacing was variable, with closer sampling (every 10-15cm) within Bed VIII and Bed IX, to enable a high-resolution correlation of the nannofossil data with the oxygen isotope record. The samples were spaced every 50 cm in the other beds (Figure 5.4).

Lithology: Dark and medium grey, highly fossiliferous silty clays interspersed with phosphatic nodules. The clays are often glauconitic, particularly near the base of the unit. Clays of the Upper Gault are lighter in colour with an overall higher carbonate content (Gale, personal communication).

Age: The section ranges from mid- to Late Albian in age (Owen 1972, 1975). A detailed stratigraphy has been established, based on beds of phosphatic nodules, shell concentrations, glauconite-rich and distinctively burrowed horizons. The succession is complete on a biostratigraphic scale with respect to the macrofossil (ammonite) zones. In this study, the focus is on the upper part of the Lower Gault and the lower part of the Upper Gault (Beds VII-X, Figure 5.4).

Environment of deposition: The Folkestone succession was deposited in a relatively shallow epicontinental sea environment at a water depth of about 60 m (Knight 1999).

Breaks in the section: The section includes numerous breaks in sedimentation represented by layers of remanié phosphatic nodules; these may represent considerable periods of time (Knight 1999). Important breaks in the latest mid- and early Late Albian include:

- Bed VIIIi of Owen (1972), in which phosphatised, remanié specimens of *Actinoceramus concentricus parabolicus* Crampton and the lowest examples of *Dipoloceras cristatum* (Brongniart) occur.

- Bed VIIIiii, or the *cristatum* Nodule Bed; abundant remanié phosphatised fossils in a shell plaster of *A. sulcatus sulcatus*.

- Bed of mature, dark and strongly worn nodules, 1.4 m above the base of Bed VIII which yield the highest *Dipoloceras* cf. *D. pseudaon* Spath, and immediately underlies the base of *M. pricei* Zone.

Sea level history: The nodule beds are interpreted as transgressive lags, which rest directly upon erosional surfaces representing sequence boundaries. The base of the Upper Albian is widely regarded as transgressive, and the *D. cristatum* or overlying *H. orbigny* Ammonite Subzone sediments commonly overlap Middle Albian sediments on massifs such as the London Platform (Gale, personal communication).

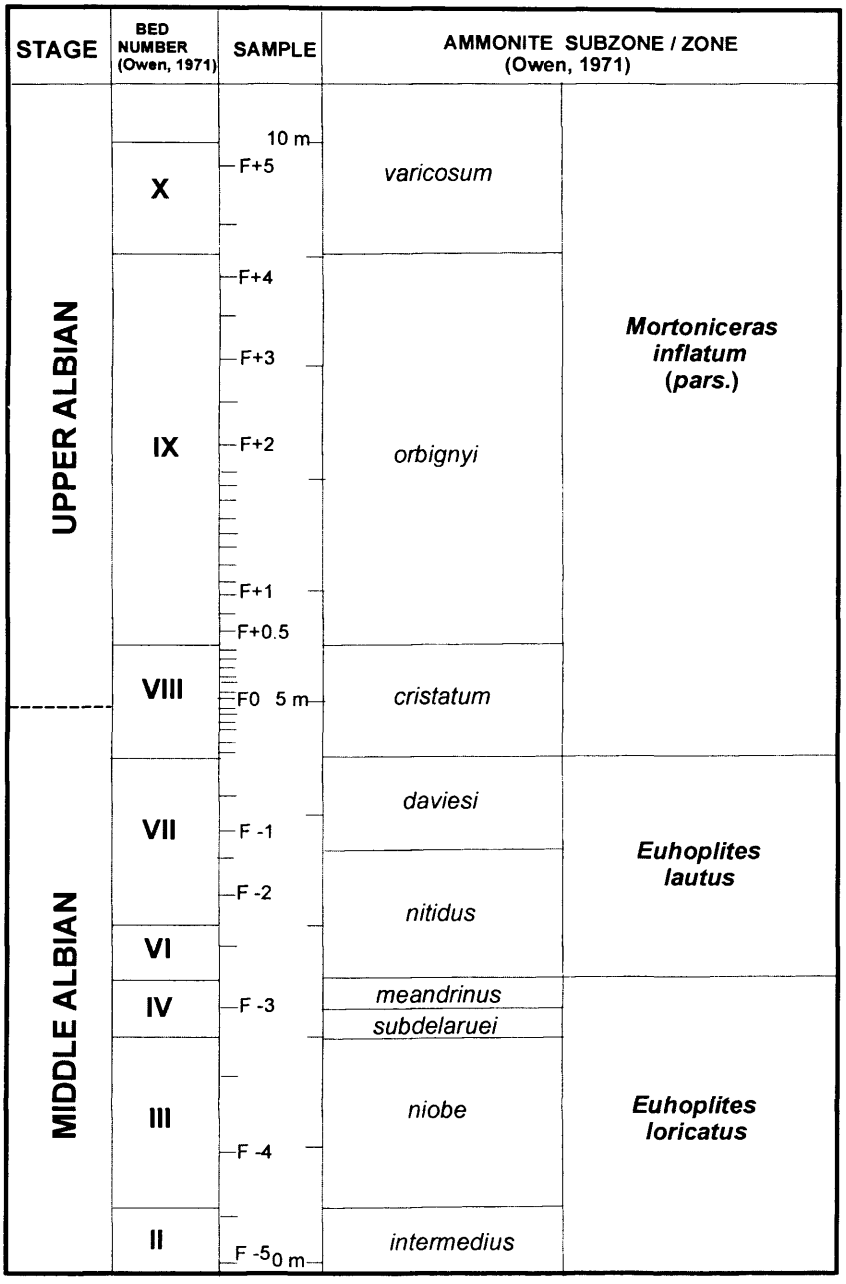

Figure 5.4 Sample details along with the ammonite zonation of the Gault Clay.

5.7 Results

5.7.1 Preservation, abundance and diversity

The nannofossil distribution in the section is presented in Appendix 2. All the 41 samples yielded abundant nannofloras. Preservation of the nannofossils varied between very good and moderate, but was predominantly good. Only one sample showed moderate preservation while a few samples were in the good-moderate category. The assemblage diversity was high, with an overall 120 species identified in the sample set. The assemblage diversity per sample was around 77 species. Due to its uniformly good preservation and high species diversity, the Gault Clay is an excellent section for studying Albian nannofossils.

5.7.2 Biostratigraphy

The biostratigraphy was established using the zonation scheme of Bown et al. (1998). The zonation of Jeremiah (1996) was applied to the samples for a comparison. Figure 5.5 is a summary diagram showing the biostratigraphy of the section. Zone BC24 to Subzone BC25b from Bown et al. (1998) were recognised in the sample set. On this basis, the age of the samples is mid- to early Late Albian. Based on the LO of *C. bicornuta*, the Middle/Upper Albian boundary falls in the sample F -0.15. Zones NAL4 to NAL9 were recognised from the zonation of Jeremiah (1996). The zonal/subzonal events identified from Bown et al. (1998) are listed below. The events are listed in order from older to younger events along with the relevant sample and the corresponding zone number.

Presence of *Tranolithus orionatus*, F-5 (lowermost sample), Zone BC24
FO *Axopodorhabdus albianus*, F-3, Subzone BC25a (base)
LO *Ceratolithina bicornuta*, F-0.15, Subzone BC25b (base)

The zonal events identified from Jeremiah (1996) are as follows:

Presence of *Crucicribrum anglicum* and *T. orionatus*, F-5 (lowermost sample), Zone NAL4
LO *Braloweria boletiformis*, F-4.5, Zone NAL5 (base)
FO *C. bicornuta*, F-2, Zone NAL6 (base)
LO *C. bicornuta*, F-0.15, Zone NAL7 (base)
FO *Staurolithites angustus*, F+3, Zone NAL9 (base)

Since *E. monechiae* or *E. turriseiffelii* were not logged in any sample, the upper part of the section is concluded to be early Late Albian in age. The recognition of all the markers was straightforward except *Tegulalithus tessellatus*, which was not logged in any of the samples. This species is reported from the lower part of the Upper Albian (*auritus* Ammonite Subzone) in the North Sea Basin and from some onshore localities in England and northern France (Crux 1991; Jeremiah 1996; Bown 2001). The species is known to have a restricted distribution and was used to define a northwest European nannofloral province (Crux 1991). According to Jeremiah (1996), *T. tessellatus* is a reliable biostratigraphic marker species in the North Sea Basin, but can be sporadic in onshore localities in England (Munday's Hill, Burwell) and northern France. The species should have been encountered in the studied samples. Its absence is probably due to its rarity, as reported by Jeremiah (1996). The absence of Zone NAL8 is therefore attributed to the rarity of this marker rather than any discontinuity in the stratigraphic record.

Bown (2001) observed coincident FO's of *T. tessellatus* and *S. angustus* in the same sample in the Upper Gault. He commented that the slightly earlier FO of *T. tessellatus* may have been concealed within the gap between samples, or the space between the events may have been obscured by a slow sedimentation rate.

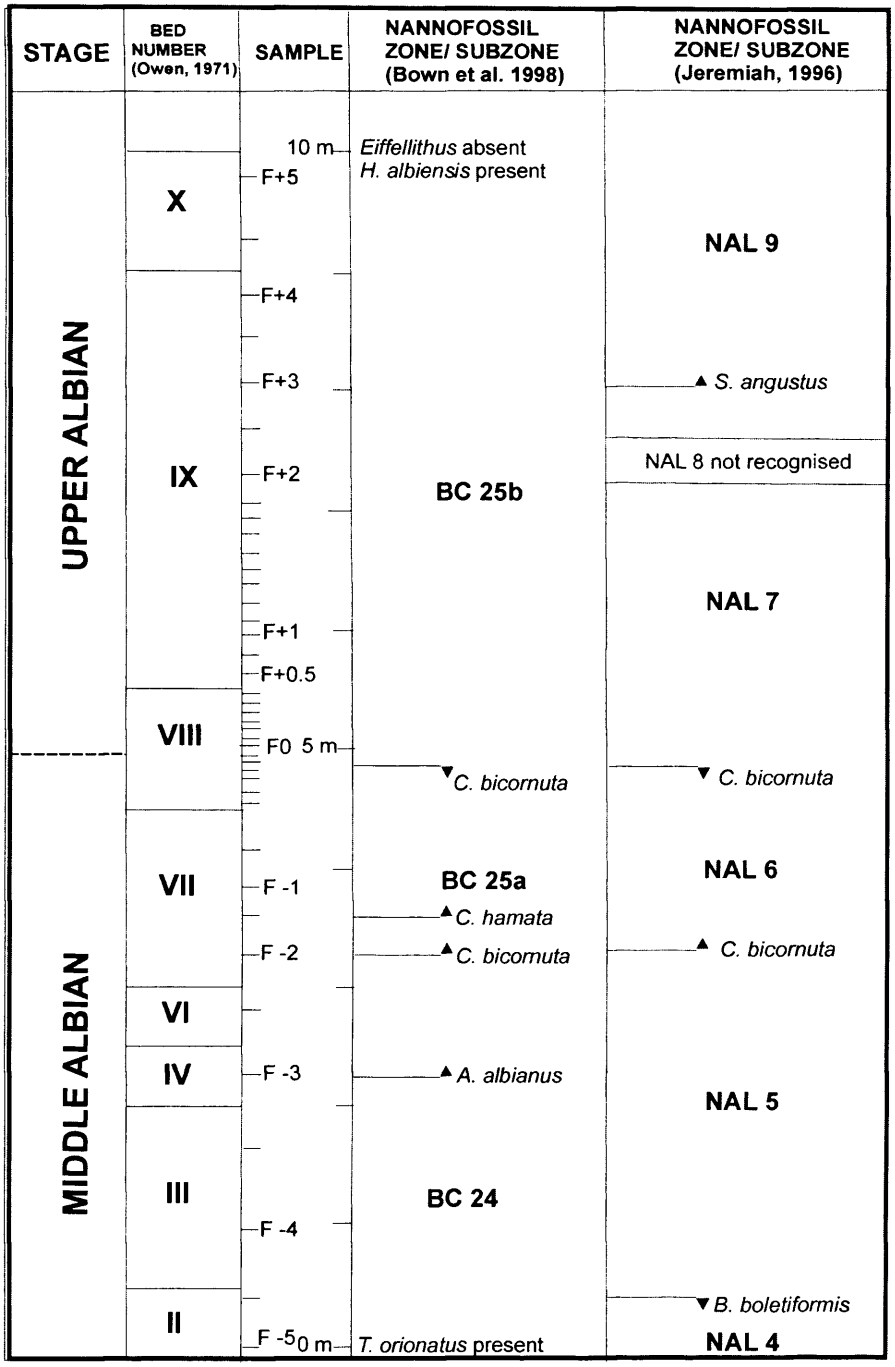

Figure 5.5 Nannofossil biostratigraphy of the Gault Clay section.

A few taxa such as *C. signum* and *O. hilli* showed discontinuous ranges in the Gault Clay. *C. signum* was discontinuous in the Middle Albian, but occurred regularly in the lower part of the Upper Albian. The species normally has its FO in the Upper Albian hence its discontinuous presence in the Middle Albian is not surprising. The rare and discontinuous distribution of *O. hilli* matches its record from the Gault Clay at Munday's Hill, from where it was originally described (Crux 1991).

A species similar to *Gartnerago praeobliquum*, logged as *G.* cf. *G. praeobliquum* was observed, albeit rarely, in the Upper Albian. It is small in size (< 6μm) with thin, narrow bars compared to the thick bars with a flaring 'arrowhead' termination seen in *G. praeobliquum* (Jakubowski, 1986, pp. 35-36). This taxon is probably a precursor to *G. praeobliquum*, based on its small size and rim/bar structure. The taxon is discussed in Chapter 8, section 8.2 (Plate 20).

The species *Radiolithus hollandicus*, whose LO was used to define Zone NAL12 in the Upper Albian, was not conclusively identified in this section. Although the LO of this taxon is outside the age range of the sample set, the difficulty in recognising this species is noteworthy. The difficulty in identifying this species was noted by Bown (2001) in the Upper Greensand Formation.

5.7.3 Palaeonvironmental Analysis

5.7.3.1 Oxygen Isotope ($\delta^{18}O$) data

The oxygen isotope data, based on bulk sediment analysis through the Lower /Upper Gault boundary (Middle/Upper Albian) is shown in Figure 5.6. The oxygen isotope values are presented in Appendix 2. The isotope values were measured on a PRISM mass spectrometer in the Department of Earth Sciences at the University of Oxford.

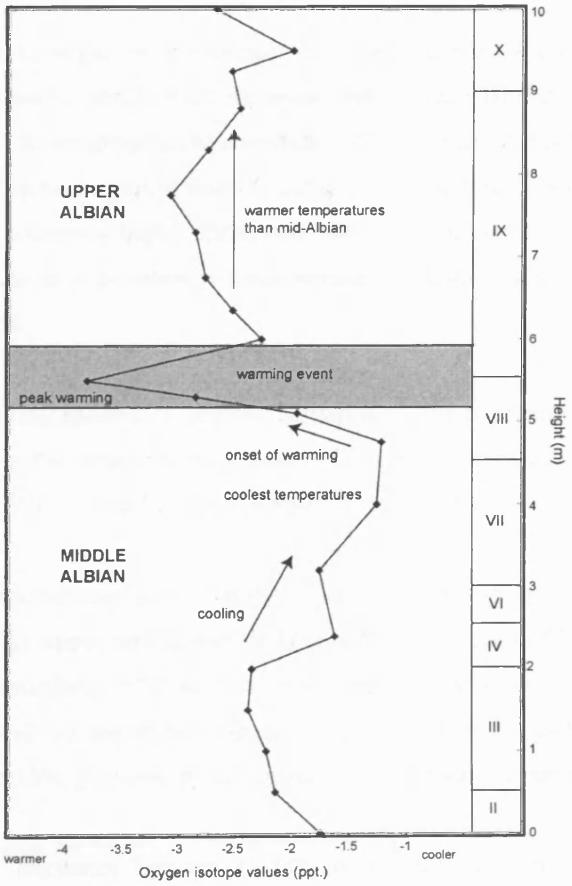

Figure 5.6 Oxygen isotope ($\delta^{18}O$) trend of the Gault Clay section.

Oxygen isotope values show considerable shifts over the 10m-sampled interval of the Gault Clay. The trend of oxygen isotopes is considered to be free from diagenetic imprints in light of the excellent preservation and high diversity of nannofossils in the samples. Some of the more delicate coccolith rims (e.g. *Corollithion*) are well preserved in the material, suggesting that the isotope signal is genuine.

From 0-2 m, at the base of the section, there is a trend towards lighter values ranging from –1.749 ppt to –2.354 ppt and then values become heavy up to 4.75 m attaining a value of –1.214 ppt. At 5.5 m, a minimum value of –3.818 ppt is reached, after a dramatic trend towards lighter values between 4.75 and 5.5 m. Following this, values reach –3.091 ppt at 7.75 m and subsequently rise to –2.681 ppt at the top of the section (10 m). Values fluctuate in the range of –2 to –3 ppt in the upper half of the section.

5.7.3.2 Quantitative nannofossil data

Around ten taxa featured prominently in abundances greater than 1-2% (of the total assemblage) in the 300 specimen counts performed on the samples. The count data is given in Appendix 2. The % abundance trends of the palaeoecologically significant taxa are discussed in this section, in stratigraphic order from older to younger samples. The % abundance trends of these taxa are shown in Figures 5.7-5.10.

B. constans (8-33%) is generally abundant in all the samples. Increases in the abundance of *B.constans* are observed in Bed II and III (~25%), lower part of Bed VIII (22%) and in the upper part of Bed IX and Bed X (> 20%). Sharp drops in the abundance of *B. constans* are noted in Bed VI (8%), upper part of Bed VIII (8%) and the lower part of Bed IX (13%). After the drop in Bed IX, *B. constans* shows a gradual rise and remains consistently high (>20%) until the top of the section, except for a minor drop in sample F+4 (15%). A decline in *B. constans* is noted around the Middle/Upper Albian boundary (around sample F0), from 22% to 8%.

The other high fertility species, *D. ignotus*, is present in low concentrations between 0-5%, even though it frequently drops to 0% values. A sharp peak in *D. ignotus* is noted in Bed II (5%) whilst minor peaks are observed in Bed VIII (2%) and in the upper part of Bed IX (2-3%).

Z. noeliae fluctuates between 9-41% in the section. It shows sharp increases in Bed III (23%), lower part of Bed VIII (28%), upper part of Bed VIII (35-41%), most parts of Bed IX (>25%) and Bed X (>25%). A decline in the abundance of *Z. noeliae*, is noticed in Bed II (9%), Bed VII (11%), Bed VIII (10%) and Bed IX (12-16%). At the Middle/Upper Albian boundary (around sample F0), the species shows a decline, from 26 to 13%, followed by a dramatic rise to 41% at the base of the Upper Albian.

Watznaueria spp. fluctuates between 11-44% in the section. The taxon is abundant in the assemblages with an average proportion of 25%. Minor drops in the percentage of *Watznaueria* spp. are

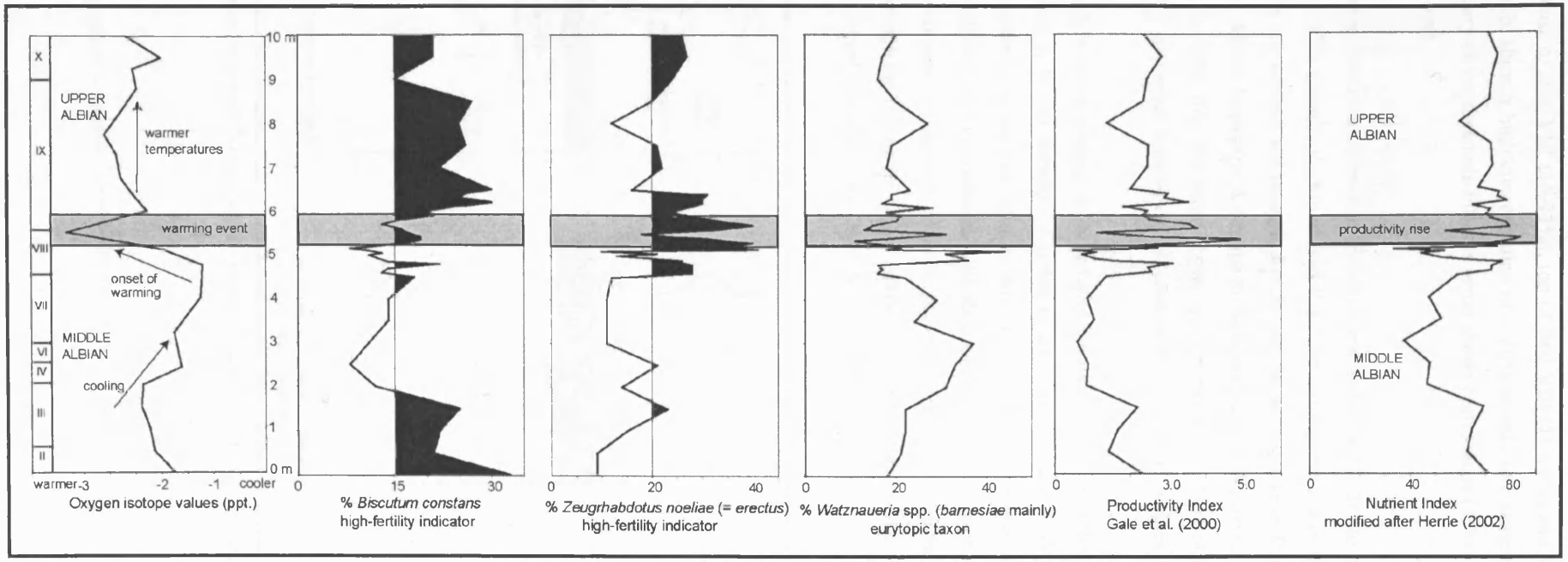

Figure 5.7 Correlation of the % abundance plots of fertility indices and *Watznaueria* spp. with the $\delta^{18}O$ trend. The trends of the Productivity Index and Nutrient Index indicate a productivity rise concomitant with the warming event.

noted at the base of Bed VIII (16-17%), top of Bed VIII (11-14%) and lower part of Bed IX (13-15%). *Watzaueria* spp. show a high concentration of > 40% in only one sample (F+0.1). At the Middle/Upper Albian boundary (around sample F0), the taxon shows high values (33%) and drops to 18% at the base of the Upper Albian.

R. parvidentatum, is present in low abundances (2-5%) at the base of the section but shows a gradual rise to 12% towards the top of Bed VII. Two sharp peaks are observed in its trend. The first peak is noted at the top of Bed VII (sample F-0.5) and the second one in Bed VIII (sample F0), around the Middle/Upper Albian boundary. A decline in the abundance of *R. parvidentatum* is observed in Bed VIII, from 11 to 1%. After this, the taxon shows low abundance (1-5%) until the top of the section. The % abundance of *T. orionatus* is between 1-7% whilst *R. asper* shows values between 0-2%.

S. primitivum is present in the samples but did not appear in the 300 specimen-count data due to its low abundance. It was therefore counted in 20 fields of view (FOV) to gain a quantitative dataset. These counts were performed on samples for which the $\delta^{18}O$ record was available. In the Middle Albian, *S. primitivum* shows rapid fluctuations in its abundance followed by a peak at 5.1 m (12 specimens per 20 FOV). A second peak is observed at 6 m (9 specimens per 20 FOV) in the section. The species shows low abundance through the rest of the Upper Albian. *F. oblongus* was also counted with *S. primitivum* but did not show significant numbers in the 20 FOV count data.

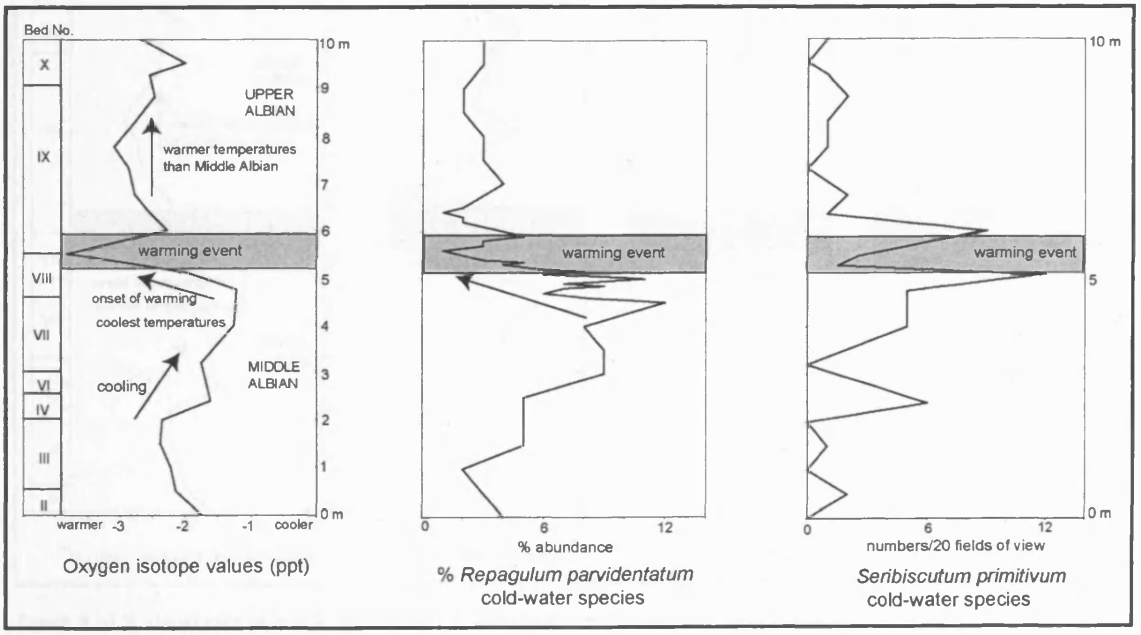

Figure 5.8 Correlation of the $\delta^{18}O$ trend with the nannofossil palaeotemperature proxies, *R. parvidentatum* and *S. primitivum*.

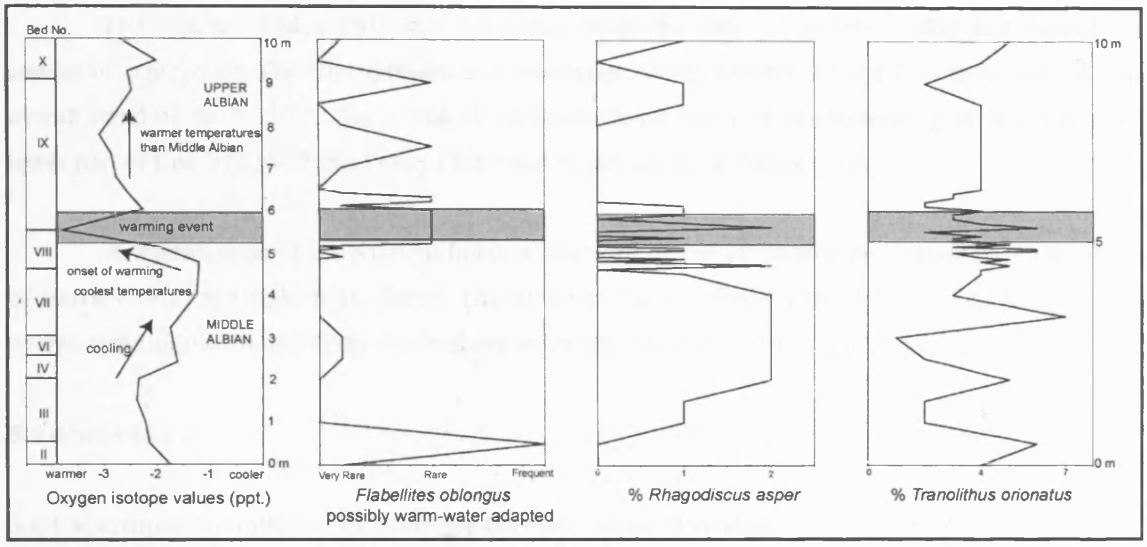

FIgure 5.9 Correlation of the $\delta^{18}O$ trend with *F. oblongus*, on the basis of which it is interpreted to have been possibly warm-warm adapted. The % abundance plots of *Rhagodiscus* spp. and *T. orionatus* show a poor correlation with the $\delta^{18}O$ trend.

The other taxa include *L. carniolensis*, *R. crenulata* and *P. columnata*. *L. carniolensis* is consistently present between 1-10% in the samples. *Retecapsa crenulata* varies between 1-3%. *P. columnata* fluctuates between 1-10%. Two sharp peaks (~10%) are observed in its trend, one at the base of Bed VIII and the other at the base of Bed IX.

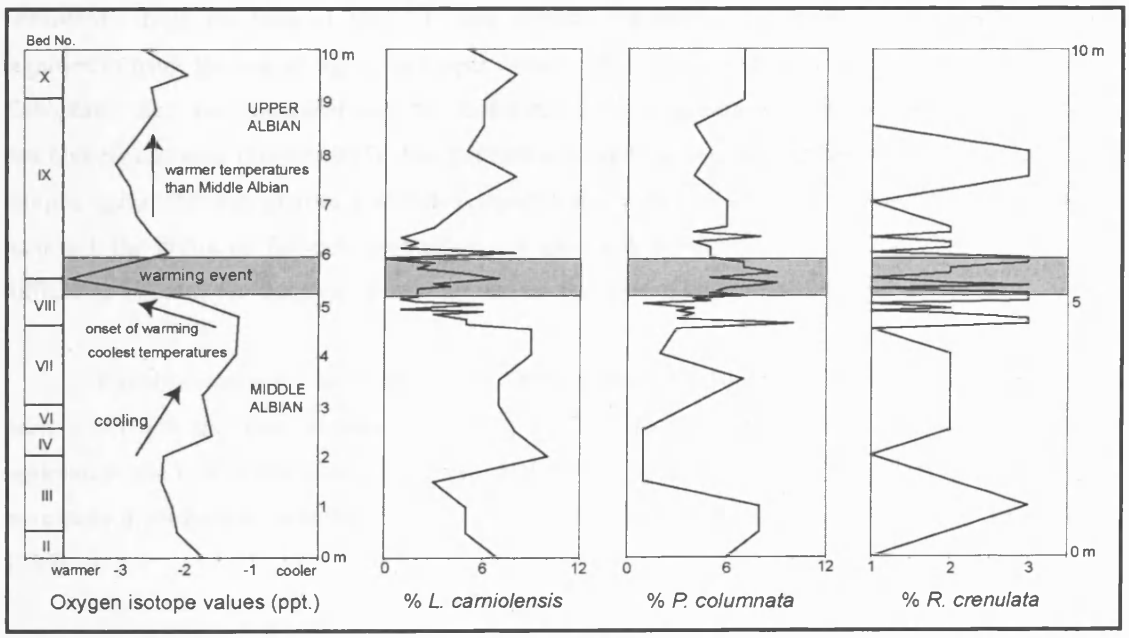

Figure 5.10 % abundance plots of *L. carniolensis*, *P. columnata* and *R. crenulata*, taxa that do not show significant changes with respect to the warming event.

5.7.3.3 Productivity Index and Nutrient Index

The Productivity Index (P), calculated using the ratio of Gale et al. (2000), shows a trend whereby a peak (4.9) is observed in the upper part of Bed VIII (5.35 m). The Productivity Index varies between values of 0.5 and 4.9 in the section.

The Nutrient Index (NI) was calculated using the ratio of Herrle (2002) and plotted for comparative purposes. The NI, expressed as a percentage, varies between 29 and 77% in the section. The overall trend of the NI is similar to that of the Productivity Index. A productivity peak is noted in the upper part of Bed VIII (5.35 m). Plots of the P and NI are shown in Figure 5.12.

A modification of the Nutrient Index is proposed herein by combining elements from the ratios of Herrle (2002) and Gale et al. (2000). The values of the modified NI range from 33 to 83%, with an overall trend similar to that of the Productivity Index and the original NI (Figure 5.12).

5.8 Discussion

5.8.1 Macropalaeontological evidence for the Late Albian warming

The first indication of a warming event in the Upper Albian came from ammonite data documented in literature (Spath 1923-43; Owen 1971, 1975, etc.). The Anglo-Paris Basin, which was dominated by hoplitinid ammonites, experienced occasional incursions of Tethyan and southern provincial ammonites during the mid-Albian (e.g. *lyelli* Ammonite Subzone). However, a more sustained invasion of Tethyan ammonites into the hoplitinid province is noted at the base of the *Dipoloceras cristatum* Ammonite Subzone (lower Upper Albian). The Tethyan ammonite genera are recorded consistently from the base of Bed VIII and continue throughout the Upper Gault. This incursion is regarded to mark the beginning of the Upper Albian, where hoplitinid ammonite genera (e.g. *Anhoplites*, *Euhoplites*, etc.) are associated with non-hoplitinid Tethyan genera such as *Hysteroceras*, *Dipoloceras* and *Oxytropidoceras* (Owen 1975). The Tethyan ammonite genera are recognised by their characteristic morphological features such as a well-developed keel, strong ribs and tubercles in the umbilical region. Although the influx of Tethyan ammonites is a good indication of the onset of a warming event, it is difficult to estimate the duration of the warming on the basis of ammonite data.

Possible routes for the migration of Tethyan ammonites into the Anglo-Paris Basin may have been either via the proto-Atlantic Ocean or by the intermittent flooding of low-lying European landmasses due to frequent transgressions in the Late Albian. Migration via the Atlantic is more likely to have been a permanent route for the entry of Tethyan ammonites into the Anglo-Paris Basin (Hancock 1989).

5.8.2 Nannofossil evidence for the Late Albian warming

The $\delta^{18}O$ record is correlated with the % abundance data of temperature-related nannofossil species in Figures 5.8 and 5.9. The $\delta^{18}O$ values have not been converted into absolute temperatures, although it is certain that at least a component of the values are controlled by palaeotemperatures. If this is correct, then the Lower Gault oxygen isotope values (*E. lautus* Ammonite Zone) record a significant and progressive temperature fall (Figure 5.6). The light oxygen isotope peak between 4.75 and 5.5 m in

the section records a rapid and probably short-lived warming event starting at the base of the Upper Albian (*D. cristatum* Ammonite Subzone). The palaeotemperature rise corresponding to the 2.5 ppt light oxygen isotope peak was of the order of several degrees (~5-6° C). Temperatures in the Upper Albian were higher than the Middle Albian.

A correlation of the % abundance of *R. parvidentatum* with the $\delta^{18}O$ trend shows an excellent correspondence between the two datasets (Figure 5.8). This is particularly evident at the Middle/Upper Albian boundary (at 5.5 m) where the light $\delta^{18}O$ peak precisely coincides with the rapid decline in the abundance of *R. parvidentatum* from 11% to 1%. The decline in *R. parvidentatum* is an independent line of evidence that supports the palaeotemperature change interpretation from the oxygen isotopes. The correlation coefficient (0.7) between % *R. parvidentatum* and $\delta^{18}O$ record suggests that there is a reasonably good level of correlation between them.

Repagulum parvidentatum is therefore considered to be an excellent cold-water indicator during the mid-Cretaceous. This is in agreement with the findings of previous authors (Wise 1983; Wise 1988; Bown et al. 1998; Street & Bown 2000). The species is known to be abundant in high-latitude sections, and frequent to rare in the temperate sections. It is however, very rare or possibly absent in the tropics. The clear understanding of its palaeoecology lends itself to its utility in palaeoenvironmental interpretation. Figure 5.11 shows the biogeographic distribution of *R. parvidentatum* during the mid-Cretaceous.

The other high-latitude species, *S. primitivum*, is regularly present in the Gault Clay, reflecting the Boreal nature of the assemblages. The high-latitude aspect of the Gault Clay assemblages is also evident from the consistent presence of *Ceratolithina* in the samples. Two species, *C. hamata* and *C. bicornuta* are regularly found in the samples. The distribution of *Ceratolithina* is known from Boreal regions (UK and the North Sea), and some high-latitude sections from the Indian Ocean, e.g., DSDP Site 258 (Lees 2002).

However, the distribution of *S. primitivum* is not comparable to *R. parvidentatum*. The reason for this is that *R. parvidentatum* is abundant in the section whereas *S. primitivum* is rare, as a result of which it did not register consistently in the counts. In the Middle Albian, *S. primitivum* shows rapid fluctuations in its abundance followed by a peak at 5.1 m (12 specimens per 20 FOV) (Figure 5.8). It then shows a decline in its abundance during the warming event (5.5 m), followed by a second peak at 6 m (9 specimens per 20 FOV) in the section. The species shows very low abundance through the rest of the Upper Albian. Although *S. primitivum* shows a decline in abundance at the peak of the warming event, its abundance record in the rest of the section is unreliable. The second peak in its abundance during warm conditions (at 6 m) is difficult to understand. It is therefore concluded that the rare occurrence of *S. primitivum* strongly limits its utility as a palaeotemperature proxy in the Gault Clay.

Figure 5.11 Bipolar distribution of *R. parvidentatum* during the mid-Cretaceous. Locations shown: 1- Argo Abyssal Plain, Indian Ocean; 2-Naturaliste Plateau, Indian Ocean; 3-Cauvery Basin, India; 4-Falkland Plateau, Southern Ocean; 5-Neuquen Basin, Argentina; 6-Shatsky Rise, Pacific Ocean; 7-Blake Nose,western Atlantic; 8-Gault Clay, England; 9-Vocontian Basin, France; 10-Umbria-Marche Basin, Italy. Data collated from this study, Lees (2002), Wise (1988), Bown & Concheyro (2004) & Erba (1992a). Palaeogeographic reconstruction is of the Late Aptian, taken from Erbacher et al. (2001).

R. asper, a putative warm-water taxon, does not show a significant correlation with the $\delta^{18}O$ data (correlation coefficient 0.44). The light oxygen isotope peak indicating warming is not supported by a corresponding increase in *R. asper*. (Figure 5.9). The overall abundance trend of *R. asper* is ambiguous as it keeps falling to 0 % values. Moreover, the % abundance of *R. asper* is very low (1-2%) in the section. In the Lower Gault (0 - 4.75 m), *R. asper* shows a consistent abundance of 2%, which is the highest value it records in the section. The warm-water affinity of *R. asper* is therefore considered dubious in this section. However, the consistent presence of *R. asper* during the cooling phase in the Middle Albian (2-4.5 m) accompanied by moderate productivity, suggests that it may be related to moderate or low fertility conditions.

Mutterlose (1989, 1996) used high abundances of *R. asper* as an indicator of warm waters in the mid-Cretaceous. However, he used circular reasoning for assuming that *R. asper* had warm-water affinities. According to him 'Assuming that Erba (1987) is correct, the hypothesis linking nannoconids to warm water is supported by the fact that *R. asper* is most abundant in those beds which yielded *Nannoconus*. Thus it is presumed that high abundances of *R. asper* and the presence of Tethyan nannoconids can be used as an indicator for warm surface waters' (Mutterlose 1989, p. 136-138). Such indirect linkages make the interpretation of *R. asper* as a warm-water species dubious.

T. orionatus does not show any correlation with the $\delta^{18}O$ data (correlation coefficient 0.029) or with % *R. parvidentatum* (Figure 5.9). Therefore *T. orionatus* is not usable as a palaeotemperature proxy and its supposed cold-water affinity (Wind 1979; Crux 1991) is rather misleading.

5.8.3 Nannofossil evidence from previous studies

Crux (1991) reported the start of a warming trend towards the end of the Middle Albian in the Gault Clay at the Munday's Hill section. He noted it at the end of the Middle Albian, on the basis of a decline in *R. parvidentatum*. According to him, this warming trend continued into the Upper Albian but was briefly interrupted in the lower *cristatum* Subzone, where *R. parvidentatum* increased in abundance. Warmer conditions returned in the *orbigny* Subzone and persisted through the lower half of the *varicosum-auritus* Subzones. During the upper half of the *varicosum-auritus* Subzones, intermediate to cold surface waters were thought to have prevailed in the region based on increased abundances of *R. parvidentatum*. A similar pattern was observed by him for the other high-latitude species such as *S. primitivum* and *B. matalosa* in the Munday's Hill section. *T. orionatus*, reported to be a high-latitude species, was found to be most abundant at the beginning of the cooling event in the Upper Albian (upper half of the *varicosum-auritus* Subzones).

Crux (1991) also reported that the warming was evident from the coiling direction observed in the planktonic and benthic foraminifera in the Munday's Hill section. The foraminifers *Gavelinella* spp. and *Hedbergella* spp. showed a predominance of dextrally coiled forms, indicative of warmer conditions, at the mid-/Late Albian boundary.

Erba et al. (1992) inferred orbitally driven cycles from the pattern of *R. parvidentatum* suggesting that cyclic variations of surface water temperature might have influenced the nannofossil patterns within the Gault Clay. It is not possible to correlate our data with that of Erba et al. (1992) because their paper does not provide sufficient information on the sample and bed details of the section they studied.

Jeremiah (1996) noted sharp increases in the abundance of *R. parvidentatum* in the Middle and Upper Albian at Copt Point. The increases in its abundance were noted in several beds, e.g., at the base of Bed II (*intermedius* Subzone), Bed III (*niobe* Subzone), the top of Bed VII (*daviesi* Subzone), Bed VIII (*cristatum* Subzone), Bed IX (*cristatum* and *orbigny* Subzones), Bed X (*varicosum* Subzone) and Bed XI (*auritus* Subzone). *R. parvidentatum* was generally reported to be abundant throughout the section in his study, even though some beds showed sharper peaks than others.

It is easier to compare the quantitative dataset from this study with that of Jeremiah (1996) since it is based on a section at Copt Point (pp. 100, Jeremiah 1996). However, since the focus of Jeremiah's work was on biostratigraphy, he did not make any interpretations from the quantitative abundance of *R. parvidentatum*. The count data of Jeremiah (1996) does not show any obvious reduction in the numbers of *R. parvidentatum* in the Upper Albian, as opposed to Crux (1991) and this study. The counts made by Jeremiah (1996) were based on 30 fields of view rather than 300 specimen counts. The difference in the method of counting or sample preparation may be a reason for the discrepancy between this dataset and that of Jeremiah (1996). The counts of *R. parvidentatum*, *R. asper* and *T. orionatus* from Crux (1991) and Jeremiah (1996) are presented in Chart 12 (Appendix 2).

5.8.4 Other taxa in the nannofossil assemblages

The genus *Nannoconus*, commonly present in Albian assemblages of the Tethyan and Atlantic regions, is very rare in the Gault Clay. This agrees well with the observations made by Jeremiah (1996) and Bown (2001) who reported sporadic occurrences of *Nannoconus* spp. in the Gault Clay. Crux (1991) did not encounter *Nannoconus* in any of the samples from Munday's Hill. The rare and sporadic occurrence of *Nannoconus* in the Gault Clay can be explained by the Boreal setting of the section, where the Tethyan-derived nannoconids did not thrive (Street & Bown 2000).

Flabellites oblongus, a species frequently encountered in Albian assemblages shows an interesting record in the Gault Clay. It shows an inconsistent presence in the Lower Gault (1-5m) but becomes relatively consistent above the Middle/Upper Albian boundary (Figure 5.9). The consistent presence of *F. oblongus* in the Upper Albian suggests that it may have been adapted to warm waters. The species is very rare, as a result of which a quantitative dataset could not be generated for it through the 20 FOV counting method.

The abundance record of taxa such as *L. carniolensis*, *P. columnata* and *R. crenulata* does not show clear trends in the Gault section (Figure 5.10). Previous studies have not been able to understand the palaeoecology of *P.columnata* or *R. crenulata*, with the conclusion being that these two taxa were cosmopolitan. This is agreed upon in this study, as both the taxa have been consistently recorded in all the four study sections (India, England, the Atlantic and Pacific). *L. carniolensis* is interpreted as an oceanic-adapted species in this study (see Chapter 7).

5.8.5 Productivity Index

The productivity index (see section 2.3, Chapter 2) of Gale et al. (2000) was calculated using the formula:

$$\text{P (Productivity Index)} = \left[\frac{\%Zeug.spp. + \%Bisc.spp.}{\%Watz.spp.}\right]$$

On the basis of this ratio, a series of productivity peaks are observed in Bed VIII (~5.3 m) and in the lower part of Bed IX (~5.6 m). A prominent peak is observed in Bed VIII (P = 4.9) coinciding with the warming event (Figure 5.7). The productivity peak reflects high percentages of *Z. noeliae* (~ 40%), a taxon occurring in the numerator of the ratio. It is worth noting that *B. constans* is relatively low in abundance during the warming event, but increases thereafter and shows consistently high percentages (>15%) in the Upper Albian. There is clearly a productivity increase in the section at this level.

Productivity Index values from the Cenomanian-Turonian Lower Chalk/White Chalk Formation from Eastbourne by Gale et al. (2000) have been compared with the Gault Clay. Although the two sections differ in age and show different preservation levels, it is still worth a comparison. 'P' values of Gale et al. (2000) are in the range of 0.5 to 1.5, whereas Gault Clay values range between 0.5 and 4.9. Thus Productivity Index in the Gault Clay is considerably higher than the Eastbourne section. This suggests temporal variations in productivity between the Cenomanian-Turonian and the Albian.

However, Gale et al. (2000) used a different counting strategy. They performed assemblage counts between 150 and 220 individuals, until 100 specimens of *Watznaueria* had been counted in a sample. As a result, % *Watznaueria* spp. was a relatively constant figure in their methodology. The method used in this study involved counting the first 300 nannofossil specimens in a sample, irrespective of *Watznaueria* spp., as a result of which % *Watznaueria* spp. varied from sample to sample. This may also have contributed to higher PI values in the Gault Clay section.

The % abundance of *Watznaueria* spp. is important, as it is the denominator of the productivity index ratio. It appears from Figure 5.7 that the % abundance trend of *Watznaueria* spp. is the inverse of the productivity index, which is explained by the nature of the ratio itself. It is important to bear in mind that closed-sum effects are involved in interpreting % abundance data of *Watznaueria* against *Biscutum* and *Zeugrhabdotus*, as these are the three dominant taxa in Albian assemblages. However, the abundance

of *Watznaueria* spp. in the Gault (11-44%) suggests that it was a ubiquitous taxon with broad palaeoecological tolerances. The fluctuations in its abundance are independent of preservation in the section, which is uniformly good. Similar arguments have been given to explain the palaeoecology of *Watznaueria* by Street & Bown (2000) and Lees et al. (2004).

5.8.6 Nutrient Index and its modification

The Nutrient Index (see section 2.3, Chapter 2) of Herrle (2002) was calculated using the formula:

$$\text{NI (Nutrient Index)} = \left[\frac{(\%D.ign. + \%Zeug.spp)}{(\%Watz.spp.) + (\%D.ign. + \%Zeug.spp.)}\right] * 100$$

The overall trend of the 'NI' and 'P' are similar, although minor differences exist due to the different taxa that are used in the two indices (Figure 5.12). The Productivity Index is based on *B. constans*, whereas the NI is based on *D. ignotus*.

Herrle (2002) computed the NI of the Early Albian Niveau Paquier (OAE1b) succession in the Vocontian Basin and the Mazagan Plateau (Atlantic Ocean). The NI values from these sections compare very well with the Gault Clay. NI values range between 25 and 80% in the Vocontian Basin and the Mazagan Plateau. The Gault Clay shows values ranging between 29 and 77%.

A modification of the Nutrient Index of Herrle (2002) is proposed here by combining elements from the ratios of Herrle (2002) and Gale et al. (2000). The modified NI is based on all the three productivity indicators, i.e., *B. constans*, *Z. noeliae* and *D. ignotus*. It is expressed as a %, similar to the ratio of Herrle (2002). The modified NI is defined as:

$$\text{NI (modified)} = \left[\frac{(\%B.const. + \%D.ign. + \%Z.noe.)}{(\%Watz.spp.) + (\%B.const. + \%D.ign. + \%Z.noe.)}\right] * 100$$

The values of the modified NI are higher ($33<NI<83$) than the NI of Herrle (2002). This is because the modified NI utilises all the three productivity-related taxa instead of only two. As all the three species, *B.constans*, *Z. noeliae* and *D. ignotus*, are related to high-fertility, it is meaningless to exclude any one of them from the ratio. Therefore the modified NI gives a better perspective of the fertility levels in the Gault section. A comparison of the trends of these three multispecies nutrient indices is shown in Figure 5.12. The overall trends of the three indices are very similar.

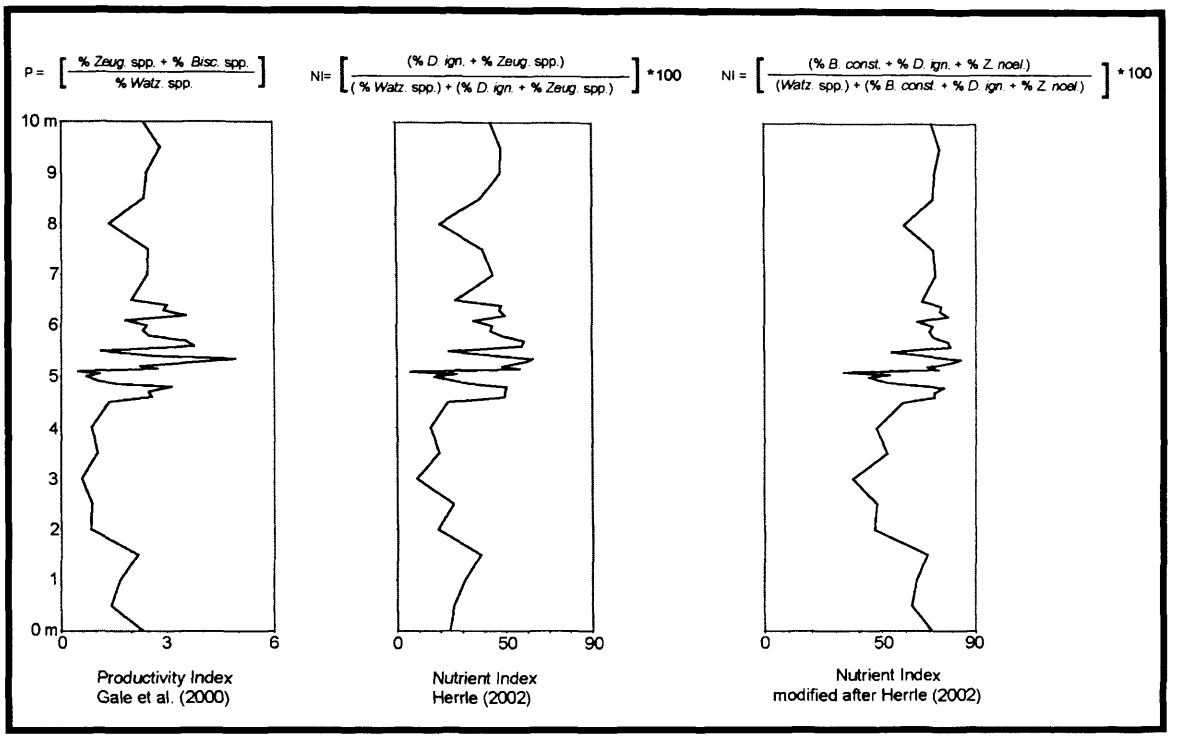

Figure 5.12 Comparison of the multispecies nutrient indices.

It is worth noting that *B. constans* and *Z. noeliae* (*erectus* of previous authors) are thought to represent different levels of high fertility. Erba (1992b) suggested this based on the observation that *B. constans* peaked in abundance prior to *Z. noeliae* in the equatorial upwelling belt of the Pacific Ocean. She observed that *Z. noeliae* was significantly abundant only in the upwelling belt, whereas *B. constans* increased in abundance at the margins of the high-fertility area. Thus *B. constans* was suggested to be sensitive to high fertility in mesotrophic environments, whereas *Z. noeliae* was sensitive to higher fertility in a more eutrophic environment. Although this study shows that *B. constans* and *Z. noeliae* peak at different times, it is difficult to point out which of these two taxa represents higher fertility than the other. In this study, *B. constans* peaks first at the base of the section in the Middle Albian. *Z. noeliae* peaks in abundance (~ 40%) during the peak of the warming event followed by peaks of *B. constans* (> 20%) after the warming peak. This order of *B. constans* peaking prior to *Z. noeliae* was observed by Erba (1992b) and Roth (1981) in the Pacific Ocean.

This study suggests that *B. constans* and *Z. noeliae* represent different levels of high fertility, as they are out-of-phase with each other. Using the hypothesis of Erba (1992b), the warming event in the Gault Clay was characterised by eutrophic conditions based on peaks of *Z. noeliae* (~ 40%), followed by mesotrophic conditions in the Upper Albian (based on peaks of *B. constans*). It is important to note that Fisher and Hay (1999) gave a contradictory hypothesis to Erba (1992b), suggesting that *Z. noeliae* represents somewhat lower fertility conditions than *B. constans*, based on correlation coefficients and diversity analysis studies. However, it is clear that a productivity increase was coincident with the warming event in this section.

5.9 Palaeoclimatic summary

Quantitative nannofossil and oxygen isotope data from the analysed samples reflect palaeoproductivity and palaeotemperature conditions in the surface waters during the mid- to early Late Albian in the Gault Clay. Starting from the base of the section (0-2 m, Middle Albian), surface-water temperatures appear to have been moderate based on oxygen isotope values, with high productivity reflected through peaks of *B. constans* (> 20%). This was followed by a cooling trend (2-4.5 m), during which productivity was moderate (NI = 37-58). The cooling was followed by a rapid and probably short-lived warming event (4.75-5.5 m) at the mid-/Late Albian boundary, deduced from the striking coincidence of a light $\delta^{18}O$ peak, a rapid decline in *R. parvidentatum* (from 11 –1%) and the ammonite record. This warming was accompanied by high productivity, reflected through high percentages of *Z. noeliae* (~ 40%). Temperatures in the Upper Albian remained higher than the Middle Albian, accompanied by high productivity shown by high percentages of *B. constans* (20-25%).

Increased abundances of *Z. noeliae* (~ 40%) coincident with the warming event suggest that surface waters were nutrient-rich. It can be hypothesised that warming in the Late Albian may have driven increased precipitation and subsequently run-off delivering more nutrients into the basin. Additionally, mixing of nutrients may have been enhanced by increased storminess and wind strength.

5.10 Conclusions

1. Using the BC zonation of Bown et al. (1998), Zone BC24 – Subzone BC25b are identified in the samples correlating with a mid- to early Late Albian age. The absence of *T. tessellatus* in the studied section combined with its reported rarity from other onshore localities in England and the North Sea Basin limits its biostratigraphic utility.

2. The coincidence of the influx of Tethyan ammonites, a light $\delta^{18}O$ peak and the decline in *R. parvidentatum* (from 11 to 1%) indicates a rapid and probably short-lived warming event starting at the Middle/Upper Albian boundary in the Weald of the Anglo-Paris Basin.

3. *R. parvidentatum* is considered to be an excellent palaeotemperature proxy for cold waters. *S. primitivum* is rare in the samples and as a result, its quantitative abundance cannot be utilised as a proxy for assessing palaeotemperatures.

4. The Nutrient Index proposed by Herrle (2002) and the Productivity Index proposed by Gale et al. (2000) have been combined to give a modified Nutrient Index. The modified Nutrient Index utilises all the three productivity indicators, *B. constans*, *Z. noeliae* and *D. ignotus*, instead of only two, and therefore gives a better perspective of the fertility levels in the Gault section.

5. A significant productivity increase based on high percentages of *Z noeliae* (~40 %) is coincident with the warming event. High productivity continued through the Upper Albian shown by peaks of *B. constans* (> 20%).

6. In terms of palaeoceanographic implications, the productivity rise accompanying the warming in the Late Albian suggests nutrient-rich surface waters in the Gault. It is hypothesised that warming may have driven increased precipitation and subsequently run-off, delivering more nutrients into the basin. Mixing may also have been enhanced by increased storminess and wind strength.

7. The warm-water affinity of *R. asper* is dubious. It is not usable as palaeotemperature proxy for the Gault Clay section. The semi-quantitative abundance of *F. oblongus* suggests that it may have been a warm-water adapted species during the mid-Cretaceous.

Chapter 6. ODP Leg 171B, Blake Nose, western North Atlantic

Abstract

A ~6 m-long section from ODP Hole 1049C, the deepest site of the Leg 171B transect across Blake Nose, western North Atlantic, was examined for its nannofossil palaeoproductivity record through the Early Albian OAE1b event. Nannofossil Subzones NC7A-B to NC8B (Roth 1978; with modifications by Bralower et al. 1993, 1995) were recognised indicating an Early Aptian to Early Albian age range for the section. The OAE1b black shale identified by Norris, Kroon, Klaus et al. (1998a) and Erbacher et al. (2001) lies within Subzone NC8B. Based on a correlation of the Blake Nose with the Vocontian Basin succession, a ~953.3 kyr-long hiatus is found to exist between the 'Kilian' and the 'Paquier' events in the studied section. There are two significant negative $\delta^{13}C$-isotope excursions in the section, Excursion 1, that lies ~2.08 m below the base of the black shale (Gröcke et al. 2002), and Excursion 2, that lies at the base of the black shale itself (Erbacher et al. 2001). In addition, a striking shift in Sr/Ca ratios, an independent proxy for nannoplankton productivity (Stoll & Schrag 2001), is noted at Excursion 1 (Gröcke et al. 2002). Nannofossil results coupled with geochemical data support the increased productivity model for the OAE 1b event in the western North Atlantic. Based on single-species proxies, multispecies nutrient indices and the Shannon-Weiner diversity index, increasing productivity proxy values are observed from Excursion 1 up section, with peaks at the base and top of the black shale. The deposition of the black shale was characterised by more stable stratified waters, evidenced by a marked decline in the productivity proxies, a minor rise in *Nannoconus*, along with high Shannon-Weiner values. The results from this study are in good agreement with Erbacher et al. (1999, 2001). Palaeotemperature data, based on $\delta^{18}O$-isotopes and the nannofossil proxies, *Rhagodiscus* spp. and *Repagulum parvidentatum* are not entirely clear, although the distribution of *R. parvidentatum* possibly suggests cooling pulses prior to both excursions. This, if true, is at variance with the interpretations of Erbacher et al. (2001) and Herrle (2002), both of which suggest warming events associated with OAE1b.

6.1 Aims

The aims of this study were as follows:

1. To evaluate the nannofossil biostratigraphy of the Aptian-Albian succession from Blake Nose (ODP Leg 171B, Hole 1049C), using established zonation schemes with a view to reappraise the initial shipboard biostratigraphy and constrain the timing of OAE1b;
2. To address the role of productivity during OAE1b, using quantitative abundance data for a suite of nannofossil species along with multispecies nutrient indices, species richness and Shannon-Weiner diversity index.
3. To correlate the nannofossil data with geochemical data ($\delta^{13}C$-isotope, $\delta^{18}O$-isotope and Sr/Ca ratios) in order to investigate the palaeoenvironment during OAE1b, and thereby understand its causal mechanism.

4. To compare the results obtained from the relative abundance (percentage-based) counting method with the absolute abundance method (fixed numbers of fields of view) and verify whether they agree or conflict with each other.

6.2 Introduction

Oceanic anoxic events (OAEs) are supraregionally- to globally correlatable black shale horizons that have associated positive carbon isotope excursions, and in some cases, precursor negative excursions (e.g., Schlanger & Jenkyns 1976; Arthur et al. 1990; Jenkyns 1995; Menegatti et al. 1998). Two of the four mid-Cretaceous OAEs have so far proven to be global in extent (OAE1a, Early Aptian, and OAE2, Cenomanian/Turonian boundary) and recognisable in all marine depositional settings, from shallow shelf to abyssal ocean basins. The co-occurring $\delta^{13}C$-isotope excursions are independent of lithological expression and identifiable in organic matter from coeval terrestrial sections (Gröcke et al. 1999; Jahren et al. 2001). Postulated mechanisms for the formation of such black shale deposits range between the two end-member models of increased primary productivity (e.g., Arthur et al. 1990; Erba 1994; Erbacher et al. 1996; Weissert et al. 1998; Jenkyns 1999; Larson and Erba 1999; Leckie et al. 2002) and enhanced preservation of organic matter (e.g., Bralower and Thierstein 1984; Erbacher et al. 2001; Herrle et al. 2003a, b), and in detail range from localised causal factors, such as basin bathymetry, terrestrial organic carbon input, runoff, and mixing (e.g., Bralower 1988; Gale et al. 2000; Erbacher et al. 2001; Herrle et al. 2003a, b), to truly global explanations invoking large scale tectonism, volcanic CO_2- and clathrate CH_4-driven global warming and the consequent climatic, oceanographic, biotic and isotopic perturbations (e.g., Arthur et al. 1990; Sinton and Duncan 1997; Jenkyns 1999; Wignall 2001; Erba 2004; Erba and Tremolada 2004).

The role of primary productivity is of particular interest to micropalaeontologists, as quantitative analyses of plankton assemblages can be used as proxies for surface-water fertility. Elevated phytoplankton and/or bacterial productivity has been cited as a major component of many of the black shale deposits, particularly of OAEs 1a and 2 (e.g., Hochuli et al. 1999; Premoli-Silva et al. 1999; Bralower et al. 2002), although palaeontological and geochemical data can be ambiguous and quite different scenarios such as stratification and low primary productivity have also been proposed (e.g., Lamolda et al. 1994; Erbacher et al. 2001). In fact, there is no consensus so far on whether a common mechanism is appropriate to explain individual OAE organic-rich deposits, although there have been a number of attempts to present unifying models (e.g., Sinton & Duncan 1997; Jenkyns 1999; Larson & Erba 1999; Erba 2004; Erba and Tremolada 2004).

The principal objective of this study was to generate a palaeoproductivity record for the Early Albian OAE1b in the western North Atlantic. To achieve this, micropalaeontological and geochemical data from the Aptian-Albian transition of Site 1049, drilled during ODP Leg 171B, on Blake Nose in the western Atlantic has been studied. The study section includes the black shale interval identified as OAE1b by Norris, Kroon, Klaus et al. (1998a) and Erbacher et al. (2001), but also incorporates the

underlying ~5 m succession, which includes another significant $\delta^{13}C$-isotope excursion and a striking shift in Sr/Ca ratios (Gröcke et al. 2002). Quantitative abundance data has been collected for a suite of nannofossil species, which are thought to represent proxies for surface-water productivity and temperature, along with multispecies nutrient indices, simple species richness and Shannon-Weiner diversity index. Sr/Ca ratios are thought to provide one of the clearest measures of productivity in the shells of carbonate-producing organisms (Stoll and Schrag 2001) and allow comparison of the nannofossil data with a powerful, independent proxy for surface-water environments. The recognition of pre-OAE1b $\delta^{13}C$-isotope and Sr/Ca excursions at Site 1049 appears to be significant for the identification and definition of these OAE events, or group of events, an issue of particular relevance to OAE1b, which is characterised in its type-area by the development of multiple black-shale levels (Bréhérét 1997; Leckie et al. 2002; Herrle 2002).

6.3 The Blake Nose setting and OAE1b

The sample material comes from ODP Hole 1049C, which is the deepest site of the Leg 171B transect across the Blake Nose (Figure 6.1), located at 30°08.54'N, 76°06.73'W, east of Florida/Georgia (USA) in the western North Atlantic (Norris, Kroon, Klaus et al. 1998a). It was drilled in 2671 m of water, close to the edge of the escarpment, which drops off to 4000 m, due to erosion of the continental slope (Norris, Kroon, Klaus et al. 1998b). Planktic/benthic foraminifera ratios of previously drilled Blake Nose sediments indicated that the Aptian-Albian at the eastern edge was deposited in water of >500m depth (Benson, Sheridan et al. 1978). According to Norris, Kroon, Klaus et al. (1998b), if the reef identified by seismic records at the western end of Blake Nose, ~67 km upslope from 1049, lay at around sea-level in the Aptian-Albian, and the gradient of the Blake Nose had been constant since then, then the deepest the 1049 sediments could have been deposited in was about 1500 m (the difference between the 1049 and the top of the reef), which means the sea-floor and its benthos was possibly influenced by mid-bathyal deep-water. Indeed, benthic foraminifera palaeodepth estimates for 1049 indicate 800-1000 m for the Albian (Norris, Kroon, Klaus et al. 1998b).

The Aptian-Albian sequence in the section is condensed (Norris, Kroon, Klaus et al. 1998a), and comprises rhythmic red-brown and green-grey nannofossil claystones and white nannofossil chalks that are interrupted by a 46 cm, very finely laminated black shale of marine origin (up to 11.5% TOC; Norris, Kroon, Klaus et al. 1998a). Bioturbated intervals indicate periods of benthic activity. They are interspersed with periods of possible anoxia during deposition. Hardgrounds, associated with Mn concentrations, occur below the black shale (at 12X-3, 110 cm; 12X-3, 120 cm; 12X-5, 98 cm). The average sedimentation rate is an apparently low ~6 m/m.y., the site receiving clays and Fe-oxides from land and debris from the platform, along with biogenic material from the water-column (Norris, Kroon, Klaus et al. 1998a).

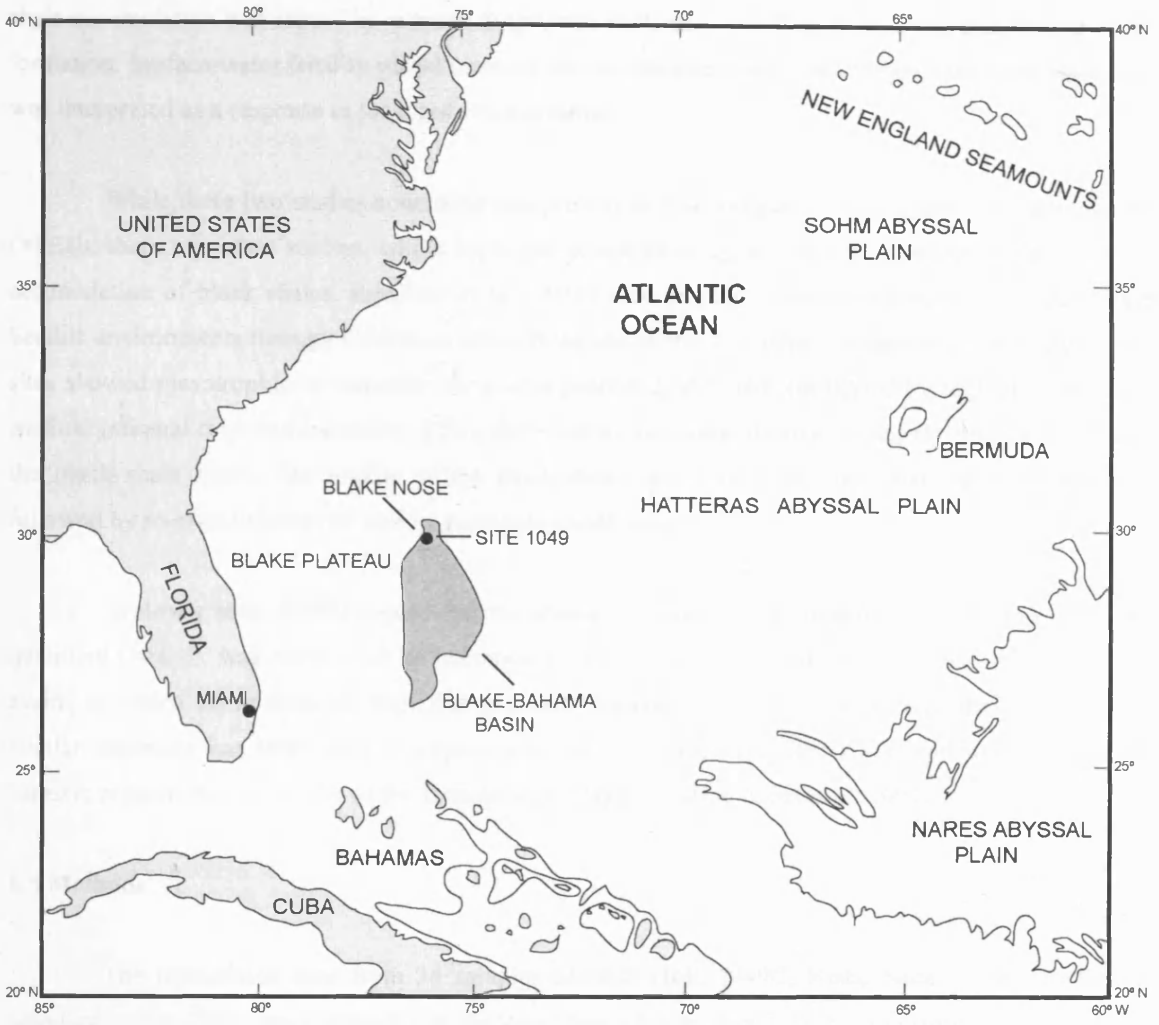

Figure 6.1 Location of ODP Site 1049 in the Blake Nose Plateau of the western Atlantic. Modified after Benson, Sheridan et al. (1978).

6.4 Previous work

Erbacher et al. (2001) analysed $\delta^{13}C$- and $\delta^{18}O$-isotope records on planktonic and benthic foraminifera through the OAE1b black shale interval and suggested that thermohaline stratification (increased temperature, decreased salinity) caused reduced deep-water ventilation, triggering black shale accumulation. Although they inferred a minor increase in primary productivity just prior to black shale deposition, it was not thought to be a primary factor controlling the positive $\delta^{13}C$ excursion. These observations prompted comparisons with the sapropel formation in the Quaternary Mediterranean, and the causal factors of increased runoff during warm periods.

Herrle (2002) presented a comprehensive review of OAE1b, along with an integrated analysis of sedimentological, geochemical and nannoplankton data, using sections from the Vocontian Basin and the central Atlantic. His observations are similar to those of Erbacher et al. (1999) but his causal mechanism for reduced ventilation differs slightly. He suggested that OAE1b deposition was characterised by monsoon-driven surface-water-temperature increases, with attendant humidity increase, and that black

shale accumulation was caused by reduced deep-water ventilation resulting from a decrease in deep-water formation. Surface-water fertility varied between the two sites he studied and through the black shale, and was interpreted as a response to localised wind-systems.

While these two studies concluded that primary productivity was not a controlling factor during OAE1b, there are other studies, which highlight productivity as, at least, a contributing factor to the accumulation of black shales. Erbacher et al. (1999) used benthic foraminiferal ecology to reconstruct benthic environments through OAE1b at Blake Nose and in the Vocontian Trough and concluded that all sites showed mesotrophic to eutrophic conditions preceding the OAE (indicated by high abundances of shallow infaunal taxa and increasing $\delta^{13}C$), followed by eutrophic dysoxic to anoxic conditions through the black shale itself. The middle of the black shale saw a reoxygenation and repopulation event, followed by re-establishment of anoxic, eutrophic conditions.

Bralower et al. (1993) argued that the absence of nannoplankton in many black shale horizons, including OAE1b, was not a result of taphonomic destruction but an indication of short-lived eutrophic events in which nannoplankton were outcompeted by organic-walled plankton, e.g., dinoflagellates. A similar argument has been used to explain extreme, low-diversity coccolith assemblages in the Late Jurassic organic-rich mudrocks of the Kimmeridge Clay Formation (Lees et al. 2004).

6.5 Methods

The nannofossil data from 34 samples of ODP Hole 1049C, Blake Nose, is presented here. Standard smear-slides were prepared in the usual way (see section 3.2). Semi-quantitative nannofossil abundances were estimated, from 142 mbsf (12X-2, 120-121cm) to 148 mbsf (12X-6, 120-121cm), and plotted as a range-chart for biostratigraphy (Table 6.1). The taxonomy generally conforms to that of Bown et al. (1998). The sample interval varied from 50 cm through the succession, down to <1 cm around the geochemical excursions. Relative abundance data was used for palaeoenvironmental interpretation based on 300-specimen counts per sample (see section 3.6.2). Additionally, a few selected taxa were counted over 20 fields of view to compare the % abundance with the absolute abundance data. Nannofossil %-abundances are plotted against sample-depth for taxa that are interpreted as having palaeoenvironmental significance (Figure 6.3). Similarly, per field of view counts of selected taxa, calculated by averaging 20 fields of view, were plotted separately against sample depth to allow a comparison of the abundance trends obtained by the two methods.

6.6 Results

6.6.1 Preservation, diversity and abundance

Thirty-three samples yielded abundant nannofloras (see Table 6.1). One sample within the OAE1b black shale interval (12X-3, 58-58.5 cm) showed low abundance (13 species). Preservation of the

nannofossils was predominantly in the good-moderate category. The assemblage diversity was high, with an overall 102 species identified in the section. The average diversity per sample was ~ 60 species.

6.6.2 Nannofossil biostratigraphy

Shipboard biostratigraphy for this leg was performed on core-catcher samples by Jean Self-Trail and David Watkins (see Norris, Kroon, Klaus et al. 1998a, fig. 13). The shipboard stratigraphy was low in resolution based on a few samples. They applied the CC biozonation of Sissingh (1977), modified by Perch-Nielsen (1985), to the succession, identifying Subzone CC7c (LO *Eprolithus antiquus* to LO *Micrantholithus obtusus*) in Core 12X and Zone CC8 (base = FO of *Prediscosphaera columnata*) in Core 11X. The nannofossil biostratigraphy has been reappraised in this study (Table 6.1) and provides a higher resolution based on more samples. The zonation schemes of Roth (1978), Sissingh (1977) and Bown et al. (1998) have been integrated in the present analysis. The ages provided (Aptian-Early Albian for CC7c and mid-Albian for CC8) follow Sissingh's and Perch-Nielsen's original correlations, which are slightly at variance with those adopted here (see below).

The biostratigraphical zones of Sissingh (1977, modified by Perch-Nielsen 1985) and Roth (1978, modified by Bralower et al. 1993, 1995), and Bown et al. (1998) have been applied to the semi-quantitative nannofossil data. The biostratigraphy of the section is shown in Table 6.1, along with the important events that are summarised on the right-hand side of the table. Samples 148.00 m to 145.89 m are assigned to Zone NC7 (Aptian; = Zone CC7b-e, BC21-22), based on the presence of *Eprolithus floralis* and the absence of *P. columnata*. Subzone NC7C is recognised, its base defined by the FO of *Rhagodiscus achlyostaurion* (at 146.10 m). Subzones NC7A and NC7B, the base of the latter defined by the LO of *Micrantholithus hoschulzii*, could not be differentiated because *M. hoschulzii* ranges here above its expected stratigraphic level, with respect to the FO's of a number of marker taxa (e.g. *Hayesites albiensis*, *P. columnata*). According to Norris, Kroon, Klaus et al. (1998a), there is a hardground between 146.51 m and 146.10 m, i. e., between Zones NC7A-B and NC7C, and so the anomalous presence of micrantholiths is possibly due to reworking. Based on correlations between nannofossil and ammonite biostratigraphies (see Bown et al. 1998, Fig. 5.2), Subzone NC7A-B is Lower to Upper Aptian and Subzone NC7C is Upper Aptian.

Samples 145.59 m to 142.00 m are assigned to Zone NC8 (uppermost Aptian-Lower Albian; = Zone CC8a, BC23), based on the presence of *P. columnata* and the absence of *Tranolithus orionatus*. Subzones NC8A and NC8B can be differentiatied, based on the FO of *H. albiensis* (at 145.00 m). These subzones have been assigned to a stage based on Kennedy et al. (2000). Therein, based on integrated macrofossil/nannofossil biostratigraphy of the proposed boundary stratotype-section at Tartonne (Alpes-de-Haute-Provence, southern France), in which the best marker for the boundary is argued to be the FO of the ammonite *Leymeriella tardefurcata* (Kennedy et al. 2000), the FO of *P. columnata* is in the Late Aptian. Although Bown (*in* Kennedy et al. 2000) did not distinguish between *H. irregularis* and *H.albiensis* in the Tartonne section, Herrle and Mutterlose (2003) show the FO of *H. albiensis* to fall below the FO of *L. tardefurcata* in the Vocontian Basin. Consequently, Subzone NC8A is Late Aptian and NC8B is Late Aptian to Early Albian in age.

ODP 171 B 1049C	SAMPLE	DEPTH (mbsf)	PRESERVATION	NANNOFOSSIL ABUNDANCE/FOV	POSSIBLE ASCIDIAN SPICULES	ABUNDANCE INORGANIC CRYSTALS	SPECIES RICHNESS	TAXON
	12X-2W, 120-121cm	142.00	G	161		R	62	
	12X-3W, 20-21cm	142.50	G	107		R	55	
	12X-3W, 42-43cm	142.72	G	75		R	50	
	12X-3W, 46-46.5cm	142.76	G-M	100		R	55	
	12X-3W, 50-50.5cm	142.80	G	150		R	61	
	12X-3W, 54-54.5cm	142.84	G-M	56		F	50	
	12X-3W, 58-58.5cm	142.88	M	<1		F	13	
	12X-3W, 64-64.5cm	142.94	G	75		R	46	
	12X-3W, 70-70.5cm	143.00	M	22		C	38	
	12X-3W, 74-74.5cm	143.04	M	75		F	33	
	12X-3W, 80-80.5cm	143.10	G	152		F	61	
	12X-3W, 86-86.5cm	143.16	G	126		R	60	
	12X-3W, 90-91cm	143.20	G	152		R	61	
	12X-3W, 120-121cm	143.50	G-M	low		R	30	
	12X-4W, 19-20cm	143.99	G-M	40+		F	66	
	12X-4W, 70-71cm	144.50	G	126		R	63	
	12X-4W, 120-121cm	145.00	G	70		R	57	
	12X-4W, 142-143cm	145.22	G-M	60		R	51	
	12X-4W, 146-147cm	145.26	G-M	65		R	59	
	12X-4W, 147-148cm	145.27	G	60		F	61	
	12X-4W, 148-149cm	145.28	G-M	62		A	61	
	12X-4W, 149-150cm	145.29	G-M	66		C	57	
	12X-5W, 0-1cm	145.30	G-M	69		C	65	
	12X-5W, 19-20cm	145.49	G	67		F	66	
	12X-5W, 20-21cm	145.50	G-M	102		C	59	
	12X-5W, 29-30cm	145.59	G-M	58	C	A	65	
	12X-5W, 59-60cm	145.89	G-M	38	A	A	59	
	12X-5W, 69-70cm	145.99	G-M	60	A	A	58	
	12X-5W, 80-81cm	146.10	G-M	32	A	A	58	
	12X-5W, 121-122cm	146.51	G-M	39	C	A	47	
	12X-5W, 130-131cm	146.60	G-M	17	A	A	51	
	12X-6W, 21-22cm	147.01	M	65	A	F	38	
	12X-6W, 70-71cm	147.50	M	45	A	A	38	
	12X-6W, 120-121cm	148.00	M	51	A	A	34	

Table 6.1 Nannofossil distribution and biostratigraphy of the study section.

DEPTH (mbsf)	148.00	147.50	147.01	146.60	146.51	146.10	145.99	145.89	145.59	145.50	145.49	145.30	145.29	145.28	145.27	145.26	145.22	145.00	144.50	143.99	143.50	143.20	143.16	143.10	143.04	143.00	142.94	142.88	142.84	142.80	142.76	142.72	142.50	142.00
SAMPLE (m)	12X-6W,120-121cm	12X-6W,70-71cm	12X-6W,21-22cm	12X-5W,130-131cm	12X-5W,121-122cm	12X-5W,80-81cm	12X-5W,69-70cm	12X-5W,59-60cm	12X-5W,29-30cm	12X-5W,20-21cm	12X-5W,19-20cm	12X-5W,0-1cm	12X-4W,149-150cm	12X-4W,148-149cm	12X-4W,147-148cm	12X-4W,146-147cm	12X-4W,142-143cm	12X-4W,120-121cm	12X-4W,70-71cm	12X-4W,19-20cm	12X-3W,120-121cm	12X-3W,90-91cm	12X-3W,86-86.5cm	12X-3W,80-80.5cm	12X-3W,74-74.5cm	12X-3W,70-70.5cm	12X-3W,64-64.5cm	12X-3W,58-58.5cm	12X-3W,54-54.5cm	12X-3W,50-50.5cm	12X-3W,46-46.5cm	12X-3W,42-43cm	12X-3W, 20-21cm	12X-2W,120-121cm
STAGE			LR.-UP. APTIAN								UPPER APTIAN																UPPER APTIAN TO LOWER ALBIAN							
NANNOFOSSIL ZONE; Bown *et al.* (1998) - BC					BC 21-22																						BC23							
NANNOFOSSIL ZONE; Roth (1978) & Bralower *et al.* (1993, 1995) - NC			NC7A-B				NC7C						NC8A														NC8B							
NANNOFOSSIL ZONE; Sissingh (1977) & Perch-Nielsen (1985) - CC					CC7b-e																	CC8a												
NANNOFOSSIL & GEOCHEMICAL EVENTS	presence *E. floralis*, *Braarudo.* spp.			FO *R. angustus*	FO *Radiolithus planus*	FO *R. achlyostaurion* hg#1		FO small *P. spinosa*	FO *P. columnata*				nannoconid 'crisis' # 1	13-C and Sr/Ca excursions				FO *H. albiensis*		brief nannoconid resurgence	nannoconid 'crisis' # 2	hg#2, 3					OAE 1b sapropel							absence *Tranolithus orionatus*
Retecapsa crenulata	F	F	R	F	R	F	R	F	F	R	C	F	F	F	F	F	F	F	F	F	R	F	F	R		R	F		R	F	R		F	
Retecapsa cf. *R. ficula*						F		F	F			R																						
Retecapsa surirella	R	F		F	R	F	R	F	F	F	C	R	F	F	F	F	F	F	F	F	R	F	F	R			R		R	F	R	F	F	F
Rhagodiscus achlyostaurion						R	R	R	R	F	R	F		C	F	F	R	F	F	F	R	F	F	F		R	F		F	F	R	F	F	F
Rhagodiscus cf. *R. achlyostaurion*															VR									VR									R	F
Rhagodiscus angustus				F	R	C	R	C	F		C	F	F	C	F	F	R	R	F	C		F	F	F	R	R	F		F	F	F	F	F	F
Rhagodiscus asper	F	F	F	C	F	C	F	C	C	F	C	C	C	C	C	C	C	F	F	F	R	F	F	F	R	R	F	VR	F	F	F	F	F	C
Rhagodiscus asper (large) group	F	F	F	C	F	C	F	C	C	F	C	C	C	C	C	C	C	F	F	F	R	F	F	F		R	F		F	F	F	F	F	F
Rhagodiscus gallagheri				R			F	R	F	F	R	F		R	R	F	F	F	F	F	R	F	F	F	R	R	F		F	F	F	F	F	F
Rhagodiscus hamptonii				R		F	F	F	R	R	R	R							VR	F								VR		R				
Rhagodiscus infinitus						R	R		F	R	F	R		R	F	R	R	R	F	F		VR	F	VR										F
Rhagodiscus splendens																													VR					
Rotelapillus laffittei	F	F	F	C	F	C	F	C	C	F	C	R	C	C	F	C	C	F	F	F	R	F	F	F	F	R	F		F	F	F	F	F	F
Staurolithites gausorhethium																													VR					
Staurolithites glaber			VR				VR																	VR						VR				
Staurolithites mutterlosei	VR		VR	R	VR	F	VR	R	R			R	F	F	R	R	R	R	R				R	VR						VR		VR	R	R
Staurolithites siesseri	C	C	C	C	F	F	F	F	C	F	F	F	C	C	F	C	C	F	F	C	R	F	F	F		R	F		R	F	R	F	R	F
Staurolithites spp.				C	R	C	C	R	F	F	C		C	C	F	C	C	C	F	C			R	R		R			F	F	F	F	F	F
Staurolithites sp. 2 + sp. 3												R							R							R		VR						R
Stoverius achylosus												R	R	F	F	C	C	R	R	F		R	F	R	F		F		R	F			R	F
Stradnerlithus geometricus																						R	F	F							F			
Tegumentum stradneri	F		F	F	F	F	F	F	F	F	F	F	F	F	F	F	F	F	F	F		F	F	R	R	R	R		R	F	R	R	R	F
Tetrapodorhabdus decorus			VR	R	R	R	R	R		R	F	R	VR					R				R		R						R		R	VR	VR
Tranolithus gabalus				F		C	F	C	C	F	C	C	C	R	R	R		R		C	R	R												
Tranolithus minimus																		R																
Tranolithus simplex															R	F	R		F			R		F			R		R	F	R	R	F	R
Tubodiscus burnettiae	R	R	R	F	F	F	F	F	F	F	R	R	R	R	R	F	R	F	R	F	R	R	F	F	R	R	R		R	F	R	F	R	R
Watznaueria barnesiae	A	A	A	C	C	A	C	A	A	C	A	A	A	A	A	A	A	A	C	C	C	A	A	C	F	F	C	R	C	A	C	C	A	A
Watznaueria biporta	F	F	F		F	R	F	F	F	F	F	F	F	F	C	F	F	F	F	F	R	F	F	F	R	R	R		R		F	F	F	F
Watznaueria britannica	F	F	F	F	R	F	F	F	F	F	F	F	F	F	F	F	F	F	F	F		F	R	F	R		R		R	F	F	R	R	R
Watznaueria fossacincta	C	C	C	F	C	F	C	F	F	C	C	F	C	C	C	C	A	C	C	F	F	C	C	C	R	F	F	VR	F	C	C	C	C	C
Watznaueria manivitiae	C	F	A	C	F	C	F	C	C	F	C	A	C	C	F	C	C	F	F	C	F	C	C	F	F	F	F	VR	F	F	F	C	C	F
Watznaueria ovata	R	R		R			R		R	R			R	R	F	F	F	R	R	R		R	R	R	VR				R		R	R		F
Zeugrhabdotus bicrescenticus					R	F	F	R	F	R	R				R			R	R	F		R	R											R
Zeugrhabdotus diplogrammus	R	F	F	F	R	F	F	F	F	F	F	R	R	F	R	F	R	F	R	F	R	R	F		F	R	R		F	F	R	F	F	F
Zeugrhabdotus embergeri	F	F	R	F	R	R	F	R	R	F	F	C	R	F	F	F	F	F	F	F	R	F	F	F	R	R	F	VR	R	F	F	F	F	F
Zeugrhabdotus cf. *Z. embergeri* (small form)		VR				F				R	R			R		R			R	F		R	R			R	R		R					
Zeugrhabdotus embergeri(side-view)	F									R				F	F	F	F	F	F			F	F	R			R		R	F	F			R
Zeugrhabdotus howei	R	F	F	F	R	F	F	F	F	R	C	F	F	F	F	C	C	C	F	F		F	F	R	R	R	R		F	R	R	F	F	F
Zeugrhabdotus noeliae	F	F	F	C	C	C	C	C	A	C	A	A	A	A	C	A	A	A	A	C	F	A	A	A	F	C	A	R	C	A	A	A	A	A
Zeugrhbdotus streetiae																			R	R			R	R	VR		R	VR	R	VR	R			VR
Zeugrhabdotus xenotus							R			F	R	R	F	R					F	F	VR	R	F	F	VR		R		R	F	R	R		

The two hardgrounds in Subzone NC8B, between 143.50 m and 143.20 m, are below the resolution recognisable by the standard biozones and hence do not affect the biostratigraphy of the section.

6.6.3 Geochemical data

There are two significant negative $\delta^{13}C$-isotope (bulk carbonate, 63-150 μm) excursions in the studied section (Fig. 6.2). As bulk $\delta^{13}C$-isotope data through the OAE1b black shale could not be obtained, due to the carbonate-free nature of the sediment, the planktonic foraminifera-derived data of Erbacher et al. (2001) has been included, in order to show the nature of the excursion, which is referred to here as Excursion 2 (base of black shale). The lower excursion, referred to here as Excursion 1, lies ~2.08 m below the base of the black shale (at 145.28 m) and was reported by Gröcke et al. (2002) as coincident with a substantial (0.6‰), positive Sr/Ca ratio shift in the bulk nannofossil size-fraction (<63 μm) and a noticeable sediment-colour change. The details of these data will be presented elsewhere (Gröcke, personal communication) but the Sr/Ca signal is thought to indicate increased productivity in the nannoplankton (Stoll & Schrag 2001).

Below Excursion 1, $\delta^{13}C$ is relatively stable at values of ~3-4‰. Excursion 1 involves a shift of ~2‰. Between Excursions 1 and 2, values remain lower at 1.5-3‰. Above the black shale, values are further reduced to between 1.5 and 2‰.

$\delta^{18}O$-isotopes (bulk carbonate, 63-150 μm) show a slight positive shift at both excursions (Fig. 6.2). Below Excursion 1, values are relatively stable, above 0. Between Excursions 1 and 2, values are below 0, dipping immediately above Excursion 1, then steadily increasing above that, to dip again just below the black shale. Values above the black shale are <-1‰. In terms of temperature, this signal equates to a stable ~10°C below Excursion 1, increasing to around 14°C around the excursion, dipping just above the excursion but then stabilising at ~12-15°C up to the black shale. Temperature peaks immediately above the black shale at ~18°C, before dropping back to ~15°C.

6.6.4 Quantitative nannofossil palaeoenvironmental proxy data

6.6.4.1 Diversity Indices (Figure 6.2)

Nannofloral preservation is moderate to good in the material studied (the sediments having been only shallowly buried and remaining poorly-lithified; Norris, Kroon, Klaus et al. 1998b), and relatively

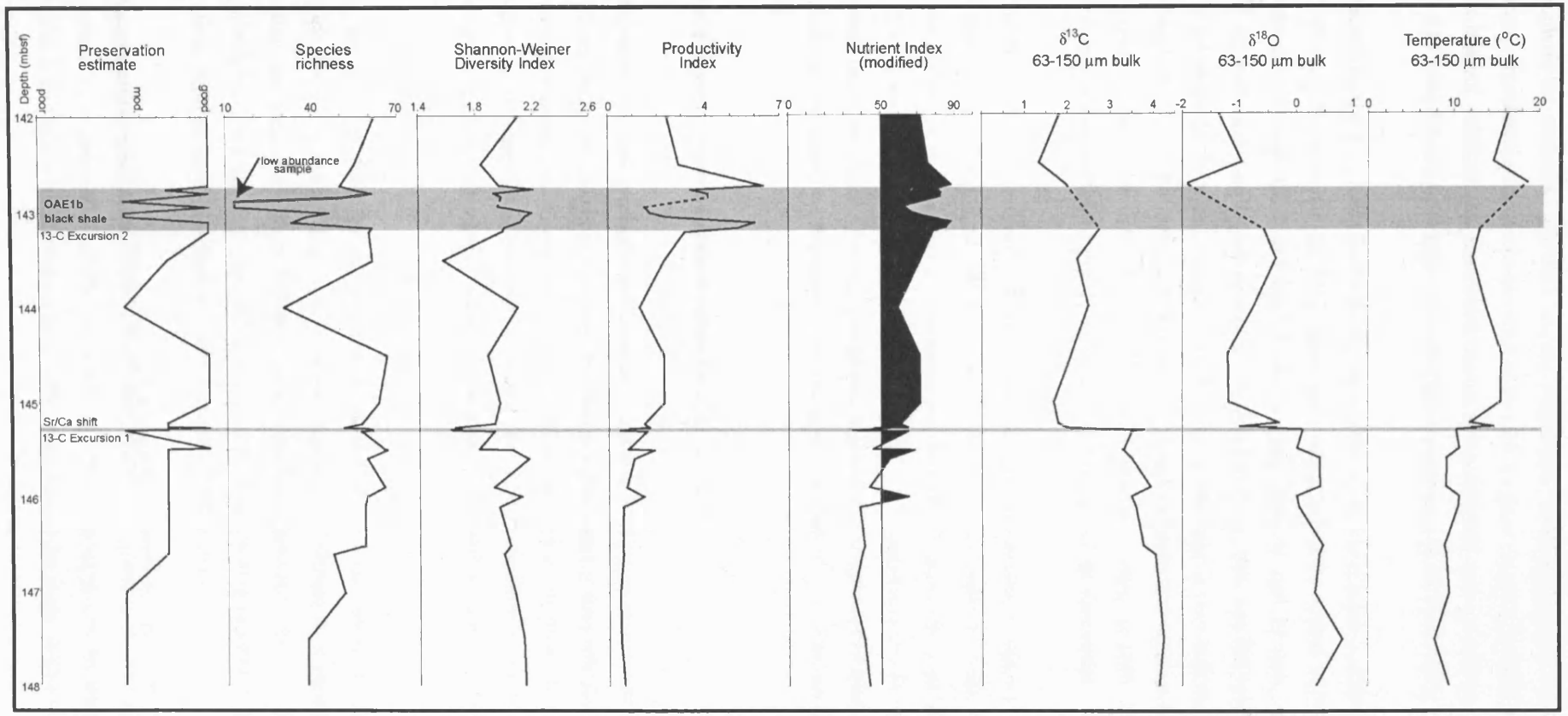

Figure 6.2 Geochemical (oxygen and carbon isotopes) and diversity indices (species richness and Shannon's index) used in palaeoceanographic interpretation of the OAE1b in the western Atlantic. Dashed lines in the isotope curves indicate carbonate-free nature of the sediment with no isotope data.

stable throughout the examined sequence, except, predictably, in the black shale interval. Consequently, the nannofossil abundance data can be assumed to provide a robust record of relative nannofloral change through this interval. Additionally, the overall species richness for the interval (102 taxa) is comparable to that determined from the coeval OAE1b (Niveau Paquier) sequence in SE France (121 taxa; Herrle 2002).

Species richness varied from 13 around the middle of the black shale (142.88 m) to 66 (at 143.99 m and 145.49 m, ~79 cm below the black shale and ~21cm below Excursion 1 respectively). Species richness increased through the lower half of the section, from 34 and 65 taxa, dropped slightly at Excursion 1 but had recovered to previous peak levels at 143.99 m. This was followed by a drop ~0.3 m below the black shale (to 30 taxa), a recovery (to 61 taxa) at the base of the black shale, and a reduction within the black shale (142.88 m) to a minimum of 13 taxa. Richness had recovered to pre-black shale levels (61 taxa) towards the end of the black shale interval, falling slightly as the black shale accumulation terminated and then rising again to 62 taxa at the top of the succession.

The Shannon-Weiner Diversity Index indicates a gradual decline in nannofossil diversity from the base of the studied section to 145.89 m. In the ~60 cm below Excursion 1, diversity peaks to 2.1 and then dips sharply at the excursion (1.6). Pre-excursion diversity is gradually re-established, peaking at 143.99 m (2.1). It then decreases sharply, reaching a value of 1.6 approximately 30 cm below the black shale. Through the black shale, diversity is relatively high (>2.0), dropping off slightly on termination of the black shale accumulation but beginning to climb again after that (to 2.1). The raw data is presented in Appendix 3.

6.6.4.2 % abundance trends of nannofossil proxies (Figure 6.3)

Biscutum constans gradually increases in abundance leading up to Excursion 1 (from 8-16%), declines ~22 cm below the excursion, recovers but then declines again at the excursion (down to ~8%). It rapidly becomes re-established above the excursion (<20%), declines at 143.99 m (12%), then rising to an acme of ~23% at the base of the black shale. Within the shale, it declines, recovers, but then declines again when black shale accumulation ceased. From here it increases to values >15% at the top of the section.

In the interval below Excursion 1, *Zeugrhabdotus noeliae* shows a gradual increase in abundance (9-29%) with a sharp drop to 15% below Excursion 1, followed by a rapid rise to 27 % at the excursion. Between Excursion 1 and the black shale, it fluctuates between ~20-30%, declining at 143.99 m (21%). Within the black shale, it rises, declines, then recovers, reaching an acme of >40% immediately above the shale, from which it falls back to ~30% at the top of the section.

Discorhabdus ignotus has a more fluctuating record compared to *Z. noeliae* and *B. constans*. Below Excursion 1, it varies from ~2-9%, but falling to ~1% at the excursion. Between Excursion 1 and the black shale, it shows a gradual increase up to ~8% at the base of the shale. Within the shale, it peaks

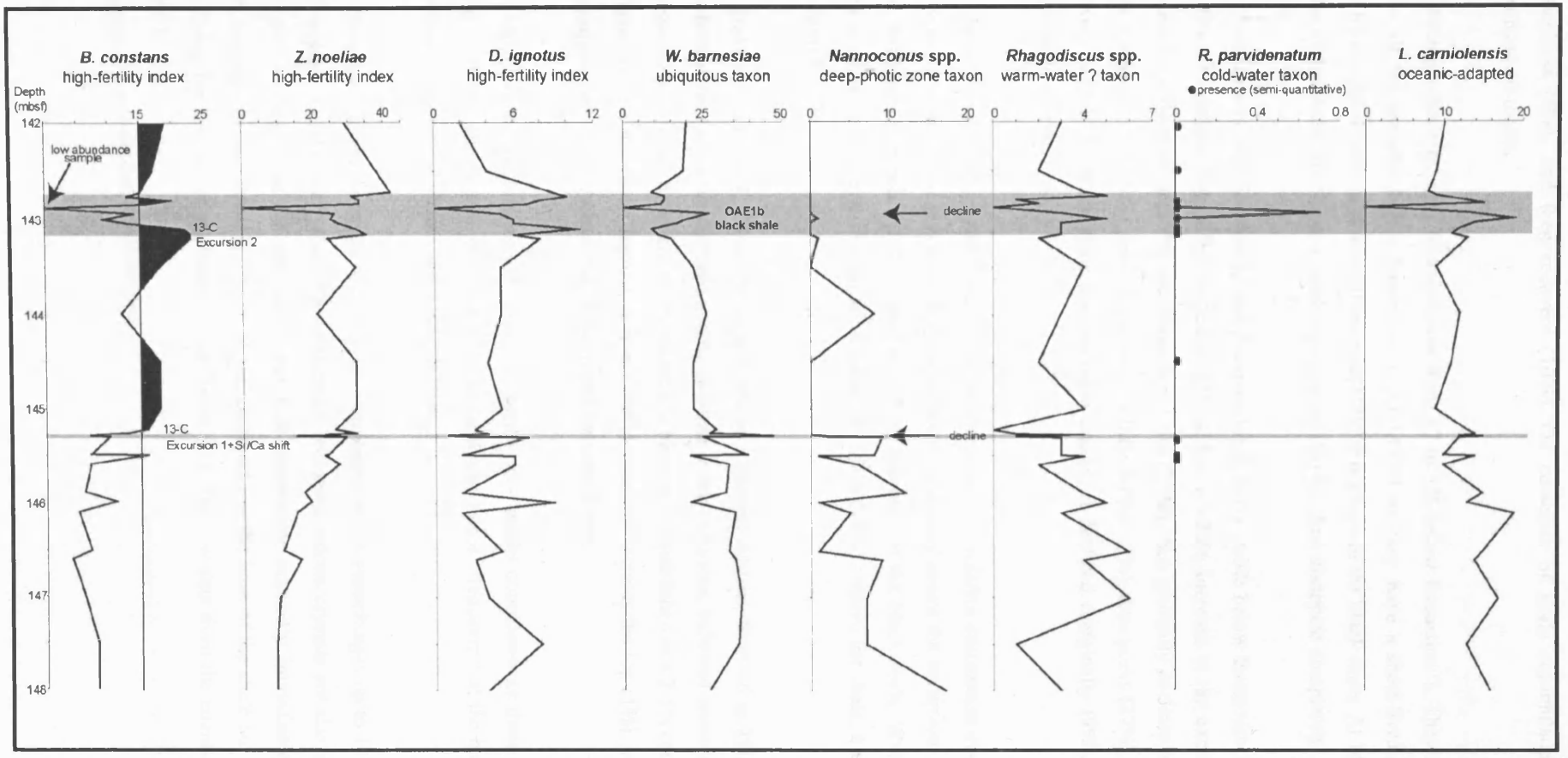

Figure 6.3 % abundance trends of taxa used in palaeoceanographic interpretation of the OAE1b in the western Atlantic.

(11%), declines (5%), and then recovers (10%). On cessation of shale accumulation, it gradually decreases from 10 to 2%.

Nannoconus spp. vary in abundance from 17 to 1% below Excursion 1. They are consistently present in all the samples below Excursion 1. At 143.99 m, they have a short-lived recovery (8%), followed by a rapid decline, and a small increase (1%) at the base of the black shale. At 143.00 m, around the middle of the shale, they have a small resurgence (1%) but then disappear completely.

Watznaueria spp. (*barnesiae* and *fossacincta*) is fairly stable below Excursion 1, varying from ~20 to 40%. It declines below the excursion (25%), has a >20% increase at the excursion, followed immediately by a sharp drop (27%), an insignificant rise (29%), then gradually declines towards the base of the black shale (15%). In the shale, it decreases a little further (9%), then peaks (27%), declines (12%) and recovers (13%). As black shale accumulation ceased, it declined marginally (9%), followed by a rapid increase to ~20%.

Below Excursion 1, *Lithraphidites carniolensis* shows a relative decrease in abundance, falling from 16% to 12% at the excursion, then rising again immediately above the excursion. From this level (14%), it fluctuates between 9-12%, rising to 13% at the base of the black shale. Within the shale, it fluctuates between 9-19% and rises to an acme at 143.00 m (19%). Above the shale, it shows a gradual increase from 8-10%.

Below Excursion 1, *Rhagodiscus* spp. shows a general decline, from ~6 to 2%. It stabilised at ~3% just below the excursion, suffered a ~2% decrease at the excursion, followed immediately by a ~3% increase and then decrease down to 0%. From here, it became re-established as a 2-5% component of the assemblages. Within the shale interval, it rises (2-5%), declines towards the top (1%), and then rises as shale accumulation ceased. Above this, it fluctuates between 2-4%.

Although *Repagulum parvidentatum* is only a very minor component of these assemblages, it does have a ~0.7% peak within the shale interval, and was found 'frequently' at the base of the shale. *Seribiscutum primitivum* is absent in the assemblages.

Possible ascidian spicules form a large component of the assemblages up to 145.59 m (~31cm below Excursion 1), at which point they disappear. Inorganic calcite crystals are also abundant below Excursion 1, increasing at the excursion, but then decreasing markedly immediately above. They gradually increase in abundance up to the shale, decreasing at the base of the shale but then increasing and stabilising for the rest of the interval (see Table 6.1). The raw data from the counts is presented in Appendix 3.

6.6.4.3 Absolute abundance (20 fields of view counts)

The absolute abundance counts are in good agreement with the percentage abundance dataset. The highest and lowest abundances in the trends of the major taxa, e.g., *B. constans*, *Z. noeliae*, *Watznaueria* spp. and *Nannoconus* spp. are found in or around the same samples in both datasets. The variability in the two datasets is minor.

6.6.4.4 Multispecies Nutrient Indices

The multispecies nutrient index of Herrle (2002), modified herein (Chapter 5, section 5.9.6) was used to estimate the fertility levels of the assemblages through the section. The productivity index (Gale et al. 2000) was also calculated for a comparison (Fig. 6.2).

Below Excursion 1, the nutrient index fluctuates between values of 35 and 65%. There is a decrease in productivity at the excursion (46%), followed by a gradual increase up to the base of the black shale (79%). The values rise within the black shale reaching a peak value of 88 in the lower part of the black shale (143.10 m). From here, the index declines (to 63%) at 142.94 m, and then rises again to reach another peak (88%) at 142.72 m, immediately above the black shale. The index reaches a value of 71% at the top of the section.

6.7 Discussion

6.7.1 Correlation of the Blake Nose section and missing time (Figure 6.4)

According to the compiled stratigraphic column of Herrle (2002, fig. 16), showing the distribution of the Vocontian Basin Aptian-Albian black shales, the Niveau Paquier (equated to OAE1b by Herrle, 2002) lies in Nannofossil Subzone NC8B and the Niveau Kilian in Subzone NC8A (both Paquier and Kilian lying within the *Hedbergella planispira* Planktonic Foraminfer Biozone). The OAE1b black shale at Blake Nose falls within Biozone NC8B and is therefore directly correlatable with the Niveau Paquier. The level of the Sr/Ca and $\delta^{13}C$-isotope excursions identified by Gröcke et al. (2002) fall within the Subzone NC8A, and so are biostratigraphically most closely correlatable to the Niveau Kilian $\delta^{13}C$-isotope excursion. Furthermore, the level of the FO of *Prediscosphaera columnata* (base Zone NC8A) has consistently been recorded above the level of the Jacob but beneath the level of the Kilian (Bown *in* Kennedy et al. 2000; Herrle 2002). This implies that Kilian is a widespread event, but for some reason, this was not expressed as black shale accumulation at Blake Nose.

No absolute time-scale correlation is attempted with the data presented here. There are numerous visible hard grounds in the Blake Nose succession, which suggest condensed sedimentation or missing sediment (and time), and indeed the sequence is significantly condensed compared to the Vocontian succession. From the Vocontian sequence, it can be seen that the base of the Kilian is ~48.2 m below the

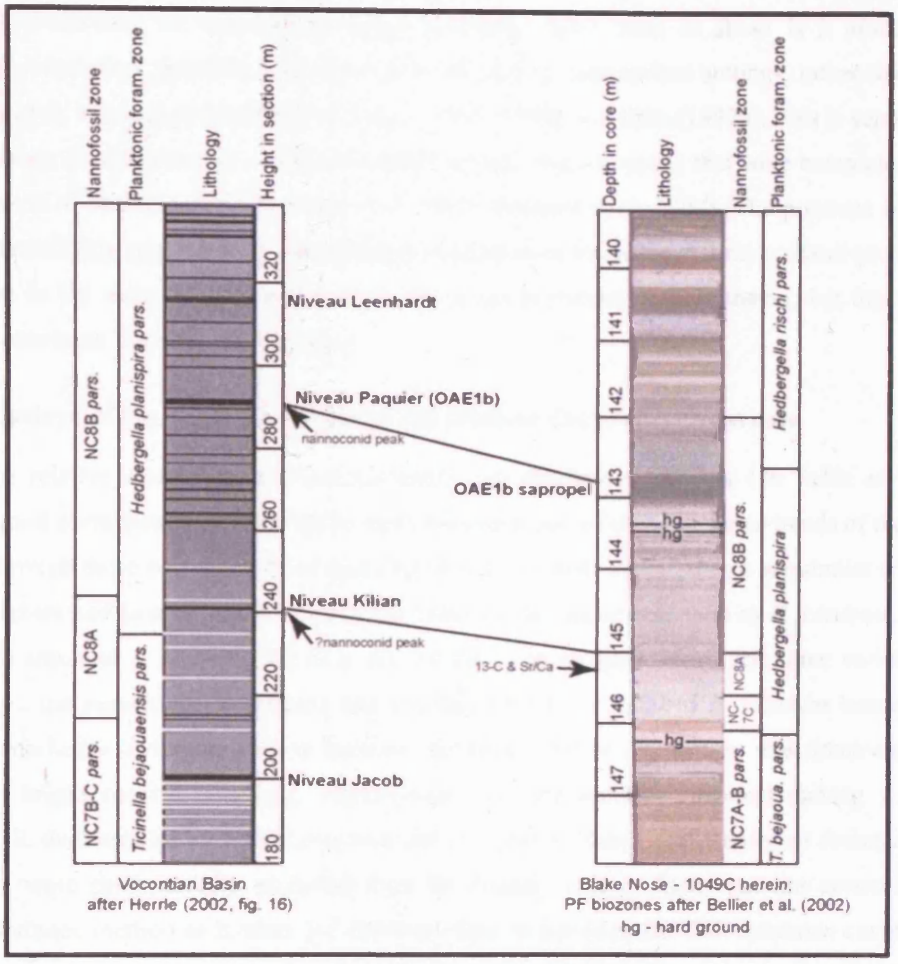

Figure 6.4 Correlation of the Blake Nose and Vocontian Basin succession with respect to the Niveau Kilian and the Niveau Paquier (OAE1b) sapropels.

base of the Paquier (Herrle 2002, fig. 16). According to Herrle, this represents ~1.3 m.y., based on a sedimentation rate of ~3.7 cm/kyr (Herrle 2002, p. 60). At Blake Nose, the 'Kilian' excursion and the base of OAE1b are ~2.08 m apart. For 1.3 m.y. to have elapsed, the sedimentation rate would have to be of the order of ~0.16 cm/kyr or 1.6 m/m.y. However, this is at odds with the calculated sedimentation rate of 0.6 cm/kyr or 6 m/m.y. (Norris, Kroon, Klaus et al. 1998b), which suggests that 953.3 kyr are missing from the succession at Hole 1049C during this measured interval!

Using $^{87}Sr/^{86}Sr$-isotopes, Gröcke (personal communication) has calculated a 90 kyr sediment gap around the 'Kilian' excursions in Hole 1049C, although they have determined that this does not entirely account for the size of the excursions. The discussion of the Sr data is beyond the scope of this chapter, however, details are available with Darren Gröcke.

6.7.2 Preservation

Preservation of nannofossils in the section is presented qualitatively in Table 6.1 and depicted graphically in Figure 6.2. The preservation values are comparable throughout, indicating that sample-to-sample abundance comparisons should be robust. The only exception to this is the sample at 142.88 m (12X-3W, 58-58.5 cm) within the black shale interval, which shows much poorer preservation and

etching, and therefore abundance values should be treated with caution. It is believed that etching and in some cases destruction of nannofossil calcite in black shales such as these is a product of post-depositional dissolution, possibly related to CCD shoaling in appropriate settings, rather than a primary ecological signal, as suggested by Bralower et al. (1993, 1994) and Erba (1992a). This is supported by the recent discovery of alkenones in comparable OAE1a black shale deposits that were completely carbonate free and barren of nannofossils (Bralower et al. 2002; Brassell et al. 2004). The presence of alkenones, which are exclusively generated by haptophytes, is conclusive evidence that nannofossil-producing algae were present in the water column and contributed to the preserved organic matter, but that their calcite tests have since been lost due to dissolution.

6.7.3 Comparison of the relative abundance and absolute abundance count data

The relative abundance (percentage-based) and absolute abundance (20 fields of view) count data show good correspondence with each other. A comparison of the abundance trends of the major taxa generated through these two methods of counting shows that their overall trends are similar (Figs. 6.5 and 6.6). The highest and lowest abundances in the trends of the major taxa such as *B. constans*, *D. ignotus*, *Watznaueria* spp. and *Z. noeliae*, fall in or around the same samples. However, some variations can be observed e.g., the percentage abundance and absolute abundance trend of *B. constans* between 146 and 148 m are markedly different. This is because the lower part of the section was dominated by large, chunky and bright nannofossils (e.g., *Nannoconus*, possible ascidian spicules) making it difficult to identify small, dark species such as *B.constans* and *D. ignotus*. Hence in the absolute abundance method, smaller taxa were preferentially excluded from the counts. This problem was not encountered in the relative abundance method as it takes 3-5 fields-of-view to complete the 300-specimen count. The small and dark taxa are easily picked up by choosing favourable fields of view in this method. Therefore a possible limitation of the absolute abundance method is that small and dark taxa such as *B. constans*, *D. ignotus* and *R. parvidentatum*, etc. are excluded from the dataset, particularly in fields-of-view dominated by chunky and bright nannofossils.

Both datasets have their advantages and disadvantages with respect to the interpretation of palaeoenvironments. The percentage abundance data accurately represents relative changes in the nannofossil assemblage composition through time. However, it suffers from closed-sum effects, i.e., the variability in the percentage of a taxon is influenced by other taxa in the assemblage. Such interdependence of percentages must be taken into account whilst interpreting the data.

Absolute abundance has the advantage of providing vital clues to sedimentological parameters in addition to the nannofloral changes, such as sedimentation rate (higher numbers represent higher rates of sedimentation) and carbonate dilution in an assemblage (high input of detrital material normally results in lower numbers of nannofossils). Closed-sum effects do not influence it as percentages are not involved, but sedimentation rates have a direct influence on absolute abundance data. Relative abundance data has been used to interpret the palaeoenvironment in this study, whereas absolute counts were performed only to verify whether they are in agreement with the percentage data or not. Both methods have their inherent advantages, although percentage abundance is preferred because it is faster and easily reproducible.

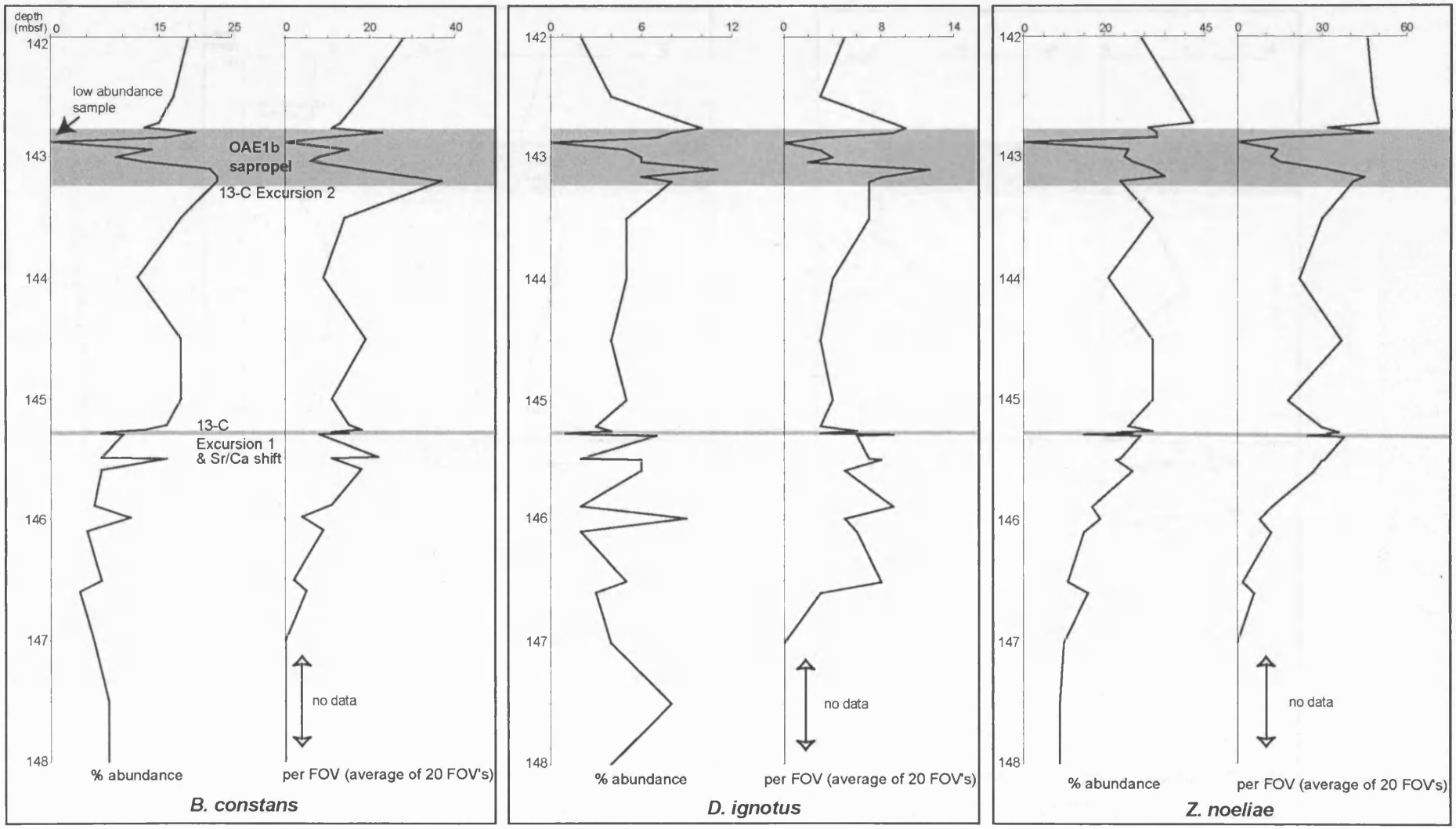

Figure 6.5 Comparison between % abundance and absolute abundance trends of (i) *B.constans*, (ii) *D. ignotus* and (iii) *Z. noeliae* in the Blake Nose section.

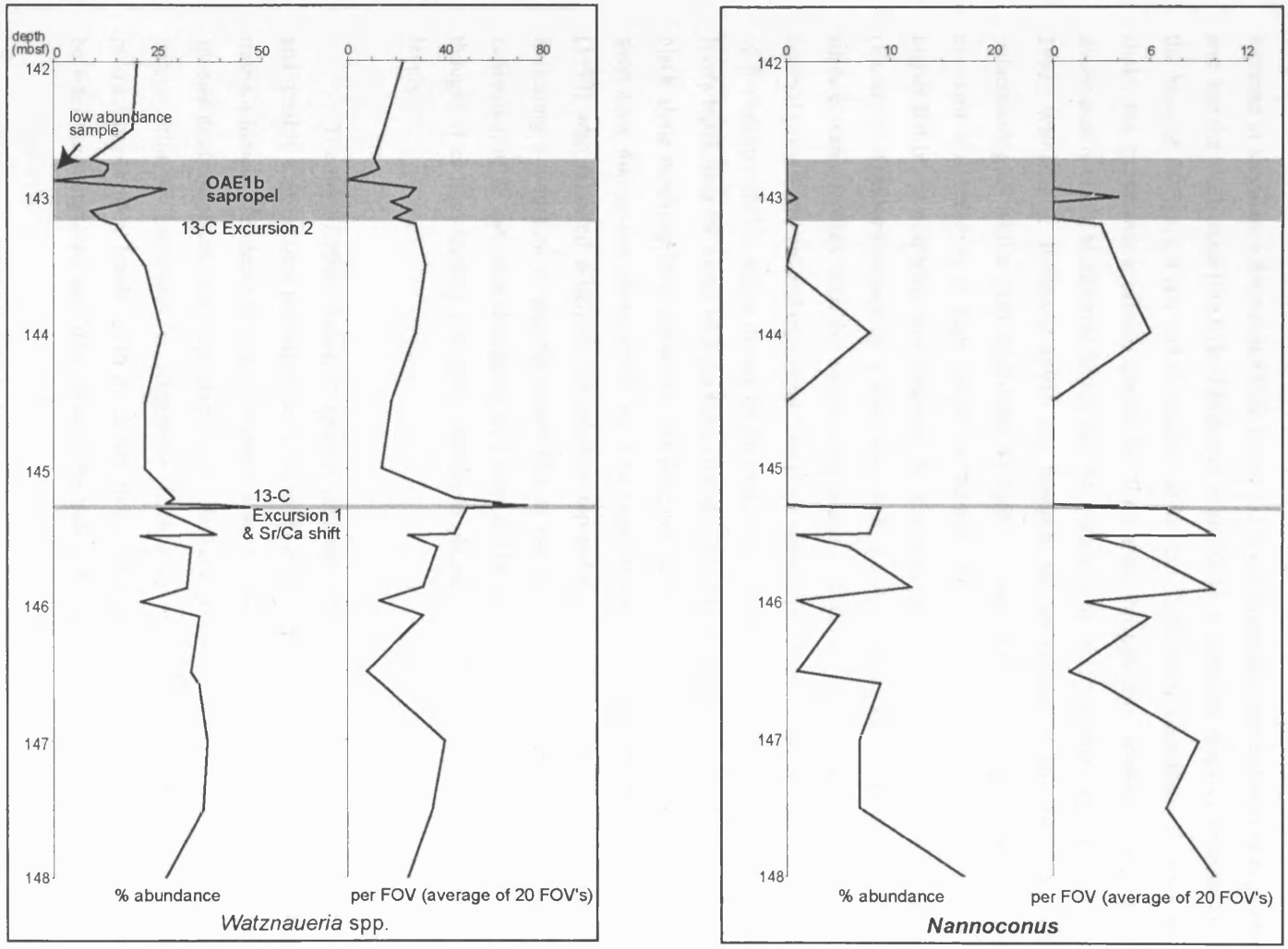

Figure 6.6 Comparison between % abundance and absolute abundance trends of (i) *Watznaueria* spp. and (ii) *Nannoconus* spp. in the Blake Nose section.

6.7.4 The Blake Nose palaeoenvironment using nannofossil and geochemical proxies

The combination of single-species proxies, multispecies nutrient indices and diversity indices provides a relatively coherent picture of the surface-water environments through the two geochemical excursions that were the focus of this study. The high-fertility indices, *Z. noeliae* and *B.constans*, both increase in abundance from around 2m below the lower excursion, and continue at high abundances up to and into the black shale (OAE1b of Erbacher et al. 2001). *B. constans* displays an abundance maximum at the base of the black shale and *Z. noeliae* at the top. Both show abundance declines within the black shale, but preservation effects cannot be discounted through this interval. The two species display abundance maxima at different levels, but this conforms to previous observations (e. g. Roth 1981; Erba 1992; Williams & Bralower 1995) and supports the interpretation that they had slightly different palaeoecologies whilst both responded to high nutrient conditions. Erba (1992b) suggested that *B. constans* was sensitive to high fertility in mesotrophic environments and *Z. noeliae* was an index of higher fertility in eutrophic environments. Such an interpretation would indicate that the lower excursion (Excursion 1), characterised by a sharp rise in *B. constans*, is associated with a significant increase in surface water fertility into the mesotrophic range, and this was maintained through the much of the interval prior to the second excursion. The black shale interval is marked at its base by maximum values of *B. constans* (23%), and at the top by the peak values of *Z. noeliae* (42%), suggesting increasing trophic levels bracketing the event with the most eutrophic conditions at the top. Both species decline within the black shale reaching their abundance minima, indicating that surface water productivity declined for a short time during this event (OAE1b). This observation correlates with the results of Erbacher et al. (1999) who reported a benthic foraminifera repopulation event within the 1049 OAE1b black shale, indicating a reduction of organic matter flux to the sea floor following the intial eutrophic event. The calibration of *B. constans* abundance by Fisher & Hay (1999) suggests levels greater than 15% may be thought of as high fertility and such a threshold places much of the section above Excursion 1 at these levels.

The third fertility-index, *D. ignotus*, although rarer in this material, displays comparable trends, and notably a abundance maximum at the base (8%) and top of the black shale (10%). The multispecies nutrient indices (Productivity Index; Nutrient Index), which primarily utilise the abundance values of the species describe above, not surprisingly show similar trends, but highlights the considerable variation in values prior to Excursion 1, suggesting fluctuating surface water environments and specifically productivity/fertility levels. Both the productivity index and the nutrient index show a gradual increase between the excursions, and high values at the base and top of the black shale.

Watznuaeria spp., which is often negatively correlated with the fertility indices, shows a gradual decline through most of the study interval, but displays considerable variation prior to Excursion 1, and a short-lived peak within the black shale. The dominant presence of *Watznaueria* spp. in all the samples (9-47%) leads to the conclusion that it is a ubiquitous Mesozoic taxon present in all environmental settings irrespective of the fertility level of the water column. The same conclusion was drawn from its abundance

in the Gault Clay section (see section 5.9.5, Chapter 5) and is in agreement with the recent findings of Lees et al. (2004).

Nannoconus, which is interpreted here as indicative of deep nutricline conditions based on a study by Erba (1994), is relatively abundant prior to Excursion 1, but with fluctuating abundance, and it declines to 1% at the excursion itself. This distribution suggests that surface water environments were fluctuating prior to the Excursion 1 but nevertheless represented a productive environment for this lower photic zone nannoplankton, most likely beneath stratified and oligotrophic surface waters. This environment disappeared above Excursion 1, replaced by meso-eutrophic surface waters and stratification breakdown. Nannoconids occur in three higher samples, abundantly at 143.99 m, and rarely at the base and in the middle of the black shale. These occurrences indicate the periodic return of stratified, less eutrophic conditions, and concur with the fertility indices and benthic foraminiferal data of Erbacher et al. (1999).

Nannoconid 'acmes' associated with OAE1b black shales have been recorded in the Vocontian Basin, in the Niveau Paquier (Bréhéret 1983; Bréhéret et al. 1986; Bown *in* Kennedy et al. 2000; Herrle 2002; Nagai et al. 2002) and Niveau Kilian (Nagai et al. 2002) and are regionally correlatable events (Bréhéret et al. 1986). The striking decline of *Nannoconus* at Excursion 1 strongly suggests the onset of more eutrophic conditions, and supports the increasing productivity model for both of these excursions. A comparable nannoconid record has been reported from widespread sites prior to OAE 1a (Erba 1994) with the decline termed the 'nannoconid crisis'. Leckie et al. (2002) suggested that a second nannoconid 'mini-crisis' similarly marked the onset of OAE1b, just prior to the black shale they interpreted as Niveau Jacob, and coincident with the extinction of the planktonic foraminfer *Planomalina cheniourensis* and the FO of *Prediscosphaera columnata*. Re-correlation of Leckie et al.'s (2002) data suggests that the onset of their OAE1b actually lies at the level of the Kilian rather than Jacob, taking into consideration that Bralower et al. (1993, fig. 2) showed that the LO of *P. cheniourensis* and the FO of *P. columnata* occurred almost coincidentally in the Late Aptian, and that the FO of the latter has been shown to lie above the Jacob but below the Kilian (Bown in Kennedy et al. 2000; Herrle 2002; herein). The nannoconid 'mini-crisis' event is reported at the level of the FO of *P. columnata* according to Leckie et al. (2002) and is therefore almost certainly correlatable to decline recorded in this study at Excursion 1. Mutterlose (1989, 1991), Erba (1994) and Herrle & Mutterlose (2003) have all noted a nannoconid acme interval of Late Aptian age, and Herrle & Mutterlose (2003) have named the termination of this event nannoconid crisis II, although they recorded consistent occurrences a considerable distance above their 'event', with a more striking near-disappearance coincident with the FO of *P. columnata*, at a level more likely to represent the 'mini-crisis' of Leckie et al. (2002).

While Leckie et al. (2002) conjectured that this nannoconid decline is part of a far-reaching calcareous plankton turnover, it should be noted that nannoconids have been recorded abundantly, albeit, short-lived, in the Niveau Paquier (Bréhéret 1983; Bréhéret et al. 1986; Bown *in* Kennedy et al. 2000; Herrle 2002; Nagai et al. 2002).

The putative warm-water species, *Rhagodiscus asper*, shows a very low abundance in the sample material and therefore it was combined with other species of the same genus (e.g., *R. angustus* and *R. achlyostaurion*) to provide a % abundance trend. However, *Rhagodiscus* spp. is variable throughout the interval (0-6%) and shows no unequivocal trends. An overall decline in its abundance precedes Excursion 1, with lowest values at and just above the excursion. Values rise above the excursion but fall at the base, in the middle, and above the black shale. These trends do not conform to earlier interpretations, which have associated warming events with OAE1b (Erbacher et al. 2001; Herrle 2002), although interpretation of the $\delta^{18}O$-isotope records are problematical and require the invocation of salinity variations (see discussion in Erbacher et al. 2001). However, the trend of *Rhagodiscus* spp. suggests that it may have been controlled by fertility, especially lower fertility conditions observed below Excursion 1. Of the two most widely recognised Cretaceous cool-water taxa, *Seribiscutum primitivum* is absent, and *Repagulum parvidentatum* is only rarely present, but notably occurs just prior to Excursion 1, and in the lower half of and above the black shale. It is most abundant at the base of the black shale. The distribution of this taxon is an indication that cooling was associated with both excursions at Site 1049.

The fluctuations in the abundance of *Lithraphidites carniolensis* are difficult to interpret in this section. Its % abundance shows a series of fluctuations (between 8-19%) throughout the section, which do not correlate with either of the excursions, or with other significant taxa. The maximum abundance of the taxon is noted twice, below Excursion 1 and within the black shale interval. The minimum abundance of the species is noted above the black shale interval towards the top of the section. *L. carniolensis* is interpreted as an oceanic-adapted taxon in this thesis, as it is significantly more abundant in open-ocean settings (Pacific Ocean, see Chapter 7). The abundance of *L. carniolensis* can reach up to 40% in such settings (Site 1207/1213, ODP Leg 198), which is clearly not the case in the Blake Nose section where the maximum abundance of the taxon is 19%. This suggests a proximal setting for the Blake Nose site. The presence of *Nannoconus*, a predominantly shelf-inhabiting taxon, in the section also supports this interpretation.

The Shannon-Weiner Diversity Index shows declining values across Excursion 1, supporting the interpretation of increasing nutrients and exploitation by fewer, opportunistic taxa. Values decline sharply at 143.50 m just below the black shale suggesting a higher productivity assemblage, but values within the black shale are relatively high, suggesting more stable environments.

In summary (Figure 6.7), there is a broad indication of increasing fertility from 146.60 m to the top of the black shale, with notably high values from Excursion 1 up section. Most of the indices fluctuate significantly prior to Excursion 1. The sharp increase in *B. constans* at Excursion 1, followed by consistently higher values suggests a switch to higher productivity surface waters, and is supported by the disappearance of *Nannoconus* and rises in *Z. noeliae* and *D. ignotus*. The interval between the two excursions has high values of the fertility indicators with lower values at 143.99 m, accompanied by a nannoconid spike, suggesting the temporary return of oligotrophic, stratified waters. The black shale interval is preceded by low diversity values and marked at the base by sharp increases in multispecies nutrient indices and high fertility species abundances (*B. constans*, *Z. noeliae*, *D. ignotus*).

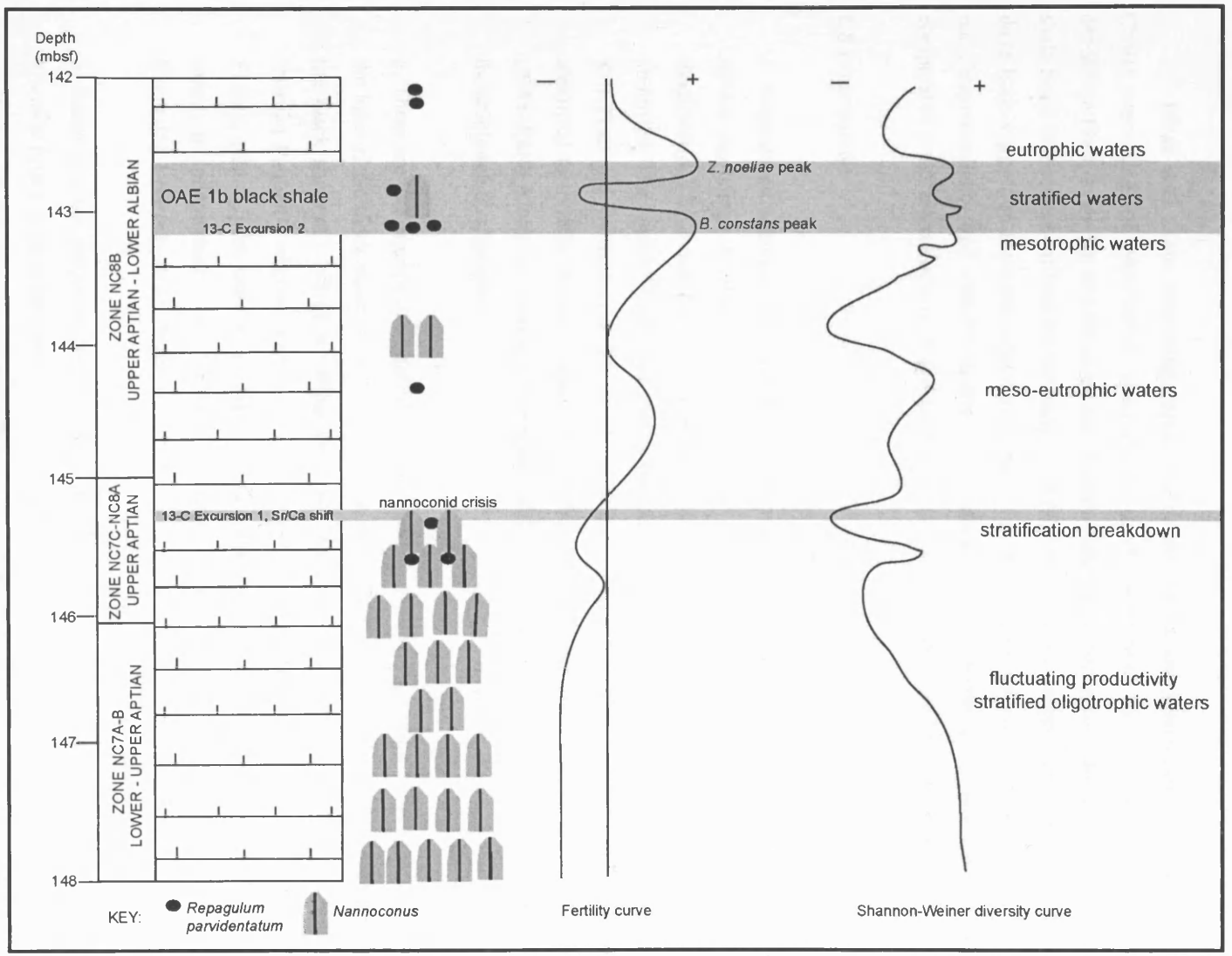

Figure 6.7 Summary diagram showing changes in important taxa along with productivity and diversity trends during the Late Aptian-Early Albian interval in the Blake Nose section.

A marked decline in these proxies along with high Shannon-Weiner values and a minor rise in *Nannoconus* indicate the re-establishment of more stable stratified environments within the black shale. The top of the black shale witnesses a sharp rise of all the high fertility indices and a possible indication of highest productivity, shown by peak *Z. noeliae* abundances (>40%) immediately above the black shale. The cold-water proxy, *R. parvidentatum*, is not very clear but may be interpreted as showing temperature decreases prior to both excursions.

These data show interesting parallels with the results and interpretations of Erbacher et al. (2001) supporting the observation of increasing productivity prior to and early in the black shale deposition (their event II), and the existence of more stable, stratified waters, during the deposition of the shale itself. We cannot confirm the warming event they postulate, as our proxies are not entirely clear and there is no suggestion from the nannofossils that there were significant variations in salinity. The results correlate remarkably well with the benthic foraminiferal results presented by Erbacher et al. (1999) with comparable peaks in productivity at the base and top of the black shale (OAE1b event).

6.8 Conclusions

1. Nannofossil Subzones NC7A-B to NC8B have been recognised giving an Early Aptian to Early Albian age range to this section. Equivalent Subzones CC7b-e to CC8a (Sissingh 1977; with modifications by Perch-Nielsen 1985) and Zones BC21-22 to BC23 (Bown et al. 1998) were also identified. The biostratigraphy has been reappraised in this study and is at slight variance with that of Self-Trail and Watkins (see Norris, Kroon, Klaus et al. 1998a, fig. 13). The OAE1b black shale identified by Norris, Kroon, Klaus et al. (1998a) and Erbacher et al. (2001), falls within Subzone CC8a (Early Albian) according to this study rather than Subzone CC7c (Late Aptian) as suggested by the shipboard stratigraphy.

2. There are two significant, negative $\delta^{13}C$-isotope excursions, Excursion 1, that lies ~2.08 m below the base of the black shale at 145.28 m (Gröcke et al. 2002), and Excursion 2, that lies at the base of the black shale at ~143.20 m (Erbacher et al. 2001). The OAE1b black shale is coeval with the 'Niveau Paquier', whereas Excursion 1 is almost certainly coeval with the 'Niveau Kilian' of SE France, although the latter is not expressed as black shales at Blake Nose. A striking shift in Sr/Ca ratios, an independent proxy for nannoplankton productivity (Stoll and Schrag 2001) is noted at Excursion 1 (Gröcke et al. 2002).

3. Based on a correlation of the Blake Nose with the Vocontian Basin succession, a ~953.3 kyr-long hiatus is found to exist between the 'Kilian' and the 'Paquier' events in the studied section. This was calculated on the basis of sedimentation rates of both these sections (Norris, Kroon, Klaus et al. 1998a; Herrle 2002).

4. Nannofossil results (single-species proxies, multispecies nutrient indices and Shannon-Weiner diversity index) coupled with geochemical data (δ^{13}C-isotope and Sr/Ca excursion) support the increased productivity model for the OAE1b at Blake Nose. Increasing productivity proxy values are observed from Excursion 1 up section, with peaks at the base (>20% *B. constans*) and top (>40% *Z. noeliae*) of the black shale. The deposition of the black shale was characterised by more stable stratified waters, evidenced by a marked decline in the productivity proxies, a minor rise in *Nannoconus*, along with high Shannon-Weiner values. This is in good agreement with Erbacher et al. (1999, 2001).

5. The striking decline of *Nannoconus* spp. at Excursion 1 in the Late Aptian correlates to the nannoconid 'mini-crisis' event of Leckie et al. (2002) and the nannoconid crisis II of Herrle & Mutterlose (2003).

6. Palaeotemperature data, based on δ^{18}O-isotope and the nannofossil proxies, *Rhagodiscus* spp. and *Repagulum parvidentatum* are not entirely clear. However, *R. parvidentatum*, which occurs just prior to Excursion 1, and at the base of the black shale (where it is most abundant), possibly suggests cooling pulses prior to both the excursions. This, if true, is at variance with the interpretations of Erbacher et al. (2001) and Herrle (2002), both of which suggest warming events associated with OAE 1b.

7. The relative abundance and the absolute abundance method of counting gave similar results. The overall similarity in the abundance trends of the major taxa implies that the palaeoenvironmental interpretation of nannofloral changes in this section is unlikely to have been influenced by the counting technique. However, a combination of both quantitative datasets is perhaps, ideal for obtaining a fuller understanding of the palaeoenvironment.

Chapter 7. Leg 198, Shatsky Rise, northwest Pacific

Abstract

This study assesses nannofossil productivity during the Early Aptian OAE1a and Early Albian OAE1b at Shatsky Rise in the northwest Pacific (Leg 198, Sites 1207 and 1213). A variation in the expression of these two mid-Cretaceous OAE's is noted at Shatsky Rise. Whilst OAE1a is represented by black shale sediments, OAE1b is devoid of black shale deposits and is characterised by siliceous sediments. Both OAE1a and OAE1b are marked by resistivity peaks in response to the chert-rich sediments that are thought to represent enhanced primary siliceous productivity in the Pacific (Robinson et al. 2004). The nannofossil record shows a marked temporal variation in the abundance trends of the productivity indicators. While all the productivity-related taxa (*Biscutum constans*, *Zeugrhabdotus noeliae* and *Discorhabdus ignotus*) are nearly absent in the OAE1a samples, they are present in relatively high numbers (2-13%) in the OAE1b-equivalent samples. This variation is attributed to differences in the scale and extent of submarine volcanism in the Pacific during the OAE1a and OAE1b intervals.

Similar values of Shannon's diversity and equitability from four coeval Early Albian sections, suggest that the palaeoequatorial Pacific may not have been a zone of long-term high productivity as suggested by the radiolarian-sourced cherts. The interpretation of chert as a high productivity proxy in the Cretaceous Pacific is therefore doubtful. The Late Albian is marked by sharp increases in the percentage abundance of *Biscutum constans* (up to 40%) in the Pacific and other coeval sections. It is hypothesised that this increase in *B. constans* may be evolutionary, rather than suggesting an increase in fertility levels globally. The mid-ocean Pacific assemblages are characterised by some features that differentiate them from shelf assemblages. These include the increased abundances of *Lithraphidites carniolensis*, *Hayesites irregularis* and *Watznaueria* spp., and the near absence of neritic taxa such as *Nannoconus* and *Braarudosphaera*.

7.1 Aims

The aims of this study were as follows:

1. To investigate the nannofossil record in samples encompassing the OAE1a and OAE1b intervals at Shatsky Rise (Sites 1207 and 1213).

2. To study the record of nannofossil productivity indicators during the OAE1a and OAE1b at Sites 1207 and 1213.

7.2 Introduction

Mid-Cretaceous nannofossil assemblages have been studied quantitatively in the last two decades to understand the dominant controls on nannoplankton productivity. These studies were pioneered by Peter

Roth and his co-workers (e.g., Roth 1981; Roth and Bowdler 1981; Roth and Krumbach 1986), and developed by Watkins (1986, 1989) and Erba (Erba 1992a, b; Erba et al. 1992; Erba 1994). The recently drilled Cretaceous sections from Leg 198 of the ODP to Shatsky Rise in the northwest Pacific Ocean offer an excellent opportunity to enhance our understanding of the palaeoequatorial Pacific palaeoceanography. Despite very poor recovery due to abundant chert, small samples of Cretaceous sediments drilled at Sites 1207 and 1213 contain relatively well-preserved assemblages of calcareous nannofossils spanning the early to mid-Cretaceous (Barremian-Cenomanian) interval.

Robinson et al. (2004) have recently investigated the Aptian-Albian depositional history for Shatsky Rise based on integration of geophysical logs with sedimentological, biostratigraphical and physical properties data from the poorly recovered chert-rich sequences at Sites 1207 and 1213. They observed that the sections included not only the black shale deposits of OAE1a, but also siliceous rich intervals that represent OAE1b. The study here is intended to follow up on their research by analysing the distribution of productivity-related nannofossil taxa (*Biscutum constans*, *Zeugrhadotus noeliae* and *Discorhabus ignotus*) in samples encompassing the OAE1a and OAE1b intervals at Shatsky Rise.

The OAE1a in the early Aptian was one of the global OAE's, and is expressed as organic-carbon-rich deposits in all marine depositional settings, irrespective of facies control, palaeolatitude or palaeowater depth (Leckie et al. 2002). Explanations of the causal mechanisms of such black shale deposits range between the two end members of increased primary productivity (e.g., Arthur et al. 1990; Erba 1994; Larson and Erba 1999; Leckie et al. 2002) and enhanced preservation of organic matter due to anoxia (e.g., Bralower & Thierstein 1984; Erbacher et al. 2001; Herrle 2003). However, global explanations invoking large-scale volcanicity and tectonism, as well as localised causal factors such as terrestrial input, stratification and mixing, have also been postulated. At Shatsky Rise, OAE1a is represented by black shale sediments that show a rise in resistivity values at the Sites 1207 and 1213.

Prior to Leg 198, early Aptian black shale records had been reported from a few other localities in the Pacific such as Sites 167, 305, 317, 463 and 866 (Winterer et al. 1973; Sliter 1989; Bralower et al. 1993; Jenkyns 1995; Jenkyns & Wilson 1999). However, quantitative nannofossil studies have not been carried out on material from these sites except Site 463 in the Mid-Pacific Mountains (Roth 1981). In addition, early Aptian sediments recovered from Sites 800, 801 and 802 (Leg 129, western Pacific) have also yielded quantitative nannofossil data (Erba 1992b).

OAE1b has generally been interpreted as a regional early Albian event, shown by a series of multiple black shale horizons in the Tethyan and Atlantic sections (e.g., Bréhéret 1983; Arthur et al. 1990; Bralower et al. 1993; Erbacher et al. 1998, 2001; Kennedy et al. 2000; Leckie et al. 2002; Herrle 2002). The first documentation of OAE1b in the Pacific Ocean is reported by Robinson et al. (2004) from Shatsky Rise, ODP Leg 198. However, OAE1b is not represented by black shale sediments, but rather siliceous sediments that are thought to represent enhanced surface water productivity. The OAE1b

sediments also show resistivity 'highs' at Sites 1207 and 1213. The marked variation in the expression of the two mid-Cretaceous OAE's in the Pacific provides the rationale for this investigation.

7.3 Previous work

The first truly pelagic organic-rich sediments from the Cretaceous were recovered during deep sea drilling in the Pacific, sparking interest and ultimately leading to the concept and theory of oceanic anoxic events (Schlanger & Jenkyns 1976). Subsequent work by Schlanger on Pacific volcanism allowed a deeper understanding of the palaeoceanography of that region (e.g., Schlanger et al. 1981). However, the understanding of mid-Cretaceous Pacific palaeoceanography leaves much to be desired owing to poor recovery of pelagic sequences, which are dominated by chert.

Quantitative mid-Cretaceous nannofossil studies were carried out by Roth (1981) on DSDP material (Sites 463, 464, 465 and 466) from the Mid-Pacific mountains and Hess Rise, where he inferred the presence of an equatorial divergence zone based on abundance patterns of *B. constans* and *Z. erectus* (= *Z. noeliae*). He noted that *B. constans* was more abundant in the tropical Pacific than it was along the eastern margin of the Atlantic. *Z. noeliae* showed a more or less similar level of abundance in the Pacific as in the Atlantic. Erba (1992b) carried out a quantitative investigation of nannofossils on material from the Sites 800, 801 and 802 (Leg 129), located south of Shatsky Rise in the Pacific. Her study utilised the potential of planktonic microfossils (nannofossils and radiolaria) to trace plate motions with respect to the palaeoequator. She noted that increases in abundances of *B. constans* and *Z. noeliae* corresponded with increases in radiolarians as sites moved closer to the equator (10-5°S), and argued that at palaeolatitudes of approximately 2°S (in the core of the upwelling zone), nannofossils were outcompeted and completely replaced by radiolarians.

7.4 Study sections

Shatsky Rise is a medium-sized large igneous province (LIP) in the northwest Pacific Ocean (Figure 7.1). The origins of the Shatsky Rise LIP can be traced back to the Tithonian-Valanginian (Early Cretaceous), due to episodic submarine volcanic eruptions at a hotspot triple junction. The volcanic activity resulted in three distinct highs on Shatsky Rise, called the Northern, Central and Southern Highs. The pelagic sediments overlying the volcanic basement range in age from the Early Cretaceous to the Recent. The palaeolatitudinal setting of Shatsky Rise during the early to mid-Cretaceous was largely restricted to the palaeoequatorial belt (0–20°N/S) (Bralower et al. 2002; Robinson et al. 2004).

Samples from two sites, 1207 and 1213, were analysed for this study. Site 1207 (37°47′N, 162°4′E) is the northernmost site in the Shatsky transect, lying 5° north of the sites of the Southern High (Figure 7.1). The site is located in lower bathyal water depth (3103 m) and recovered a late Barremian to Holocene section. Recovery was excellent in the late Campanian to Holocene section, but poor in the late Barremian to early Campanian, where chert layers were very common. Two holes, 1207A and

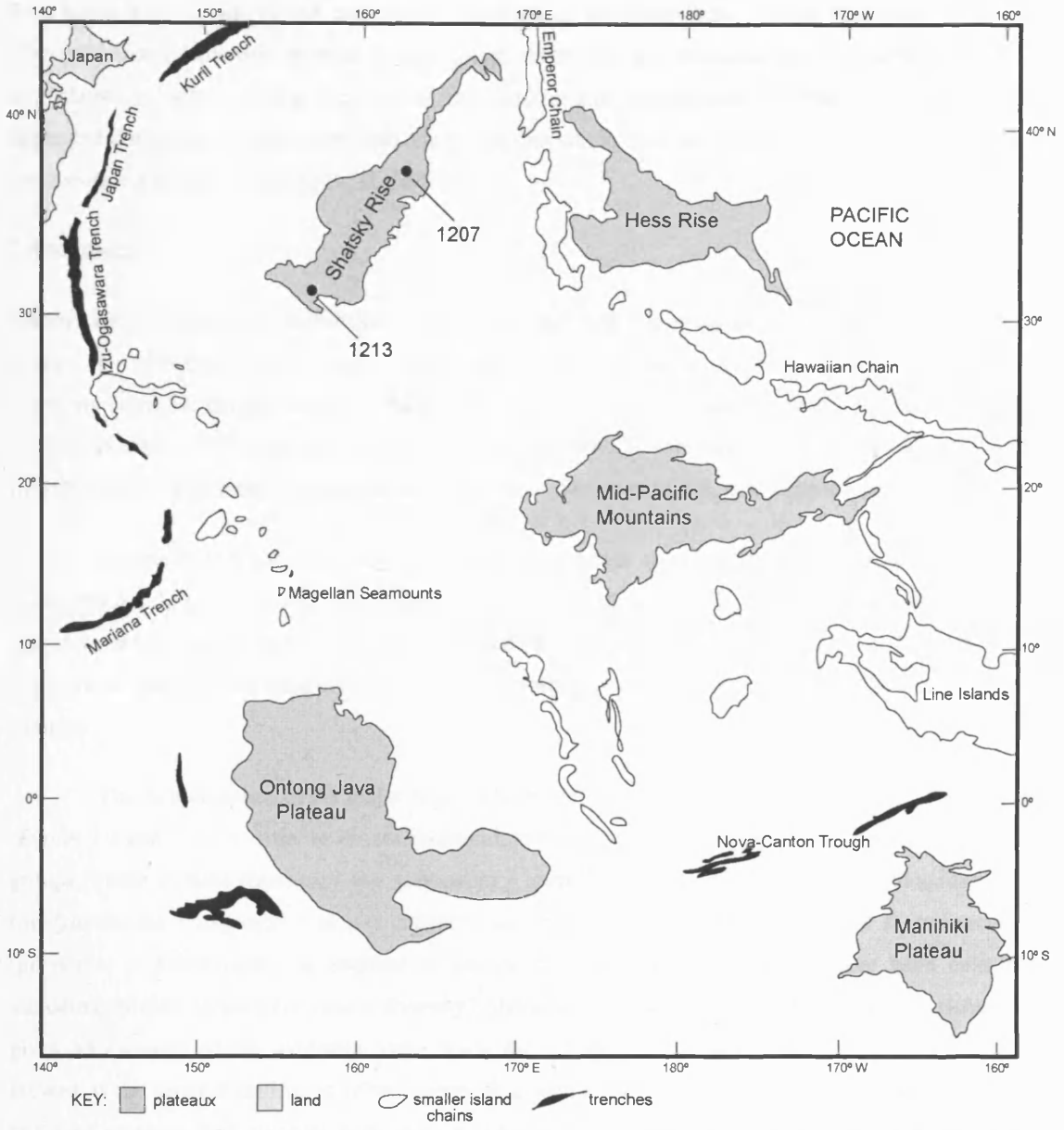

Figure 7.1 Present-day location of Shatsky Rise Sites 1207 and 1213 in the northwest Pacific Ocean. Modified after Kelley (2003).

1207B were drilled at this site. The lithology in the Cretaceous part of the section comprises nannofossil oozes with common chert layers. The occurrence of common chert from the early Campanian to the base of the hole suggests that the site remained within the equatorial divergence zone from the Aptian until the early Campanian. An early Aptian C_{org}-rich claystone horizon, which is considered to be the equivalent of the Selli horizon deposited during the OAE1a, was recovered from this site (Bralower et al. 2002). However, there is no evidence of organic carbon accumulation during the early Albian OAE1b anywhere on Shatsky Rise (Robinson et al. 2004).

Site 1213 (31°34′N, 157°17′E) is the southernmost and deepest site on the Shatsky Rise transect, located in lower bathyal (3883 m) water depth on the southern flank of the Southern High. The main objective of drilling this site was to core a relatively deepwater mid- and Lower Cretaceous sequence.

Two holes were cored, 1213A and 1213B, the base of the latter being earliest Berriasian in age. The lithologic units of this site are more diverse compared to 1207 and comprise chert, porcellanite, limestone and claystone with variable amounts of radiolarians and nannofossils in them. C_{org}-rich sediments deposited during the OAE1a were recovered from this site in Core 1213B-8R. The two sites are ~900 km apart from each other (Bralower et al. 2002).

7.5 Methods

Sample choice was totally controlled by core recovery and the presence of favourable lithologies. In general, small samples were scraped from vugs in chert pieces at an interval of 9-10 m. However, relatively complete sample sets are available through the interval of interest with good recovery around OAE1a. A total of 37 samples were analysed quantitatively, 21 samples from Site 1207 and 16 samples from Site 1213. The sample spacing is, on an average, one per core, i.e., one sample every 9 m.

Standard 300+ specimen counts were used to generate quantitative nannofossil data (see Chapter 3, section 3.6.2, 3.6.3). Smear slides were used to carry out the counts. The evaluation of preservation was done while logging the slides (prior to counting) and all the samples were evaluated to be in the moderate to good (M-G) category. Preservation of nannofossils was found to be largely consistent in the samples.

The % abundance of the major taxa (>2%) is plotted against depth to show the abundance trends (Figure 7.2 and 7.4). In order to ensure taxonomic consistency, certain species were merged into generic groups. These include *Retecapsa* spp. (*crenulata* + *surirella* + small *Retecapsa* rims), *Rhagodiscus* spp. (*achlyostaurion* + *angustus* + *asper*), *Staurolithites* spp. (*siesseri* + small forms) and *Watznaueria* spp. (*barnesiae* + *fossacincta*). In addition to abundance trends, diversity indices have been calculated, including species richness (or simple diversity), Shannon's diversity and equitability. Species richness (S) gives an estimate of the available niche space for the phytoplankton community. Equitability (E) is viewed as the relative utilisation of the energy flux within the ecosystem. Shannon's diversity (H) is an unbiased measure that involves both species richness and equitability. These diversity indices give an idea of the stability of the photic zone where the phytoplankton community lived and also the distribution of nutrients that were available for these communities. They allow a direct comparison of samples independently. A more detailed discussion of these indices can be found in Watkins (1989) and Fisher and Hay (1999).

7.6 Results

7.6.1 Preservation, abundance and diversity

7.6.1.1 Section 1207B

All twenty-one samples yielded abundant nannofossils. An overall 135 species were identified in the section, with an average diversity of ~41 species per sample. Preservation of the nannofossils was predominantly in the moderate-good (M-G) category.

7.6.1.2 Section 1213A-B

Fifteen samples yielded abundant nannofossils. One sample (198-1213B-8R-1, 3 cm) showed moderate abundance, with a low diversity of 13 species in the sample. An overall 146 species were identified in the section, with an average diversity of ~37 species per sample. Preservation was predominantly in the moderate-good (M-G) category.

7.6.2 Biostratigraphy

The biostratigraphic framework of the two sections, 1207B and 1213A-B is summarised briefly here. The NC zones/subzones of Roth (1978, 1983), Bralower (1987), Bralower et al. (1993) and the UC zones of Burnett (1998) have been applied to the sections. Accordingly, section 198-1207B-45R through 24R ranges from Subzone NC5d/e to Zones UC1-2 (Late Barremian to Early Cenomanian). Samples 198-1213B-9R-1, 17-18 cm through 198-1213A-9R CC range from Zones NC6 to UC2 (Early Aptian to Early Cenomanian). Range charts are presented in Appendix 4 (Chart 22, 23); age-depth plots and summary diagrams can be found in Bown (*in press*).

7.6.3 % abundance and diversity indices

The nannofossil abundance in both sections is uniformly high and the overall preservation is moderate to good (M-G). Since dissolution, etching or overgrowth is not observed in any of the samples, they are suitable for generating count data. *Watznueria* spp., *B. constans* and *Z. noeliae* are the dominating taxa that show wide fluctuations (0-50%) in both sections. Their abundance variations are documented for the OAE1a and OAE1b. The other abundant taxa are *Discorhabdus ignotus, Lithraphidites carniolensis, Hayesites irregularis, Retecapsa* spp. and *Rhagodiscus* spp.

7.6.3.1 Section 1207B (Figures 7.2 and 7.3)

The OAE1a sample counted is 198-1207B-44R-CCi, falling within Nannofossil Zone NC6. This sample is closest to the black shales, which are barren of nannofossils. Five samples (198-1207B-38R through 34R) encompass the OAE1b (Subzone NC8A-B) in this section. The abundance record of the productivity-related taxa are described first, followed by other abundant taxa and the diversity indices.

B. constans, ranging between 0 and 48% in the section, is absent in the OAE1a sample. It is low in abundance during the OAE1b interval, varying between 4-9%. *Z. noeliae*, ranging between 0 and 17% in the section, is present at very low levels (2%) in the OAE1a sample. In the OAE1b interval, the taxon

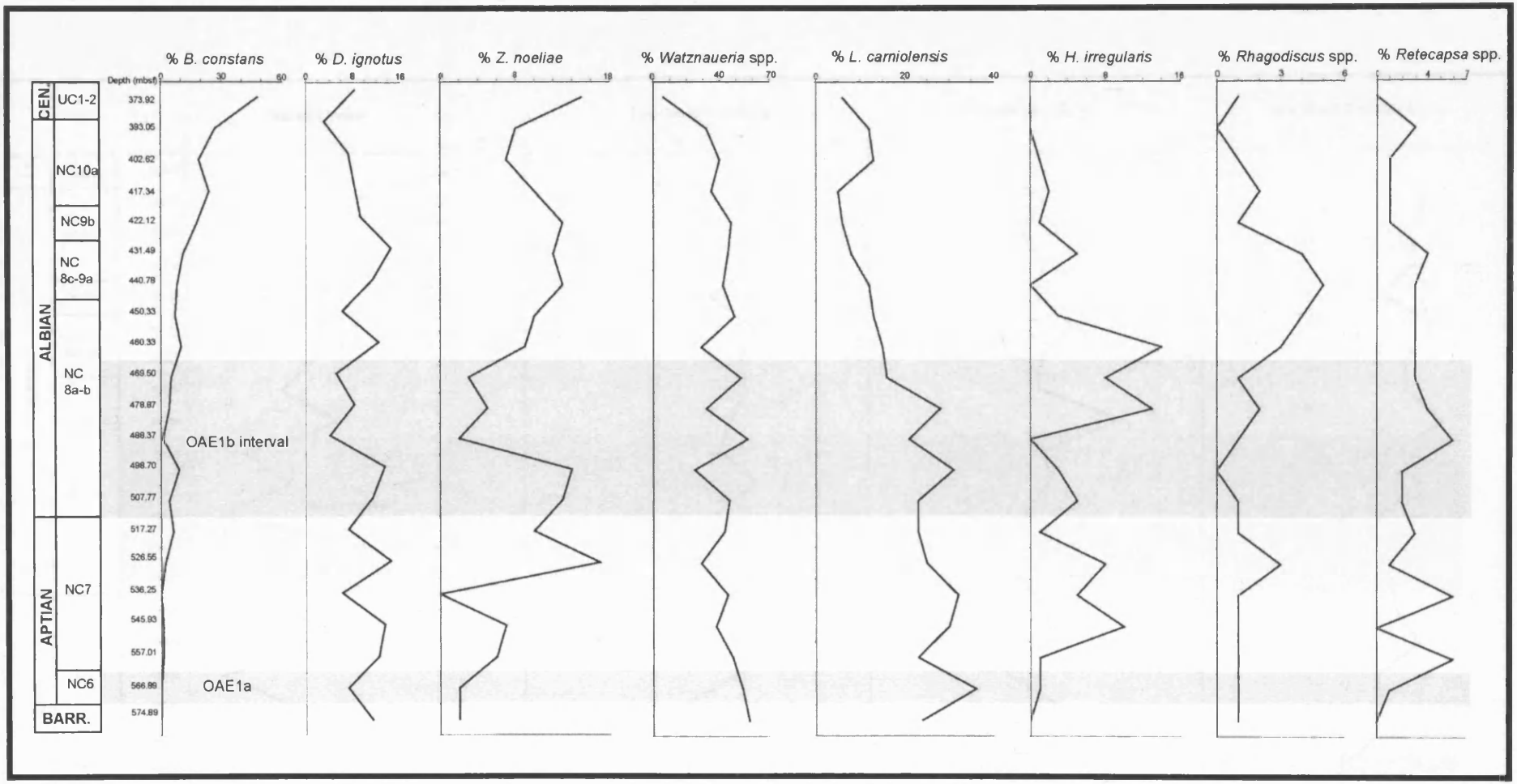

Figure 7.2 Variations in the % abundances of major nannofossil taxa during the mid-Cretaceous at Shatsky Rise, 198-1207B. Both OAE1a and OAE1b intervals are marked by resistivity peaks (Robinson et al. 2004).

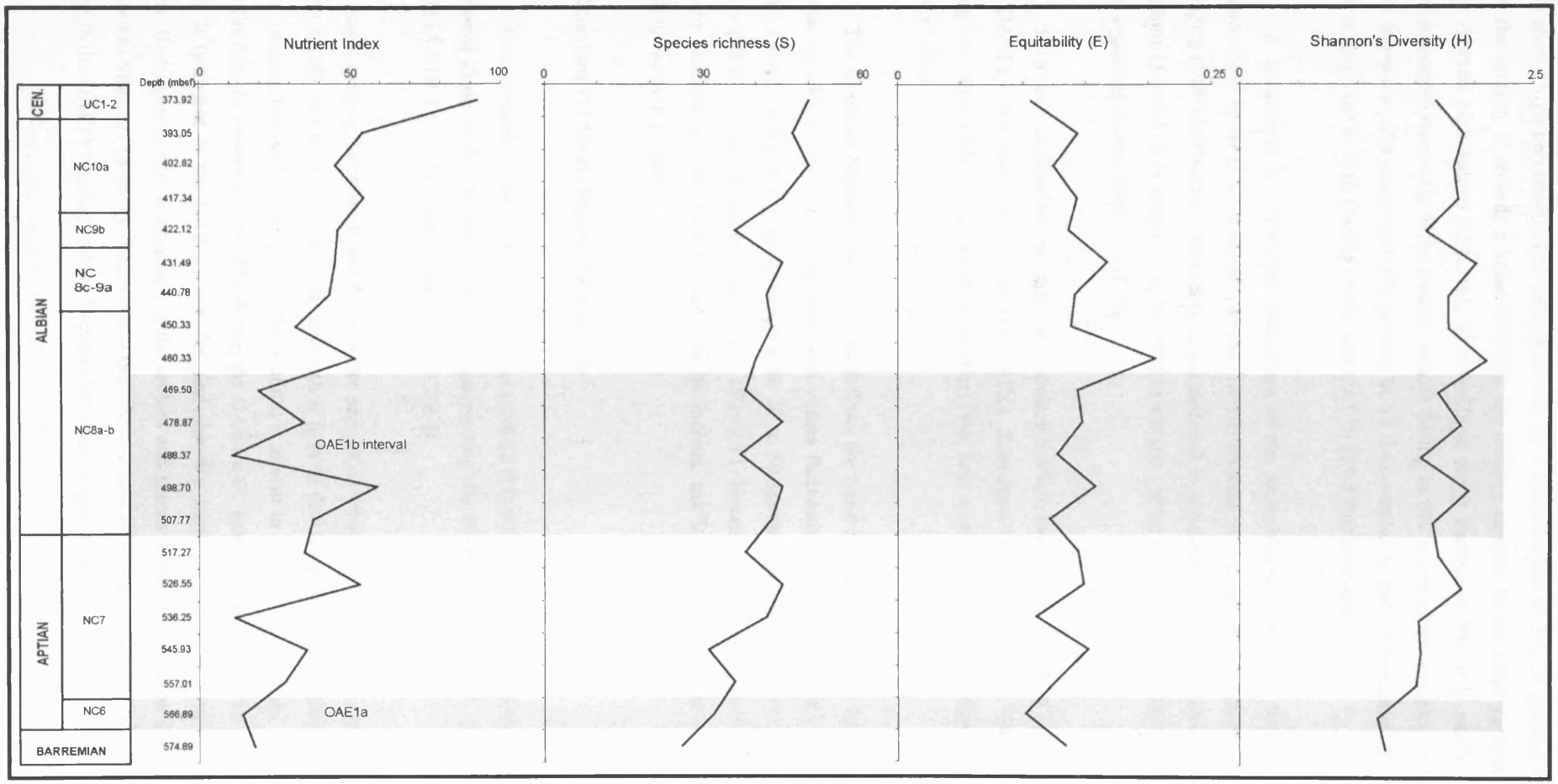

Figure 7.3 Variations in the Nutrient Index and diversity indices during the mid-Cretaceous at Shatksy Rise, 198-1207B.

initially shows high percentages (13-14%) followed by a sharp decline to 3%. *D. ignotus*, ranges from 3-14% in the section. It records a value of 7% in the OAE1a sample. In the OAE 1b interval, the taxon initially records high values (11-13%), followed by a sharp decline to 5%. It is worth noting that *D. ignotus* features consistently in the counts without falling to 0% in any of the samples. *Watznaueria* spp. (mainly *barnesiae* and *fossacincta*) is present in all the samples in the section ranging between 6 and 58%. It is dominant in both OAE1a (54%) and OAE1b (25-53%) intervals.

H. irregularis is a common component of the assemblages at Shatsky Rise. It shows a low abundance (1%) in the OAE1a sample. In the OAE1b interval, it registers a peak value of 13% in one of the samples (198-1207B-35R). Similarly, *L. carniolensis* is consistently present in all the samples in high proportions (5-36%). It is abundant in the OAE1a sample (36%) as well as the OAE1b interval, where it records a gradual decline from 31 to 15%.

Taxa such as *Rhagodiscus* spp. vary between 0-5% in the section and show low abundance, both in the OAE1a (1%), and OAE1b intervals (0-3%). *Retecapsa* spp. vary between 0-6% in the section, showing low abundance in the OAE1a sample (1%), and a slightly higher abundance in the OAE1b interval (2-6%).

The modified Nutrient Index broadly follows the trend of the productivity indicators. It shows a low value of 14% in the OAE1a sample, with values fluctuating between 11 and 59% in the OAE1b interval. Species richness (S) values range from 26 to 50 species per sample in the section. Shannon's diversity (H) in the assemblages ranges from 1.18 to 2.11. Equitability (E) varies between 0.10 and 0.21. No sharp changes are observed in the diversity indices, but they show a pattern of gradual increase through the section (Figure 7.3).

7.6.3.2 Section 1213A-B (Figures 7.4 and 7.5)

Two samples cover the OAE1a interval (198-1213B-9R-1 and 198-1213B-8R-1), falling within Nannofossil Zone NC6. The four samples encompassing the OAE1b include 198-1213B-3R-1 through 198-1213A-21R-CC, falling within Subzones NC8A-B.

B. constans, ranging between 0 and 35% in the section, is absent in the OAE1a samples. It is present between 7-10% in the OAE1b interval, although it falls to 0% in one of the samples (1213B-2R-1). *Z. noeliae*, ranging between 0 and 27% in the section, is absent in the OAE1a samples, whereas it records values fluctuating between 1 and 8% during the OAE1b. *D. ignotus* varies between 0 and 10 % in the section. It is absent in the OAE 1a samples, and shows a rapid decline from 8 to 2% in the OAE1b samples. *Watznaueria* spp. is abundant in the section and shows higher % values in Site 1213 (12-75%) compared to Site1207 (6-58%). *Watznaueria* spp. show values of 39 and 70% in the two OAE1a samples, whereas in the OAE1b interval, values fluctuate between 29 and 53%.

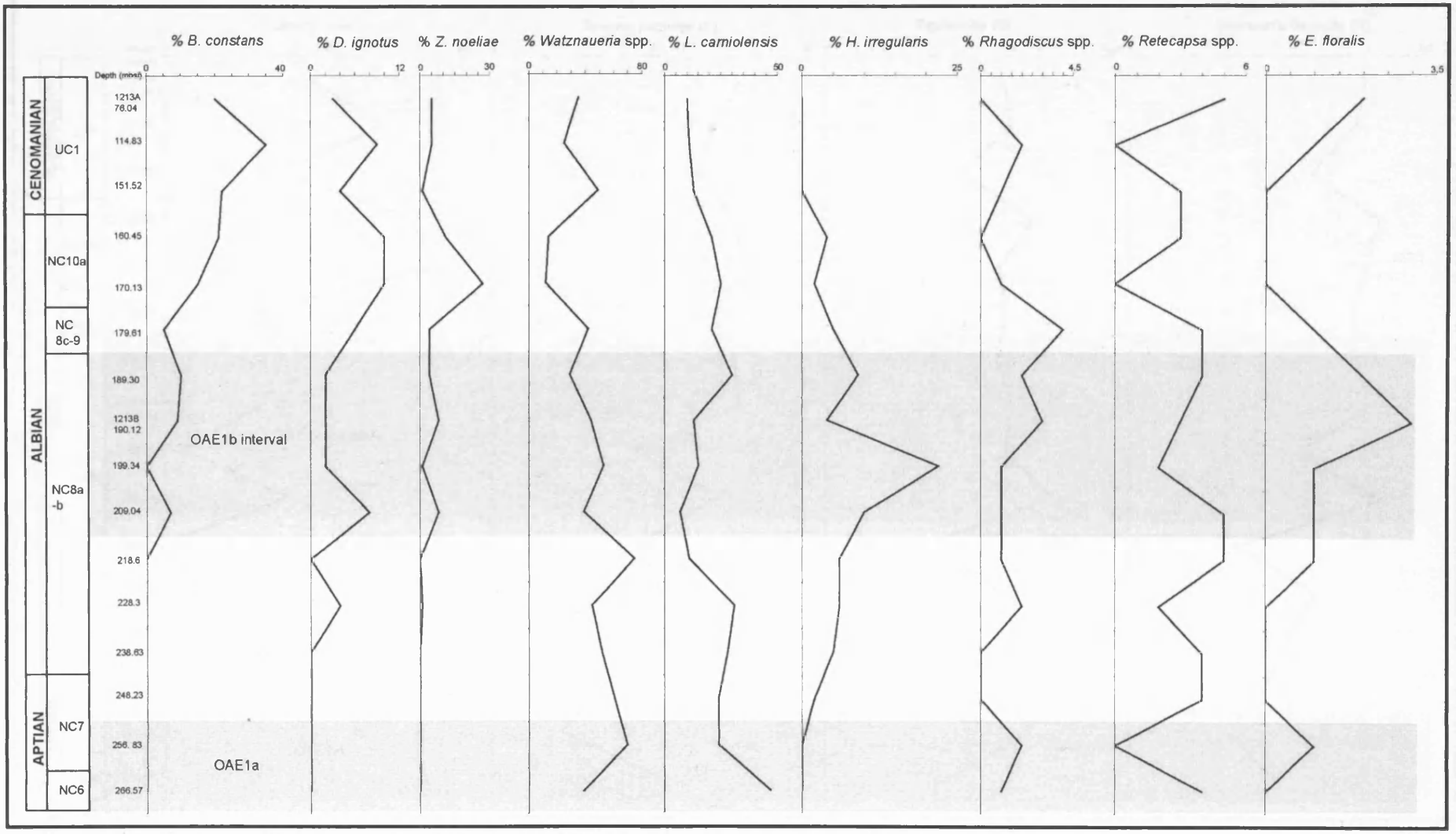

Figure 7.4 Variations in the % abundances of major nannofossil taxa during the mid-Cretaceous at Shatsky Rise, 198-1213A-B. Both OAE 1a and OAE1b intervals are marked by resistivity peaks (Robinson et al. 2004)

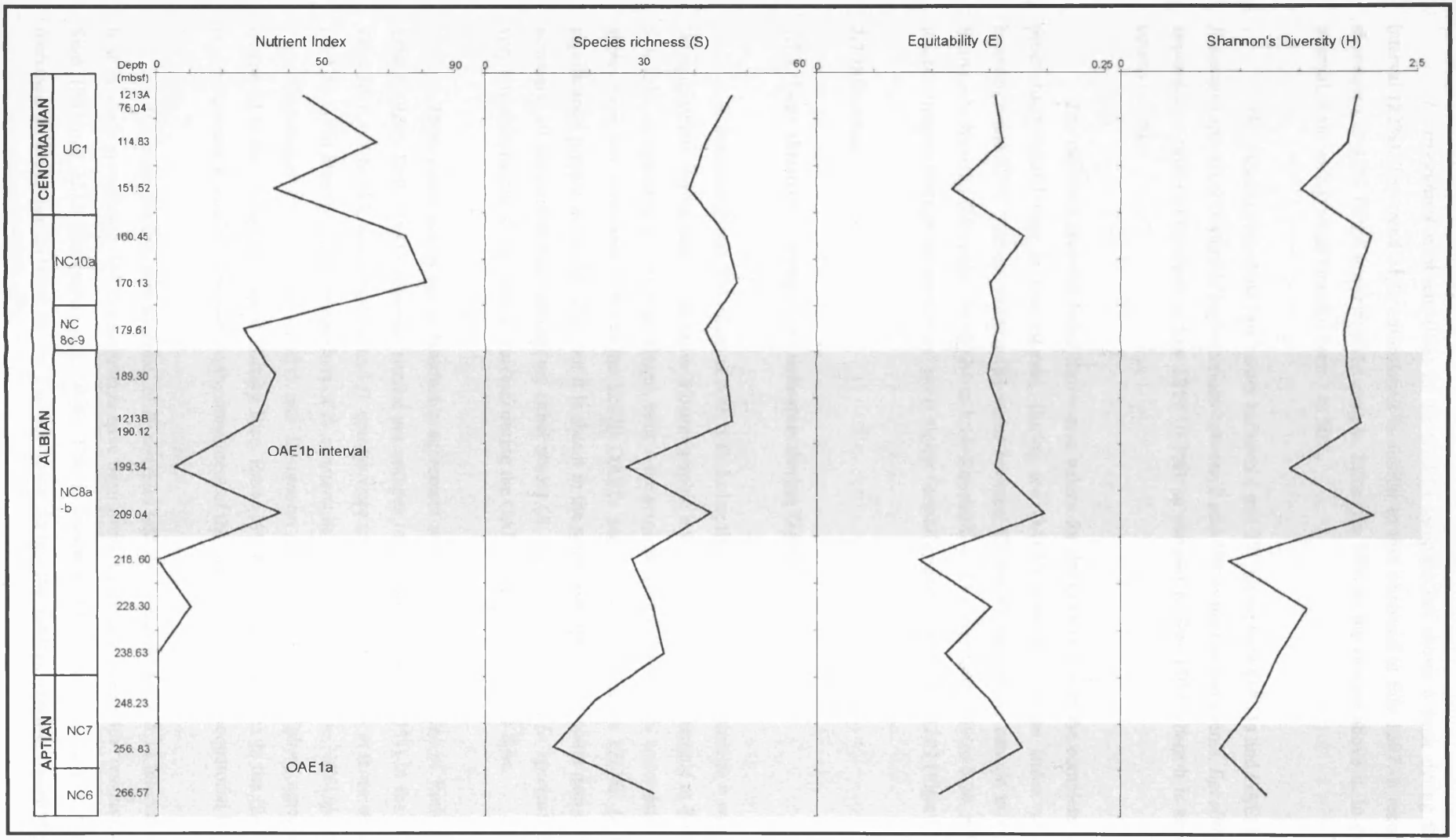

Figure 7.5 Variations in the Nutrient Index and diversity indices during the mid-Cretaceous at Shatksy Rise, 198-1213A-B.

H. irregularis is absent (0%) in the OAE1a samples, but shows a peak during the OAE1b interval (22%). The trend of *L. carniolensis* is similar to that observed at Site 1207. It records a high abundance of 47% in the lower OAE1a sample, falling to 24% in the sample above it. In the OAE1b interval, it shows a gradual increase from 7 to 30%.

Rhagodiscus spp. show low values between 1 and 3% during both OAE1a and OAE1b intervals. *Retecapsa* spp. records slightly higher values between 2 and 5% during the two events. *Eprolithus floralis* appears as a minor component in Site 1213 (0-3%), in contrast to Site 1207 where it is absent in the counts (<1%).

The modified Nutrient Index shows zero values for the OAE1a due to the complete absence of productivity-related taxa in that interval. During the OAE1b interval, Nutrient Index values range between 5 and 37%. Species richness (S) varies between 13 and 47 species per sample in this section. Shannon's diversity (H) ranges from 0.84 to 2.14. Equitability (E) varies from 0.09 to 0.20. All the three indices increase through the section and show higher variability compared to Site 1207 (Figure 7.5).

7.7 Discussion

7.7.1 'Near absence' of productivity indicators during OAE1a

B. constans shows 0% values at both sites during the OAE1a interval, although it was logged as 'Frequent/Few' during semi-quantitative biostratigraphic analysis of the OAE1a sample at Site 1207. At Site 1213, *B. constans* is completely absent, both in the semi-quantitative and the % count data. *Z. noeliae* shows very low abundance (2%) in the 1207B OAE1a sample, but is absent in 1213B. *D. ignotus* is significantly present in 1207B (7%), but it is absent in the semi-quantitative and count data in 1213B. In summary, all the high-fertility species are either absent (*B. constans*, *Z. noeliae*, *D. ignotus*) or occur in very low abundances (*D. ignotus*, *Z. noeliae*) during the OAE1a interval at Shatsky Rise.

These observations are in reasonable agreement with the previous studies of Roth (1981) and Erba (1992b). Roth (1981) observed similar percentages of *B. constans* (0 to <1%) in the Nannofossil Zone NC6 at Site 463, and *Z. noeliae* and *D. ignotus* were recorded between 1-2% in those samples. Erba (1992b) found slightly higher proportions of *B. constans* in the Early Aptian (Zone NC6) at Site 800 (0-7%). Percentages of *Z. noeliae* (1-5%) and *D. ignotus* (4-6%) were also higher, especially when compared to the studied samples at Shatsky Rise. Erba (1992b) described changes in the fluctuations of *B. constans* and *Z. noeliae* in relation to the movement of the site across the palaeoequatorial belt.

The cause for the 'near absence' of *B. constans* and *Z. noeliae* in the OAE1a interval at Shatsky Rise is worth speculating. OAE1a sediments have been found to be associated with 'resistivity highs' at Sites 1207 and 1213 (Robinson et al. 2004). This is indicative of increased silica flux and thereby, increased siliceous productivity in the Pacific basins during the OAE1a (Premoli Silva et al. 1989;

Coccioni et al. 1992; Bralower et al. 1994; Erba 1994; Menegatti et al. 1998; Erba & Tremolada 2004). Increased siliceous primary productivity in the Pacific is strongly suggested to have been volcanic-driven (Ontong Java, Manihiki and Carribean LIP eruption), more specifically by the availability of hydrothermal plume-derived nutrients such as Fe, Zn and other biolimiting metals (Sinton & Duncan 1997; Larson & Erba 1999; Leckie et al. 2002, Erba 2004).

The correspondence between 'resistivity highs' and the 'near absence' of nannoplankton productivity indicators clearly shows the inverse relationship between siliceous and carbonate productivity at Shatsky Rise. A plausible explanation for this could be that these taxa faced severe competition from the siliceous plankton, such as radiolarians, and were temporarily outcompeted by them. However, radiolarians being zooplankton presumably responded to increases in productivity by means of primary producers, i.e., nannoplankton or other phytoplankton groups. So it is possible that nannoplankton faced direct competition from some other phytoplankton group. This however does not explain as to why the productivity-related nannofossil taxa were more severely affected during the OAE1a interval. For instance, *L. carniolensis*, a nannolith species, shows very high abundances (~30%) during this interval implying that it successfully faced competition against other phytoplankton. It is possible that the hydrothermal-derived nutrients (e.g. Fe) that are thought to have triggered siliceous plankton productivity were favourable to *L. carniolensis*.

Alternatively, it is likely that the toxicity of specific metals introduced in large quantities into the Pacific basins by extensive submarine volcanism was detrimental to the productivity-related taxa. Such biolimiting metals are known to have adverse effects on calcification in extant nannoplankton species (Brand 1994). Moreover, the inhibitory effect of metal toxicity has been cited as one of the reasons for reduced occurrences of *B. constans* during and after the OAE2 event (Erba 2004). It is likely that similar mechanisms came into play during the OAE1a, resulting in the absence of *B. constans* and other productivity-related taxa at Shatsky Rise.

It can be questioned whether fertility levels during the OAE1a interval were really very high as implied by the chert-rich sequences recovered from the Pacific. This further implies the question whether chert is a good indicator of high productivity or not. Due to slower oceanic circulation mechanisms and weaker wind forces during the Cretaceous (Barron et al. 1993, 1995), it is possible that the palaeoequatorial divergence belt was not as fertile as it is in the modern ocean. Therefore if trophic levels were lower than the threshold for *B. constans* and *Z. noeliae*, these taxa would not have been abundant, as is the case observed in the OAE1a interval. It is also possible that the mid-ocean setting was not favourable to *B.constans* and *Z. noeliae*, which are known to be more abundant in shelf settings.

7.7.2 Productivity indicators during OAE1b

B. constans shows a relatively higher abundance in the OAE1b interval at both sites. In 1207B, percentages range between 4-9 % (Subzone NC8A-B), whereas in 1213B, they are in the range of 7-10%.

Z. noeliae shows higher abundance too, between 3-13% at both sites. *D. ignotus* shows similar abundances as *Z. noeliae*, i.e., between 2-13% at both sites. In summary, the productivity indicators show markedly increased abundances in the OAE1b interval, compared to the OAE1a interval.

At Blake Nose, in the western Atlantic, high percentages of *B. constans* (~20%) and *Z. noeliae* (~40%) were observed, bracketing the OAE1b sapropel (Chapter 6, section 6.7.4). This led to the conclusion that the OAE1b at Blake Nose was strongly linked with increased productivity. Herrle (2002) also noted high values of the Nutrient Index in the Niveau Paquier succession in the Vocontian Basin (mean value of NI: 49.9%). The Niveau Paquier succession was, in fact, characterised by high frequency fertility changes of surface waters, associated with warmer and more humid phases. This was suggested to be related to localised climatic phenomena such as enhanced monsoonal activity and stronger winds. The Nutrient Index and the abundance record of the productivity-related taxa are lower at Shatsky Rise compared to coeval Atlantic and Tethyan sections.

OAE1b sediments show resistivity peaks at Shatsky Rise, similar to OAE1a sediments (Robinson et al., 2004). The productivity indicators show higher abundance in the OAE1b interval compared to OAE1a. There is clearly a temporal variation in nannofossil productivity with respect to the OAE1a and OAE1b intervals in the Pacific. It is hypothesised that this is directly related to differences in the scale and extent of volcanism during the two events. Reduced rates of submarine volcanism during the Early Albian OAE1b would have limited the supply of toxic metals introduced via hydrothermal plumes (Sinton & Duncan 1997; Duncan & Bralower 2002; Leckie et al. 2002). This may have boosted the productivity of *B. constans* and *Z. noeliae*, which are suggested to have suffered metal toxicity during OAE1a. In other words, the reduced presence of toxic metals may have promoted the growth of these taxa during OAE1b.

Increased upwelling due to equatorial divergence cannot be invoked as an explanation for the temporal variation in the abundance of the productivity-related taxa during OAE1a and OAE1b. This is because both sites remained at the same palaeolatitudes (0-5°N/S) in the core of the upwelling zone, between 120 and 100 Ma (Bralower et al. 2002). Therefore the upwelling rate must have been fairly constant between the early Aptian and the early Albian.

7.7.3 Palaeoecology of *Watznaueria*, *Hayesites irregularis*, *Lithraphidites carniolensis*, *Rhagodiscus*, absence of *Nannoconus*

Watznaueria spp. is the most abundant taxon in the mid-Cretaceous samples at Shatsky Rise (Figures 7.2 and 7.4). The uniformly high abundance of *Watznaueria* reflects its dominance in the nannoplankton assemblages from the Pacific basin. Previously, *Watznaueria barnesiae* has been interpreted as a preservation index with >40% concentrations indicating dissolution and/or diagenetic alteration (e.g., Roth and Bowdler 1981; Roth and Krumbach 1986). Its abundance is understood to increase with increasing dissolution as delicate taxa get progressively dissolved and the assemblage

becomes largely *Watznaueria*-dominated. This interpretation is not supported by the observations made in this study. The samples at Shatsky Rise show uniform preservation (moderately good) without obvious signs of etching, overgrowth or dissolution, yet there are very high abundances of *Watznaueria* spp. (>40%) in the samples. This strongly suggests that the dominance of *Watznaueria* does not bear a direct relationship with the preservation in a sample. Its dominance is more a reflection of its broad palaeoecological tolerance rather than resistance to dissolution. This is evident from the fact that one sample (198-1207B-27R) with the highest species diversity (50 species) has 40% *Watznaueria* in it, whereas another sample (198-1207B-24R) with the same diversity (50 species) has only 6% *Watznaueria*. Both samples show similar preservation, but wide variations in the percentages of *Watznaueria*. This suggests that the abundance fluctuations of *Watznaueria* are a primary ecological response rather than related to preservation effects. Similar observations have been made by Street & Bown (2000) and Lees et al. (2004) recently.

It is also observed that *Watznaueria* is more abundant in open-ocean settings compared to neritic settings (e.g., Blake Nose). This is evident from the significantly higher percentages of the taxon at Shatsky Rise (up to 70%) as opposed to Blake Nose where it does not exceed 45% by proportion. Lees et al. (2004) have recently interpreted watznauerian palaeoecology in light of its exclusive presence in the Jurassic Kimmeridge Clay Formation stone band microlaminae (showing pristine preservation) in southern England. They have interpreted that *Watznaueria* had an opportunistic, r-selected palaeoecological strategy, and compared it to the extant coccolithophore *E. huxleyi*. They also suggest that there is considerable differentiation in the palaeocological strategies within the *Watznaueria* plexus, with different members forming a morphologic continuum.

The consistent presence and high abundance of *Hayesites irregularis* at Shatsky Rise suggests that it is a low-latitude, tropical taxon with warm-water affinities. This is supported by observations from the coeval Atlantic section, European epicontinental assemblages and sections from SE India, where *H. irregularis* is either absent or sporadic. Erba (1992b) noted peaks in the abundance of the taxon in the upper Aptian with decreases in the Albian, leading to similar interpretations on its palaeoecology. Bown (*in press*) has similar observations on *H. irregularis* at Shatsky Rise. However, *H. irregularis* is a biostratigraphic marker species with its FO at the base of the Aptian and LO around the Albian/Cenomanian boundary. Its abundance trend starting with low abundance in the early Aptian, a peak around the Aptian/Albian boundary followed by a decline towards the Late Albian may reflect its evolutionary history rather than its palaeoecological strategy (Figures 7.2 and 7.4).

Lithraphidites carniolensis is another taxon that shows unusually high abundances (>25%) at Shatsky Rise. Similar to *H. irregularis*, such high abundances of *L. carniolensis* have not been observed in the other study sections. Roth (1981) observed abundant *L. carniolensis*, reaching up to 14% in the Lower Aptian (Zone NC6) at Site 463. Erba (1992b) however, reported low percentages (0-4%) of the taxon in the early Aptian from the western Pacific. The data from Shatsky Rise supports the interpretation

that *L. carniolensis* is an oceanic-adapted species (Thierstein 1976; Roth and Bowdler 1981; Eshet & Almogi-Labin 1996; Bown, *in press*).

In addition to its high abundance, it is also observed that the abundance trend of *L. carniolensis* is the inverse of *B. constans* (Figures 7.2 and 7.4). This is a notable feature suggesting that these two taxa were probably controlled by different sets of nutrients. It is possible that Fe, a limiting nutrient, was favourable to *L. carniolensis* and inhibitory to *B. constans*. Iron fertilisation is suggested to have increased in the Pacific, particularly during OAE1a, as a result of heightened submarine volcanism and oceanic crustal production (Larson & Erba 1999; Leckie et al., 2002). This agrees well with the observed peaks in *L. carniolensis* during the OAE1a interval.

Rhagodiscus spp. do not show a clear trend in both sections and are a minor component of the assemblages (0-5%). *R. asper* did not register significant numbers in the count data and was therefore combined with other *Rhagodiscus* species.

The palaeoecological affinities of minor taxa such as *Retecapsa* spp. and *E. floralis* are difficult to interpret from their abundance trends (Figures 7.2 and 7.4). The absence of nannoconids in the Pacific is striking, although not surprising. It is very rare in both sections. *Nannoconus* is known to be abundant only in neritic settings of the Tethyan and Atlantic regions (Street & Bown 2000). Its rarity in the mid-oceanic environment is therefore not unusual.

7.7.4 Global rise in *B. constans* in the Late Albian – evolutionary or environmental?

The Family Biscutaceae, a group of non-imbricating placoliths that radiated in the Pliensbachian (Early Jurassic) and persisted till the end of the Cretaceous, is one of the most important Mesozoic nannofossil families. The genus *Biscutum*, after which the family takes its name, appeared in the Pliensbachian with early forms such as *B. novum*, *B. grande* and *B. dubium*, which did not survive beyond the Jurassic, but radiated into other forms that lasted till the end of Mesozoic. *B. dubium* is supposed to have evolved into *B. constans*, a species that was environmentally sensitive and survived till the end of the Maastrichtian. *B. constans* is an important species in the mid-Cretaceous and is, in fact, dominant in most nannofossil assemblages of that age. Related species such as *D. ignotus*, are usually less conspicuous than *B. constans* in mid-Cretaceous assemblages but can be dominant under specific palaeoceanographic conditions, particularly in high-fertility environments.

The trend of *B. constans*, from the observations made in this study, is that of fairly high abundances (~10%) in the Early and mid-Albian. This is also observed in the Cauvery Basin, Gault Clay and Blake Nose assemblages that have been quantitatively analysed. Additional samples from the Vocontian Basin (SE France) have also yielded high numbers of *B. constans* in the *T. orionatus* Zone (BC24, Middle Albian). This pattern of increasing abundances of *B. constans* from the early/mid- into the Late Albian is interesting, particularly the sharp increase that is observed in the Late Albian. High

abundances of *B. constans* in the Late Albian (*E. turriseiffelii* Zone) are observed in all the study sections (Table 7.1).

Location	Details	Author	% *B. constans*
Central Pacific (DSDP Sites)	Site 463, Mid-Pacific Mountains	Roth, 1981	16%
	Site 464, Northern Hess Rise		13-39%
	Site 465, Southern Hess Rise		~30%
	Site 466, Southern Hess Rise		>30%
Western Pacific, ODP Leg 129	Site 800	Erba, 1992	~25%
	Site 801		~25%
Northwest Pacific, ODP Leg 198, Shatsky Rise	Site 1207	this study	19-48%
	Site 1213		15-35%
	Site 1214		16%
SE India (outcrop)	Karai Formation, Cauvery Basin		14%
SE France (outcrop)	Col de Palluel Section, Vocontian Basin		18%
SE England (borehole)	Selborne boreholes, Sel 1		17%

Table 7.1: % abundance data for *B. constans* in the Late Albian *E. turriseiffelii* Zone NC10 and younger sediments.

The Shatsky Rise sections (1207B and 1213A-B) show very high abundances of *B. constans* (>20%, reaching up to 48%) throughout the Late Albian and in the Early Cenomanian. This is in good agreement with the results of Roth (1981) and Erba (1992b). Roth (1981) recorded high percentages of *B. constans* (>25%, reaching up to 49%) at Sites 465 and 466 in the Pacific. Sites 463 and 464 showed comparatively lower percentages (>15%, reaching up to 30%), but this was attributed either to poor preservation (Site 464) or to the palaeolatitudinal position of Site 463 outside the equatorial high-productivity zone. Figure 7.6 illustrates the sharp increases in *B.constans* during the Late Albian in the Pacific sections.

Erba (1992b) noted similar trends in the patterns of *B. constans* and *Z. noeliae* within the *E. turriseiffelii* Zone in the equatorial Pacific, where both species increased dramatically to values greater than 20%. This was interpreted in terms of the different levels of fertility of the two taxa, with higher levels of fertility accorded to *Z. noeliae* than *B.constans*.

It is worth speculating if the prominent peaks of *B. constans* in the Late Albian are related to primary environmental signals or if they have an evolutionary aspect to them. Although *B. constans* and

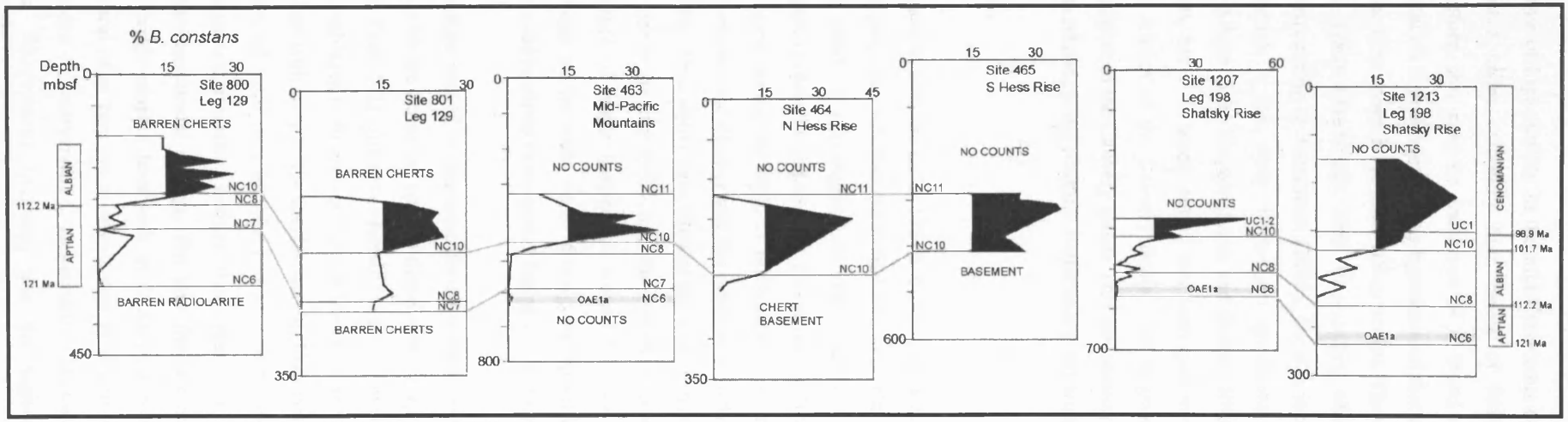

Figure 7.6. Rise in the % abundance of *B. constans* in the Late Albian Nannofossil Zone NC10 across the Pacific basin. Data from Leg 129 is taken from Erba (1992). Data for Sites 463, 464 and 465 from Roth (1981).

Z. noeliae are indicative of high fertility in the mid-Cretaceous oceans, it is unlikely that all the study sections were deposited under extremely high levels of fertility to allow *B. constans* to peak simultaneously. Therefore, this may be indicative of a broad evolutionary change in *B. constans*. Although this interpretation is preliminary, it is hypothesised that new niches opened up for this species beyond the high-productivity zones in the Late Albian oceans. There is evidence of an increase in the size of *B.constans* in the Albian (Tremolada 2002; this study), which may be related to the suggested evolutionary change. According to Tremolada (2002), the size increase occurs in the mid-Albian in the Tethyan regions, although in this study, large-sized specimens of *B. constans* (~8 μm) have been observed in the Early Albian in the Cauvery Basin and Shatsky Rise. The timing of this size increase may have been diachronous, but it is worth noting that increased numbers of large-sized *B. constans* are observed in the Late Albian of the Cauvery Basin. The large-sized morphotypes continue to occur throughout the Cenomanian in the Cauvery Basin. This speculation of a temporal variability in *Biscutum*, particularly in the Late Albian, being possibly evolutionary in nature needs further research.

7.7.5 Diversity Indices

Species richness in both the cores 1207B and 1213A-B is fairly high, with an average diversity of >35 species per sample. This indicates the availability of a relatively large niche space for the various species in the surface waters. It also suggests an overall stability in the depositional environment with many species evenly partitioning the niche space. This agrees well with the general palaeoceanography of the tropical Pacific region during the early to mid-Cretaceous. In the absence of major ice caps, the temperature gradient between the equator and the poles was fairly low (e.g. Barron 1983; Barron et al. 1995; Frakes et al. 1992). This would have allowed the trade winds to blow at fairly constant rates rather than fluctuate in response to the seasonality, as is the case in the modern ocean (Barron et al. 1993, 1995). Additionally, the absence of major landmasses around Shatsky Rise would have contributed to the constancy of the strength of the trade winds driving the upwelling. It can therefore be said that the equatorial Pacific was a fairly stable environment during the mid-Cretaceous.

The Shatsky Rise record is characteristic of oceanic nannofossil assemblages. This becomes clear by comparing it with the European epicontinental assemblages, the Atlantic and the Cauvery Basin shelf assemblages (see Table 7.2). Species richness is slightly lower in oceanic assemblages (~60 species) compared to shelf assemblages (~70 species). The majority of nannofossil species (~80%) in the tropical Pacific are cosmopolitan with only a few species setting them apart from coeval shelf or epicontinental assemblages. Examples of such taxa include *L. carniolensis* and *H. irregularis*, both taxa that are conspicuously more abundant in oceanic settings. *Watznaueria* spp. is also observed to be more abundant in oceanic settings than continental settings. The taxa that are noticeably absent or patchy in oceanic assemblages are the neritic-adapted taxa such as *Braarudosphaera*, *Broinsonia*, *Micrantholithus* and *Nannoconus* spp. Several other taxa are relatively rare or absent in mid-ocean environments. Examples include *Cyclagelosphaera* (*C. margerelii*, *C. reinhardtii*), *Calciosolenia fossilis*, *Octocyclus reinhardtii*, *Percivalia fenestrata*, *Rhagodiscus splendens* and the high-latitude taxa (*R. parvidentatum*, *S.*

primitivum). Taxa such as *Gaarderella granulifera*, *Braloweria boletiformis* and *Ceratolithina* are also absent at Shatsky Rise.

Locality	Age/ NF Zone	No. of samples	Preservation	Simple diversity	Shannon's Diversity	Equitability
Karai Formation, Section 1	mid-Albian, BC24	2	G-M	60-69	1.99-2.13	0.12
Karai Formation Section 1	Late Albian BC27	3	G-M	43-67	1.53-2.19	0.11-0.15
Gault Clay Formation	mid-Albian, BC24-25a	16	G	48-70	1.8-2.37	0.09-0.19
Blake Nose, western Atlantic	Early Albian NC8B	10	G-M	13-61	1.99-2.20	0.08-0.26
Shatsky Rise (1207,1213)	Early Albian NC8A-B	4-5	G-M	27-47	1.43-2.14	0.12-0.20

Table 7.2: Comparison of the diversity indices between the four study sections. Values given here show the range of the diversity indices in the samples. Preservation: G-Good, M-Moderate.

Shannon's diversity index was calculated for the four palaeoenvironmentally disparate study sections, i.e., India, England, Blake Nose and the Pacific, in order to make comparisons. As diversity critically depends on the time interval, the indices are compared only between coeval sections. Shannon's diversity and equitability values are comparable in the four coeval Albian sections. There is very little variability between them. Shannon's diversity ranges between 1.43 and 2.37 in the four localities, whereas equitability values are between 0.08 and 0.26.

The similar values of equitability and Shannon's index in the four Early Albian sections suggest that the palaeoequatorial Pacific may not necessarily have been a very high productivity setting. This questions the interpretation of chert as a high productivity indicator in the Mesozoic Pacific Ocean. The interpretation of radiolarian-rich chert as a high productivity proxy is based on a comparison with the modern silica cycle in which diatoms play the dominant role as phytoplankton. However, diatoms and radiolaria are essentially different plankton groups in terms of their ecological strategies and may not be directly comparable as productivity proxies.

Mesozoic chert deposits are known to have been controlled by other factors. High Si content has been equated with clastic-sediment-starved pelagic deposition in the Late Jurassic Tethyan Ocean (Weissert 1989). It has also been suggested that temperature may be the fundamental control on siliceous plankton, particularly diatoms (Berger et al. 1989). Therefore Si-rich and organic carbon-rich sediments

are rarely associated in the geological record (Kuhnt et al. 1986). Although it is not conclusive, Shannon's diversity comparisons strongly suggest that fertility in the palaeoequatorial Pacific may have been relatively moderate rather than high. This has also been postulated by Robinson et al. (2004).

7.8 Conclusions

1. The nannofossil record in samples encompassing the OAE1a and OAE1b intervals at Shatsky Rise (Sites 1207 and 1213) shows marked variations in the abundance trends of the productivity indicators. During the Early Aptian OAE1a interval, all the productivity indicators are either absent (*B. constans*, *Z. noeliae*, *D. ignotus*) or occur in very low abundances (*D.ignotus* and *Z. noeliae*). The correspondence between the 'resistivity highs' suggesting increased siliceous productivity (Robinson et al. 2004) and the 'near absence' of the nannofossil productivity taxa is noteworthy. Possible reasons for this could be competition from other phytoplankton groups for nutrients and/or the inhibitory effects of metal toxicity introduced by extensive submarine volcanism in the Pacific Basin.

2. Nannofossil productivity indicators show relatively increased abundances in the Early Albian OAE1b interval (2-13%). This may be directly related to differences in the scale and extent of volcanism during the two OAE intervals. Reduced rates of submarine volanism in the Pacific, and consequently the reduced production of toxic metals may have boosted the productivity of *B.constans* and *Z. noeliae* during the OAE1b interval.

3. The majority of nannofossil species at Shatsky Rise are cosmopolitan with only a few species setting them apart from coeval shelf assemblages. *Watznaueria* spp. is more abundant in oceanic settings (up to 70%) compared to shelf environments where it usually does not exceed 45% by proportion. The dominance of *Watznaueria* is thought to be a reflection of its palaecological strategy rather than resistance to dissolution. *L. carniolensis* is abundant (>25%) in the Pacific assemblages and is interpreted as an oceanic-adapted taxon. The increased abundances of *L. carniolensis*, especially in the OAE1a interval, may be related to Fe-fertilisation as a result of heightened submarine volcanism. The consistent presence of *H. irregularis*, suggests that it was a low-latitude, tropical species with warm-water affinities. Neritic taxa (*Braarudosphaera*, *Broinsonia* and *Nannoconus*) are very rare or absent in oceanic assemblages of the Pacific.

4. A marked increase in the % of *B. constans* (reaching up to 48%) in the Late Albian *E. turriseiffelii* Zone is noted across the Pacific and in other coeval study sections. This increase in *B. constans* continues into the Early Cenomanian and perhaps, even younger sediments. It is hypothesised that this may be indicative of a broad evolutionary change in *B. constans*, rather than an increase in fertility levels globally.

5. Diversity indices such as species richness suggest that the equatorial Pacific was a fairly stable environment during the mid-Cretaceous with a relatively large niche space shared by many species.

The similar values of Shannon's diversity and equitability in four coeval early Albian sections suggests that the equatorial Pacific may not have been a high productivity setting as suggested by the radiolarian-sourced cherts. The interpretation of chert as a high-productivity proxy in Mesozoic ocean systems, especially in the Pacific is questionable.

Chapter 8. Palaeobiogeography

8.1 Introduction

The aim of this study was to test the hypothesis that mid-Cretaceous nannofloras were cosmopolitan. The hypothesis that the mid-Cretaceous (Aptian-Albian) was a period of nannofloral homogenisation with cosmopolitan species worldwide was proposed by Mutterlose and co-workers (e.g. Mutterlose 1992b; Mutterlose & Kessels 2000) and Bown (2001). It is well known that Early Cretaceous nannofloras showed marked provinciality, inferred on the basis of endemic species, bipolar high-latitude distribution of certain taxa, abundance changes and the existence of climatic belts (Mutterlose 1992a, b; Street and Bown 2000). For the Early Cretaceous, most authors recognise provinces such as the Boreal, Tethyan and Austral. The Boreal Province is used for northern high-palaeolatitudes, the Tethyan Province covers the equatorial tropical to subtropical palaeolatitudes, whereas the Austral Province is used for the southern high-palaeolatitudes (Street 1998). According to Mutterlose (1992b), provincialism diminished during the Aptian-Albian, which led to the homogenisation of Boreal and Tethyan taxa and the disappearance of nannofloral realms.

This study tests if these provinces are recognisable in Albian-Cenomanian nannofossil assemblages from samples broadly representing different palaeobiogeographic zones (PBZ). In order to carry out the analysis, nannofossil assemblages from the Cauvery Basin have been compared, both qualitatively and quantitatively, with assemblages from Europe and the Pacific. Samples from three established datum-levels, i.e., FO of *T. orionatus* (Middle Albian), FO of *E. turriseiffelii* (Upper Albian) and the FO of *C. kennedyi*/LO of *W. britannica* (Lower Cenomanian) were examined. In addition to the sample from the datum-level, one sample above and one below the datum-level were also examined for qualitative comparisons. This was done to homogenise the effects of preservation in the different sample localities. However, for generating quantitative data, only the sample at the datum-level was counted (see Chapter 3, section 3.6.4). The following sample localities have been used in this analysis:

1. **SE France**: A total of 14 smear slides (PG 26-30; ColP 54-62) from the Middle and Upper Albian datum-levels were examined from the Col de Pré-Guittard section in the Vocontian Basin. This section was proposed as a potential candidate GSSP for the base of the Albian in Kennedy et al. (2000). Two slides (Risou +16, +20) from the Lower Cenomanian datum-level were examined from the Mt. Risou section in the same region. The Mt. Risou section was proposed as a potential candidate GSSP for the base of the Cenomanian in Gale et al. (1996). This region is broadly representative of the Tethyan Province.

2. **S. England**: Six slides (Sel 1-50, 54, 55; Sel 2- 41.5, 45.5, 49.5) from the Middle and Upper Albian datum-levels were examined from the British Geological Survey (BGS)-Selborne (Sel&2) boreholes in Hampshire. Two slides from the Lower Cenomanian datum-level were examined from the section at the Folkestone Warren, in Kent (Warren 7, 8). This region is broadly representative of the Boreal Province.

3. **Shatsky Rise, Pacific Ocean**: Twelve slides covering the Middle Albian, Upper Albian and Lower Cenomanian datum-levels were examined from ODP Leg 198, Holes 1213A (17R-21R), 1214A (7R-10R) and 1207B (25R-27R). The LO of *W. britannica* was used as the Lower Cenomanian datum-level instead of *C. kennedyi* due to the absence of the latter species in all the sites located at Shatsky Rise (Bown, personal communication). Shatsky Rise was located at mid-oceanic tropical palaeolatitudes during the Albian.

4. **Cauvery Basin, SE India**: A total of 9 slides from Karai Formation, Section 1 were examined from the Middle Albian, Upper Albian and Lower Cenomanian datum-levels. Samples examined include KA 18-KA 27 (Middle Albian), KA 180-189 (Upper Albian), and KA 332.5-341.5 (Lower Cenomanian). Cauvery Basin is broadly representative of the Austral Province during the Albian.

8.2 Results

All forty-five samples from the four localities show abundant and diverse (~ 130 species) nannofossil assemblages with preservation varying from poor to good. The majority of the samples however show moderate-good preservation. Range charts and biostratigraphy for the Col de Pré-Guittard, Mt. Risou, Selborne and Shatsky Rise sections are published in Kennedy et al. (2000), Gale et al. (1996), Bown (2001) and Bown (*in press*) respectively. The presence/absence-based distribution of the taxa in the four localities, at each of the three datum-levels is presented in Appendix 1.

Results based on qualitative comparisons of assemblages (Figures 8.1-8.3) show that for all the datum-levels (Middle Albian, Upper Albian and Lower Cenomanian), >80 % of the taxa are present in all four regions. From Figs. 8.1-8.3 (b), it can be observed that > 40 species are present at all the study sites, whereas < 5 species are restricted to one site. This indicates that the majority of the taxa during the Albian and Early Cenomanian were cosmopolitan.

Quantitative data collected from samples at each of the datum-levels show important trends in mid-Cretaceous palaeobiogeography. Around 10-12 taxa are present above concentrations of 2% in all the regions during the mid-Albian, Late Albian and Early Cenomanian (Figure 8.1-8.3). The assemblages are markedly uneven in their composition, dominated by three taxa, *Watznaueria barnesiae*, *Bisutum constans* and *Zeugrhabdotus noeliae*. The relative proportions of the different taxa present in proportions above 2% are shown in Figures 8.1-8.3 (c). The count data is attached in Appendix 1.

8.3 Discussion

8.3.1 Comparison of nannofossil assemblages between India, Europe and the Pacific

Qualitative comparisons show that the Boreal, Tethyan and Austral provinces cannot be clearly recognised in the nannofossil assemblages from England, France or India during the Albian and Early

Cenomanian. This is because the majority of taxa were cosmopolitan in their distribution, as shown by results obtained in this study (Figures 8.1-8.3). Only a few taxa show restricted distribution in Albian assemblages. These include *Braloweria boletiformis,* which is restricted to NW Europe (England and the North Sea Basin). *Gaarderella granulifera* and *Tegulalithus tessellatus* are known mainly from Europe (England and France), but have been reported from the Indian Ocean recently (Lees 2002). The genus *Ceratolithina* (*C. bicornuta* and *C. hamata*) is common in samples from England, but is rare in France. These two taxa are reported from the Indian Ocean (Bown et al. 1998; Lees 2002). The Tethyan genus *Nannoconus*, is common to abundant in samples from France, but is very rare or absent in all other localities (England, India and the Pacific). The neritic-adapted genera *Braarudosphaera* and *Micrantholithus* show a distribution restricted mainly to samples from France. They are sporadic in all other localities. *R. parvidentatum* and *S. primitivum* were adapted to high-latitudes, and are therefore found consistently in samples from the Cauvery Basin and England. Practically all other taxa were cosmopolitan during the Albian.

The Cauvery Basin assemblages do not show any marked Austral features, even though the palaeolatitudinal position of India during the Albian (~60°S) was in the Austral Zone. The only taxa that suggest the high-latitude palaeoposition of the Cauvery Basin are *R. parvidentatum* and *S. primitivum*, both of which are consistently present in the assemblages. In fact, it is the absence or rare presence of some distinctive Austral taxa that makes the palaeobiogeographic affinities of the Cauvery Basin difficult to comprehend.

S. falklandensis is rare in the Cauvery Basin and is restricted to only one sample. The limited presence of this species prevents its utility as a conclusive indicator of Austral latitudes for the Cauvery Basin. This species was first described from the Falkland Plateau (DSDP Sites 327 and 330) where it was reported to be common to abundant (Wise & Wind 1977). It has also been reported from ODP Sites 765/766, near the Exmouth Plateau in the Indian Ocean (Bown, personal communication). Similarly, another Austral species, *Z. kerguelenensis*, described from the Kerguelen Plateau in the Southern Ocean (Watkins *in* Wise et al. 1992), is rare and sporadic in the Cauvery Basin.

The palaeobiogeographic distribution of the *incertae sedis* genus *Ceratolithina* is puzzling. The taxon is absent in the Cauvery Basin assemblages, although it is reported from the Naturaliste Plateau (DSDP Sites 257, 258 and 259) in the Indian Ocean, which was located at similar palaeolatitudes as the Cauvery Basin (~ 60°S) (Lees 2002; Bown, personal communication). The palaeoecological affinities of this taxon are not entirely clear, but it is possible that the taxon was shelf-restricted in the Naturaliste Plateau region, and was unable to migrate through the deep waters of the Indian Ocean towards the Indian peninsula.

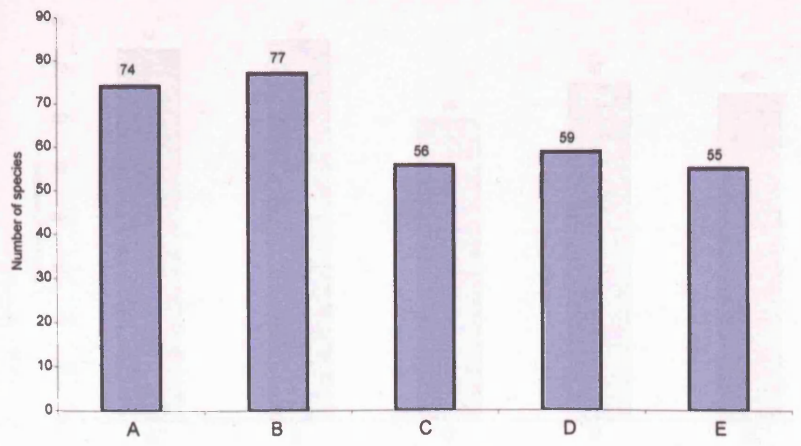

a. Species richness

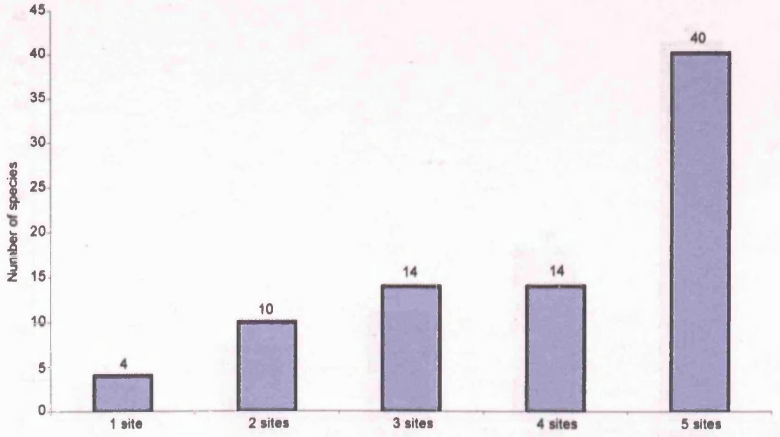

b. Number of species logged vs. number of sites studied

KEY:

A: Karai Section 1, India, sample KA22.5
B: Shatsky Rise, Pacific Ocean, 198-1213A-20R
C: Shatsky Rise, Pacific Ocean, 198-1214A-9R
D: Col de Palluel section, France, Col PG 29
E: Selborne, S. England, Sel2/45.5

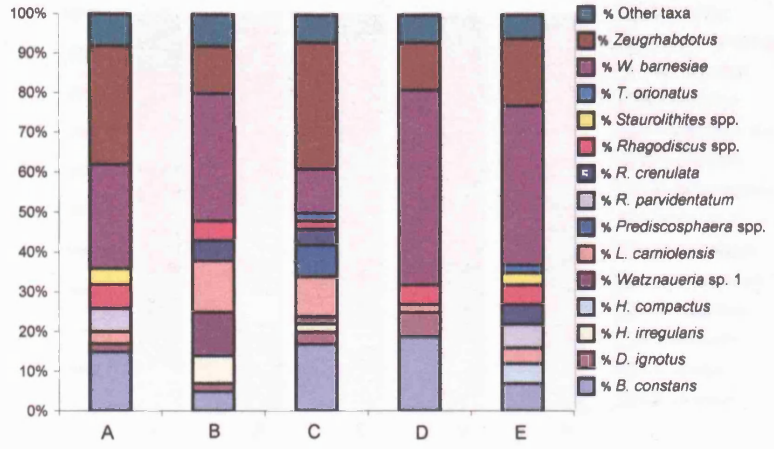

c. Taxa present above 2% based on count data

Figure 8.1 Plots summarising the cosmopolitan distribution of nannofloras at the *T. orionatus* datum-level (mid-Albian) based on data from five studied sites.

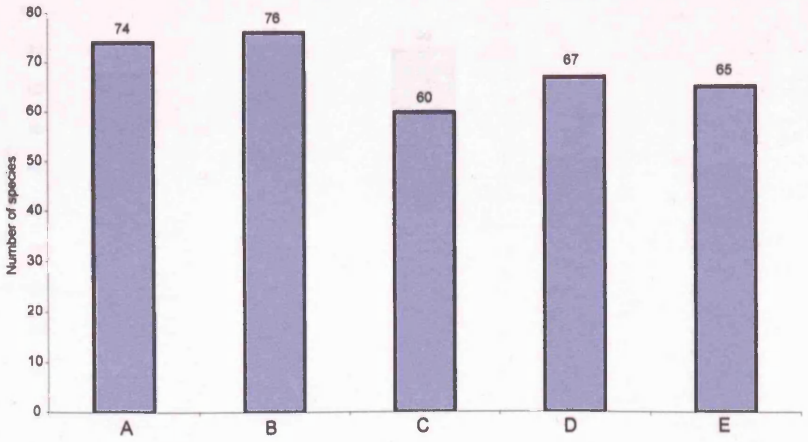

a. Species richness

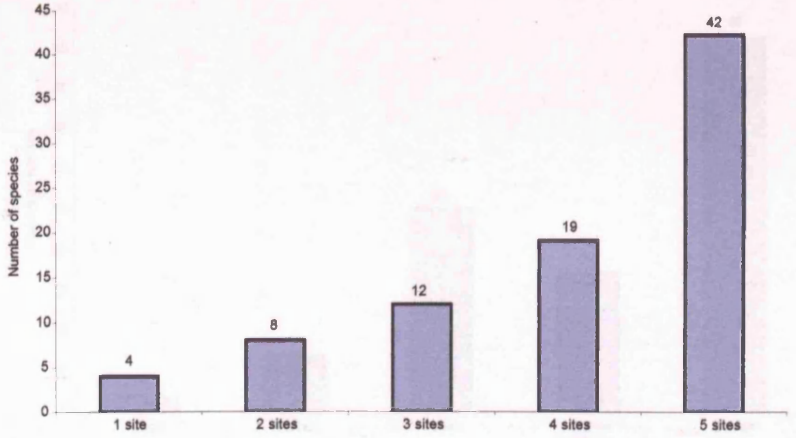

b. Number of species logged vs. number of sites studied

KEY:

A: Karai Section 1, India, sample KA 184.5
B: Shatsky Rise, Pacific Ocean, 198-1213A-19R
C: Shatsky Rise, Pacific Ocean, 198-1214A-8R
D: Col de Palluel section, France, Col P59
E: Selborne, S. England, Sel1/54

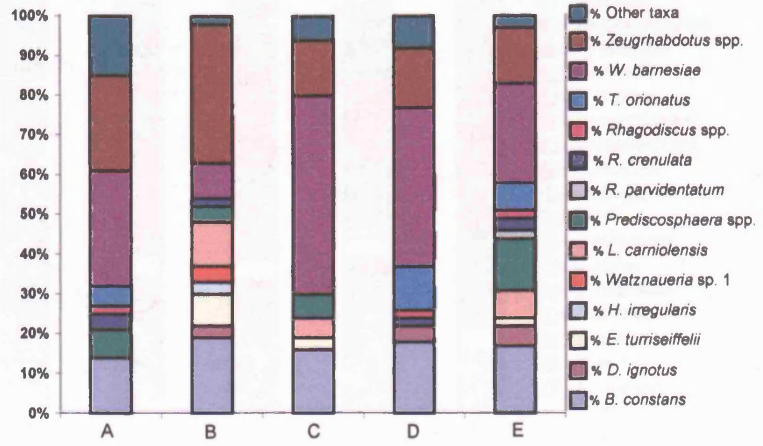

c. Taxa present above 2% based on count data

Figure 8.2 Plots summarising the cosmopolitan distribution of nannofloras at the *E. turriseiffelii* datum-level (Late Albian) based on data from five studied sites.

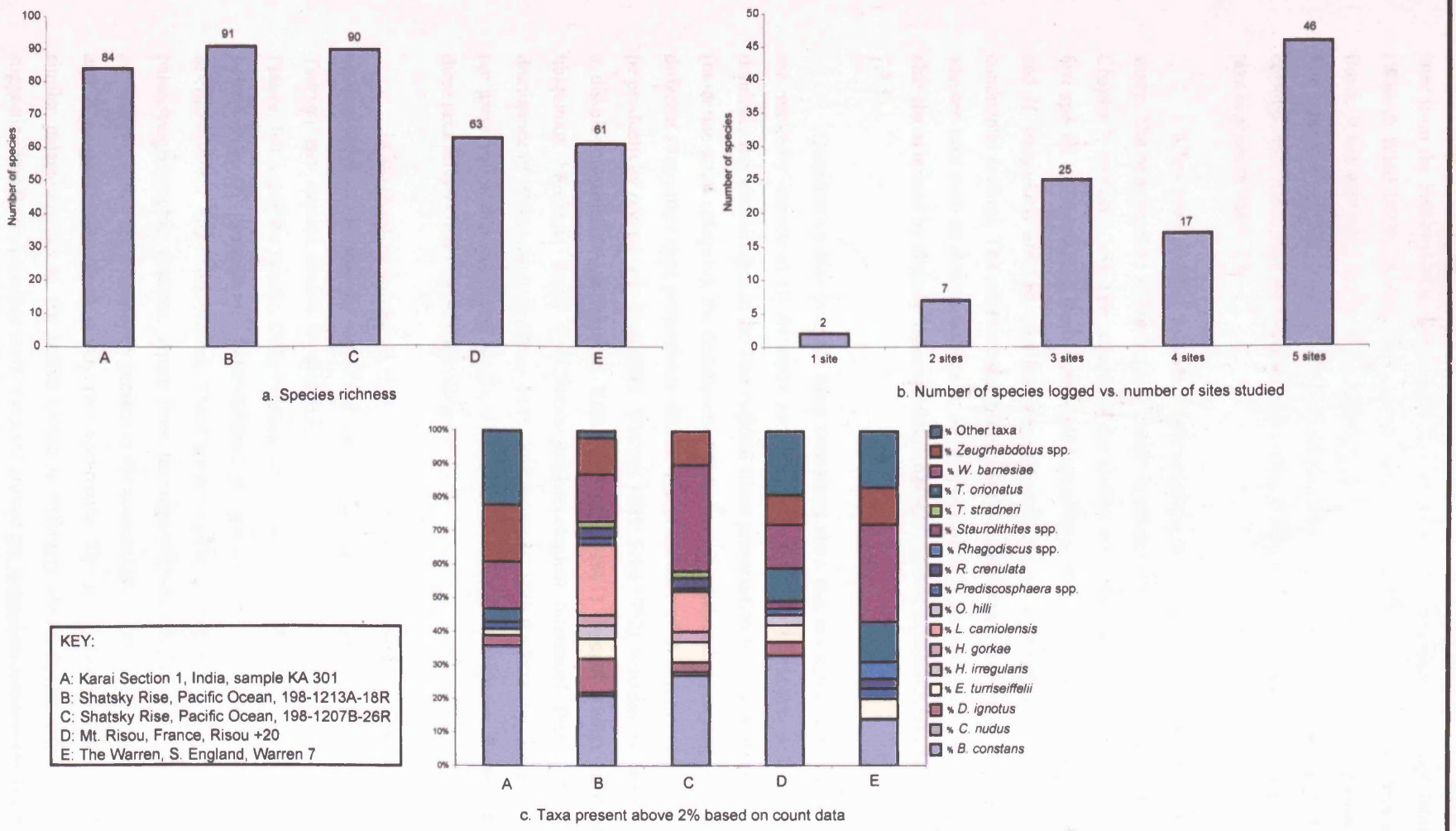

Figure 8.3 Plots summarising the cosmopolitan distribution of nannofloras at the FO of *C. kennedyi*/LO of *W. britannica* datum-level (Early Cenomanian) based on data from the five studied sites.

Laguncula dorotheae, which was reported first from the Gault Clay in England (Black 1971) and later from the Falkland Plateau, has been suggested to have a preference for high-latitude environments (Wise & Wind 1977). The taxon is found to be fairly consistent in samples from France and the Cauvery Basin. It has also been found in the Indian Ocean at DSDP Site 257 (Bown, personal communication). The presence of this taxon in the Vocontian Basin (SE France) suggests that it may have been cosmopolitan rather than restricted to high latitudes. A palaeobiogeographic summary of some important taxa is given in Table 4.3.

It has been possible to make direct comparisons between shelf and oceanic assemblages in this study. The Shatsky Rise in the tropical Pacific is characteristic of oceanic nannofossil assemblages (see Chapter 7, section 7.7.5). The majority of the species in the tropical Pacific are cosmopolitan, with only a few species differentiating them from shelf assemblages from India, England or France. *L. carniolensis* and *H. irregularis* are two taxa that are conspicuously more abundant in oceanic assemblages than continental settings. The oceanic assemblages from the Pacific are marked by the near absence of neritic-adapted taxa such as *Braarudosphaera*, *Micrantholithus* and *Nannoconus*. The oceanic assemblages are also characterised by slightly lower species richness compared to continental sites (see Chapter 7, section 7.7.5)

Quantitative data from the three time-slices show that mid-Cretaceous nannofossil assemblages are markedly uneven in all the study sections. Three taxa (*W. barnesiae*, *B. constans* and *Z. noeliae*) dominate the assemblages in the four regions. Since preservation is broadly similar in the study sections (moderate-good category), the dominance of these taxa is attributed to varying productivity levels at the different sites rather than preservation effects. The abundance of *B. constans* and *Z. noeliae* is known to be productivity related (e.g. Roth 1981; Watkins 1989; Erba 1992), whereas *Watznaueria* is interpreted as a dissolution-resistant species (e.g. Roth & Bowdler 1981). Recent studies have interpreted it as a ubiquitous Mesozoic taxon with broad palaeoecological tolerances (Street & Bown 2000). The dominance of *Watznaueria* in all the study sections agrees with the latter hypothesis that its abundance is not preservation dependent and is related to a primary ecological response. Further discussion on these three taxa follows in the subsequent chapters.

In summary, it is confirmed in this study that Albian and Early Cenomanian nannofloras were cosmopolitan in distribution, as a result of which palaeobiogeographic provinces such as the Boreal, Tethyan and Austral cannot be distinctly recognised in the nannofossil assemblages from England, France, India and the Pacific. Only 7-8 taxa show restricted distribution during the Albian. These are *B. boletiformis*, *T. tessellatus*, *Ceratolithina*, *R. parvidentatum*, *S. primitivum*, *Braarudosphaera*, *Micrantholithus* and *Nannoconus*. The Cauvery Basin assemblages do not show marked Austral palaeobiogeographic features. Apart from the high-latitude taxa such as *R. parvidentatum* and *S. primitivum*, which are consistently present in the assemblages, other Austral taxa such as *S. falklandensis* and *Z. kerguelenensis* show a very rare occurrence. The genus *Ceratolithina*, reported from roughly similar palaeolatitudes in the Indian Ocean is strikingly absent in the Cauvery Basin assemblages, suggesting that it was probably shelf-restricted around the Naturaliste Plateau area in the Indian Ocean.

Taxon	**Cauvery Basin** (Karai Formation)	**SE France** (Mt. Risou, Col de Pré-Guittard sections)	**S.England** (Selborne boreholes, the Warren section)	**western Pacific** (Leg 198, Shatsky Rise)	**Palaeobiogeographic preferences**
Braarudosphaera **spp.**	Trace occurrence	Rare and sporadic (Col de Pré-Guittard); Frequent-Rare, continuous (Mt. Risou)	Rare and sporadic	Trace occurrence	Consistent presence in **Tethyan shelf** settings
Braloweria boletiformis	Absent	Rare, in one sample only (Mt. Risou)	Rare and fairly continuous	Absent	Restricted to **England** and the North Sea (**NW Europe**)
Ceratolithina bicornuta	Absent	Absent	Absent in Selborne, present in the Gault Clay and the North Sea	Absent	Not clear, **possibly restricted to high latitudes**
C. hamata	Absent	Rare and discontinuous (Mt. Risou)	Rare and fairly continuous	Absent	Not clear, present in **Europe and the Indian Ocean**
Crucibiscutum. hayi	Rare and continuous, early appearance in the Early Albian	Rare and discontinuous	Rare and continuous	Absent	**Possibly high-latitude** origins
Gaarderella granulifera	Absent	Frequent-Rare, fairly continuous (Mt. Risou)	Rare and sporadic	Absent	Observed in **Europe** and the Indian Ocean (Site 258)
Gartnerago segmentatum	Frequent, small-sized forms observed in the Late Albian	Outside the age range of samples	Outside the age range of samples	Absent	**Possibly high-latitude** origins
Hayesites irregularis	Rare and sporadic	Indistinguishable from *H. albiensis* (Col de Pré-Guittard), absent in Mt. Risou	Absent	Common-Abundant throughout	**Tropical oceanic** species
Laguncula dorotheae	Rare and fairly continuous	Rare and fairly continuous (Col de Pré-Guittard)	Absent	Absent	**Rare taxon**, but probably cosmopolitan
Lithraphidites carniolensis	Frequent and continuous	Common-Frequent, continuous	Frequent and continuous	Abundant throughout	**Oceanic**-adapted species
Nannoconus **spp.**	Absent	Rare-Frequent, fairly continuous	Rare and sporadic	Trace occurrence	**Tethyan** taxon
Repagulum parvidentatum	Common-Frequent, continuous	Common and continuous (Col de Pré-Guittard) Rare and discontinuous (Mt. Risou)	Common-Frequent, continuous	Absent	**High-latitude** bipolar species
Seribiscutum primitivum	Rare and continuous (Albian-Early Cenomanian); sporadic (mid-Cenomanian -Turonian)	Rare and continuous (Col de Pré-Guittard); Rare and discontinuous (Mt. Risou)	Rare and continuous	Absent	**High-latitude** bipolar species
Sollasites falklandensis	Rare, in one sample only	Absent	Absent	Absent	**High-latitude** species
Tegulalithus tessellatus	Absent	Rare and continuous (Mt. Risou)	Rare and fairly continuous	Absent	**Rare taxon**, observed in Europe and the Indian Ocean (Site 258).

Table 8.1 Palaeobiogeographic summary of selected taxa during the mid-Cretaceous. Abundant: >10/field of view (FOV); Common: 1-10/FOV; Frequent: 1 per 10 FOV's; Rare: 1 per >10 FOV's. 'Sporadic' indicates few occurrences at irregular points in time. 'Trace occurrence' means only one or two specimens observed. 'Discontinuous' means present but not consistently.

8.4 Conclusions

1. Palaeobiogeographic comparisons of nannofossil assemblages from India with coeval assemblages from England, France and the Pacific confirm the hypothesis that the majority of the taxa during the Albian were cosmopolitan. Palaeobiogeographic provinces such as the Boreal, Tethyan and Austral cannot be clearly recognised in the assemblages from these four regions. Only 7-8 taxa show restricted distribution in the Albian, e.g., *B. boletiformis*, *T. tessellatus*, *Nannoconus* and *Braarudosphaera.*

2. The Cauvery Basin assemblages do not show marked Austral features. Apart from the consistent presence of *R. parvidentatum* and *S. primitivum*, no other Austral taxa are regularly found in the assemblages. Both *S. falklandensis* and *Z. kerguelenensis*, known to be Austral taxa, show a very rare distribution in the Karai Formation. The absence of *Ceratolithina* in the Cauvery Basin suggests that it was shelf-restricted in the Naturaliste Plateau region of the Indian Ocean.

Chapter 9. Taxonomy

Since taxonomy is not the main focus of this study, taxonomic descriptions are kept to a minimum and synonymy lists omitted. The first section in this chapter lists all the species cited in the text, figures, plates and data spreadsheets. More than 90% of the species encountered in this study are well established and therefore a repetition of their description is deemed unnecessary. The second section in this chapter is a taxonomic discussion of a few important species, including the description of four new species. The taxonomy applied herein follows the guidelines of Bown and Young (1997) and Bown et al. (1998). The descriptive terminology used herein follows the guidelines of Young et al. (1997), and the following abbreviations have been used in taxonomic descriptions: LM – Light Microscope, XPL – cross polarised light, PC – phase contrast illumination. All observations are based on LM study. The taxa are illustrated in Plates 1-30. The plates are separated on the basis of the study area. Plates 1-16 show nannofossils from the Cauvery Basin, 17-22 from the Gault Clay, and 23-30 from the western Atlantic. Only those bibliographic references that are not included in Perch-Nielsen (1985) and Bown (1998) are included in the reference list.

9.1 Taxonomic list

The species are listed below in alphabetical order; first by generic name followed by the type species and then by the species name. The names in bold are those species that are further discussed or described.

Ahmuellerella Reinhardt, 1964;
Type species: *Ahmuellerella limbitenuis* Reinhardt, 1964
A. octoradiata (Górka, 1957) Reinhardt, 1966
A. cf. *A. octoradiata* (Górka, 1957) Reinhardt, 1966

Amphizygus Bukry, 1969;
Type species: *Amphizygus brooksii* Bukry, 1969
A. brooksii Bukry, 1969

Assipetra Roth, 1973;
Type species: *Micula infracretacea* Thierstein, 1973
A. terebrodentarius (Applegate et al. *in* Covington and Wise, 1987) Rutledge and Bergen *in* Bergen, 1994

Axopodorhabdus Wind & Wise *in* Wise & Wind, 1977;
Type species: *Podorhabdus cylindratus* Noël, 1965
A. albianus (Black, 1967) Wind & Wise *in* Wise & Wind, 1977
A. dietzmannii (Reinhardt, 1965) Wind & Wise, 1983

Biscutum Black *in* Black & Barnes, 1959;
Type species: *Biscutum testudinarium* Black *in* Black & Barnes 1959
B. constans (Górka, 1957) Black *in* Black & Barnes, 1959
B. gaultensis (Mutterlose, 1992) Bown *in* Kennedy et al. 2000

Braarudosphaera Deflandre, 1947;
Type species: *Pontosphaera bigelowi* Gran & Braarud, 1935
B. africana Stradner, 1961
B. cf. *B. primula* Black, 1973

B. stenorhetha Hill, 1976
Braarudosphaera sp. 1
Braarudosphaera sp. 2
Braarudosphaera sp. 3

Braloweria (Black, 1972) Crux, 1991;
Type species: *Braloweria boletiformis* (Black, 1972) Crux, 1991
B. boletiformis (Black, 1972) Crux, 1991

Broinsonia Bukry, 1969;
Type species: *Broinsonia dentata* Bukry, 1969
B. cenomanica (Black, 1973) Bown 2001
B. enormis (Shumenko, 1968) Manivit, 1971
B. galloisii (Black, 1973) Bown *in* Kennedy et al. 2000
B. matalosa (Stover, 1966) Burnett *in* Gale et al. 1996
B. stenostaurion Hill, 1976
B.* cf. *B. viriosa (Jeremiah, 1996) Bown *in* Kennedy et al. 2000

Bukrylithus Black, 1971;
Type species: *Bukrylithus ambiguus* Black, 1971
B. ambiguus Black, 1971

Calciosolenia (Gran, 1912) Young et al., 2003;
Type species: *Calciosolenia murrayi* Gran, 1912
C. fossilis (Deflandre in Deflandre & Fert, 1954) Bown *in* Kennedy et al. 2000

Calculites Prins & Sissingh *in* Sissingh 1977;
Type species: *Tetralithus obscurus* Deflandre, 1959
C. percernis Jeremiah, 1996
***C. karaiensis* sp. nov.**

Ceratolithina Martini, 1967;
Type species: *Ceratolithina hamata* Martini, 1967
C. bicornuta Perch-Nielsen, 1988
C. cruxii Perch-Nielsen, 1988
C. hamata Martini, 1967

Chiastozygus Gartner, 1968;
Type species: *Zygodiscus*? *amphipons* Bramlette & Martini, 1964
C. bifarius Bukry, 1969
C. litterarius (Górka, 1957) Manivit, 1971
C. platyrhethus Hill, 1976
C. cf. *C. amphiphons* (Bramletter & Martini, 1964) Gartner, 1968
C. spissus Bergen *in* Bralower & Bergen, 1998
C. stylesii Burnett, 1998
C. synquadriperforatus Bukry, 1969
C. trabalis (Górka, 1957) Burnett, 1998
***Chiastozygus* spp. (small)**

Corollithion Stradner, 1961;
Type species: *Corollithion exiguum* Stradner, 1961
C. exiguum Stradner, 1961
C.? *madagaskarensis* Perch-Nielsen, 1973
C. kennedyi Crux, 1981
C. protosignum Worsley, 1971
C. signum Stradner, 1963

Corollithion? sp. 1

Cretarhabdus Bramlette and Martini, 1964;
Type species: *Cretarhabdus conicus* Bramlette and Martini, 1964
C. conicus Bramlette and Martini, 1964
C. multicavus Bukry, 1969
C. striatus (Stradner, 1963) Black, 1973

Cribrosphaerella Deflandre *in* Piveteau, 1952;
Type species: *Cribrosphaerella ehrenbergii* Arkhangelsky, 1912
C. ehrenbergii (Arkhangelsky, 1912) Deflandre *in* Piveteau, 1952

Crucibiscutum Jakubowski, 1986;
Type species: *Cruciplacolithus salebrosus* Black, 1971
C. hayi (Black, 1973) Jakubowski, 1986

Crucicribrum Black, 1973;
Type species: *Crucicribrum anglicum* Black, 1973
C. anglicum Black, 1973

Cyclagelosphaera Noël, 1965;
Type species: *Cyclagelosphaera margerelii* Noël, 1965
C. margerelii Noël, 1965
C. reinhardtii (Perch-Nielsen, 1968) Romein, 1977
C. rotaclypeata Bukry, 1969

Cylindralithus Bramlette and Martini, 1964;
Type species: *Cylindralithus serratus* Bramlette and Martini, 1964
C. biarcus Bukry, 1969
C. coronatus Bukry, 1969
C. nudus Bukry, 1969
C. sculptus Bukry, 1969
C. serratus Bramlette and Martini, 1964

Discorhabdus Noël, 1965;
Type species: *Rhabdolithus patalus* Deflandre and Fert, 1954
D. ignotus (Górka, 1957) Perch-Nielsen, 1968

Eiffellithus Reinhardt, 1965;
Type species: *Zygolithus turriseiffelii* Deflandre and Fert, 1954
E. gorkae Reinhardt, 1965
E.? hancockii Burnett, 1998
E. monechiae Crux, 1991
E. turriseiffelii (Deflandre *in* Deflandre and Fert, 1954) Reinhardt, 1965
Eiffellithus sp. 1

Eprolithus Stover, 1966;
Type species: *Lithastrinus floralis* Stradner, 1962
E. apertior Black, 1973
E. floralis (Stradner, 1962) Stover, 1966
E. moratus (Stover, 1966) Burnett, 1998
E. octopetalus Varol, 1992

Flabellites Thierstein, 1973;
Type species: *Watznaueria oblonga* Bukry, 1969
F. oblongus (Bukry, 1969) Crux *in* Crux et al., 1982

Gaarderella Black, 1973;
Type species: *Gaarderella granulifera* Black, 1973
G. granulifera Black, 1973

Gartnerago Bukry, 1969;
Type species: *Arkhangelskiella concava* Gartner, 1968
G. chiasta Varol, 1991
G. nanum Thierstein, 1974
G. cf. *G. nanum* Thierstein, 1974
G. praeobliquum Jakubowski, 1986
G.* cf. *G. praeobliquum Jakubowski, 1986
G. segmentatum (Stover, 1966) Thierstein, 1974
G. theta (Black *in* Black and Barnes, 1959) Jakubowski, 1986

Grantarhabdus Black, 1971;
Type species: *Grantarhabdus meddii* Black, 1971
G. coronadventis (Reinhardt, 1966) Grün *in* Grün and Allemann, 1975

Haqius Roth, 1978;
Type species: *Coccolithites circumradiatus* Stover, 1966
H. circumradiatus (Stover, 1966) Roth, 1978

Hayesites Manivit, 1971;
Type species: *Hayesites albiensis* Manivit, 1971
H. albiensis Manivit, 1971
H. cf. *H. albiensis* Manivit, 1971
H. irregularis (Thierstein *in* Roth and Thierstein, 1972) Applegate et al. *in* Covington and Wise, 1987

Helenea Worsley, 1971;
Type species: *Helenea staurolithina* Worsley, 1971
H. chiastia Worsley, 1971

Helicolithus Noël, 1970;
Type species: *Discolithus anceps* Górka, 1957
H. compactus (Bukry, 1969) Varol & Girgis, 1994
H. trabeculatus (Górka, 1957) Verbeek, 1977

Hemipodorhabdus Black, 1971;
Type species: *Hemipodorhabdus latiforatus* Black, 1971
H. gorkae (Reinhardt, 1969) Grün *in* Grün and Allemann, 1975
H. cf. *H. gorkae* (Reinhardt, 1969) Grün *in* Grün and Allemann, 1975

Laguncula Black, 1971;
Type species: *Laguncula dorotheae* Black, 1971
L. dorotheae Black, 1971
L. montrisouensis Burnett, 1997

Lapideacassis Black, 1971;
Type species: *Lapideacassis mariae* Black, 1971
L. blackii Perch-Nielsen *in* Perch-Nielsen and Franz, 1977
L. cornuta (Forchheimer & Stradner, 1973) Wind & Wise *in* Wise & Wind, 1977
L. glans Black, 1971
L. mariae Black, 1971

Lithraphidites Deflandre 1963;

Type species: *Lithraphidites carniolensis* Deflandre, 1963
L. acutus Verbeek and Manivit *in* Manivit et al., 1977
L. carniolensis Deflandre, 1963
L. pseudoquadratus Crux, 1981
L. cf. *L. pseudoquadratus* Crux, 1981

Loxolithus Noël, 1965;
Type species: *Cyclolithus armilla* Black *in* Black and Barnes, 1959
L. armilla (Black *in* Black and Barnes, 1959) Noël, 1965
***L. bicyclus* sp. nov.**

Manivitella Thierstein, 1971;
Type species: *Crucicolithus pemmatoideus* Deflandre *in* Manivit, 1965
M. pemmatoidea (Deflandre *in* Manivit, 1965) Thierstein, 1971
***M. fibrosa* sp. nov.**

Micrantholithus Deflandre *in* Deflandre and Fert, 1954
Type species: *Micrantholithus flos* Deflandre, 1950?
M. hoschulzii (Reinhardt, 1966) Thierstein, 1971
M. obtusus Stradner, 1963
Micrantholithus sp. 1
Micrantholithus sp. 2

Microrhabdulus Deflandre, 1959;
Type species: *Microrhabdulus decoratus* Deflandre, 1959
M. belgicus Haye and Towe, 1963
M. decoratus Deflandre, 1959

Nannoconus Kamptner, 1931;
Type species: *Nannoconus steinmanni* Kamptner, 1931
Nannoconus truitti group Brönnimann, 1955

Octocyclus Black, 1972;
Type species: *Octocyclus magnus* Black, 1972
O. reinhardtii (Bukry, 1969) Wind & Wise *in* Wise & Wind, 1977

Orastrum Wind & Wise *in* Wise & Wind, 1977;
Type species: *Orastrum asarotum* Wind &Wise *in* Wise &Wind, 1977
O. perspicuum Varol *in* Al-Rifaiy et al., 1990

Owenia Crux, 1991;
Type species: *Owenia hilli* Crux, 1991
O. hilli Crux, 1991

Percivalia Bukry, 1969;
Type species: *Percivalia porosa* Bukry, 1969
P. fenestrata (Worsley, 1971) Wise, 1983
P.? howardii Bown *in* Kennedy et al. 2000
P.* cf. *P. hauxtonensis Black, 1973

Pickelhaube Applegate et al., *in* Covington and Wise, 1987;
Type species: *Pickelhaube furtiva* (Roth, 1983) Applegate et al., *in* Covington & Wise, 1987
P. furtiva (Roth, 1983) Applegate et al., *in* Covington & Wise, 1987
P.* cf. *P. furtiva (Roth, 1983) Applegate et al., *in* Covington & Wise, 1987

Placozygus Hoffmann, 1970;
Type species: *Glaukolithus? fibuliformis* Reinhardt, 1964
P.* cf. *P. fibuliformis (Reinhardt, 1964) Hoffmann, 1970

Prediscosphaera Vekshina, 1959;
Type species: *Coccolithophora cretacea* Arkhangelsky, 1912
P. columnata (Stover, 1966) Perch-Nielsen, 1984
P. cretacea (Arkhangelsky, 1912) Gartner, 1968
P.* cf. *P. ponticula (Bukry, 1969) Perch-Nielsen, 1984
P. spinosa (Bramlette & Martini, 1964) Gartner, 1968

Quadrum Prins & Perch-Nielsen *in* Manivit et al., 1977;
Type species: *Quadrum gartneri* Prins & Perch-Nielsen *in* Manivit et al., 1977
Q. eneabrachium Varol, 1992
Q. octobrachium Varol, 1992

Radiolithus Stover, 1966;
Type species: *Radiolithus planus* Stover, 1966
R. planus Stover, 1966
R.* cf. *R. planus Stover, 1966

Repagulum Forchheimer, 1972;
Type species: *Discolithus parvidentatus* Deflandre & Fert, 1954
R. parvidentatum (Deflandre & Fert, 1954) Forchheimer, 1972

Retecapsa Black, 1971;
Type species: *Retecapsa brightoni* Black, 1971
R. cf. *R. angustiforata* Black, 1971
R. crenulata (Bramlette & Martini, 1964) Grün *in* Grün and Allemann, 1975
R. cf. *R. ficula* (Stover, 1966) Burnett, 1998
R. surirella (Deflandre & Fert, 1954) Grün *in* Grün and Allemann, 1975

Rhagodiscus Reinhardt, 1967;
Type species: *Discolithus asper* Stradner, 1963
R. achlyostaurion (Hill, 1976) Doeven, 1983
R.* cf. *R. achlyostaurion (Hill, 1976) Doeven, 1983
R. angustus (Stradner, 1963) Reinhardt, 1971
R. asper (Stradner, 1963) Reinhardt, 1967
R. asper (large) group
R. gallagheri Rutledge and Bown, 1996
R. hamptonii Bown *in* Kennedy et al., 2000
R. infinitus (Worsley, 1971) Applegate et al. in Covington and Wise, 1987
R. reniformis Perch-Nielsen, 1973
R. reniformis Perch-Nielsen, 1973
R. splendens (Deflandre, 1953) Verbeek, 1977

Rotelapillus Noël, 1973;
Type species: *Rotelapillus radians* Noël, 1973

R. laffittei (Noël, 1957) Noël, 1973

Seribiscutum Filewicz et al., *in* Wise and Wind, 1977;
Type species: *Seribiscutum bijugum* Filewicz et al., *in* Wise and Wind, 1977
S. primitivum (Thierstein, 1974) Filewicz et al., *in* Wise and Wind, 1977

Sollasites Black, 1967;

Type species: *Sollasites barringtonensis* Black, 1967
S. falklandensis Filewicz et al., *in* Wise and Wind, 1977
S. horticus (Stradner et al., *in* Stradner & Adamiker, 1966) Cepek and Hay, 1969

Staurolithites Caratini, 1963;
Type species: *Staurolithites laffittei* Caratini, 1963
S. angustus (Stover, 1966) Crux, 1991
S. crux (Deflandre & Fert, 1954) Caratini, 1963
S. gausorhethium (Hill, 1976) Varol & Girgis, 1994
S. glaber (Jeremiah, 1996) Burnett, 1998
S. laffittei s. l. Caratini, 1963
S. mutterlosei Crux, 1989
S. rotatus Jeremiah, 1996
S. siesseri Bown *in* Kennedy et al., 2000
Staurolithites sp. 1
Staurolithites sp. 2
Staurolithites sp. 3

Stoverius Perch-Nielsen, 1986;
Type species: *Chiphragmalithus achylosus* Stover, 1966
S. achylosus (Stover, 1966) Perch-Nielsen, 1986

Stradnerlithus Black, 1971;
Type species: *Stradnerlithus comptus* Black, 1971
S. geometricus (Górka, 1957) Bown and Cooper, 1989

Tegumentum Thierstein *in* Roth and Thierstein, 1972;
Type species: *Tegumentum stradneri* Thierstein *in* Roth and Thierstein, 1972
T. stradneri Thierstein *in* Roth and Thierstein, 1972

Tetrapodorhabdus Black, 1971;
Type species: *Tetrapodorhabdus coptensis* Black, 1971
T. coptensis Black, 1971
T. decorus (Deflandre *in* Deflandre & Fert, 1954) Wind & Wise *in* Wise & Wind, 1977

Tranolithus Stover, 1966;
Type species: *Tranolithus manifestus* Stover, 1966
T. gabalus (Stover, 1966) Köthe, 1981
T. minimus (Bukry, 1969) Perch-Nielsen, 1984
T. orionatus (Reinhardt, 1966) Reinhardt, 1966
***T. simplex* sp. nov.**

Tubodiscus Thierstein, 1973;
Type species: *Tubodiscus verenae* Thierstein, 1973
T. burnettiae Bown *in* Kennedy et al., 2000

Watznaueria Reinhardt, 1964;
Type species: *Watznaueria angustoralis* Reinhardt, 1964
W. barnesiae (Black, 1959) Perch-Nielsen, 1968
W. biporta Bukry, 1969
W. britannica (Stradner, 1963) Reinhardt, 1964
W. fossacincta (Black, 1971) Bown, 1989
W. manivitiae s. l. Bukry, 1973
W. ovata Bukry, 1969

Zeugrhabdotus Reinhardt, 1965;

Type species: *Zygolithus erectus* Deflandre & Fert, 1954
Z. bicrescenticus (Stover, 1966) Burnett *in* Gale et al., 1996
Z. biperforatus (Gartner, 1968) Burnett, 1998
Z. diplogrammus (Deflandre *in* Deflandre & Fert, 1954) Burnett *in* Gale et al., 1996
Z. embergeri (Noël, 1958) Perch-Nielsen, 1984
Z.* cf. *Z. embergeri (Noël, 1958) Perch-Nielsen, 1984
Z. howei Bown *in* Kennedy et al., 2000
Z. cf. *Z. howei* Bown *in* Kennedy et al., 2000
Z. kerguelenensis Watkins *in* Wise et al., 1992
Z. noeliae Rood et al., 1971
Z. streetiae Bown *in* Kennedy et al., 2000
Z. xenotus (Stover, 1966) Burnett *in* Gale et al., 1996

9.2 Systematic Palaeontology

HETEROCOCCOLITHS

Family Chiastozygaceae (Rood et al., 1973) Varol and Girgis, 1994

***Chiastozygus* spp. (small)**

Plate 1, figs. 16-20

Remarks: Small specimens of *Chiastozygus*, usually <5.0 μm in size, with unicyclic or faintly bicyclic rims and a simple diagonal cross were regularly logged at all the sites.

Occurrence:

Karai Formation: Lower Albian (Zone BC23) – Lower Turonian (Zone UC6).

Gault Clay Formation: Middle - Upper Albian (Zones BC24-BC25b).

Leg 171B, Hole 1049C: Lower Albian (Zone BC23).

Leg 198, Hole 1207B: Trace occurrence, Upper Aptian (Zone NC7) – Lower Cenomanian (Zones UC1/2).

Zeugrhabdotus* cf. *Z. embergeri (Noël, 1958) Perch-Nielsen, 1984

Plate 3, figs. 11-15; Plate 23, figs. 26-28

Remarks: Used herein for small (<7.0 μm) bicyclic loxolith rims possessing a thick, robust, birefringent transverse bar bearing a spine. The spine divides the bar into two parts. The spine base appears as a prominent black spot under XPL. A variety of morphologies are included in this species with respect to the bar and spine morphology. Some forms appear darker than others under XPL.

Occurrence:

Karai Formation, Section 1: Middle Albian (Zone BC24) – Lower Turonian (Zone UC6).

Karai Formation, Section 2: Upper Albian (Zone BC27) - Upper Cenomanian (Zones UC3-4).

Gault Clay Formation: Middle - Upper Albian (Zone BC25).

Leg 171B, Hole 1049C: Upper Aptian (Zones BC21-22) - Lower Albian (Zone BC23).

Leg 198, Hole 1207B: Lower Albian (Subzone NC8a-b) - Lower Cenomanian (Zone UC1-2).
Leg 198, Hole 1213A/B: Lower Albian (Subzones NC8a-b) – Lower Cenomanian (Zone UC2).

Zeugrhabdotus kerguelenensis Watkins, 1992

Plate 2, figs. 9-10

Remarks: Used herein for side views of loxolith coccoliths with a very broad spine. The specimens are easier to identify in side view than in plan view. Sizes are in the range of 5-8 μm. Very rare and sporadic distribution in the Cauvery Basin (Karai Formation, Section 2).

***Loxolithus bicyclus* sp. nov.**

Plate 1, figs. 23-26

1998 *Loxolithus* sp. 2, Bralower and Bergen, p. 75, pl. 1, fig. 2

Derivation of name: From '*cyclus*' in Latin meaning cycle, referring to the two cycles clearly observed in this species.

Diagnosis: Medium to large-sized elliptical muroliths with a bicyclic rim and an open central area. The inner rim cycle is bright and spiralled.

Differentiation: The species is readily distinguished from *L. armilla* by its bicyclic rim. *L. armilla* has a unicyclic rim.

Dimensions: Length 6-10 μm, width c. 5 μm. 20 specimens measured.

Holotype: Plate 1, figure 23 (fig. 24 is the same specimen).

Type locality: Karai Formation, Cauvery Basin, SE India.

Type level: Lower Cenomanian, sample GR 16, Zones UC1-2.

Abundance: Rare

Occurrence:
Karai Formation, Section 1: Middle - Upper Cenomanian (Zones UC3-UC4).
Karai Formation, Section 2: Upper Albian (Zone BC27) - Lower Turonian (Zone UC6).

Staurolithites laffittei s.l.

Plate 1, figs. 35-42; Plate 17, figs. 21-22

Remarks: Refers here to the small-sized (<7 μm), unicyclic to faintly bicyclic species of *Staurolithites* with a simple axial cross in the central area. It is difficult to assign a species name to these taxa because of their nondescript morphology. The taxonomy of *Staurolithites* is problematic because of the broad range of morphologies it encompasses in the absence of a cohesive classification strategy. Frequently observed throughout the mid-Cretaceous (Aptian-Turonian) in all the studied regions.

Placozygus* cf. *P. fibuliformis (Reinhardt, 1964) Hoffmann, 1970

Plate 4, figs. 1-3

Remarks: Although the range of this species is reported to be Turonian-Maastrichtian (Burnett 1998), it is frequently observed in Albian-Cenomanian sediments in all the study sections. Empty rims without the complex transverse central area bar were frequently encountered.

***Tranolithus simplex* sp. nov.**

Plate 2, figures 33-42

Derivation of name: From '*simplex*', Latin for simple, referring to the simply constructed bars in the central area.

Diagnosis: A small to medium-sized species of *Tranolithus* with the central area spanned by two narrow and disjunct transverse bars directly apposed to each other. The two bars are simply constructed and appear darker than the rim in XPL. The bars terminate with a forked end especially under high focus. No spine base is visible.

Differentiation: This species is sometimes confused with the Jurassic/Cretaceous species *Z. erectus*. The difference is that *Z. erectus* has very bright (high birefringence) transverse bars with a spine. The transverse bar in *Z. erectus* can be disjunct or continuous and the spine base appears as a black spot in XPL. This species of *Tranolithus* has dark and long bars without any obvious spine base.

The species has been placed under the genus *Tranolithus* and not under *Zeugrhabdotus* because its overall LM appearance is closer to other *Tranolithus* species, e.g., *T. orionatus* and *T. gabalus*. However, in view of the poor understanding of this generic group in terms of phylogeny, this is not definitive.

Dimensions: Length 5.0-7.5 μm, width c. 3.0 μm. 20 specimens measured.

Holotype: Plate 2, figure 40 (figs. 40-42 are the same specimen).

Paratype: Plate 2, figure 35 (figures 36-37 are the same specimen).

Type locality: Karai Formation, Cauvery Basin, SE India.

Type level: Lower Cenomanian; sample KA 373 (Subzone UC2a).

Abundance: Frequent – Rare.

Range: Albian – Turonian, possibly extends further into the Late Cretaceous.

Occurrence:
Karai Formation, Section 1: Lower Albian (Zone BC23) – Lower Turonian (Zone UC6).
Karai Formation, Section 2: Upper Albian (Zone BC27) – Lower Turonian (Zone UC6).
Gault Clay Formation: Middle - Upper Albian (Zones BC24-BC25b).
Leg 171B, Hole 1049C: Lower Albian (intra Zone BC23).

Family Rhagodiscaceae Hay, 1977

Percivalia* cf. *P. hauxtonensis Black, 1973
Plate 17, figs. 38-42; Plate 18, figs. 1-10

Remarks: Medium-sized (5-7 μm), elliptical muroliths with a pronounced bright inner cycle and a central area having a thick 'x' shaped cross. A well-developed spine base is present at the centre. The x-shaped cross appears like a broad bridge, spanning almost two-thirds of the central area.

These specimens match the SEM description of *P. hauxtonensis*, which was described as having 'a specialised central area surmounted on the distal side by a broad bridge and a well-developed spine.' The holotype of Black, 1973 (pl. 31, figs. 10-14) is comparable to the specimens observed here. Size range and age of the taxon also match well with Black's original description. Bralower and Bergen (1998) described this species under LM as having a bright central plate with two longitudinal perforations. However, their LM images of *P. hauxtonensis* (pl. 2, fig. 1, p. 62) are clearly of a different species from the one that is being discussed here.

Occurrence:
Gault Clay Formation: Middle - Upper Albian (Subzones BC25a - BC25b).

Rhagodiscus* cf. *R. achlyostaurion (Hill, 1976) Doeven, 1983

Plate 6, figs. 3-8

Remarks: A taxon very similar to *R. achylostaurion* with a prominent and robust spine base. The spine base appears to be raised compared to the rim. The central area is otherwise granular, similar to *R. achlyostaurion*. Dimensions are comparable to *R. achlyostaurion* with an average length of c. 6 μm and a width of c. 4 μm. It is difficult to confirm whether this is a preservational difference or an intraspecific variation. Comparable to *Rhabdolithina swinnertoni* Black, 1971 that has a large spine, but since its holotype is a SEM it is difficult to ascertain if this is the same species.

Occurrence:

Karai Formation, Section 1: Lower – Middle Albian (Zone BC23-25).

Karai Formation, Section 2: Upper Albian (Zone BC27) – Lower Cenomanian (Zones UC1-2).

Gault Clay Formation: Middle - Upper Albian (Subzones BC25a - BC25b).

Leg 171B, Hole 1049C: Lower Albian (intra Zone BC23).

Rhagodiscus asper (Stradner, 1963) Reinhardt, 1967 Group

Plate 5, figs. 40-42; Plate 6, fig. 2; Plate 24, figs. 22-42

Remarks: Murolith coccoliths with a broad central area spanned by a granular plate that usually bear a spine. The rim is unicyclic. They are usually large-sized (>8.0 μm). A variety of morphologies conforming to this description were observed in Aptian-Cenomanian sediments in all the studied regions. They have been split into a number of species by Bown (*in press*). In this study, they were broadly logged as *R. asper* large-sized group.

Rhagodiscus reniformis Perch-Nielsen, 1973

Plate 6, figs. 20-23; Plate 18, fig. 18

Remarks: Although the range of this species is reported to be Turonian-Maastrichtian (Burnett 1998), it is frequently logged in the mid-Cretaceous. The morphology of the specimens observed in this study is comparable to the SEM holotype and the SEM/LM paratypes of this species. The stratigraphic range of this species is extended here in light of its consistent presence from the mid-Albian.

Published range: Turonian-Maastrichtian (Burnett, 1998).

Modified range: mid-Albian – Maastrichtian.

Occurrence:

Karai Formation, Section 1: Middle Albian (Zone BC25) – Lower Turonian (Zone UC6).

Karai Formation, Section 2: Upper Albian (Zone BC27) – Lower Turonian (Zone UC6).

Gault Clay Formation: Middle - Upper Albian (Subzones BC25a - BC25b).
Leg 198, Hole 1207B: Trace occurrence in the Lower Cenomanian (Zones UC1-2).

Family Axopodorhabdaceae Bown and Young, 1987

Octocyclus reinhardtii (Bukry 1969) Wind & Wise *in* Wise & Wind, 1977
(Synonym: *Octocyclus magnus* Black, 1972)
Plate 8, figs. 26, 27; Plate 18, fig. 39

Remarks: There is some confusion regarding the nomenclature of these two species. The definition of the two species reveals that they have identical morphologies. Bukry (1969) defined *O. reinhardtii* as a species similar to *A. dietzmannii* in most respects but with eight large and round perforations in the central area, symmetrical to the long and short axes of the ellipse. The TEM holotype of *reinhardtii* is that of a partly broken specimen. The species was originally described with an Early Santonian age. Black (1972) described *O. magnus* similarly, but from the Albian Gault Clay. The characteristic features of *O. magnus* were its large size, a tubular spine in the centre and eight large windows or perforations arranged symmetrically in the central area along the principal axes of the ellipse. The holotypes of both the species are TEM images and therefore not useful in LM study. The size-ranges of the two taxa are comparable. Both are large coccoliths with an average length of approximately 10-12 μm, although Black described a broader size range for *O. magnus* (8.4-19 μm).

Under the LM, it is impossible to differentiate between the two species based on morphology or size. Thus *O. magnus* is regarded here as a junior synonym of *O. reinhardtii*.

Dimensions: >8.0 μm (length).

Occurrence:
Karai Formation, Section 1: Middle Albian (Zone BC24) – Lower Turonian (Zone UC6).
Karai Formation, Section 2: Upper Albian (Zone BC27) – Upper Cenomanian (Zones UC3-4).
Gault Clay Formation: Middle - Upper Albian (Zones BC24 - BC25b).

Tetrapodorhabdus decorus (Deflandre in Deflandre & Fert, 1954)
Wind & Wise *in* Wise & Wind, 1977
Tetrapodorhabdus coptensis Black, 1971

Plate 8, figs. 23-25

Remarks: The morphology of *T. coptensis* is very similar to that of *T. decorus*. Both have a podorhabdid rim with a hollow spine base and four perforations separated by offset cross bars. The holotypes of these species are not helpful in understanding their relationship. The holotype of *T. coptensis* is a SEM whereas

that of *T. decorus* is a LM side view showing a tall, flaring spine. It is therefore impossible to correlate the two holotypes. There is not much difference between the two species under LM in plan view, except that they differ in size, as per their original descriptions (*decorus* 11.5 μm; *coptensis* ~7 μm). *T. decorus* has a more conspicuous spine base compared to *T. coptensis*. In this study, specimens <8 μm were logged as *T. coptensis* whilst those >8 μm were assigned to *T. decorus*. Both species range throughout the mid-Cretaceous (Aptian-Turonian), and are observed in all the study sections.

FAMILY Biscutaceae Black, 1971

Biscutum constans (Górka, 1957) Black *in* Black and Barnes, 1959
Plate 8, figs. 30-33

Remarks: Large coccoliths of *B. constans* (>5 μm) are common to frequent in the mid-Cretaceous. Erba (*in* Premoli Silva et al., 1989) misidentified large-sized specimens of *B. constans* as *B. magnum* in the Albian. Tremolada (2002) reported the FO of large *B. constans* in the Middle Albian Zone NC9 in the Umbria-Marche Basin (central Italy). According to him, the FO of large *B. constans* follows the FO of *A. albianus*. This observation is not agreed upon in this study because large *B. constans* is found at the base of the Albian at the FO of *P. columnata* datum-level in the Cauvery Basin.

Occurrence:
Karai Formation, Section 1: Lower Albian (Zone BC23) - Lower Turonian (Zone UC6)
Gault Clay Formation: Middle - Upper Albian (Zones BC24 - BC25b).
Leg 198, Hole 1207B/1213A-B: Lower Albian (Zone NC8) – Lower Cenomanian (Zone UC2).

Family Cretarhabdaceae Thierstein, 1973

Pickelhaube* cf. *P. furtiva (Roth, 1983) Applegate et al., in Covington and Wise, 1987
Plate 11, fig. 14; Plate 25, figs. 33-35

Remarks: Used herein for broadly elliptical placoliths with two moderately birefringent shields of comparable width and an open central area. The taxon is very rare.

Occurrence:
Karai Formation, Section 1: Lower Albian (Zone BC23) – Middle Albian (Zone BC25).
Karai Formation, Section 2: Lower Cenomanian (Zones UC1-2); present in one sample only.
Gault Clay Formation: Middle - Upper Albian (Zones BC24 - BC25b).
Leg 171B, Hole 1049C: Lower Aptian (Zone BC21-22) – Lower Albian (Zone BC23)
Leg 198, Hole 1207B: Upper Aptian (Zone NC7) - Lower Albian (lower Zone NC8).

Cretarhabdus* cf. *C. multicavus Bukry, 1969

Plate 10, figs. 40-42; Plate 11, figs. 1-5; Plate 19, figs. 34-39

Remarks: Used herein for small to medium-sized (<7 μm) coccoliths with a heavy *Cretarhabdus* like shield and a central plate with a reinforced longitudinal bar. There are 2-3 perforations in each quadrant, which appear as black dots in XPL. The holotype of this species is a SEM that shows offset cross bars. However, the cross bars do not appear offset under LM. The species is rare in the mid-Cretaceous.

Occurrence:

Karai Formation, Section 1: Middle Albian (Zone BC25) – Lower Turonian (Zone UC6).

Karai Formation, Section 2: Upper Albian (Zone BC27) - Upper Cenomanian (Zones UC3-4).

Gault Clay Formation: Middle - Upper Albian (Subzones BC25a-BC25b).

Family Prediscosphaeraceae Rood et al., 1971

Prediscosphaera* cf. *P. ponticula (Bukry, 1969) Perch-Nielsen, 1984

Plate 10, figs. 8-15; Plate 19, figs. 10-12

Remarks: Used here for large-sized (>7 μm), broadly circular species of *Prediscosphaera* with 'x' shaped cross bars at the centre. '*Ponticula*' was originally described as a subspecies of *Prediscosphaera cretacea* with a circular outline, a proportionately broader rim and 4 slender auxillary bars extending from the margin of the central area to the inner ends of the principal cross bars (Bukry, 1969). The additional bars are almost never seen, possibly due to preservation. Hence the taxon is referred to as *P.* cf. *P. ponticula*.

Occurrence:

Karai Formation, Sections 1 & 2: Lower Cenomanian (Zone UC2) – Lower Turonian (Zone UC6).

Gault Clay Formation: Upper Albian (Subzone BC25b).

Family Tubodiscaceae Bown and Rutledge *in* Bown and Young, 1997

***Manivitella fibrosa* sp. nov.**

Plate 11, figs. 29-36; Plate 19, fig. 42

Derivation of name: From '*fibra*' in Latin meaning fibres, referring to the fibrous appearance of the coccolith.

Diagnosis: Large, elliptical placolith rim composed of two narrow shields and a third, narrow collar-cycle that is variable in height. The central area is broad and vacant. The overall LM image is dark but the

collar cycle is bright compared to the distal cycle. The outline of the distal cycle is diffuse, giving a fibrous appearance under XPL. Under PC, the rim appears as a dark band of uniform thickness.

Differentiation: The species is readily distinguished from *M. pemmatoidea* in two ways:

1. Its overall appearance (under XPL) is darker than *M. pemmatoidea.*
2. The fibrous appearance is not seen in *M. pemmatoidea.*

The species is not directly comparable to *M. pecten* (Black, 1973) or *M. gronosa* (Stover, 1966) in terms of its morphology. These two species are described in Black (1973).

Dimensions: Length 8.0-11 μm, width c. 5 μm. 20 specimens measured.

Holotype: Plate 11, figure 31.

Paratype: Plate 11, figure 29 (fig. 30 is the same specimen under PC).

Type locality: Karai Formation, Cauvery Basin, SE India.

Type level: Upper Albian, sample KA 278.5, (Zone BC27).

Abundance: Frequent – Rare.

Range: Early Albian – mid-Cenomanian, possibly extends into the Late Cretaceous.

Occurrence:
Karai Formation, Section 1: Middle Albian (Zone BC24) – Middle Cenomanian (Zone UC3).
Karai Formation, Section 2: Upper Albian (Zone BC27) – Middle Cenomanian (Zone UC3).
Gault Clay Formation: Middle - Upper Albian (Zones BC24 - Zone BC25b).
Leg 171B, Hole 1049C: Upper Aptian (Zone BC21-22) – Lower Albian (Zone BC23).
Leg 198, Hole 1207B: Upper Aptian (Zone NC7) – Upper Albian (Subzone NC9B).
Leg 198, Hole 1213A/B: Berriasian (Subzone NK2a) – Middle Cenomanian (Zone UC3).

Family Watznaueriaceae Rood et al., 1971

Watznaueria manivitiae s. l. Bukry, 1973
Plate 12, figs. 10-11

Remarks: Used herein for large-sized (>8 μm) elliptical coccoliths having watznauerian shields and a relatively elongate central area aligned with the long axis of the ellipse. Displays high birefringence

colours (high order yellow to orange) under XPL. Although *manivitiae* is strictly speaking a Jurassic species, it is observed in the mid-Cretaceous. Hence it is called *manivitiae sensu lato* here.

Occurrence:

Karai Formation, Section 1: Lower Albian (Zone BC23) – Lower Turonian (Zone UC6).

Karai Formation, Section 2: Upper Albian (Zone BC27) – Lower Turonian (Subzone UC6).

Gault Clay Formation: Middle - Upper Albian (Zones BC24 - BC25b).

Leg 171B, Hole 1049C: Upper Aptian (Zone BC21-22) – Lower Albian (Zone BC23).

FAMILY Arkhangelskiellaceae Bukry (1969) Bown & Hampton *in* Bown & Young, 1997

Broinsonia galloisii (Black, 1973) Bown *in* Kennedy et al., 2000

Plate 12, figs. 21-23; Plate 20, figs. 7-9

Remarks: Bown recombined *Acaenolithus galloisii* (Black, 1973) to *Broinsonia galloisii* for substantive reasons (see discussion by Bown *in* Kennedy et al. 2000, p. 651). He also differentiated *B. galloisii* from the related form *B. matalosa* on the basis of size. Specimens ranging in size from 4.0-5.5 μm were classified under *galloisii* whereas *matalosa* was used for specimens >8.0 μm in his study. In my view, this size-based division poses problems because there are *Broinsonia* specimens that fall in the size range of 5.5-8 μm throughout the Albian-Cenomanian. They have to be called *B.* cf. *B. matalosa* or *B.* cf. *B. galloisii*. In order to remove the ambiguity of the 'cf. *galloisii/matalosa*' category, it is proposed here that the upper limit of the size range of *B. galloisii* be raised to 7 μm. Thus *B. galloisii* should cover all small and medium sized specimens of *Broinsonia*. There is no morphological difference between *B. matalosa* and *B. galloisii* under LM except the size. Since Stover (1966) defined *B. matalosa* in the size range of 7-11μm, it is appropriate to use 7μm as the cut-off between *B. galloisii* and *B. matalosa*.

Dimensions: 3.5-7.0 μm, 20 specimens measured.

Occurrence:

Karai Formation, Section 1: Lower Albian (Zone BC23) – Lower Turonian (Zone UC6).

Karai Formation, Section 2: Upper Albian (Zone BC27) – Upper Cenomanian (Zones UC3-4)

Gault Clay Formation: Middle - Upper Albian (Zones BC24-25b).

Leg 171B, Hole 1049C: Lower Albian (Zone BC23).

Leg 198, Hole 1207B/1213A-B: Trace occurrence, Lower Albian (Zone NC8) – Middle Cenomanian (Zone UC3).

Broinsonia* cf. *B. viriosa (Jeremiah, 1996) Bown *in* Kennedy et al. 2000

Plate12, figs. 41-42; Plate 13, figs. 1-3

Remarks: Specimens resembling *B. viriosa* (Jeremiah, 1996) were encountered in the Middle Albian (samples KA 31.5 - KA 99) in the Karai Formation. Although their occurrence is clearly outside the range of the species (Late Aptian - earliest Albian), the specimens had the typical appearance of *B. viriosa* with a large central opening and a massive cross, and were therefore logged as *B.* cf. *B. viriosa*. The size of the specimens observed (6.5–7.5 μm) is smaller than the usual size of *B. viriosa* (>8.0 μm).

Occurrence:
Karai Formation, Section 1: Middle Albian (Zones BC24 - BC25).

Family Kamptneriaceae Bown and Hampton *in* Bown and Young, 1997

Gartnerago segmentatum (Stover, 1966) Thierstein, 1974
Gartnerago obliquum (Stradner, 1963) Noël, 1970
Plate 13, figs. 33-42

Remarks: *G. segmentatum* could not be differentiated from *G. obliquum* in this study. *G. obliquum* was originally described by Stradner (1963) as an imperforate coccolith with a wide central area having an oblique cross. Thierstein (1974) opined that the main feature of *G. obliquum* were the two rows of perforations along the long axis of the coccolith. *G. segmentatum*, on the other hand, was first described (under LM) as a large species (9-12 μm) having a base plate made of 8 radially arranged wedge shaped blocks resembling propeller blades (Stover, 1966). According to Thierstein (1974), the two species are 'conspecific morphotypes' with similar stratigraphic ranges. He commented that the two species are not easily distinguishable, especially under LM, as intermediate specimens occur frequently. He also stated that the abundances of the two morphotypes show a reciprocal relationship depending on the preservation in a sample.

Perch Nielsen (1985) commented that *G. obliquum* includes many of the different large *Gartnerago* species and has a large central plate divided into eight parts. The FO of *G. obliquum* was placed in the Early Turonian by Perch-Nielsen (1985). Burnett (1998) identified the two species separately and placed their FO's close to each other in the Early Cenomanian, the FO of *G. segmentatum* preceding the FO of *G. obliquum*.

G. obliquum could not be conclusively identified in the Karai Formation in spite of the overall moderate-good preservation in the samples. It is difficult to distinguish between the two species under LM because of their similar morphology. The perforations that are supposed to be a characteristic feature of *G. obliquum* are not visible under LM.

Occurrence:

Karai Formation, Section 1: Lower Cenomanian (Zone UC2) – Lower Turonian (Zone UC6).

Gartnerago* cf. *G. praeobliquum Jakubowski, 1986

Plate 13, figs. 23-32; Plate 20, figs. 17-22

Remarks: Small-sized (<6 μm) specimens bearing a strong resemblance to *Gartnerago praeobliquum* (Jakubowski, 1986) were encountered in the Upper Albian-Cenomanian sediments from the Gault Clay and Cauvery Basin. These specimens show the characteristic bright outer cycle and the dark inner cycle with an axial cross that is typical of *G. praeobliquum* (in XPL). The differences being that these specimens are small in size, and have thin axial cross bars minus the flaring 'arrowhead' termination. Specimens are rare and inconsistent in occurrence.

Occurrence:

Karai Formation, Section 1: Middle Cenomanian (Subzone UC3a-b) – Upper Cenomanian (Subzone UC3e-5).

Karai Formation, Section 2: Upper Albian (Zone BC27) – Lower Turonian (Zone UC6).

Gault Clay Formation: Upper Albian (Subzone BC25b).

Gartnerago* cf. *G. nanum Thierstein, 1974

Plate 14, figs. 1-6

Remarks: Used herein for small to medium sized (5-8 μm) specimens of *Gartnerago* that differ from the SEM holotype of Thierstein (1974) in lacking an axial cross in the central area opening. This species is almost certainly different from *G. nanum* and needs a new name. Bown (*in press*) has renamed this species as *G. ponticulus*. Further details can be found in that paper.

Occurrence:

Karai Formation, Section 1: Lower Cenomanian (UC2-UC3).

Karai Formation, Section 2: Upper Albian (BC27) – Lower Cenomanian (UC3).

HOLOCOCCOLITHS

Family Calyptrosphaeraceae Boudreaux & Hay, 1969

***Calculites karaiensis* sp. nov.**

Plate 14, figs. 38-42; Plate 15,1-9

Derivation of name: From '*Karai*', the stratigraphic unit in which it was noticed.

Diagnosis: An elliptical, small-sized species of *Calculites* with a narrow rim made up of 6-7 blocks. The blocks extinguish separately on rotating the stage and are asymmetric. The sutures between the blocks are irregular. The surface of the holococcolith appears to be smooth under LM with a central pore or depression.

Differentiation: The species is distinguished by the multiple blocks (6-7) that are asymmetric. The other mid-Cretaceous species, *C. percernis* has only four blocks. Owing to the limited understanding of holococcolith taxonomy, the generic placement of this species under *Calculites* is tentative.

Dimensions: Length 4.5-5.5 μm, width c. 3.0 μm. 30 specimens measured.

Holotype: Plate 14, figure 41 (fig. 42 is the same specimen).

Paratype: Plate 14, figure 38 (figs. 39-40 are the same specimen).

Type locality: Karai Formation, Cauvery Basin, SE India.

Type level: Lower Turonian, sample KA 459.3 (Subzone UC6b).

Abundance: Frequent/Few, present in one sample only.

Occurrence: Lower Turonian.

NANNOLITHS

Family Polycyclolithaceae (Forchheimer, 1972) Varol, 1992

Radiolithus* cf. *R. planus Stover, 1966
Plate 16, figs. 16-23; Plate 21, figs. 30-36

Remarks: A degree of confusion has arisen over the nomenclature of the high-walled *Radiolithus* group. The genus *Radiolithus* was originally described by Stover (1966) as circular in plan view with nine radial segments and a low, narrow rim. The cross sectional outline of the genus was described as 'U'-shaped giving it a flat appearance. *R. planus* was described by Stover (1966) as 'composed of eight or nine radial segments that appear as a rosette in plan view with a rounded to angular outer margin. The outer margins can be rounded, bilobed or pointed but are generally all of the same shape on individual specimens.' No holotype was designated for this species. The LM images of the species in the paper (pl. 7, p. 163, figs. 22-24) are not in tune with the generic description of *Radiolithus*, because the shield appears to have a high wall made of petal shaped elements that are characteristic of the genus *Eprolithus*. This invalidates the holotype and in effect, no holotype exists for this species.

Burnett (1988) produced very good SEM and LM illustrations of *R. planus* to clarify its taxonomy. In her view, the structure of *R. planus* is relatively simple. Under the SEM in plan view, nine blocks interdigitate with zig-zag sutures to form a low cylinder, surrounding a central diaphragm. In side view, the wall is composed of two layers, the upper layer having half the height of the lower and the cross-sectional view is 'U' shaped. Burnett (1988) described the range of *R. planus* as Albian-Santonian.

Varol (1992) classified *Radiolithus* based on the height of the wall. He formulated two groups, i.e., the low-wall (<4 μm) or the *R. planus* group and the high-wall (>4 μm) or the *R. orbiculatus* group. According to him, these two groups can be identified in plan view by their birefringence. This classification appears to be superficial due to lack of SEM perspective and was therefore not used. In this study, all specimens other than *R. planus* that show a considerably thick outer margin were logged as *R.* cf. *R. planus*.

Occurrence (*Radiolithus* cf. *R. planus*):
Karai Formation, Section 1: Middle Albian (Zone BC25) – Lower Turonian (Zone UC6).
Karai Formation, Section 2: Upper Albian (Zone BC27) - Lower Turonian (Zone UC6).
Gault Clay Formation: Middle - Upper Albian (Zones BC24 - BC25b).
Leg 171B, Hole 1049C: Upper Aptian (Zone BC21-22) – Lower Albian (Zone BC23).

UNCERTAIN POLYCYCLOLITHS

Assipetra terebrodentarius (Applegate et al. *in* Covington and Wise, 1987) Rutledge and Bergen *in* Bergen, 1994

Plate 26, figs. 22-42

Remarks: Used herein for blocky nannoliths made up of numerous complexly intergrown calcite blocks joined along radial sutures. The shape varies from broadly circular to rectangular. Specimens show high birefringence colours. The species has been split into two subspecies based on size (Tremolada & Erba, 2002). However, there is some discrepancy with regards to the size of the holotype. Hence the classification of Tremolada and Erba (2002) was not used in this study.

PLATE 1 - CAUVERY BASIN, KARAI FORMATION, SECTIONS 1 & 2

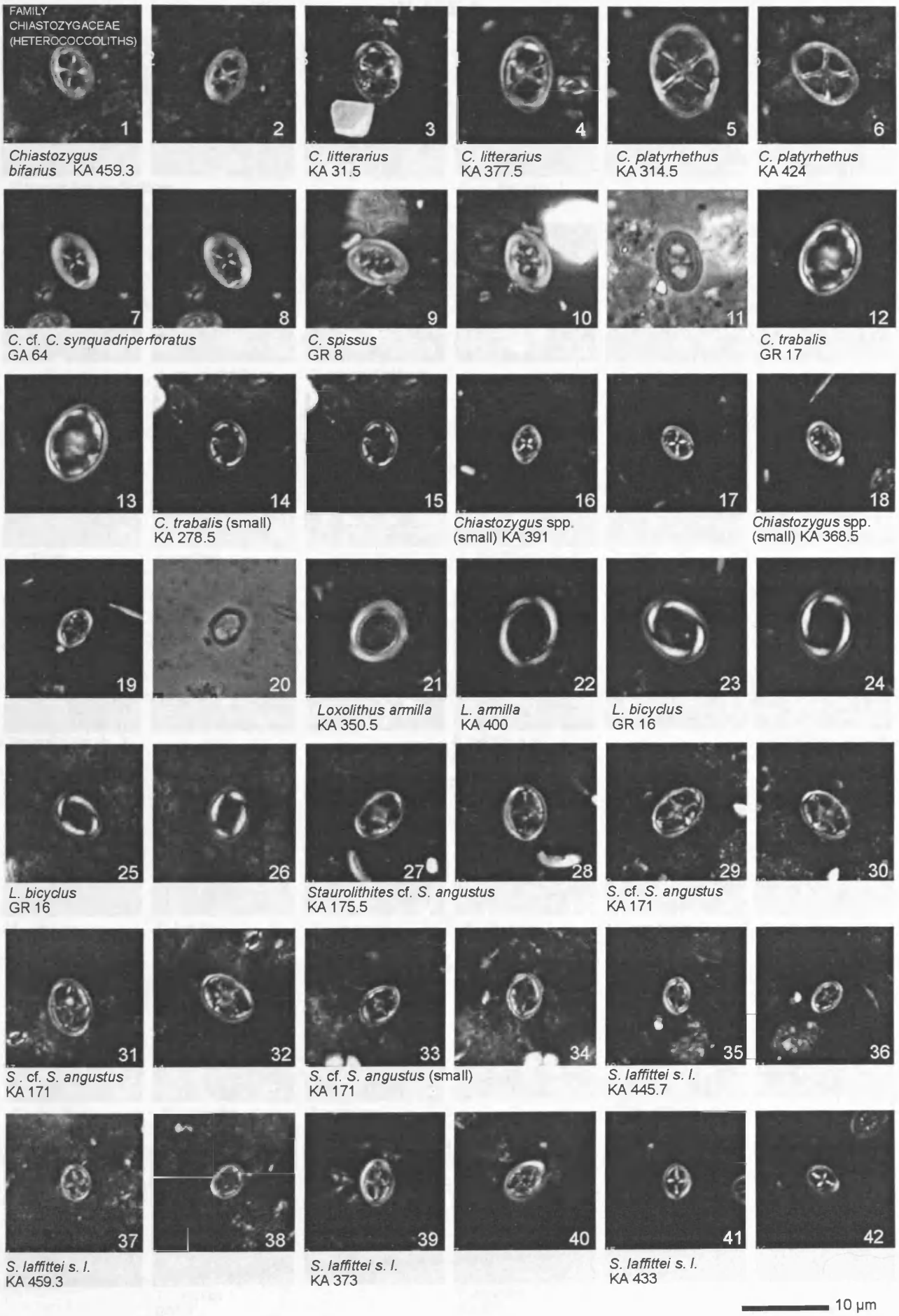

Chiastozygus bifarius KA 459.3

C. litterarius KA 31.5

C. litterarius KA 377.5

C. platyrhethus KA 314.5

C. platyrhethus KA 424

C. cf. *C. synquadriperforatus* GA 64

C. spissus GR 8

C. trabalis GR 17

C. trabalis (small) KA 278.5

Chiastozygus spp. (small) KA 391

Chiastozygus spp. (small) KA 368.5

Loxolithus armilla KA 350.5

L. armilla KA 400

L. bicyclus GR 16

L. bicyclus GR 16

Staurolithites cf. *S. angustus* KA 175.5

S. cf. *S. angustus* KA 171

S . cf. *S. angustus* KA 171

S. cf. *S. angustus* (small) KA 171

S. laffittei s. l. KA 445.7

S. laffittei s. l. KA 459.3

S. laffittei s. l. KA 373

S. laffittei s. l. KA 433

10 µm

PLATE 2

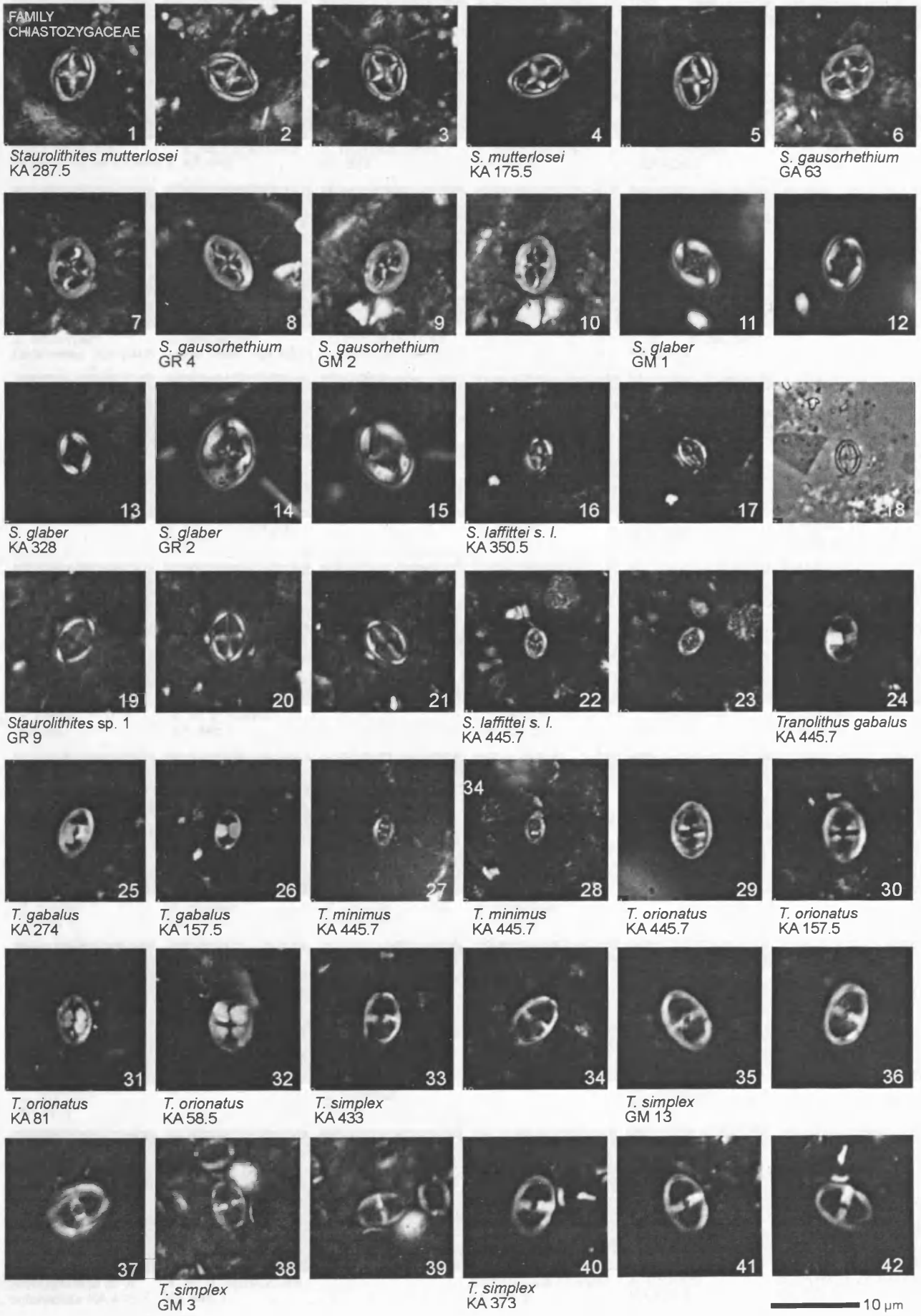
FAMILY
CHIASTOZYGACEAE
1
2
3
4
5
6
Staurolithites mutterlosei
KA 287.5
S. mutterlosei
KA 175.5
S. gausorhethium
GA 63
7
8
9
10
11
12
S. gausorhethium
GR 4
S. gausorhethium
GM 2
S. glaber
GM 1
13
14
15
16
17
18
S. glaber
KA 328
S. glaber
GR 2
S. laffittei s. l.
KA 350.5
19
20
21
22
23
24
Staurolithites sp. 1
GR 9
S. laffittei s. l.
KA 445.7
Tranolithus gabalus
KA 445.7
25
26
27
34
28
29
30
T. gabalus
KA 274
T. gabalus
KA 157.5
T. minimus
KA 445.7
T. minimus
KA 445.7
T. orionatus
KA 445.7
T. orionatus
KA 157.5
31
32
33
34
35
36
T. orionatus
KA 81
T. orionatus
KA 58.5
T. simplex
KA 433
T. simplex
GM 13
37
38
39
40
41
42
T. simplex
GM 3
T. simplex
KA 373
10 µm

PLATE 3

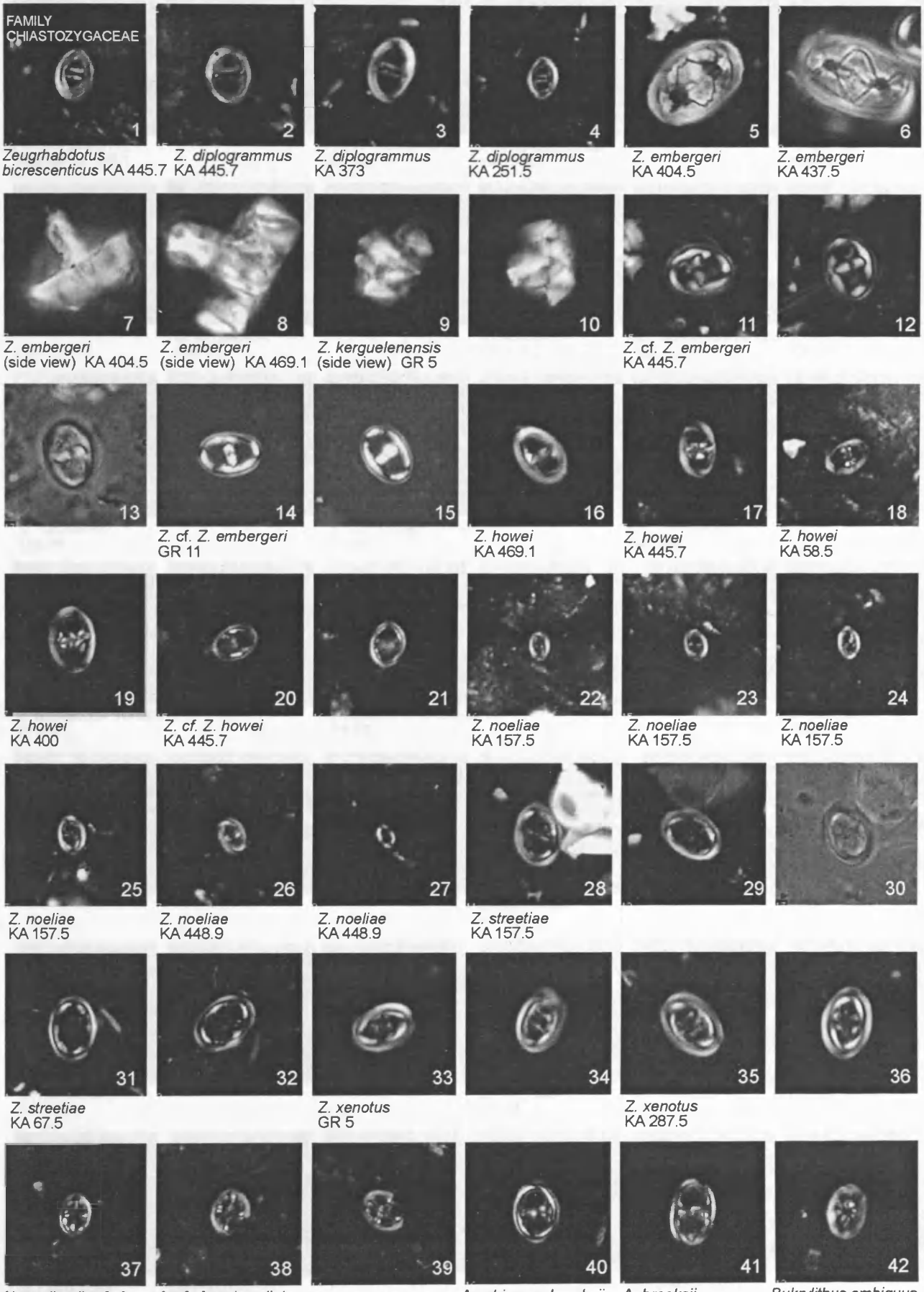

Zeugrhabdotus bicrescenticus KA 445.7

Z. diplogrammus KA 445.7

Z. diplogrammus KA 373

Z. diplogrammus KA 251.5

Z. embergeri KA 404.5

Z. embergeri KA 437.5

Z. embergeri (side view) KA 404.5

Z. embergeri (side view) KA 469.1

Z. kerguelenensis (side view) GR 5

Z. cf. *Z. embergeri* KA 445.7

Z. cf. *Z. embergeri* GR 11

Z. howei KA 469.1

Z. howei KA 445.7

Z. howei KA 58.5

Z. howei KA 400

Z. cf. *Z. howei* KA 445.7

Z. noeliae KA 157.5

Z. noeliae KA 157.5

Z. noeliae KA 157.5

Z. noeliae KA 157.5

Z. noeliae KA 448.9

Z. noeliae KA 448.9

Z. streetiae KA 157.5

Z. streetiae KA 67.5

Z. xenotus GR 5

Z. xenotus KA 287.5

Ahmuellerella cf. *A. octoradiata* KA 445.7

A. cf. *A. octoradiata* KA 445.7

Amphizygus brooksii KA 451.9

A. brooksii KA 428.5

Bukrylithus ambiguus KA 428.5

10 µm

PLATE 4

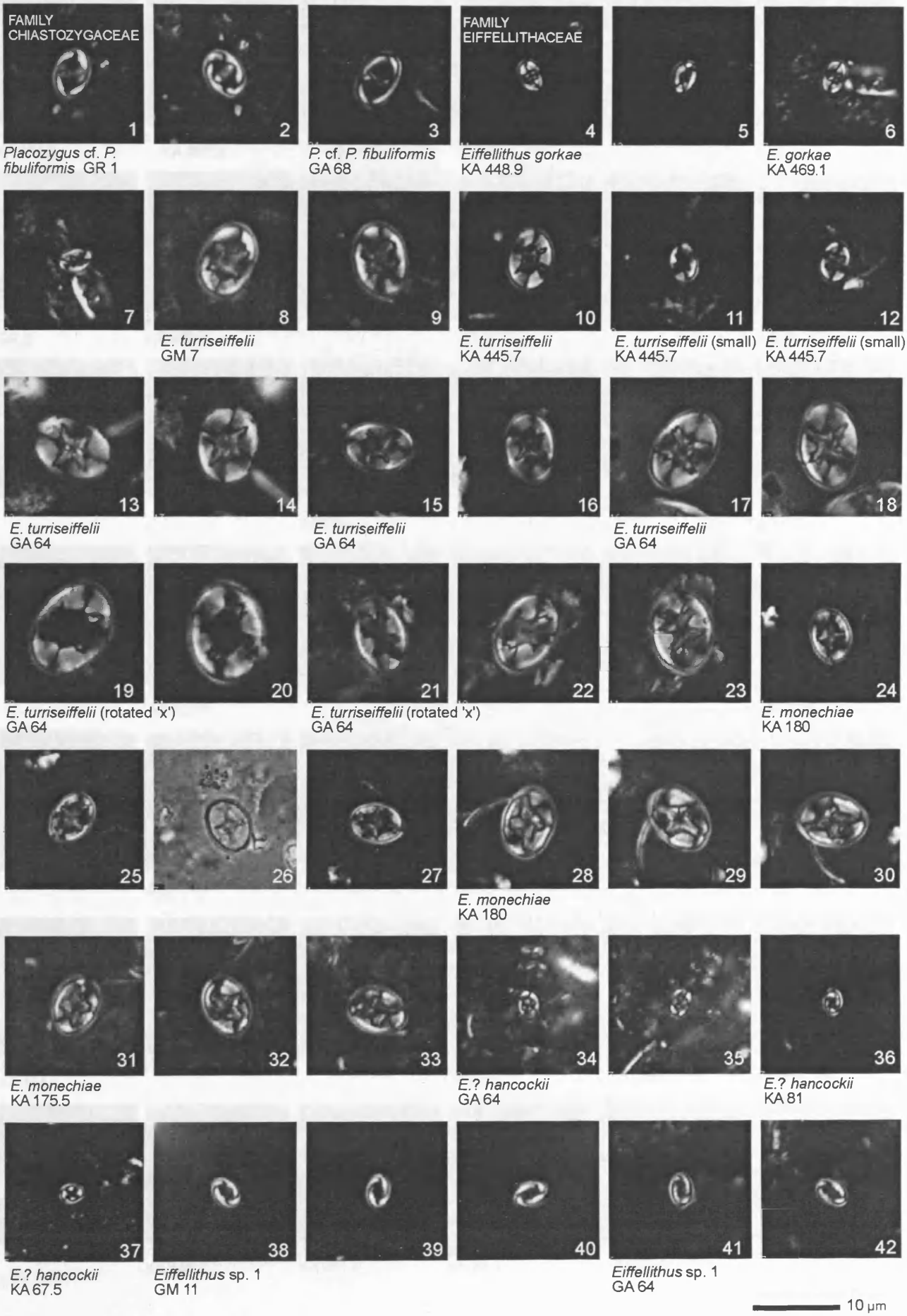

Placozygus cf. *P. fibuliformis* GR 1

P. cf. *P. fibuliformis* GA 68

Eiffellithus gorkae KA 448.9

E. gorkae KA 469.1

E. turriseiffelii GM 7

E. turriseiffelii KA 445.7

E. turriseiffelii (small) KA 445.7

E. turriseiffelii (small) KA 445.7

E. turriseiffelii GA 64

E. turriseiffelii GA 64

E. turriseiffelii GA 64

E. turriseiffelii (rotated 'x') GA 64

E. turriseiffelii (rotated 'x') GA 64

E. monechiae KA 180

E. monechiae KA 180

E. monechiae KA 175.5

E.? hancockii GA 64

E.? hancockii KA 81

E.? hancockii KA 67.5

Eiffellithus sp. 1 GM 11

Eiffellithus sp. 1 GA 64

10 µm

PLATE 5

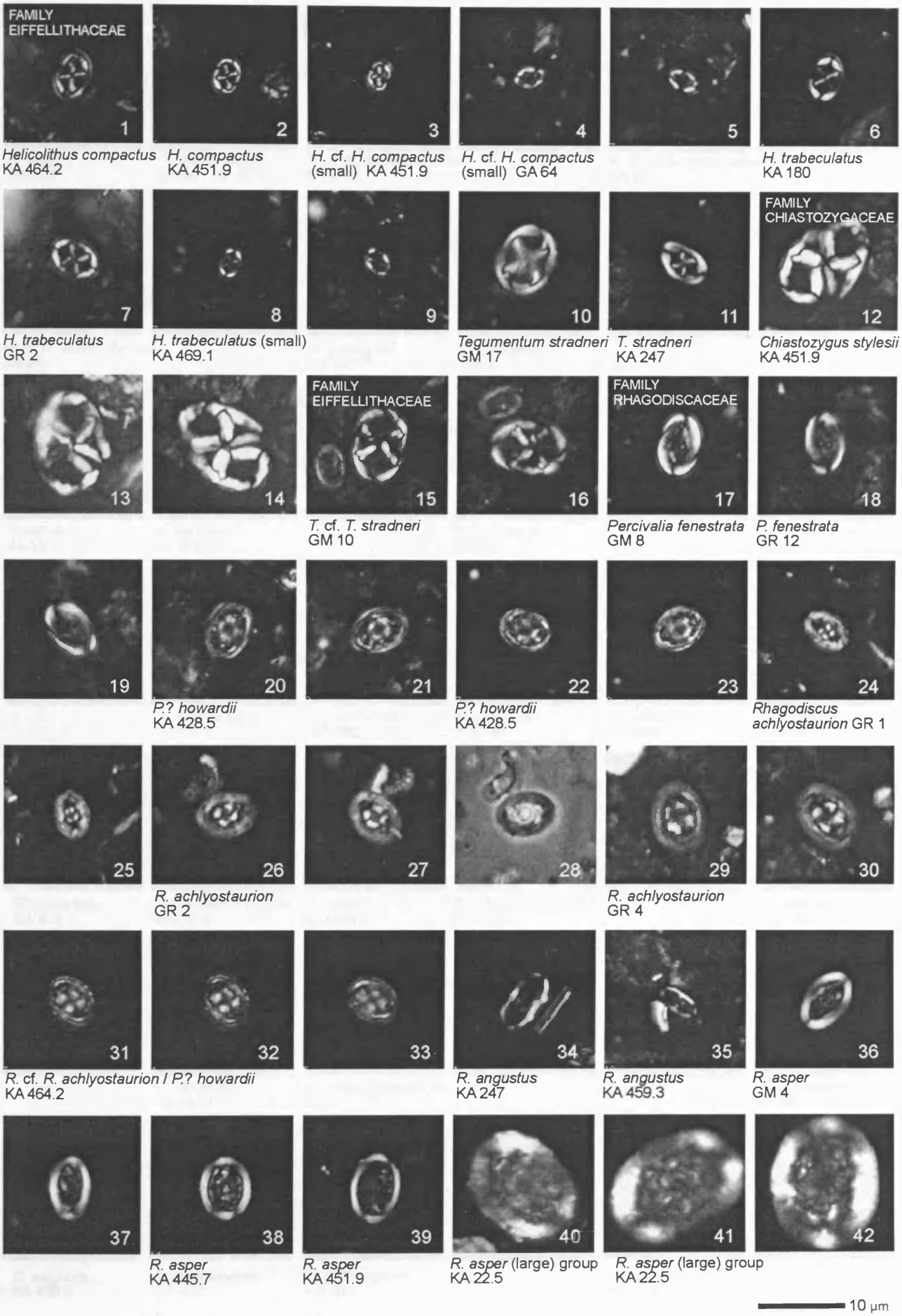
FAMILY EIFFELLITHACEAE
1
2
3
4
5
6
Helicolithus compactus KA 464.2
H. compactus KA 451.9
H. cf. H. compactus (small) KA 451.9
H. cf. H. compactus (small) GA 64
H. trabeculatus KA 180
7
8
9
10
11
FAMILY CHIASTOZYGACEAE
12
H. trabeculatus GR 2
H. trabeculatus (small) KA 469.1
Tegumentum stradneri GM 17
T. stradneri KA 247
Chiastozygus stylesii KA 451.9
13
14
FAMILY EIFFELLITHACEAE
15
16
FAMILY RHAGODISCACEAE
17
18
T. cf. T. stradneri GM 10
Percivalia fenestrata GM 8
P. fenestrata GR 12
19
20
21
22
23
24
P.? howardii KA 428.5
P.? howardii KA 428.5
Rhagodiscus achlyostaurion GR 1
25
26
27
28
29
30
R. achlyostaurion GR 2
R. achlyostaurion GR 4
31
32
33
34
35
36
R. cf. R. achlyostaurion / P.? howardii KA 464.2
R. angustus KA 247
R. angustus KA 459.3
R. asper GM 4
37
38
39
40
41
42
R. asper KA 445.7
R. asper KA 451.9
R. asper (large) group KA 22.5
R. asper (large) group KA 22.5
10 µm

PLATE 6

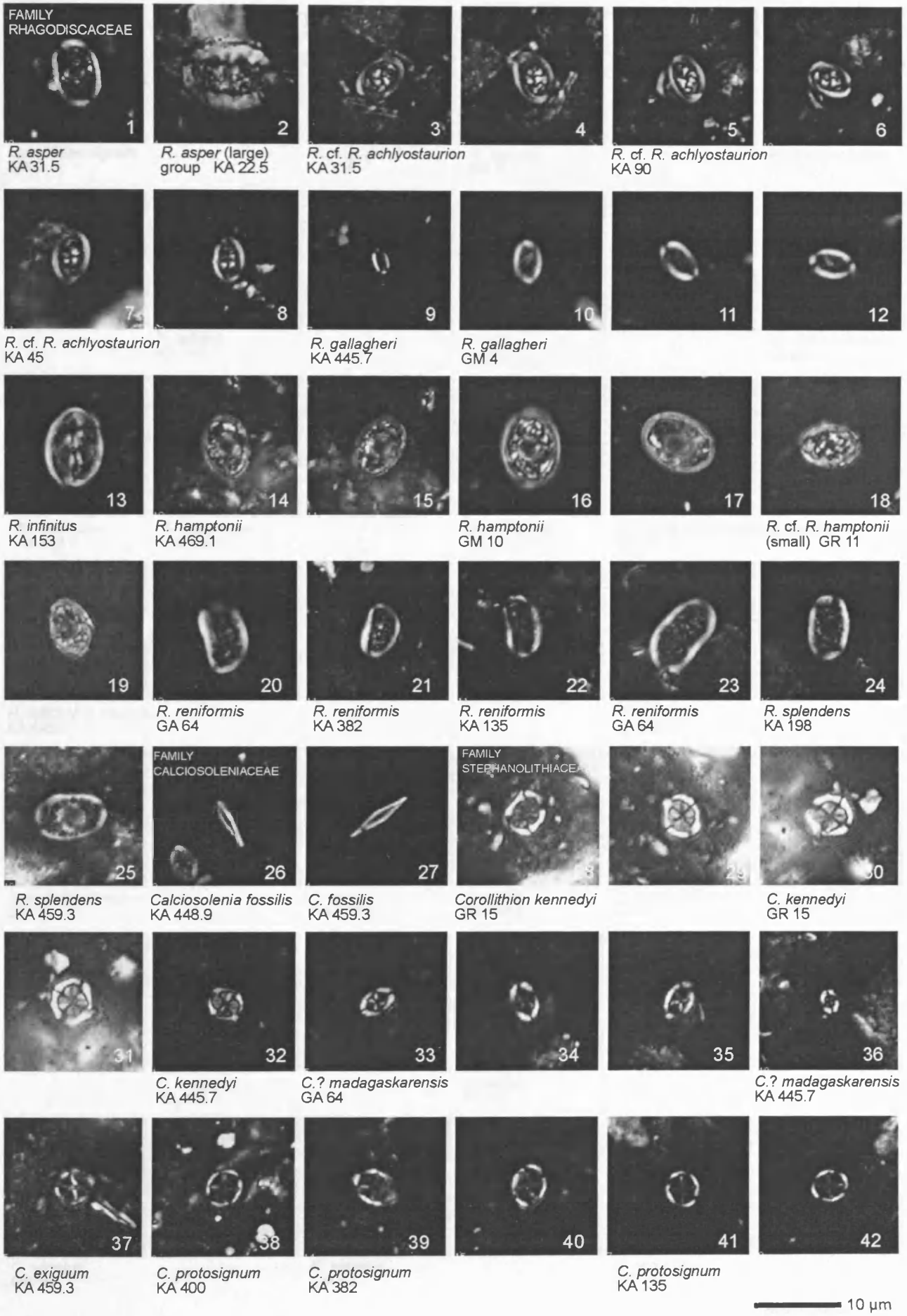

R. asper
KA 31.5

R. asper (large)
group KA 22.5

R. cf. *R. achlyostaurion*
KA 31.5

R. cf. *R. achlyostaurion*
KA 90

R. cf. *R. achlyostaurion*
KA 45

R. gallagheri
KA 445.7

R. gallagheri
GM 4

R. infinitus
KA 153

R. hamptonii
KA 469.1

R. hamptonii
GM 10

R. cf. *R. hamptonii*
(small) GR 11

R. reniformis
GA 64

R. reniformis
KA 382

R. reniformis
KA 135

R. reniformis
GA 64

R. splendens
KA 198

R. splendens
KA 459.3

Calciosolenia fossilis
KA 448.9

C. fossilis
KA 459.3

Corollithion kennedyi
GR 15

C. kennedyi
GR 15

C. kennedyi
KA 445.7

C.? madagaskarensis
GA 64

C.? madagaskarensis
KA 445.7

C. exiguum
KA 459.3

C. protosignum
KA 400

C. protosignum
KA 382

C. protosignum
KA 135

10 µm

PLATE 7

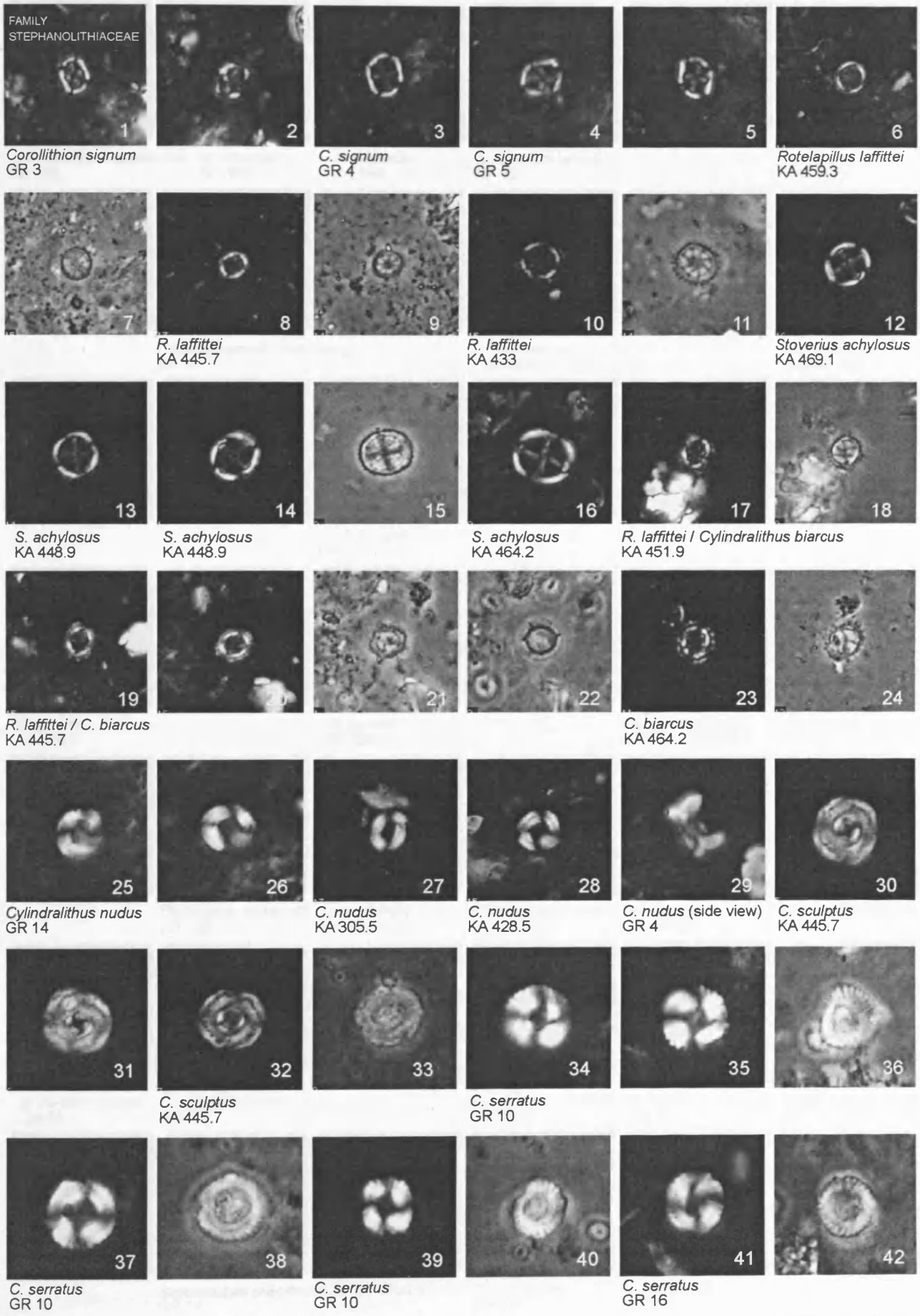
FAMILY
STEPHANOLITHIACEAE
1
2
3
4
5
6
Corollithion signum
GR 3
C. signum
GR 4
C. signum
GR 5
Rotelapillus laffittei
KA 459.3
7
8
9
10
11
12
R. laffittei
KA 445.7
R. laffittei
KA 433
Stoverius achylosus
KA 469.1
13
14
15
16
17
18
S. achylosus
KA 448.9
S. achylosus
KA 448.9
S. achylosus
KA 464.2
R. laffittei / Cylindralithus biarcus
KA 451.9
19
21
22
23
24
R. laffittei / C. biarcus
KA 445.7
C. biarcus
KA 464.2
25
26
27
28
29
30
Cylindralithus nudus
GR 14
C. nudus
KA 305.5
C. nudus
KA 428.5
C. nudus (side view)
GR 4
C. sculptus
KA 445.7
31
32
33
34
35
36
C. sculptus
KA 445.7
C. serratus
GR 10
37
38
39
40
41
42
C. serratus
GR 10
C. serratus
GR 10
C. serratus
GR 16
10 µm

PLATE 8

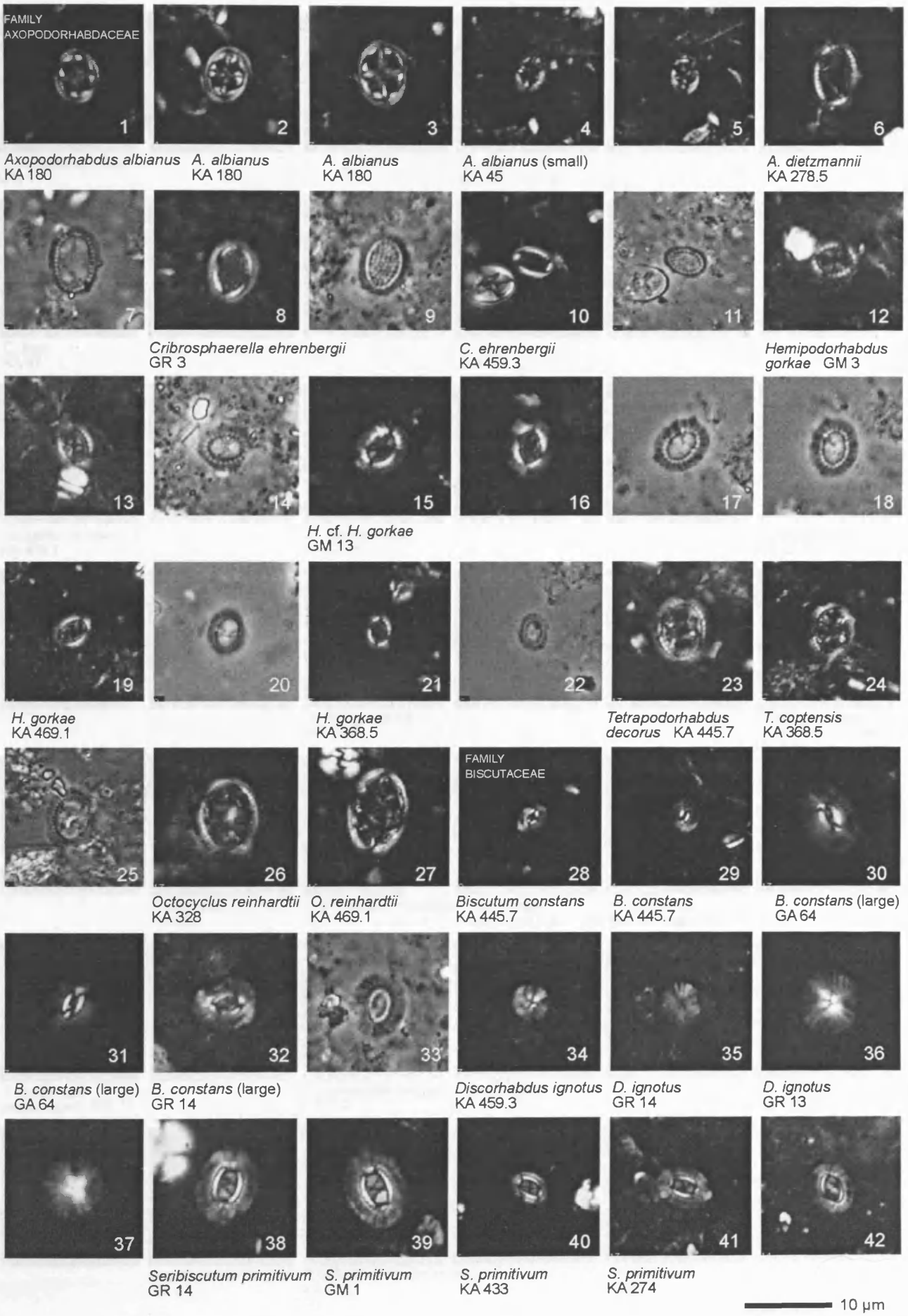
FAMILY
AXOPODORHABDACEAE
1
2
3
4
5
6
Axopodorhabdus albianus KA 180
A. albianus KA 180
A. albianus KA 180
A. albianus (small) KA 45
A. dietzmannii KA 278.5
7
8
9
10
11
12
Cribrosphaerella ehrenbergii GR 3
C. ehrenbergii KA 459.3
Hemipodorhabdus gorkae GM 3
13
14
15
16
17
18
H. cf. H. gorkae GM 13
19
20
21
22
23
24
H. gorkae KA 469.1
H. gorkae KA 368.5
Tetrapodorhabdus decorus KA 445.7
T. coptensis KA 368.5
25
26
27
FAMILY
BISCUTACEAE
28
29
30
Octocyclus reinhardtii KA 328
O. reinhardtii KA 469.1
Biscutum constans KA 445.7
B. constans KA 445.7
B. constans (large) GA 64
31
32
33
34
35
36
B. constans (large) GA 64
B. constans (large) GR 14
Discorhabdus ignotus KA 459.3
D. ignotus GR 14
D. ignotus GR 13
37
38
39
40
41
42
Seribiscutum primitivum GR 14
S. primitivum GM 1
S. primitivum KA 433
S. primitivum KA 274
10 µm

PLATE 9

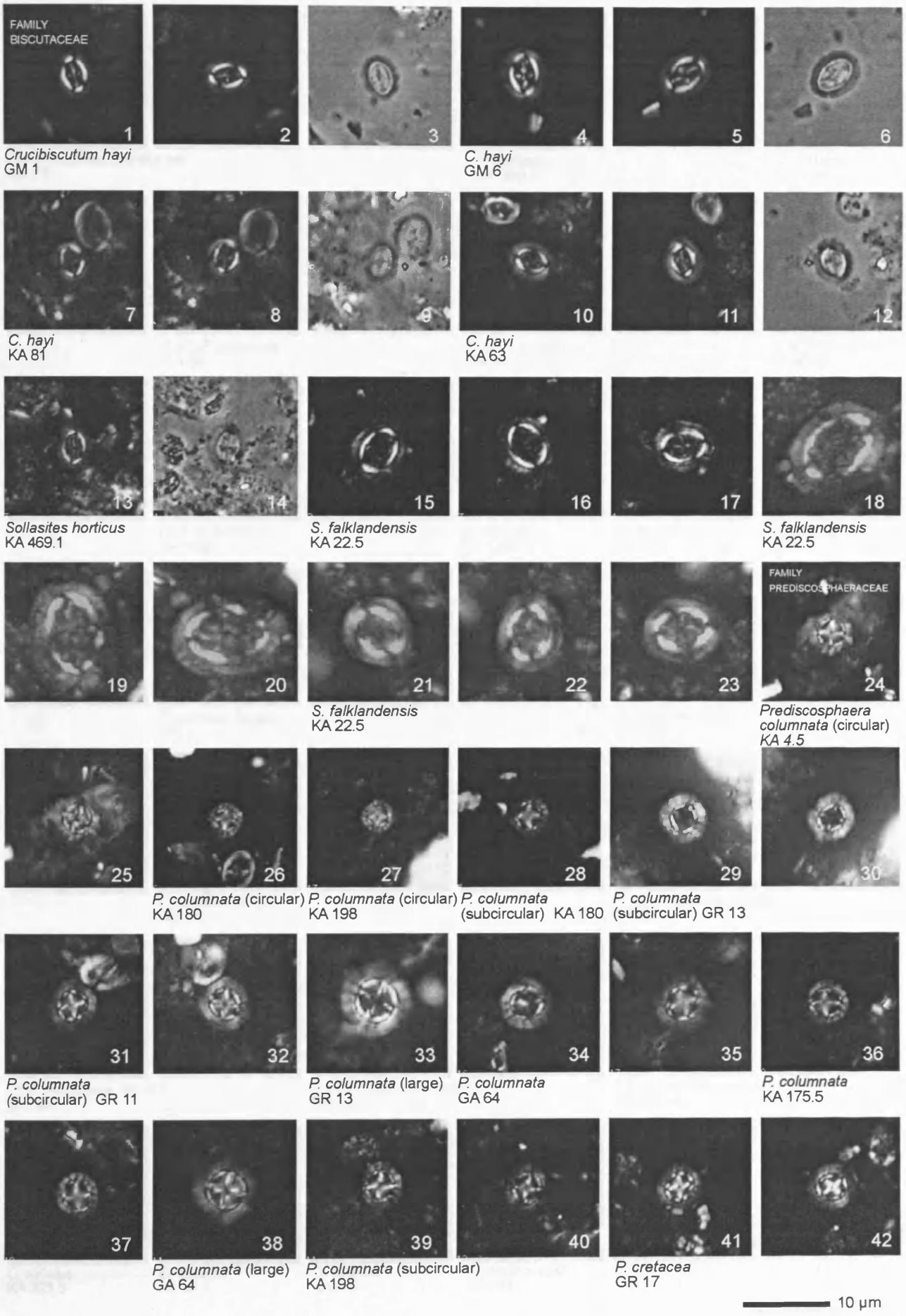
FAMILY
BISCUTACEAE
1
2
3
4
5
6
Crucibiscutum hayi
GM 1
C. hayi
GM 6
7
8
9
10
11
12
C. hayi
KA 81
C. hayi
KA 63
13
14
15
16
17
18
Sollasites horticus
KA 469.1
S. falklandensis
KA 22.5
S. falklandensis
KA 22.5
19
20
21
22
23
FAMILY
PREDISCOSPHAERACEAE
24
S. falklandensis
KA 22.5
Prediscosphaera
columnata (circular)
KA 4.5
25
26
27
28
29
30
P. columnata (circular)
KA 180
P. columnata (circular)
KA 198
P. columnata
(subcircular) KA 180
P. columnata
(subcircular) GR 13
31
32
33
34
35
36
P. columnata
(subcircular) GR 11
P. columnata (large)
GR 13
P. columnata
GA 64
P. columnata
KA 175.5
37
38
39
40
41
42
P. columnata (large)
GA 64
P. columnata (subcircular)
KA 198
P. cretacea
GR 17
10 µm

PLATE 10

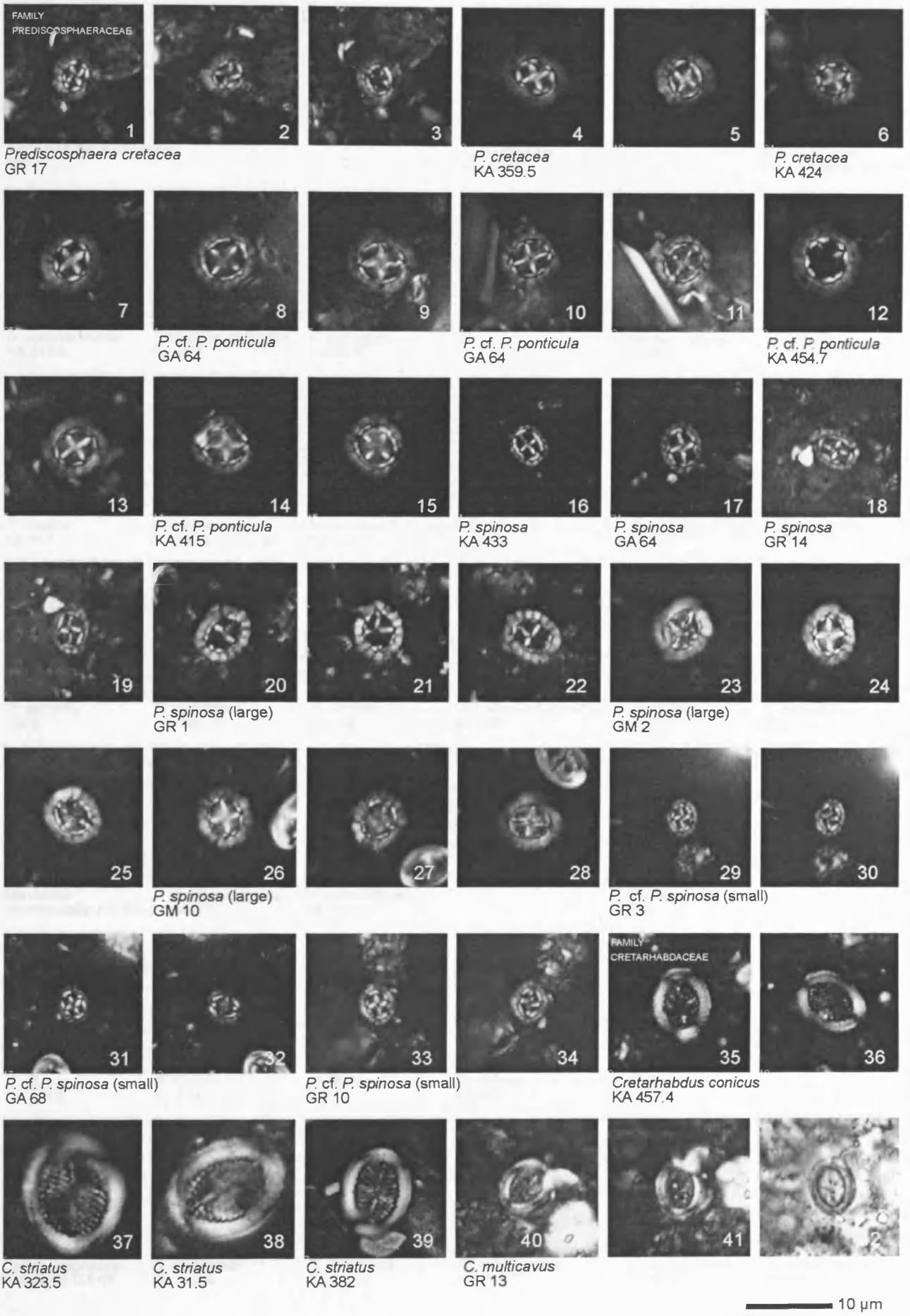
FAMILY
PREDISCOSPHAERACEAE
1
2
3
4
5
6
Prediscosphaera cretacea
GR 17
P. cretacea
KA 359.5
P. cretacea
KA 424
7
8
9
10
11
12
P. cf. P. ponticula
GA 64
P. cf. P. ponticula
GA 64
P. cf. P. ponticula
KA 454.7
13
14
15
16
17
18
P. cf. P. ponticula
KA 415
P. spinosa
KA 433
P. spinosa
GA 64
P. spinosa
GR 14
19
20
21
22
23
24
P. spinosa (large)
GR 1
P. spinosa (large)
GM 2
25
26
27
28
29
30
P. spinosa (large)
GM 10
P. cf. P. spinosa (small)
GR 3
31
32
33
34
FAMILY
CRETARHABDACEAE
35
36
P. cf. P. spinosa (small)
GA 68
P. cf. P. spinosa (small)
GR 10
Cretarhabdus conicus
KA 457.4
37
38
39
40
41
42
C. striatus
KA 323.5
C. striatus
KA 31.5
C. striatus
KA 382
C. multicavus
GR 13
10 µm

PLATE 11

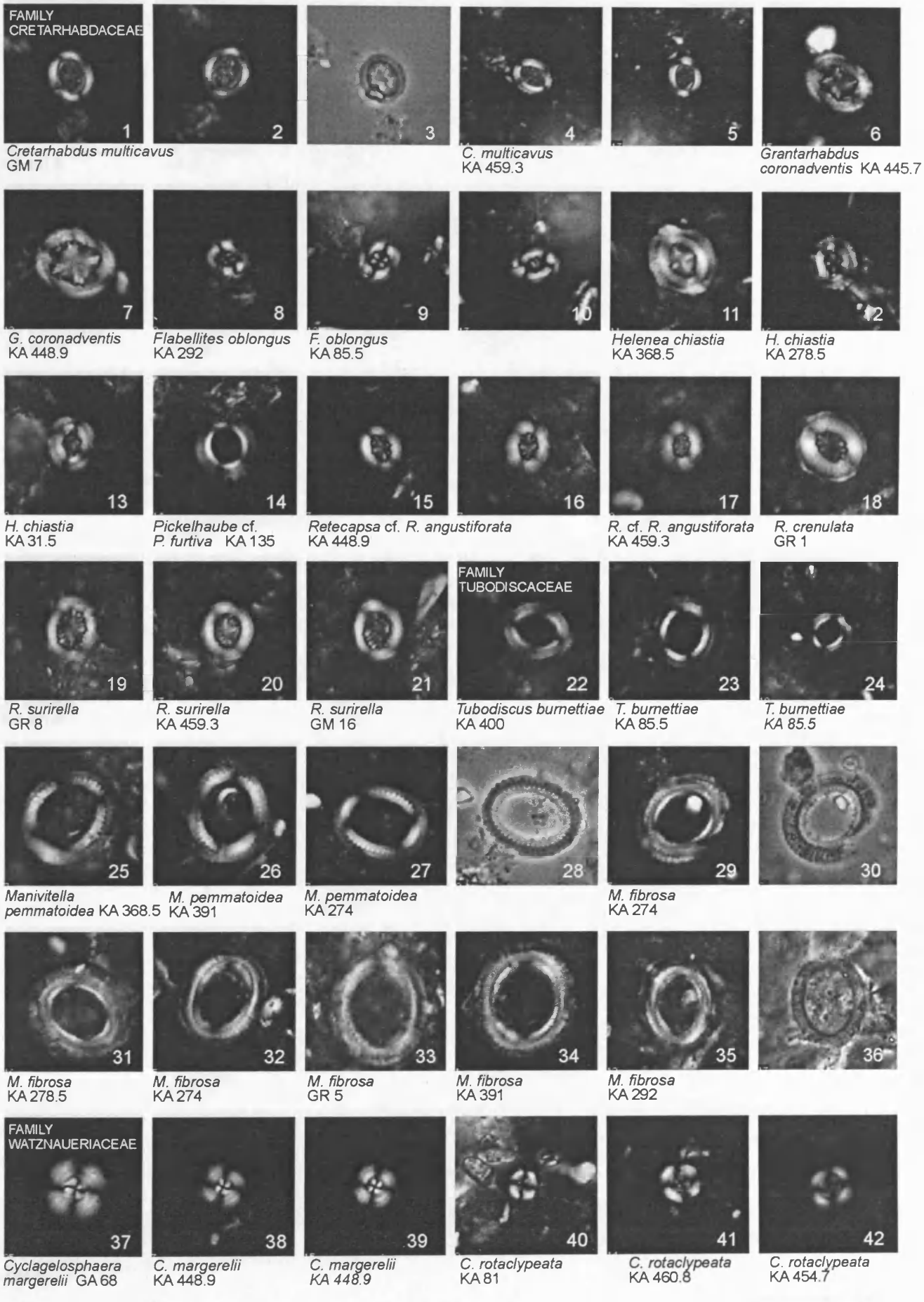
FAMILY
CRETARHABDACEAE
1
2
3
4
5
6
Cretarhabdus multicavus
GM 7
C. multicavus
KA 459.3
Grantarhabdus
coronadventis KA 445.7
7
8
9
10
11
12
G. coronadventis
KA 448.9
Flabellites oblongus
KA 292
F. oblongus
KA 85.5
Helenea chiastia
KA 368.5
H. chiastia
KA 278.5
13
14
15
16
17
18
H. chiastia
KA 31.5
Pickelhaube cf.
P. furtiva KA 135
Retecapsa cf. R. angustiforata
KA 448.9
R. cf. R. angustiforata
KA 459.3
R. crenulata
GR 1
19
20
21
FAMILY
TUBODISCACEAE
22
23
24
R. surirella
GR 8
R. surirella
KA 459.3
R. surirella
GM 16
Tubodiscus burnettiae
KA 400
T. burnettiae
KA 85.5
T. burnettiae
KA 85.5
25
26
27
28
29
30
Manivitella
pemmatoidea KA 368.5
M. pemmatoidea
KA 391
M. pemmatoidea
KA 274
M. fibrosa
KA 274
31
32
33
34
35
36
M. fibrosa
KA 278.5
M. fibrosa
KA 274
M. fibrosa
GR 5
M. fibrosa
KA 391
M. fibrosa
KA 292
FAMILY
WATZNAUERIACEAE
37
38
39
40
41
42
Cyclagelosphaera
margerelii GA 68
C. margerelii
KA 448.9
C. margerelii
KA 448.9
C. rotaclypeata
KA 81
C. rotaclypeata
KA 460.8
C. rotaclypeata
KA 454.7
10 µm

PLATE 12

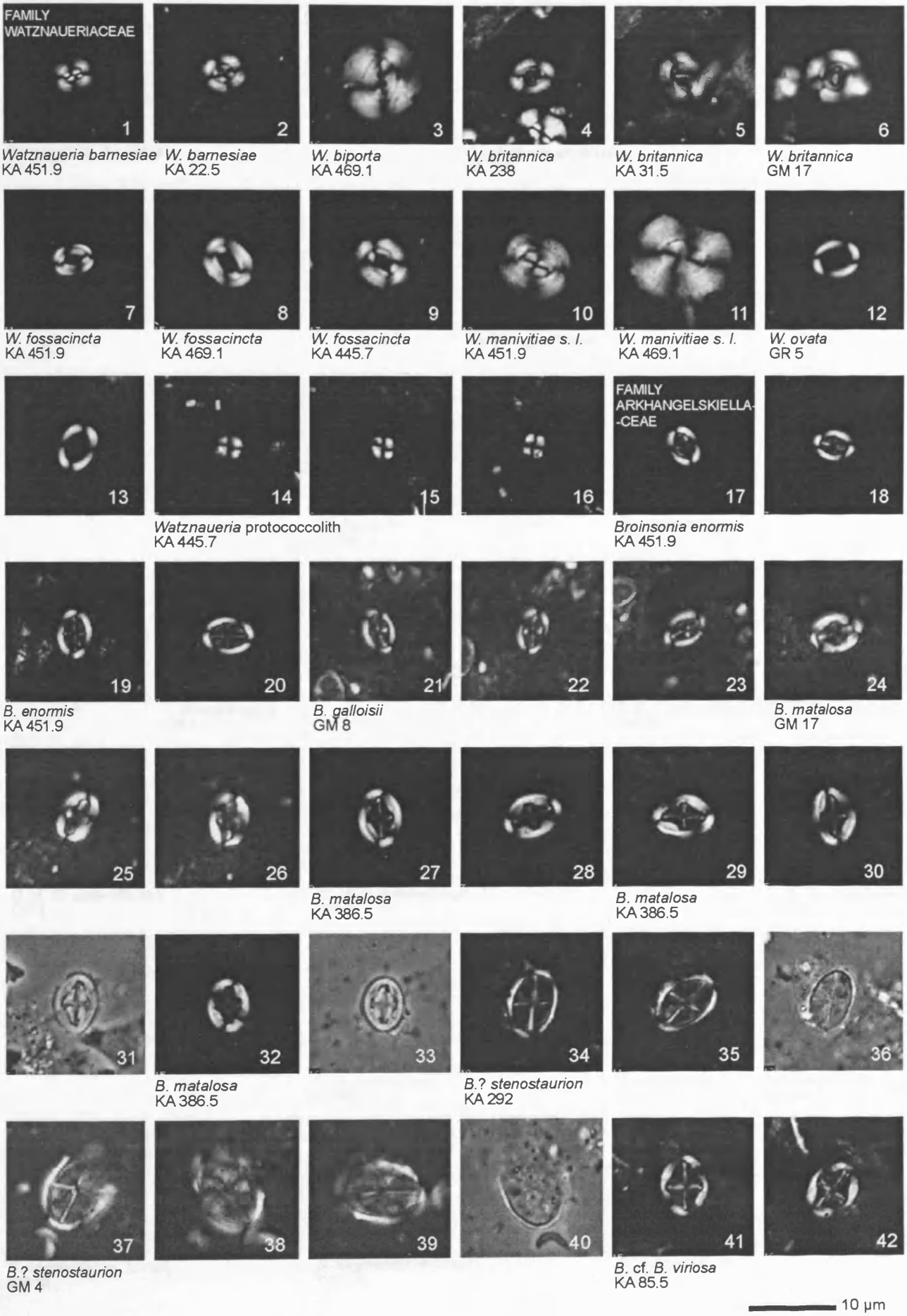
FAMILY WATZNAUERIACEAE
1
2
3
4
5
6
Watznaueria barnesiae KA 451.9
W. barnesiae KA 22.5
W. biporta KA 469.1
W. britannica KA 238
W. britannica KA 31.5
W. britannica GM 17
7
8
9
10
11
12
W. fossacincta KA 451.9
W. fossacincta KA 469.1
W. fossacincta KA 445.7
W. manivitiae s. l. KA 451.9
W. manivitiae s. l. KA 469.1
W. ovata GR 5
13
14
15
16
FAMILY ARKHANGELSKIELLA--CEAE
17
18
Watznaueria protococcolith KA 445.7
Broinsonia enormis KA 451.9
19
20
21
22
23
24
B. enormis KA 451.9
B. galloisii GM 8
B. matalosa GM 17
25
26
27
28
29
30
B. matalosa KA 386.5
B. matalosa KA 386.5
31
32
33
34
35
36
B. matalosa KA 386.5
B.? stenostaurion KA 292
37
38
39
40
41
42
B.? stenostaurion GM 4
B. cf. B. viriosa KA 85.5
10 µm

PLATE 13

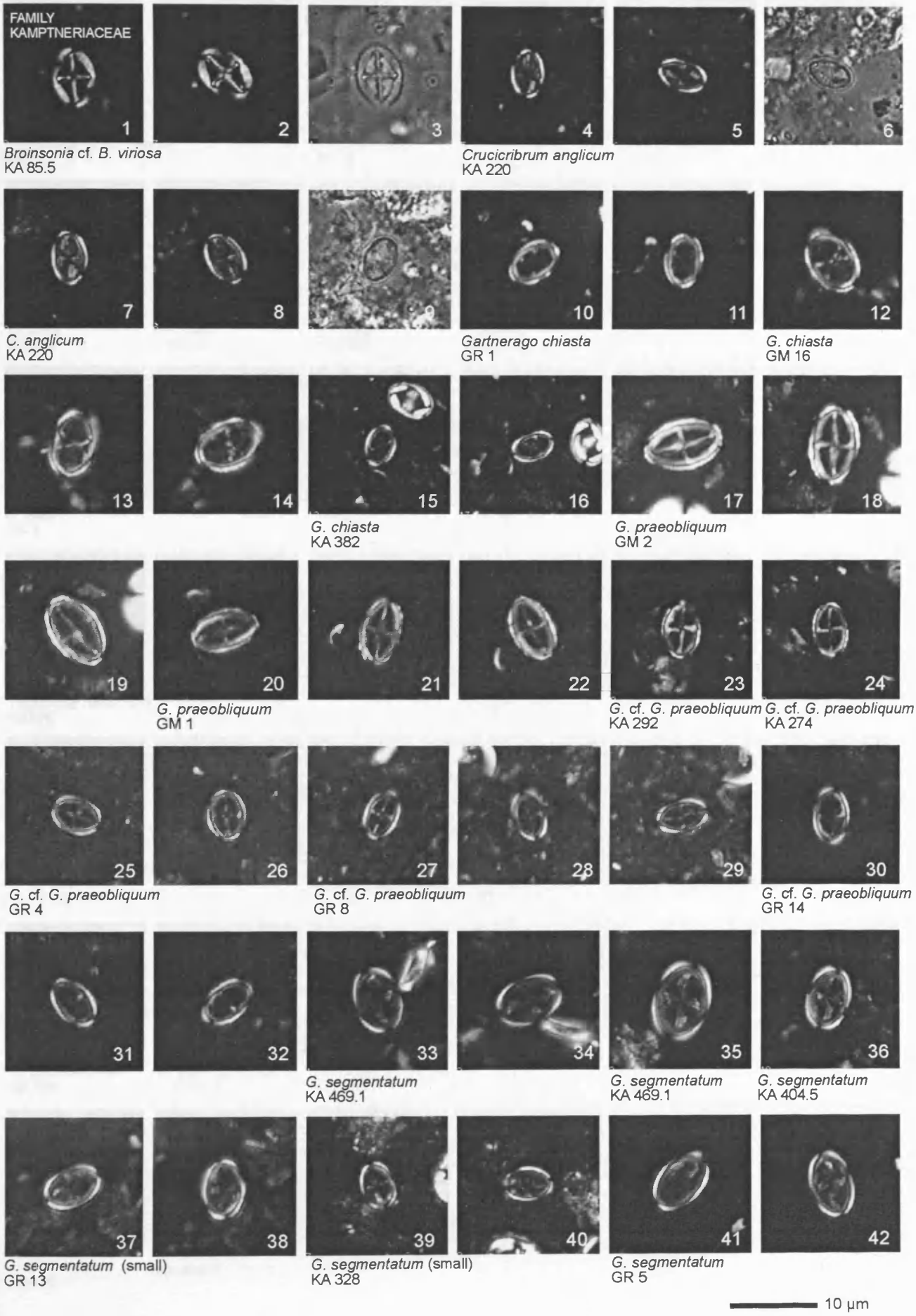
FAMILY
KAMPTNERIACEAE
1
2
3
4
5
6
Broinsonia cf. B. viriosa
KA 85.5
Crucicribrum anglicum
KA 220
7
8
9
10
11
12
C. anglicum
KA 220
Gartnerago chiasta
GR 1
G. chiasta
GM 16
13
14
15
16
17
18
G. chiasta
KA 382
G. praeobliquum
GM 2
19
20
21
22
23
24
G. praeobliquum
GM 1
G. cf. G. praeobliquum
KA 292
G. cf. G. praeobliquum
KA 274
25
26
27
28
29
30
G. cf. G. praeobliquum
GR 4
G. cf. G. praeobliquum
GR 8
G. cf. G. praeobliquum
GR 14
31
32
33
34
35
36
G. segmentatum
KA 469.1
G. segmentatum
KA 469.1
G. segmentatum
KA 404.5
37
38
39
40
41
42
G. segmentatum (small)
GR 13
G. segmentatum (small)
KA 328
G. segmentatum
GR 5
10 µm

PLATE 14

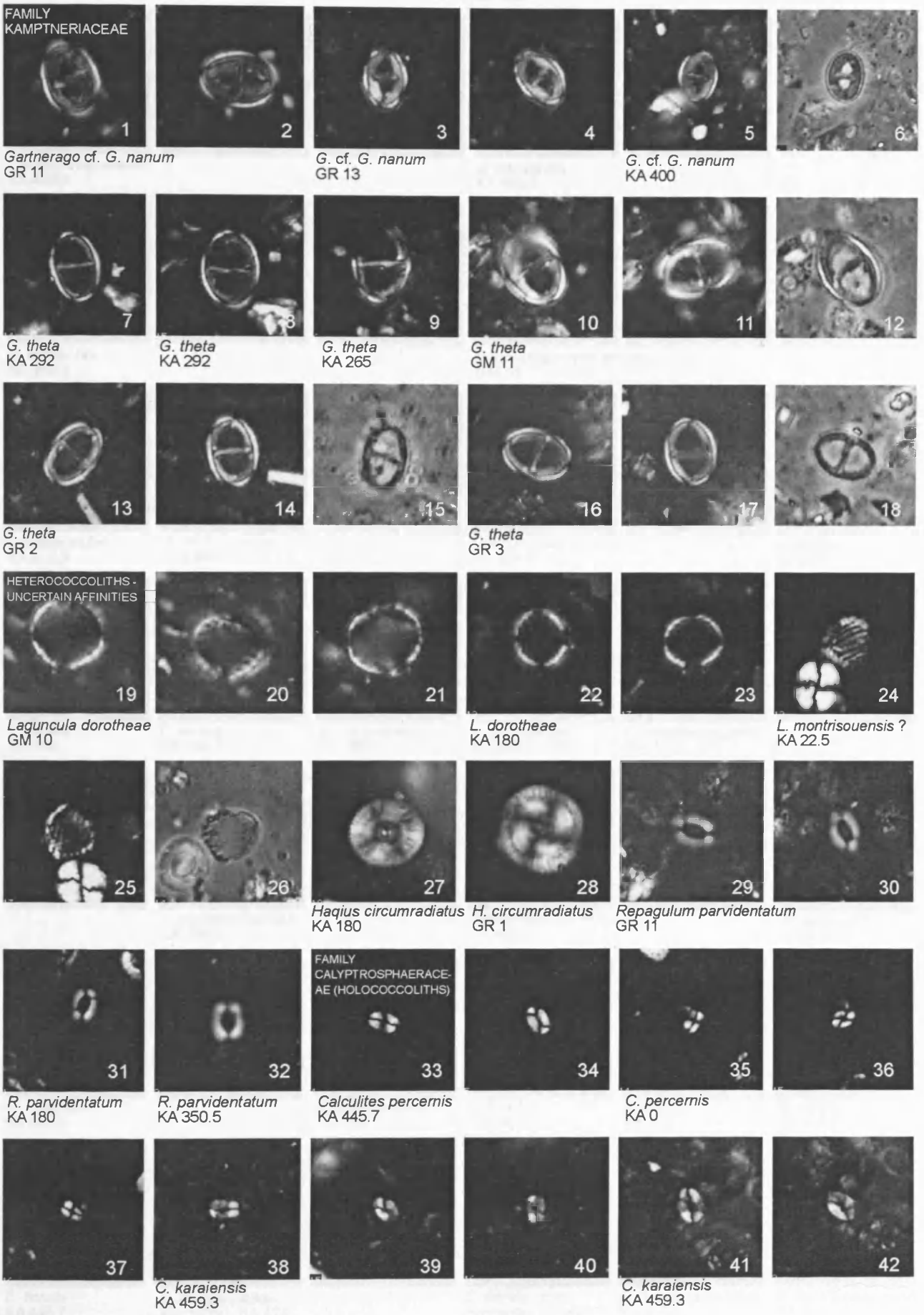
FAMILY KAMPTNERIACEAE
1
2
3
4
5
6
Gartnerago cf. G. nanum
GR 11
G. cf. G. nanum
GR 13
G. cf. G. nanum
KA 400
7
8
9
10
11
12
G. theta
KA 292
G. theta
KA 292
G. theta
KA 265
G. theta
GM 11
13
14
15
16
17
18
G. theta
GR 2
G. theta
GR 3
HETEROCOCCOLITHS - UNCERTAIN AFFINITIES
19
20
21
22
23
24
Laguncula dorotheae
GM 10
L. dorotheae
KA 180
L. montrisouensis ?
KA 22.5
25
26
27
28
29
30
Haqius circumradiatus
KA 180
H. circumradiatus
GR 1
Repagulum parvidentatum
GR 11
31
32
FAMILY CALYPTROSPHAERACEAE (HOLOCOCCOLITHS)
33
34
35
36
R. parvidentatum
KA 180
R. parvidentatum
KA 350.5
Calculites percernis
KA 445.7
C. percernis
KA 0
37
38
39
40
41
42
C. karaiensis
KA 459.3
C. karaiensis
KA 459.3
10 µm

PLATE 15

Calculites karaiensis
KA 459.3

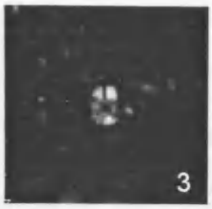

C. karaiensis
KA 459.3

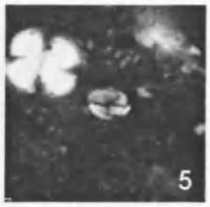

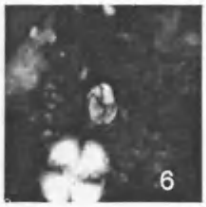

C. karaiensis
KA 459.3

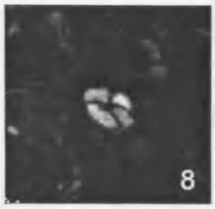

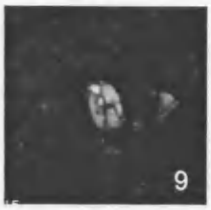

Braarudosphaera africana ?
GM 10

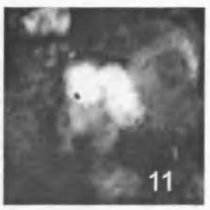

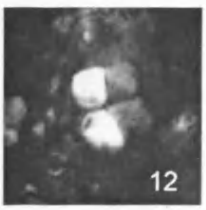

Lapideacassis glans
KA 428.5

L. cf. *L. cornuta*
KA 469.1

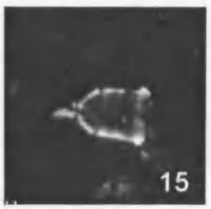

Lithraphidites acutus
KA 404.5

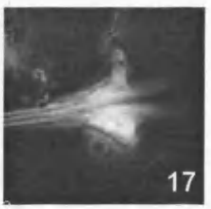

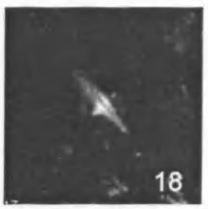

L. acutus
KA 433

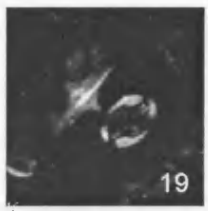

L. acutus
KA 433

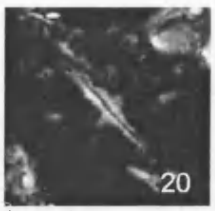

L. acutus
KA 445.7

L. carniolensis
KA 469.1

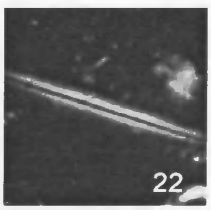

L. carniolensis
KA 368.5

L. pseudoquadratus
GR 17

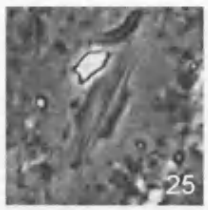

L. pseudoquadratus
KA 404.5

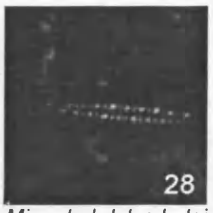

Microrhabdulus belgicus
KA 459.3

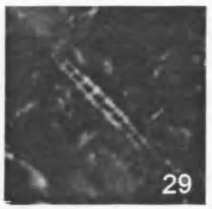

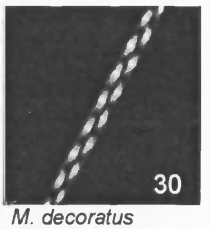

M. decoratus
KA 448.9

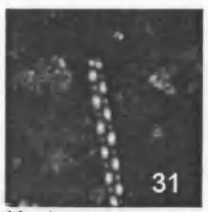

M . decoratus
KA 448.9

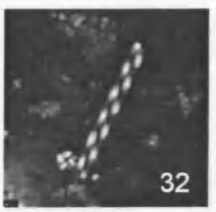

Eprolithus floralis
KA 135

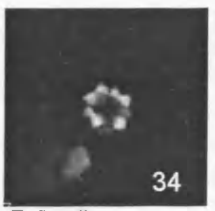

E. floralis
KA 292

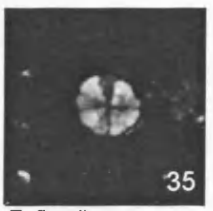

E. floralis
KA 319

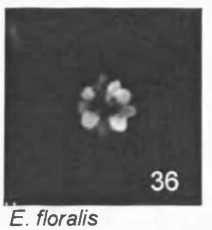

E. floralis
KA 445.7

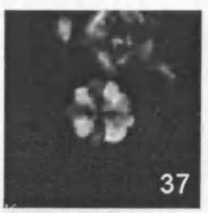

E. floralis
KA 445.7

E. floralis (spiky elements) KA 424

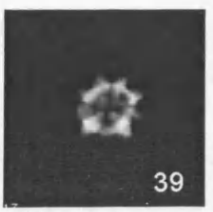

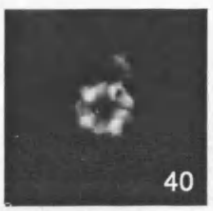

E. floralis (spiky elements) KA 424

E. floralis (side view)
KA 305.5

E. floralis (side view)
KA 424

10 µm

PLATE 16

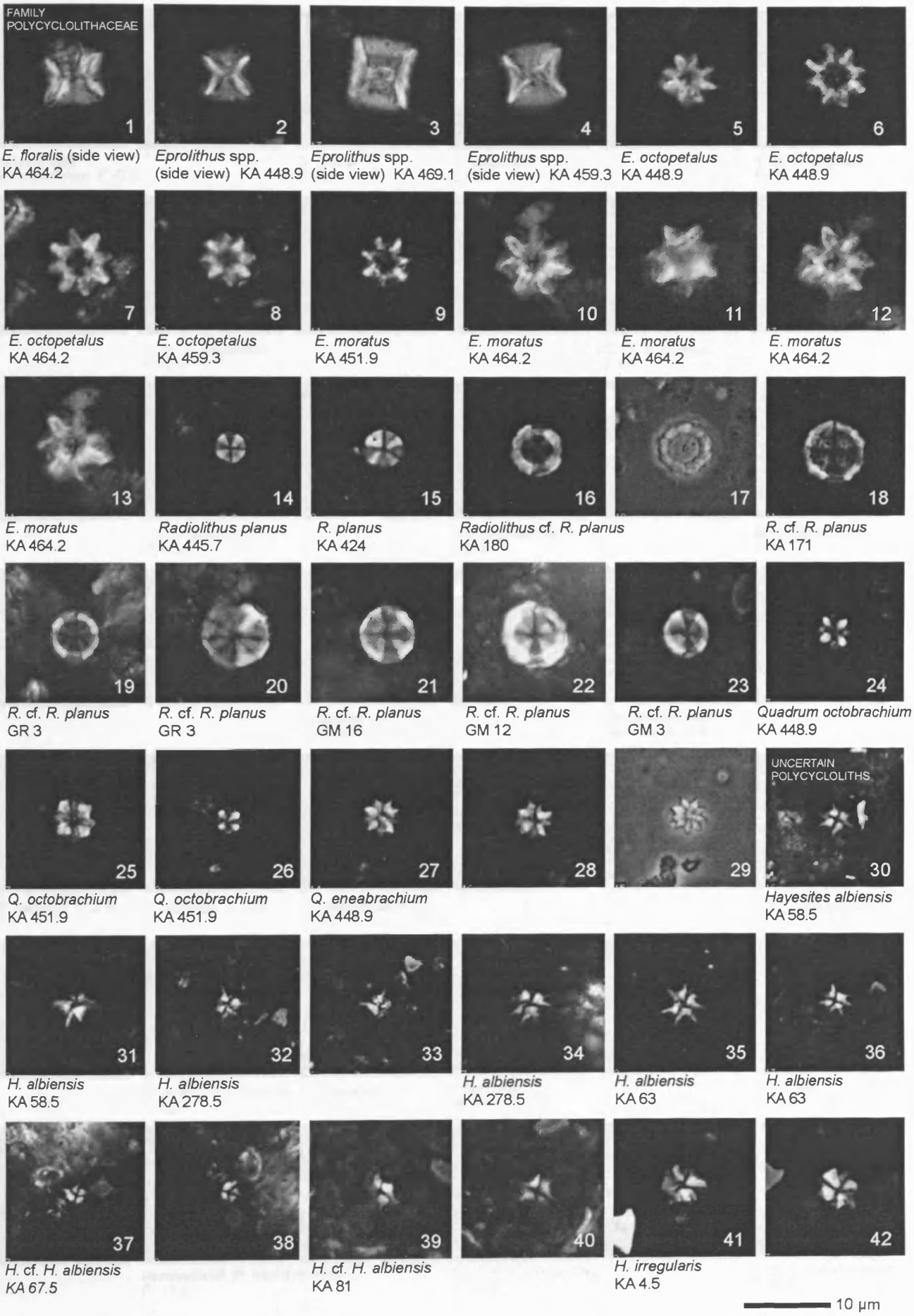

E. floralis (side view) KA 464.2

Eprolithus spp. (side view) KA 448.9

Eprolithus spp. (side view) KA 469.1

Eprolithus spp. (side view) KA 459.3

E. octopetalus KA 448.9

E. octopetalus KA 448.9

E. octopetalus KA 464.2

E. octopetalus KA 459.3

E. moratus KA 451.9

E. moratus KA 464.2

E. moratus KA 464.2

E. moratus KA 464.2

E. moratus KA 464.2

Radiolithus planus KA 445.7

R. planus KA 424

Radiolithus cf. *R. planus* KA 180

R. cf. *R. planus* KA 171

R. cf. *R. planus* GR 3

R. cf. *R. planus* GR 3

R. cf. *R. planus* GM 16

R. cf. *R. planus* GM 12

R. cf. *R. planus* GM 3

Quadrum octobrachium KA 448.9

Q. octobrachium KA 451.9

Q. octobrachium KA 451.9

Q. eneabrachium KA 448.9

Hayesites albiensis KA 58.5

H. albiensis KA 58.5

H. albiensis KA 278.5

H. albiensis KA 278.5

H. albiensis KA 63

H. albiensis KA 63

H. cf. *H. albiensis* KA 67.5

H. cf. *H. albiensis* KA 81

H. irregularis KA 4.5

10 µm

PLATE 17 - GAULT CLAY, SE ENGLAND

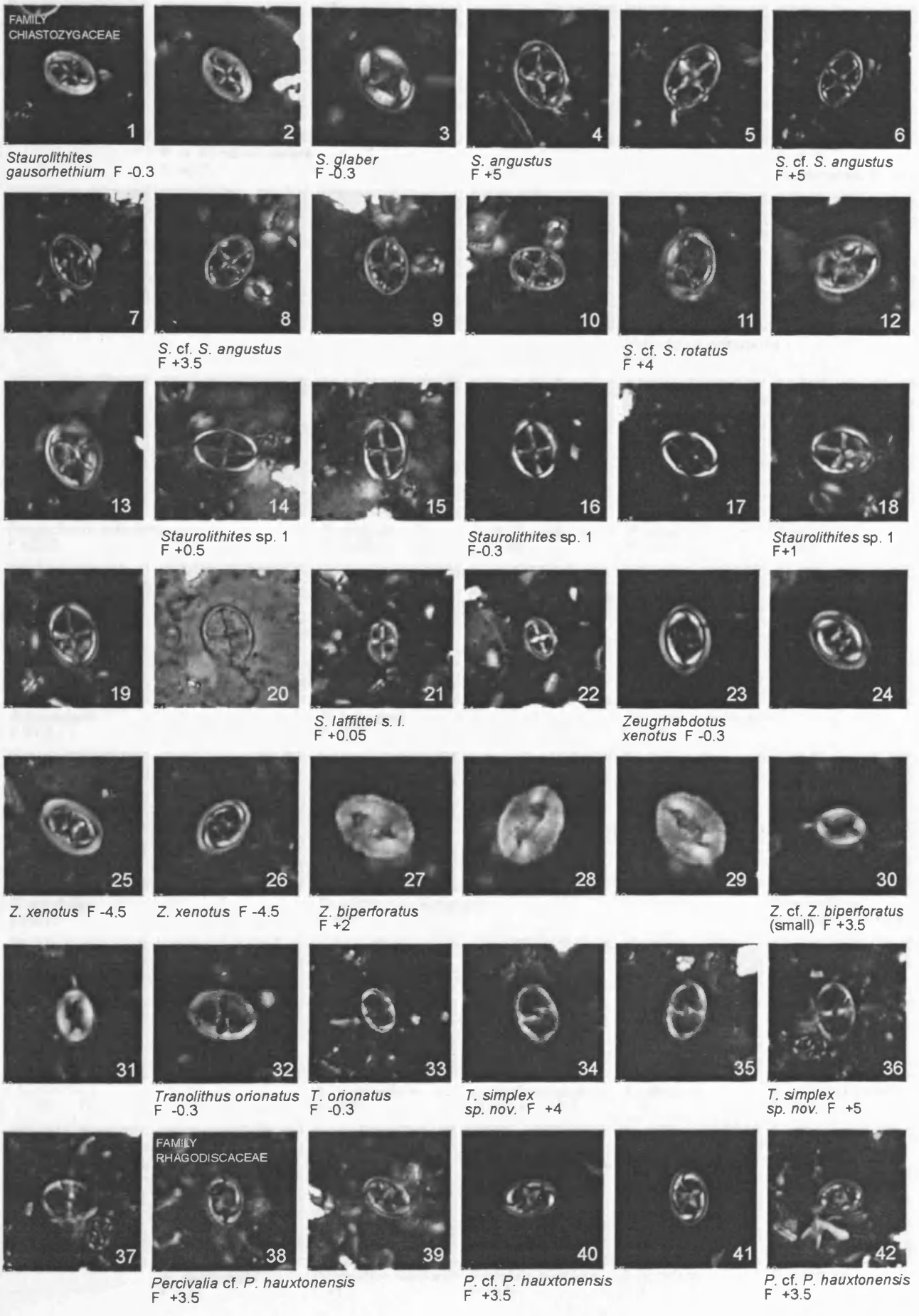

Staurolithites gausorhethium F -0.3

S. glaber F -0.3

S. angustus F +5

S. cf. *S. angustus* F +5

S. cf. *S. angustus* F +3.5

S. cf. *S. rotatus* F +4

Staurolithites sp. 1 F +0.5

Staurolithites sp. 1 F-0.3

Staurolithites sp. 1 F+1

S. laffittei s. l. F +0.05

Zeugrhabdotus xenotus F -0.3

Z. xenotus F -4.5

Z. xenotus F -4.5

Z. biperforatus F +2

Z. cf. *Z. biperforatus* (small) F +3.5

Tranolithus orionatus F -0.3

T. orionatus F -0.3

T. simplex sp. nov. F +4

T. simplex sp. nov. F +5

Percivalia cf. *P. hauxtonensis* F +3.5

P. cf. *P. hauxtonensis* F +3.5

P. cf. *P. hauxtonensis* F +3.5

10 µm

PLATE 18

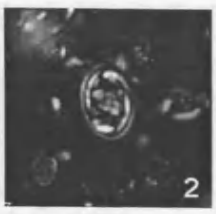

P. cf. *P. hauxtonensis*
F +0.7

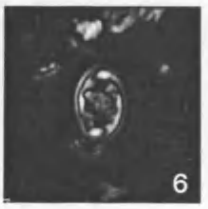

P. cf. *P. hauxtonensis* F +0.9

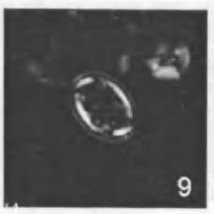

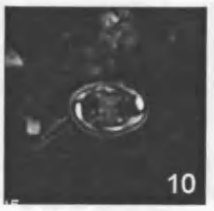

Helicolithus compactus
F +5

Rhagodiscus achlyostaurion
F +0.35

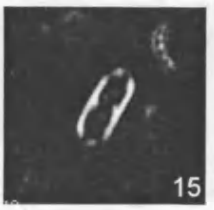

R. angustus
F +0.35

R. cf. *R. angustus*
F +0.35

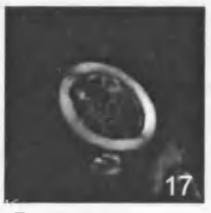

R. asper
F +0.5

R. reniformis
F +4.5

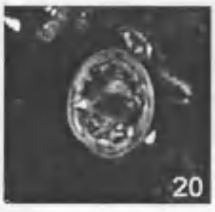

R. hamptonii
F +1.5

R. hamptonii
F +2.5

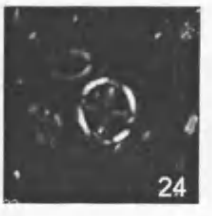

Stoverius achylosus
F +0.6

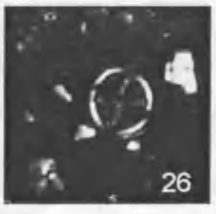

S. achylosus
F +0.15

Corollithion protosignum
F +1.1

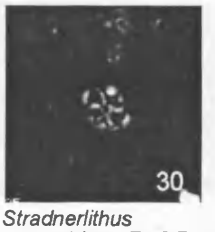

Stradnerlithus geometricus F +3.5

S. geometricus
F +4.5

Axopodorhabdus albianus F +0.9

A. albianus
F -3

A. albianus (small)
F +0.5

A. dietzmannii
F +0.5

Octocyclus reinhardtii
F +1

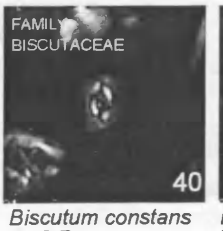

Biscutum constans
F +3.5

B. constans
F -1

B. constans
F -5

10 µm

PLATE 19

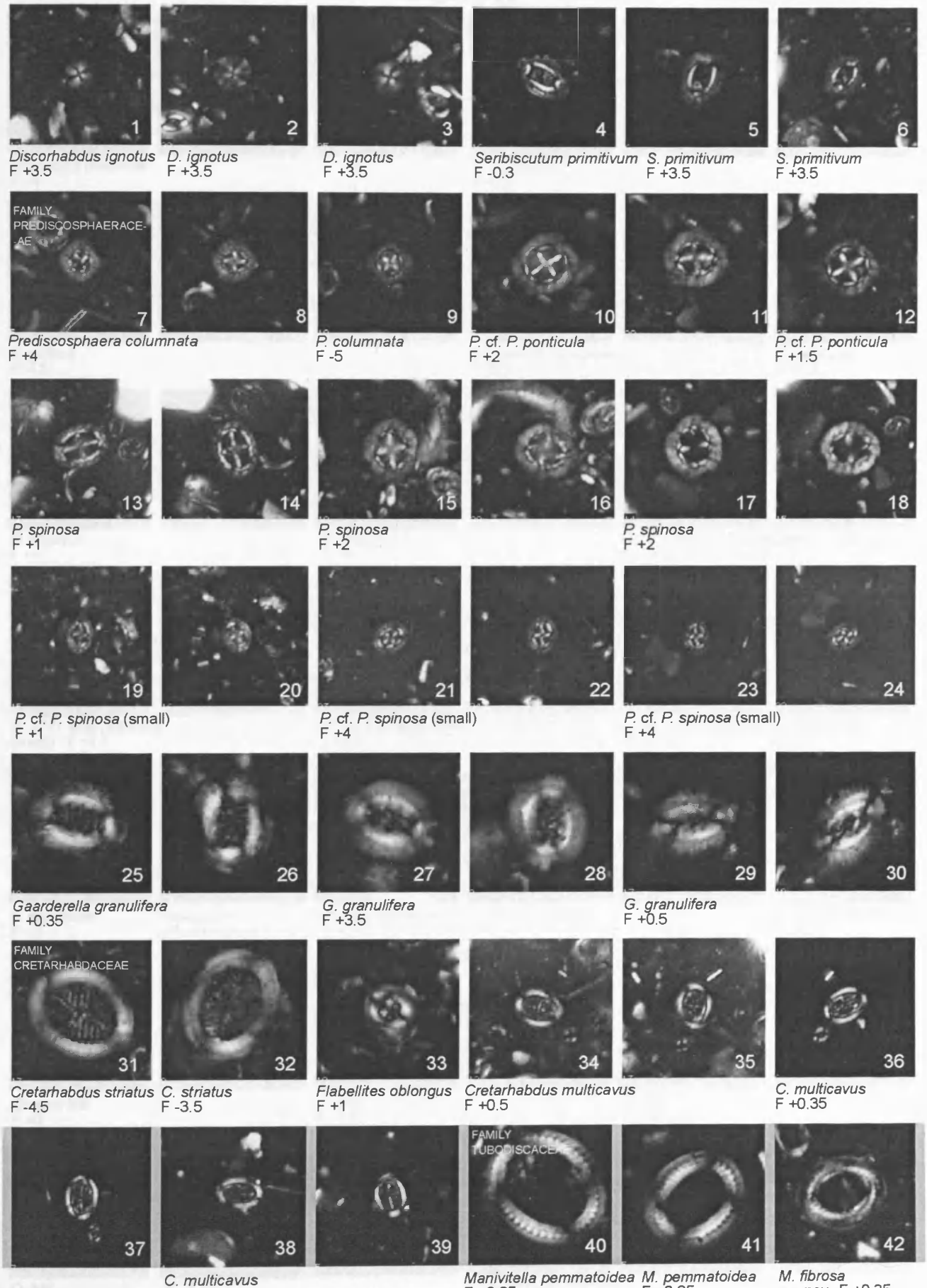
1
2
3
4
5
6
Discorhabdus ignotus F +3.5
D. ignotus F +3.5
D. ignotus F +3.5
Seribiscutum primitivum F -0.3
S. primitivum F +3.5
S. primitivum F +3.5
FAMILY PREDISCOSPHAERACEAE
7
8
9
10
11
12
Prediscosphaera columnata F +4
P. columnata F -5
P. cf. P. ponticula F +2
P. cf. P. ponticula F +1.5
13
14
15
16
17
18
P. spinosa F +1
P. spinosa F +2
P. spinosa F +2
19
20
21
22
23
24
P. cf. P. spinosa (small) F +1
P. cf. P. spinosa (small) F +4
P. cf. P. spinosa (small) F +4
25
26
27
28
29
30
Gaarderella granulifera F +0.35
G. granulifera F +3.5
G. granulifera F +0.5
FAMILY CRETARHABDACEAE
31
32
33
34
35
36
Cretarhabdus striatus F -4.5
C. striatus F -3.5
Flabellites oblongus F +1
Cretarhabdus multicavus F +0.5
C. multicavus F +0.35
37
38
39
FAMILY TUBODISCACEAE
40
41
42
C. multicavus F +0.35
Manivitella pemmatoidea F +0.35
M. pemmatoidea F +0.35
M. fibrosa sp. nov. F +0.35
10 µm

PLATE 20

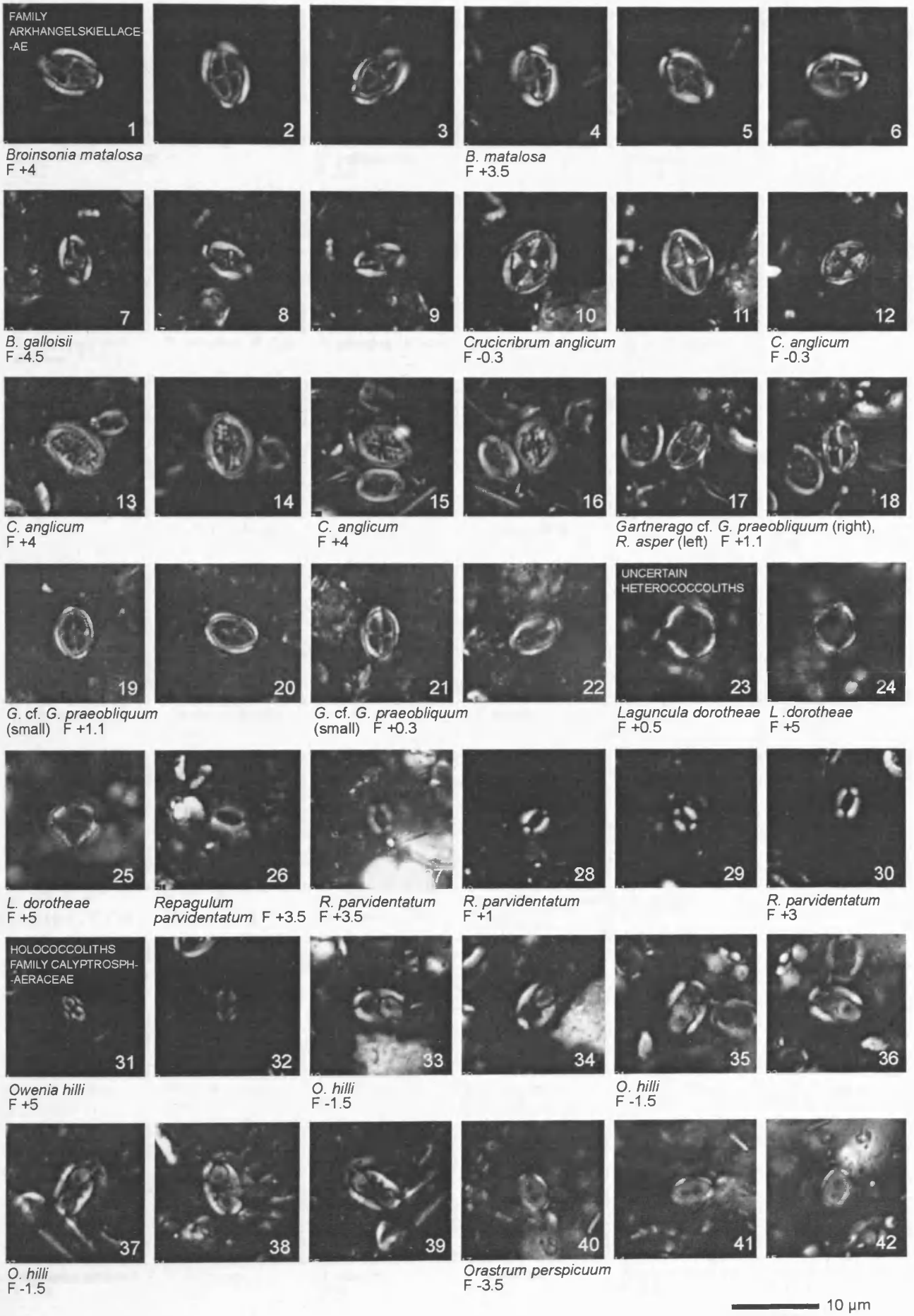
FAMILY ARKHANGELSKIELLACE--AE
1
2
3
4
5
6
Broinsonia matalosa F +4
B. matalosa F +3.5
7
8
9
10
11
12
B. galloisii F -4.5
Crucicribrum anglicum F -0.3
C. anglicum F -0.3
13
14
15
16
17
18
C. anglicum F +4
C. anglicum F +4
Gartnerago cf. G. praeobliquum (right), R. asper (left) F +1.1
19
20
21
22
UNCERTAIN HETEROCOCCOLITHS
23
24
G. cf. G. praeobliquum (small) F +1.1
G. cf. G. praeobliquum (small) F +0.3
Laguncula dorotheae F +0.5
L .dorotheae F +5
25
26
28
29
30
L. dorotheae F +5
Repagulum parvidentatum F +3.5
R. parvidentatum F +3.5
R. parvidentatum F +1
R. parvidentatum F +3
HOLOCOCCOLITHS FAMILY CALYPTROSPH--AERACEAE
31
32
33
34
35
36
Owenia hilli F +5
O. hilli F -1.5
O. hilli F -1.5
37
38
39
40
41
42
O. hilli F -1.5
Orastrum perspicuum F -3.5
10 µm

PLATE 21

Orastrum perspicuum
F -3.5

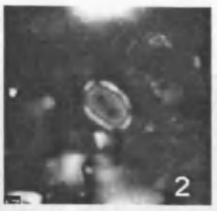

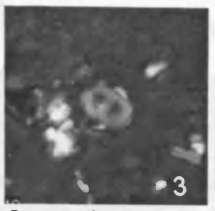

O. perspicuum
F -3.5

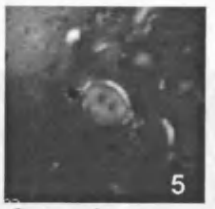

O. perspicuum
F -3.5

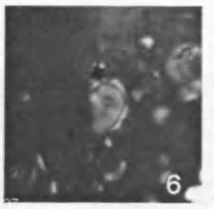

Braarudosphaera africana F +0.5

B. africana F -0.3

B. africana F +0.5

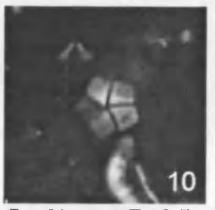

B. africana F +3.5

B. cf. *B. primula*
F +5

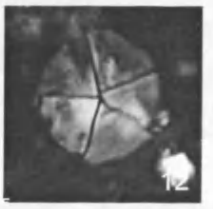

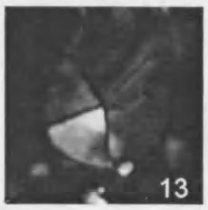

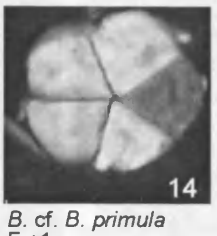

B. cf. *B. primula*
F +1

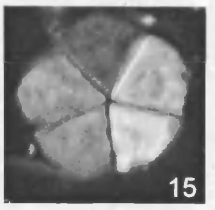

B. stenorhetha
F +4

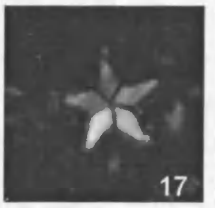

B. stenorhetha
F +2

B. stenorhetha
F +2

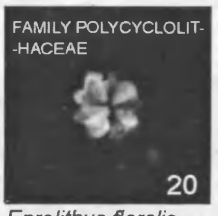

Eprolithus floralis
F +5

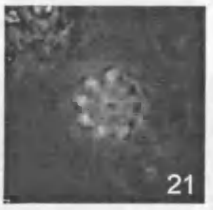

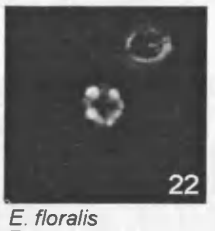

E. floralis
F +1.3

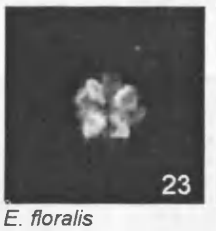

E. floralis
F +3

E. floralis
F +3.5

E. apertior ?
(side-view) F +3.5

E. floralis
(side-view) F +5

Eprolithus spp.
(side-view) F +5

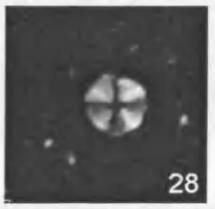

Radiolithus planus
F +0.5

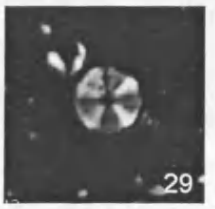

R. planus
F -0.3

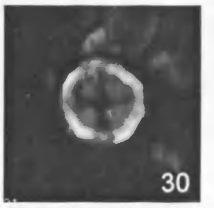

R. cf. *R. planus*
F +4

R. cf. *R. planus*
F +4

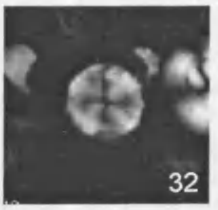

R. cf. *R. planus*
F +4

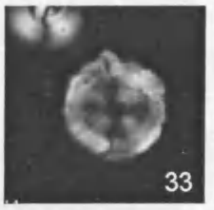

R. cf. *R. planus*
F -1.5

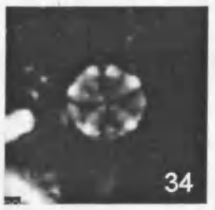

R. cf. *R. planus*
F +0.35

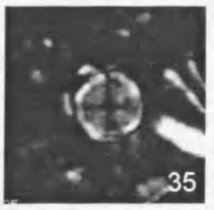

R. cf. *R. planus*
F +0.35

R. cf. *R. planus*
F +1.2

Hayesites albiensis
F -0.3

H. albiensis
F -0.3

H. albiensis
F +4

H. albiensis
F +1.0

Nannonconus x-s
F -0.3

Nannonconus x-s
F -0.5

10 µm

PLATE 22

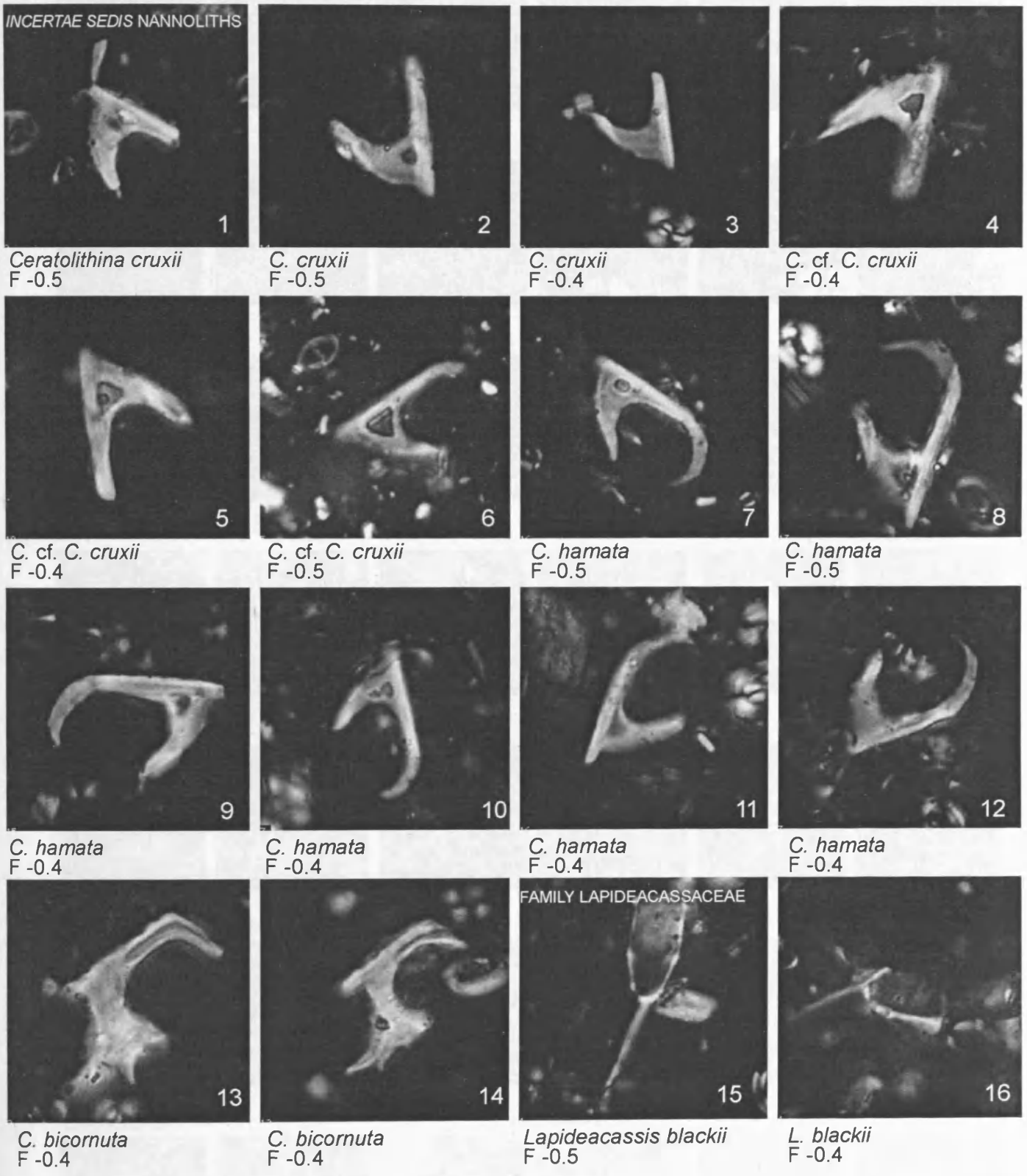

Ceratolithina cruxii
F -0.5

C. cruxii
F -0.5

C. cruxii
F -0.4

C. cf. *C. cruxii*
F -0.4

C. cf. *C. cruxii*
F -0.4

C. cf. *C. cruxii*
F -0.5

C. hamata
F -0.5

C. hamata
F -0.5

C. hamata
F -0.4

C. hamata
F -0.4

C. hamata
F -0.4

C. hamata
F -0.4

C. bicornuta
F -0.4

C. bicornuta
F -0.4

Lapideacassis blackii
F -0.5

L. blackii
F -0.4

PLATE 23 - ODP LEG 171B, HOLE 1049C, BLAKE NOSE

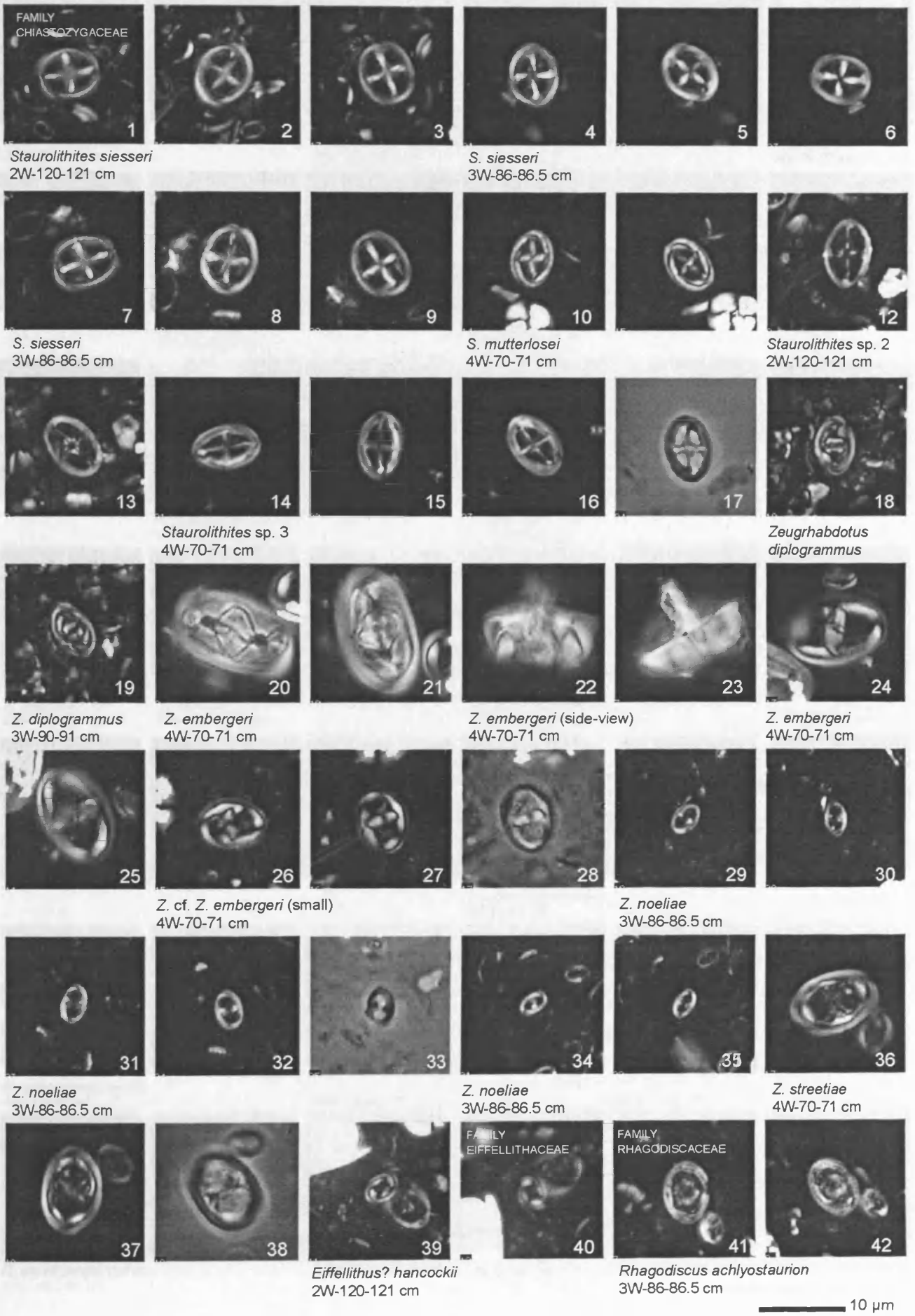

PLATE 24

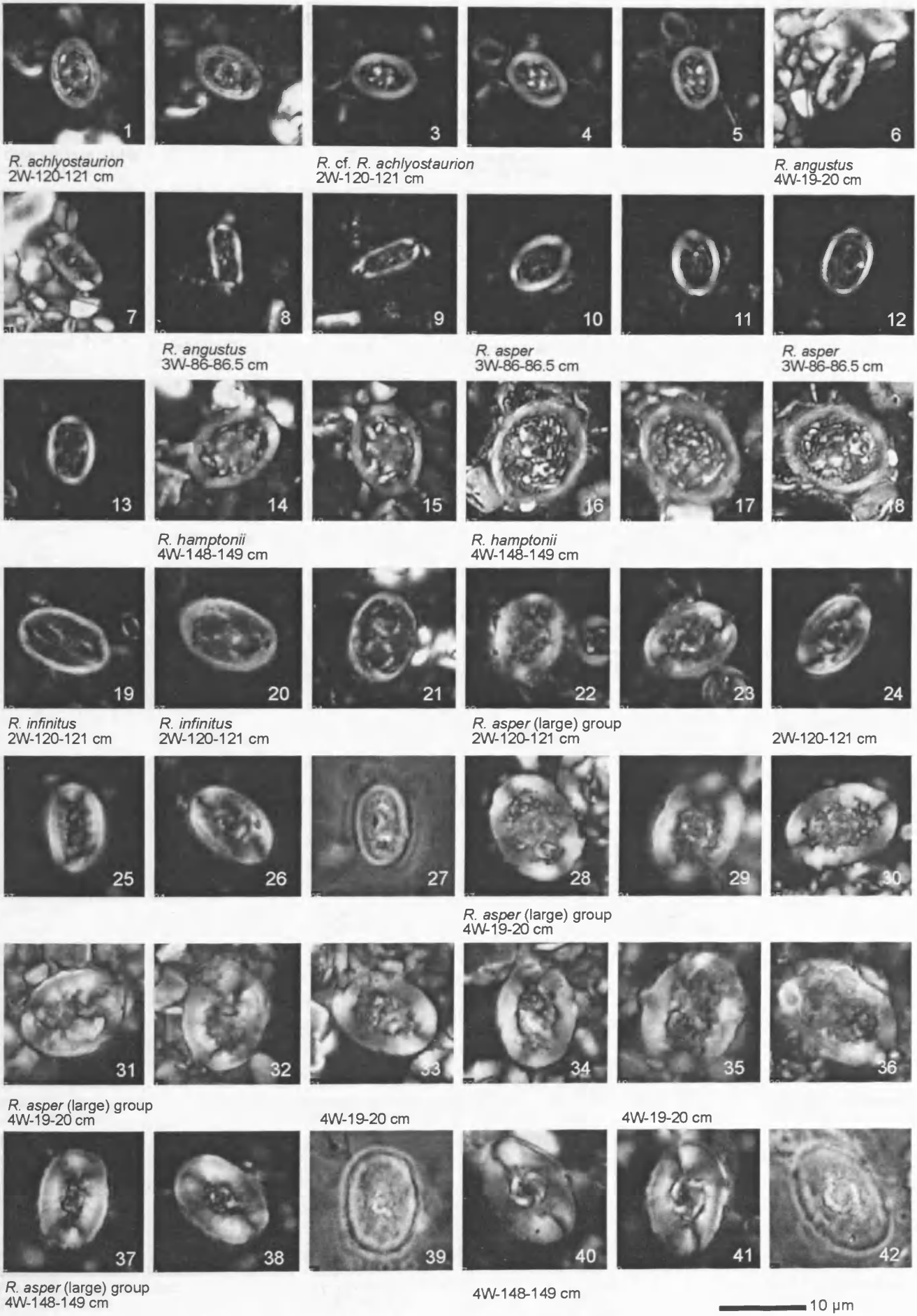
1
3
4
5
6
R. achlyostaurion
2W-120-121 cm
R. cf. R. achlyostaurion
2W-120-121 cm
R. angustus
4W-19-20 cm
7
8
9
10
11
12
R. angustus
3W-86-86.5 cm
R. asper
3W-86-86.5 cm
R. asper
3W-86-86.5 cm
13
14
15
16
17
18
R. hamptonii
4W-148-149 cm
R. hamptonii
4W-148-149 cm
19
20
21
22
23
24
R. infinitus
2W-120-121 cm
R. infinitus
2W-120-121 cm
R. asper (large) group
2W-120-121 cm
2W-120-121 cm
25
26
27
28
29
30
R. asper (large) group
4W-19-20 cm
31
32
34
35
36
R. asper (large) group
4W-19-20 cm
4W-19-20 cm
4W-19-20 cm
37
38
39
40
41
42
R. asper (large) group
4W-148-149 cm
4W-148-149 cm
10 µm

PLATE 25

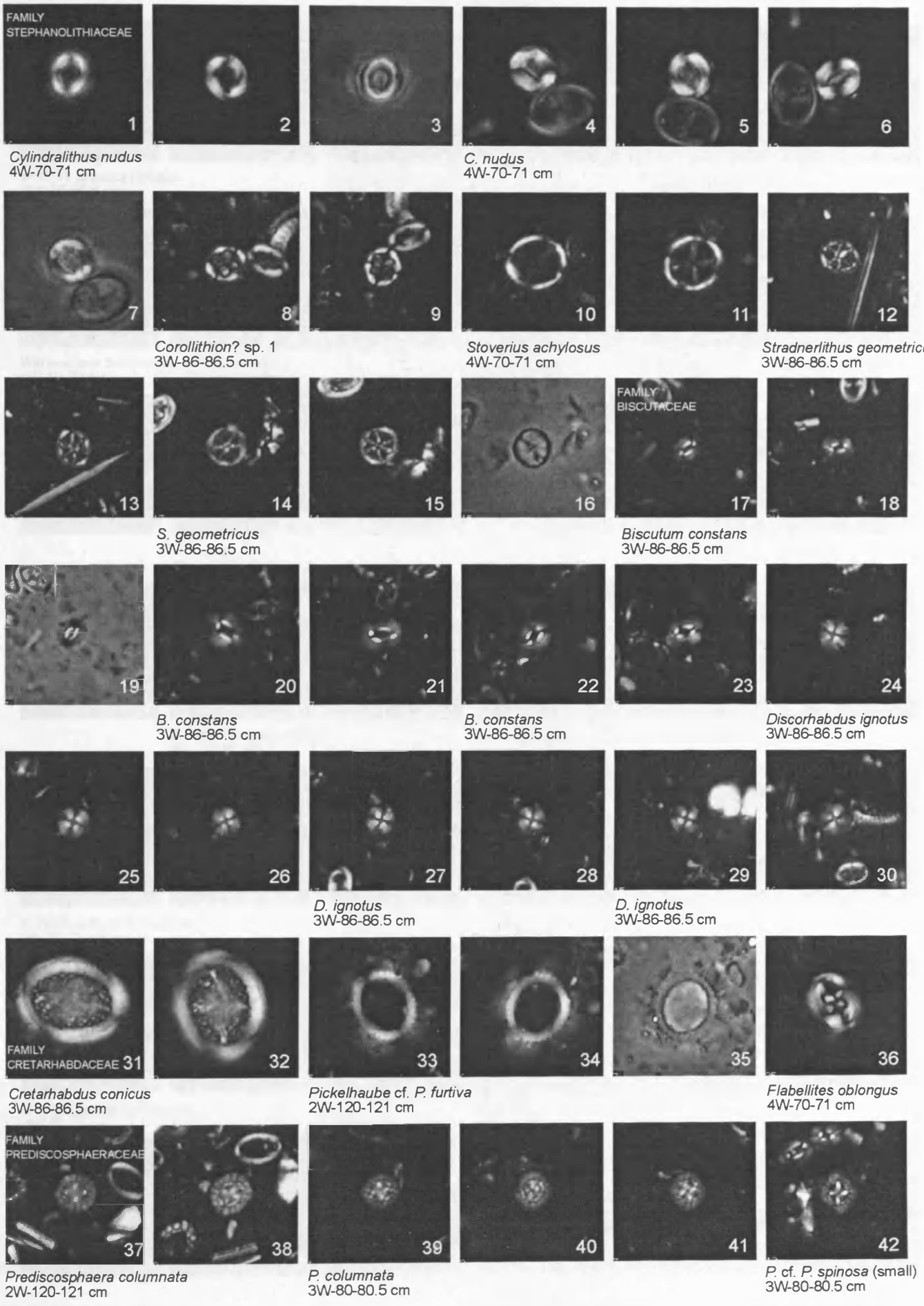
FAMILY STEPHANOLITHIACEAE
1
2
3
4
5
6
Cylindralithus nudus
4W-70-71 cm
C. nudus
4W-70-71 cm
7
8
9
10
11
12
Corollithion? sp. 1
3W-86-86.5 cm
Stoverius achylosus
4W-70-71 cm
Stradnerlithus geometricus
3W-86-86.5 cm
13
14
15
16
FAMILY BISCUTACEAE
17
18
S. geometricus
3W-86-86.5 cm
Biscutum constans
3W-86-86.5 cm
19
20
21
22
23
24
B. constans
3W-86-86.5 cm
B. constans
3W-86-86.5 cm
Discorhabdus ignotus
3W-86-86.5 cm
25
26
27
28
29
30
D. ignotus
3W-86-86.5 cm
D. ignotus
3W-86-86.5 cm
FAMILY CRETARHABDACEAE 31
32
33
34
35
36
Cretarhabdus conicus
3W-86-86.5 cm
Pickelhaube cf. P. furtiva
2W-120-121 cm
Flabellites oblongus
4W-70-71 cm
FAMILY PREDISCOSPHAERACEAE
37
38
39
40
41
42
Prediscosphaera columnata
2W-120-121 cm
P. columnata
3W-80-80.5 cm
P. cf. P. spinosa (small)
3W-80-80.5 cm
10 µm

PLATE 26

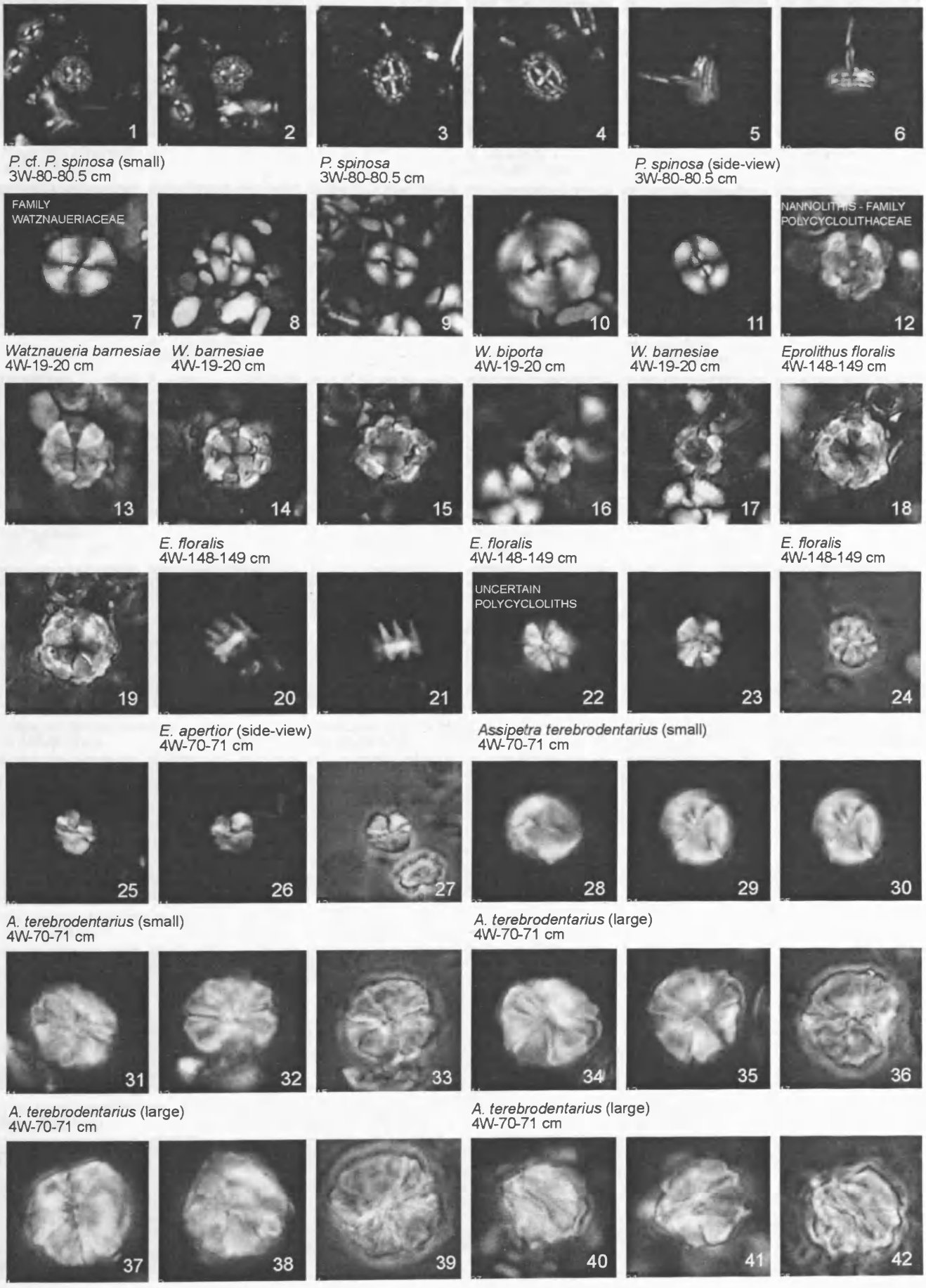
1
2
3
4
5
6
P. cf. P. spinosa (small)
3W-80-80.5 cm
P. spinosa
3W-80-80.5 cm
P. spinosa (side-view)
3W-80-80.5 cm
FAMILY
WATZNAUERIACEAE
7
8
9
10
11
NANNOLITHS - FAMILY
POLYCYCLOLITHACEAE
12
Watznaueria barnesiae
4W-19-20 cm
W. barnesiae
4W-19-20 cm
W. biporta
4W-19-20 cm
W. barnesiae
4W-19-20 cm
Eprolithus floralis
4W-148-149 cm
13
14
15
16
17
18
E. floralis
4W-148-149 cm
E. floralis
4W-148-149 cm
E. floralis
4W-148-149 cm
19
20
21
UNCERTAIN
POLYCYCLOLITHS
22
23
24
E. apertior (side-view)
4W-70-71 cm
Assipetra terebrodentarius (small)
4W-70-71 cm
25
26
27
28
29
30
A. terebrodentarius (small)
4W-70-71 cm
A. terebrodentarius (large)
4W-70-71 cm
31
32
33
34
35
36
A. terebrodentarius (large)
4W-70-71 cm
A. terebrodentarius (large)
4W-70-71 cm
37
38
39
40
41
42
A. terebrodentarius (large)
4W-19-20 cm
A. terebrodentarius (large)
4W-19-20 cm
10 µm

PLATE 27

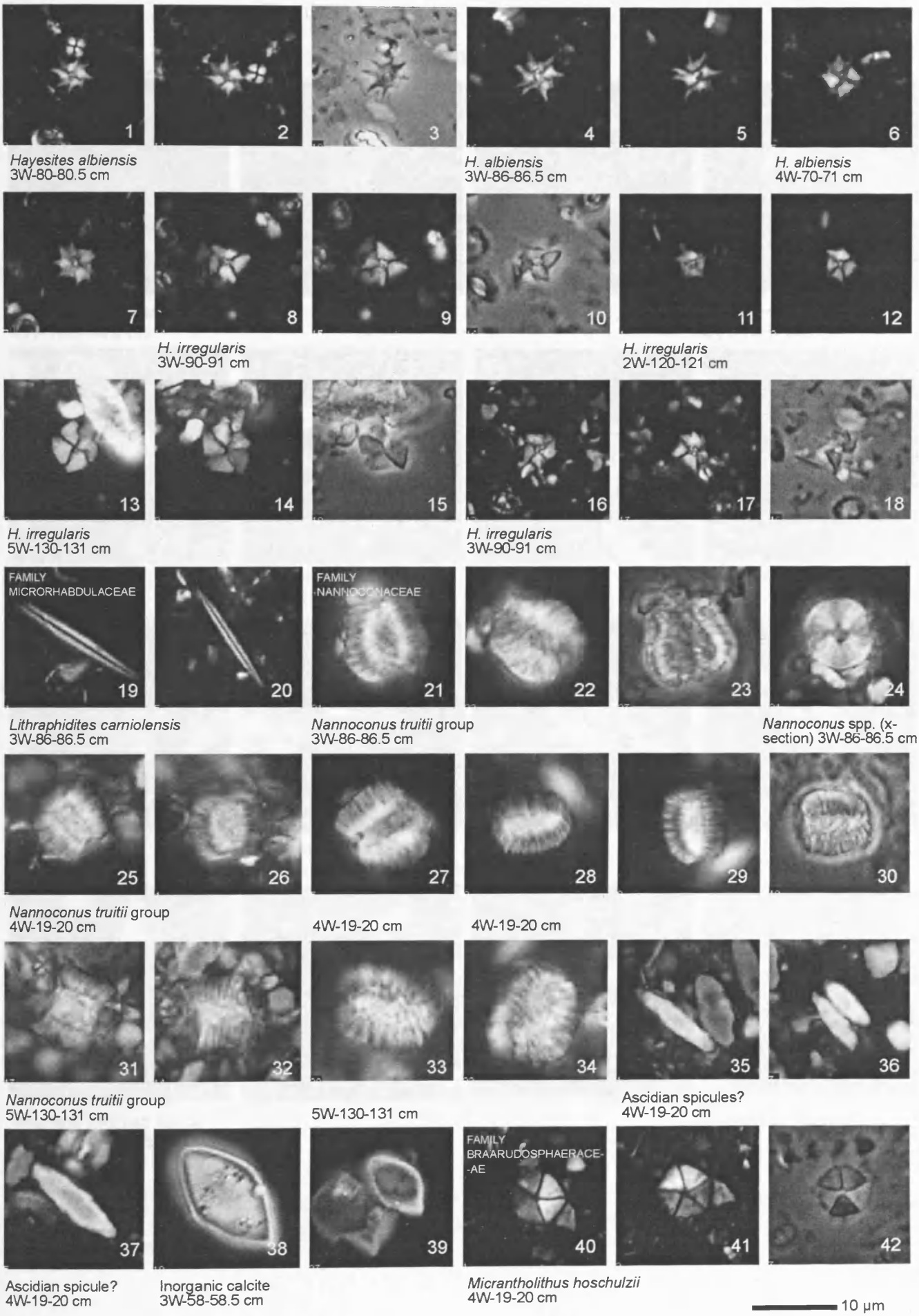

Hayesites albiensis
3W-80-80.5 cm

H. albiensis
3W-86-86.5 cm

H. albiensis
4W-70-71 cm

H. irregularis
3W-90-91 cm

H. irregularis
2W-120-121 cm

H. irregularis
5W-130-131 cm

H. irregularis
3W-90-91 cm

Lithraphidites carniolensis
3W-86-86.5 cm

Nannoconus truitii group
3W-86-86.5 cm

Nannoconus spp. (x-section) 3W-86-86.5 cm

Nannoconus truitii group
4W-19-20 cm

4W-19-20 cm

4W-19-20 cm

Nannoconus truitii group
5W-130-131 cm

5W-130-131 cm

Ascidian spicules?
4W-19-20 cm

Ascidian spicule?
4W-19-20 cm

Inorganic calcite
3W-58-58.5 cm

Micrantholithus hoschulzii
4W-19-20 cm

10 µm

PLATE 28

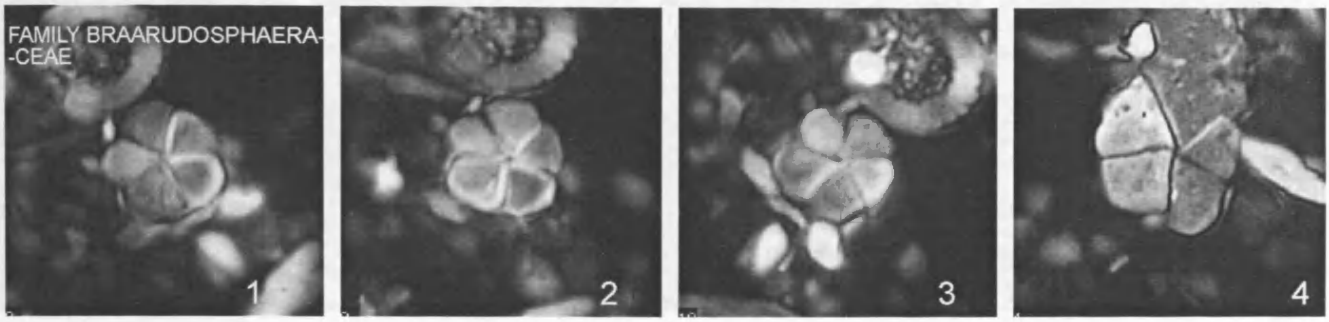

Braarudosphaera sp. 1
4W-148-149 cm

Braarudosphaera sp. 2
4W-148-149 cm

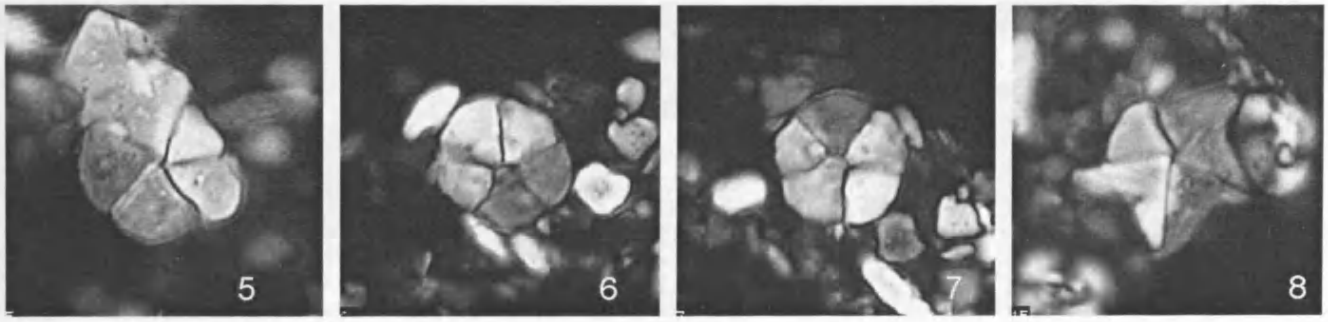

Braarudosphaera sp. 3
4W-148-149 cm

Micrantholithus sp. 1
(small) 4W-148-149 cm

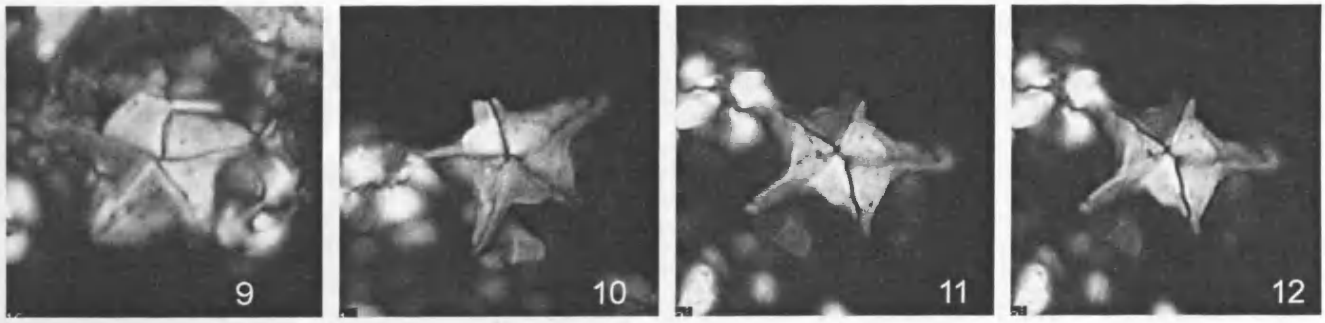

Micrantholithus sp. 1
(small) 4W-148-149 cm

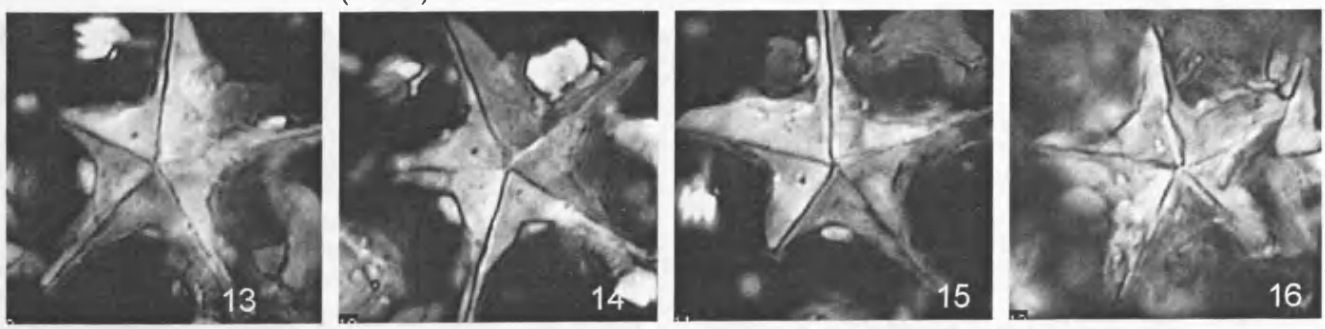

Micrantholithus sp. 2
(large) 4W-148-149 cm

Micrantholithus sp. 2
(large) 4W-148-149 cm

10 µm

PLATE 29

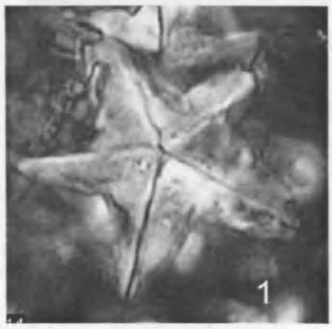

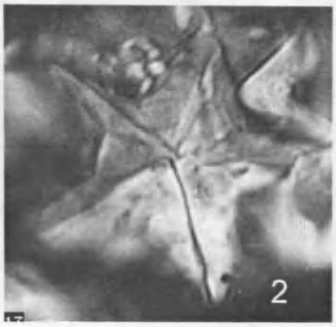

Micrantholithus sp. 2
4W-148-149 cm

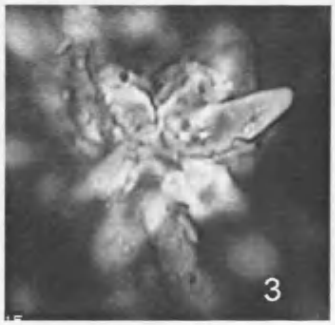

Ascidian spicules?
4W-148-149 cm

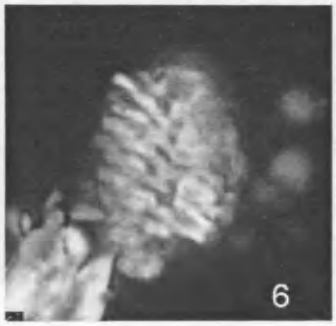

Nannoconus truitii group
4W-148-149 cm

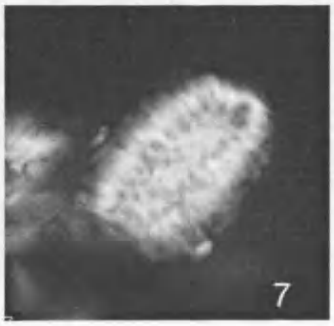

Excursion 1 field of view
4W-148-149 cm

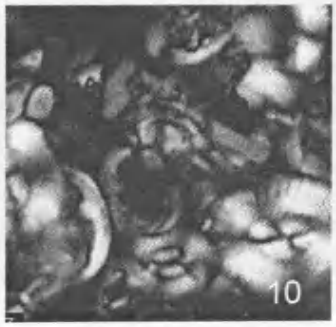

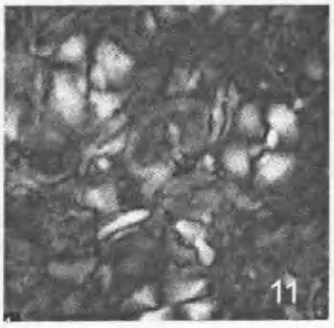

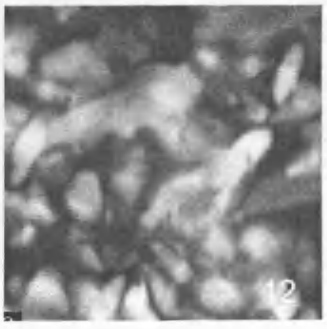

pre-Excursion 1 field of
view, 6W-120-121 cm

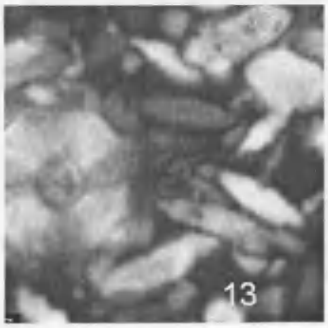

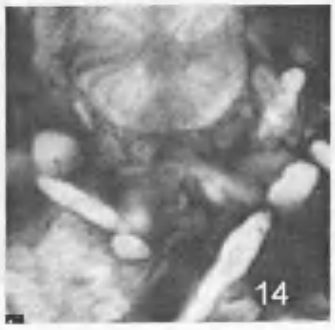

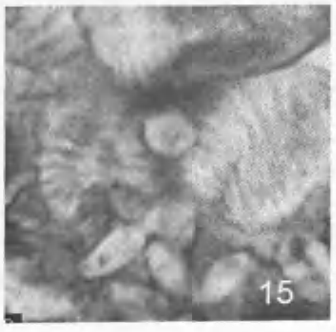

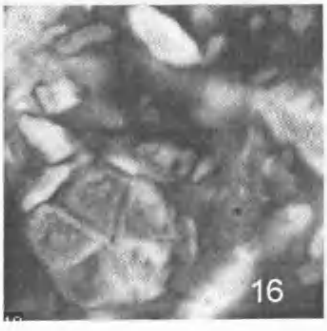

10 µm

PLATE 30

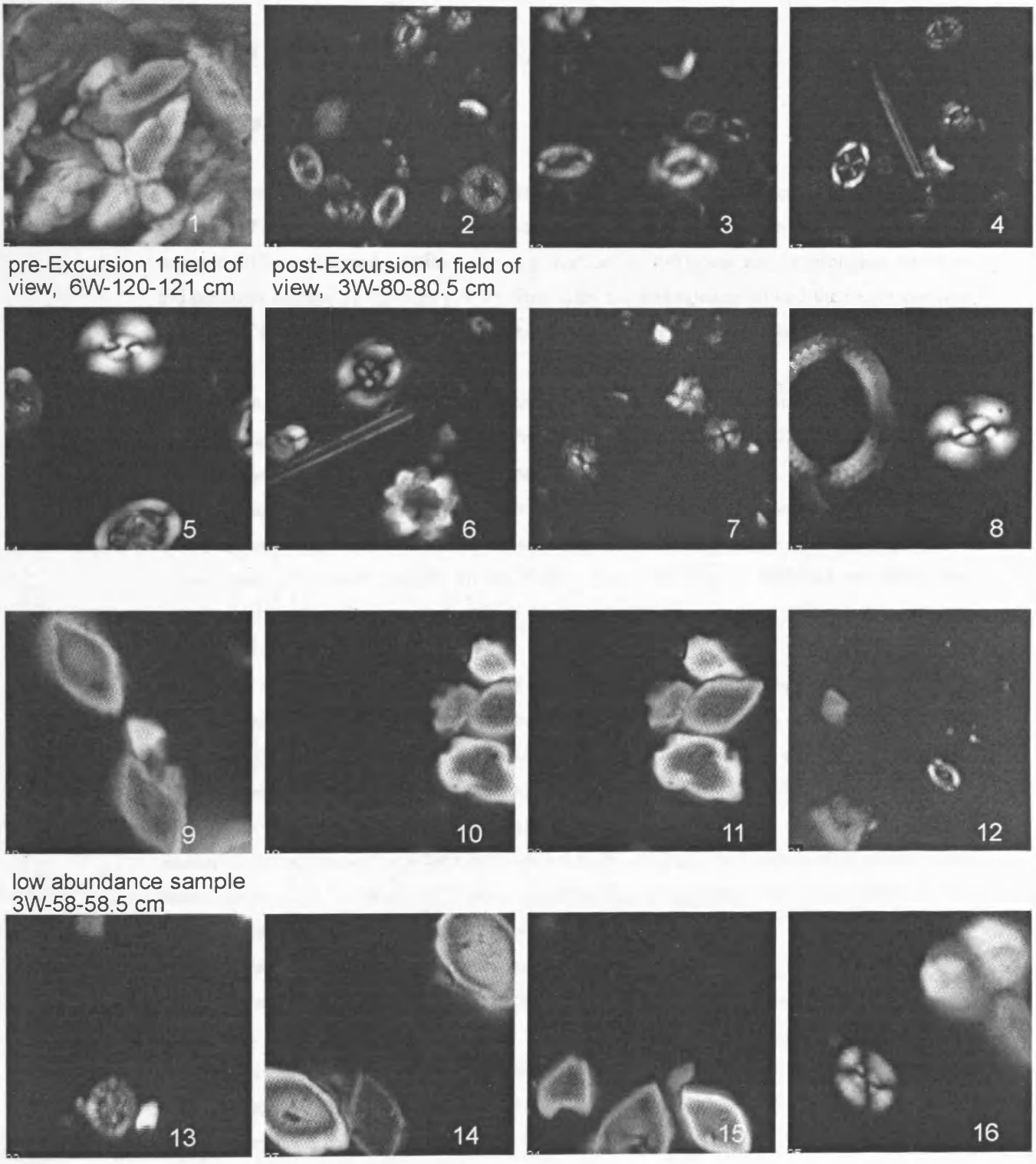
1
2
3
4
pre-Excursion 1 field of view, 6W-120-121 cm
post-Excursion 1 field of view, 3W-80-80.5 cm
5
6
7
8
9
10
11
12
low abundance sample 3W-58-58.5 cm
13
14
15
16
10 µm

Chapter 10. Conclusions

10.1 Cauvery Basin stratigraphy

10.1.1 Biostratigraphy

- The Albian-Cenomanian nannofossil biostratigraphy of the Cauvery Basin, based on two new sections of the Karai Formation, has been significantly improved in this study. Previous nannofossil biostratigraphy of the basin (e.g. Kale et al. 2000) was low in resolution, based on the zonation scheme of Sissingh (1977). This study has additionally utilised the recent zonation schemes of Bown et al. (1998) and Burnett (1998) that offer increased resolution.

- The Albian zones, BC23-BC27 of Bown et al. (1998), are based on a series of robust, cosmopolitan marker taxa such as *Prediscosphaera columnata*, *Tranolithus orionatus*, *Axopodorhabdus albianus* and *Eiffellithus turriseiffelii*, making their application relatively straightforward irrespective of the zonation that is used. There are a few secondary events in the BC zonation of Bown et al. (1998), such as the LO's of *Braloweria boletiformis* and *Ceratolithina bicornuta* that are known mainly from NW Europe (England and North Sea region), and are therefore not applicable to the Cauvery Basin.

- A number of problems were encountered when applying the Cenomanian zonation of Burnett (1998). Two zonal markers proposed by her for the first time, *Gartnerago segmentatum* (Zone UC2) and *Cylindralithus biarcus* (Zone UC4), could not be used for the Karai Formation. *G. segmentatum* displays diachroneity with respect to the FO of *Corollithion kennedyi* in the two study sections, and is therefore problematic. *C. biarcus* was very rare and sporadic in Karai Section 1 and absent in Karai Section 2. It is therefore not practical as a marker species. Both these species are reported to have a stratigraphic range from the Cenomanian to the Maastrichtian (Burnett 1998). Some of the secondary events (e.g. FO's of *Helicolithus anceps* and *Quadrum intermedium*) are not recognised in the Cauvery Basin although they have been identified in the Indian Ocean (Burnett 1998). Their absence is more likely due to their rarity rather than stratigraphic problems. Other secondary markers such as *Gartnerago chiasta* and *Watznaueria britannica* are slightly displaced in the Cauvery Basin with respect to their stratigraphic position within Zone UC1 (Burnett 1998), and were therefore not easily applicable as secondary zonal events.

- The nannofossil events at the Albian/Cenomanian boundary in the Cauvery Basin correlate reasonably well with the proposed GSSP at Mt. Risou (southern France), although there are inconsistencies with respect to the stratigraphic order of events such as the LO's of *Watznaueria britannica* and *Staurolithites glaber*. The boundary was tentatively identified in the Karai

sections using the FO of *Corollithion kennedyi*, supported by a number of additional events such as the FO's of *Gartnerago* cf. *G. nanum* and *Gartnerago chiasta*, and the LO's of *Hayesites albiensis* and *Staurolithites glaber*. Precise demarcation of the boundary will be possible after calibrating the nannofossil data with the ammonite data (Gale, in prep.).

- *Gartnerago* cf. *G. nanum* shows potential as a new marker species with respect to its first and last occurrence. It has a short stratigraphic range from the Early Cenomanian (close to the FO of *C. kennedyi*) to the mid-Cenomanian (Zone UC3) in the Cauvery Basin. In addition to its easy identification, the species occurs frequently in both study sections, thereby showing biostratigraphic utility. The species was also recognised in Europe and the Pacific study areas.

- Based on nannofossil biostratigraphy, the Cenomanian/Turonian boundary appears to be incomplete in both sections, indicated by the simultaneous last occurrences of *Lithraphidites acutus* and *Helenea chiastia* in the same sample. This resulted in the absence of Zone UC5 (LO of *L. acutus*) of the Upper Cenomanian. The boundary was bracketed by the LO of *Helenea chiastia* and the FO of *Eprolithus octopetalus* in Karai Section 1. No definitive Turonian markers were identified in Karai Section 2.

10.1.2 Palaeobiogeographic differences

- Qualitative comparisons of coeval assemblages from three time-slices (mid-Albian, Late Albian and Early Cenomanian) from four different palaeogeographic settings have confirmed the overall cosmopolitan nature of Albian-Early Cenomanian nannofloras, previously suggested by Mutterlose (1992b) and Bown (2001). Palaeobiogeographic provinces such as the Boreal, Tethyan and Austral cannot be clearly recognised in the overall nature of the assemblages from England, France, India and the Pacific. However, some subtle palaeobiogeographic differences are observed between these areas, which are summarised below.

- **Europe (England and France):** In this study, two species, *Ceratolithina hamata* and *Braloweria boletiformis*, were restricted to samples from England, where they showed a continuous presence. In southern France, these species showed a rare and sporadic presence. *Ceratolithina bicornuta* was found only in samples from England. *Gaarderella granulifera* was found consistently in sections from England and France. It was absent in samples from India and the Pacific. The genus *Nannoconus* showed a stronger presence in France compared to England, where it was rare in occurrence. *Nannoconus* was practically absent in samples from India and the Pacific, confirming the earlier interpretation of its neritic-adapted, Tethyan distribution (e.g., Street & Bown 2000).

- **Cauvery Basin**: The nannofossil assemblages showed the consistent presence of the two high-latitude forms, *Repagulum parvidentatum* and *Seribiscutum primitivum*, but did not contain other

distinctive Austral forms such as *Sollasites falklandensis* or *Zeugrhabdotus kerguelenensis*. Very rare occurrences of these two forms were observed in the Karai Formation. The Cauvery Basin assemblages therefore did not show marked Austral affinities. The distribution of the *incertae sedis* genus *Ceratolithina* is puzzling. It is commonly occurring in the Gault Clay. The taxon is also reported from the Indian Ocean (Bown et al. 1998; Lees 2002) but is absent in the Cauvery Basin assemblages. Although the palaeobiogeographic preferences of *Ceratolithina* are not clearly understood, it is possible that the taxon was shelf-restricted and was unable to migrate through deep waters between the Naturaliste Plateau (off Australia, Sites 257 and 258) and the Cauvery Basin.

- **Shatsky Rise (ODP Leg 198):** The nannofossil assemblages from the tropical Pacific Ocean showed certain characteristic 'oceanic' features that set them apart from coeval shelf assemblages from England, France and India. For example, *Lithraphidites carniolensis* is abundantly present throughout in the Pacific section and was almost certainly an oceanic-adapted taxon. *Hayesites irregularis* is commonly present, suggesting that it was adapted to low-latitude warmer waters. The neritic-adapted, Tethyan genus *Nannoconus* is virtually absent in the tropical Pacific. *Watznaueria* spp. is more abundant, comprising up to 70% of the assemblages, compared to shelf assemblages where it usually does not exceed 45% by proportion.

10.2 Palaeoceanography

10.2.1 Palaeoclimate interpretation

- A major warming event is postulated at the mid-/Late Albian boundary in the Weald (Gault Clay) of the Anglo-Paris Basin. Nannofossil data give strong support to the oxygen isotope and ammonite data for this warming event. The cold-water species *Repagulum parvidentatum* shows a rapid decline in its percentage abundance from to 11 to 1% in Bed VIII of the Gault Clay, which precisely coincides with the warming evidenced by a light oxygen isotope peak and the influx of Tethyan ammonites. This confirms that *R. parvidentatum* is an excellent nannofossil proxy for palaeotemperatures in the Gault Clay section. Benthic and planktic foraminifera such as *Gavenlinella* spp. and *Hedbergella* spp. are known to show a change in their coiling directions in the Munday's Hill section of the Gault Clay supporting this temperature change (Crux 1991). A significant productivity increase based on high percentages of *Zeugrhabdotus noeliae* (~40%) is coincident with this rapid and probably short-lived warming event. The productivity rise suggests nutrient-rich waters in the Weald during the Late Albian, which is likely to have been driven by increased precipitation and run-off, as a result of the warming.

10.2.2 Proxy testing

- The principal productivity proxies, *Biscutum constans* and *Zeugrhabdotus noeliae*, are significantly more abundant in neritic environments (e.g. Gault Clay, Blake Nose) than mid-ocean settings (Shatsky Rise). Hence they are usable as fertility proxies primarily in shelf sections. *Discorhabdus ignotus* is a minor productivity proxy in shelf sections because its average abundance (mean: 5%) is lower than that of *B. constans* and *Z. noeliae* (mean: 15%). This partly conflicts with the results of Herrle (2002) who ignored *B. constans* in the high-fertility group in neritic (Vocontian Basin) and upwelling sites (Mazagan Plateau), despite its higher abundance (10-20%) than *D. ignotus* (5-8%).

- The genus *Watznaueria* (*barnesiae* and *fossacincta*) constitutes the most abundant taxon in all mid-Cretaceous nannofossil assemblages. The dominance of *Watznaueria* does not bear a direct relationship with the preservation in a sample. For example, in the Shatsky Rise sections, high abundances of *Watznaueria* (> 40%) were observed in uniformly moderate to well-preserved samples. Therefore the dominance of *Watznaueria* reflects its broad palaeoecological tolerance rather than resistance to dissolution. This is in agreement with the observations of Street & Bown (2000) and Lees et al. (2004), which suggest *Watznaueria* to be an r-selected, ubiquitous Mesozoic taxon similar to the extant species *Emiliania huxleyi*.

- The Nutrient Index (NI) proposed by Herrle (2002) and the Productivity Index proposed by Gale et al. (2000) have been combined herein to give a modified Nutrient Index for the quantitative estimation of fertility conditions (see Chapter 5). The nature of the modified NI is similar to the ratio of Herrle (2002), but utilises all the three productivity proxies, i.e., *Biscutum constans*, *Zeugrhabdotus noeliae* and *Discorhabdus ignotus*, instead of only two. This index has been applied on the Gault Clay, Blake Nose and Shatsky Rise sections and its trend is similar to that obtained by using the original ratio of Herrle (2002). However, the modified NI appears to give a better perspective of fertility levels, as *B. constans* is included in the ratio.

- The utility of the principal nannofossil palaeotemperature proxies have been tested in this study. *Repagulum parvidentatum* is an excellent proxy for cold waters as evidenced in the Gault Clay section (see Chapter 5). *Seribiscutum primitivum* is low in abundance, and is therefore not usable as a cold-water proxy in the Gault Clay. The semi-quantitative abundance of *Flabellites oblongus* in the Gault suggests that it may possibly have been warm-water adapted. *Rhagodiscus asper*, a putative warm-water taxon, does not show any significant correlation with the $\delta^{18}O$ record either in the Gault Clay or in the Blake Nose section. Its abundance trend in the Shatsky Rise is also not clear. The species is consistently low in abundance (~2%), and is a minor component of the nannofossil assemblages in all the sections. Its warm-water affinity is concluded to be dubious. The fluctuations in the abundance of *R. asper* however, suggest that it may have been sensitive to lower-fertility conditions. *Tranolithus orionatus*, a species with

supposedly cold-water affinities is unusable as a palaeotemperature proxy because it shows no correlation with the $\delta^{18}O$ values in the Gault Clay section.

10.2.3 Nannofossil productivity record at the OAE1a and OAE1b

- The nannofossil productivity record of the Early Albian OAE1b in the western Atlantic (ODP Leg 171B) along with geochemical data ($\delta^{13}C$-isotope and Sr/Ca excursions) supports the increased productivity model for this anoxic event at the Blake Nose Plateau. This is based on the increased productivity levels from Excursion 1 up section, (see Chapter 6) with peaks at the base (>20% *B. constans*) and top (>40% *Z. noeliae*) of the black shale. The deposition of the black shale was characterised by more stable, stratified waters, evidenced by a marked decline in the productivity proxies, a minor rise in *Nannoconus*, along with high Shannon-Weiner values. The increased productivity model for the OAE1b is in good agreement with the results of Erbacher et al. (1999, 2001). Benthic foraminiferal data also suggests that eutrophic conditions prevailed before and during the OAE, indicated by the presence of infaunal as well as opportunistic genera such as *Gyrodinoides* and *Pseudobolivina*. The termination of OAE1b is suggested to have been caused by a change from eutrophic to mesotrophic conditions and characterised by a gradual repopulation of the sea floor, starting with opportunistic benthic foraminiferal taxa in bathyal sections (Erbacher et al. 1999). Planktonic foraminifera at this time were generally the small, inconspicuous forms belonging to the genus *Hedbergella* that tend to be abundant, as observed in the western Tethyan Col de Palluel section (SE France). The absence of large planktonic foraminifera is considered to be due to evolutionary factors rather than the result of an expanded oxygen minimum zone destroying the habitat of larger deep-dwelling forms, as suggested in Bréhéret et al. (1986).

- Nannofossil productivity proxies show marked temporal variations in abundance with respect to the OAE1a and OAE1b events at Shatsky Rise in the Pacific Ocean (Sites 1207 and 1213). During the Early Aptian OAE1a interval, all the productivity proxies are either absent (*B. constans*, *Z. noeliae*, *D. ignotus*) or occur in very low abundances (*D.ignotus* and *Z. noeliae*). The correspondence between 'resistivity highs' indicating enhanced siliceous productivity (Robinson et al. 2004) and the 'near absence' of nannofossil productivity taxa clearly indicates their inverse relationship. Radiolarians show high rates of evolutionary turnover (extinction and radiation) at or near the OAEs (Erbacher & Thurow 1997). Planktonic foraminifera and calcareous nannoplankton were likewise influenced to varying degrees by the OAEs (Leckie et al. 2002).

- The nannofossil productivity indicators show relatively increased abundances in the Early Albian OAE1b interval (2-13%). This may be directly related to differences in the scale of volcanism during the two OAE events. Reduced rates of submarine volcanism during OAE1b

compared to OAE1a may have boosted the productivity of *B. constans* and *Z. noeliae* during the OAE1b interval at Shatsky Rise.

- Diversity indices such as species richness suggest that the equatorial Pacific was a fairly stable environment during the mid-Cretaceous with a relatively large niche space shared by many species. The similar values of Shannon's diversity and equitability between four coeval early Albian sections, i.e., Cauvery Basin, Gault Clay, Blake Nose and Shatsky Rise, suggest that the palaeoequatorial Pacific may not necessarily have been a zone of long-term high productivity. The interpretation of chert as a productivity proxy is questionable when applied to Mesozoic ocean systems, especially the chert-dominated Pacific Ocean.

- A marked increase in the % of *Biscutum constans* (reaching up to 48%) in the Late Albian *Eiffellithus turriseiffelii* Zone is noted in the Pacific and other coeval samples covered in this study. This increase in *B. constans* continues into the Early Cenomanian and younger sediments. Such an increase may be indicative of a broad evolutionary change in *B. constans*, rather than its sensitivity to ocean fertility.

10.3 Taxonomy

- Based on LM observations, four new species, *Calculites karaiensis*, *Loxolithus bicyclus*, *Manivitella fibrosa* and *Tranolithus simplex* are described in this study.

10.4 Recommendations for future work

- A SEM study of *Cylindralithus biarcus* is necessary to clarify its taxonomy, in light of the observations made in this study.

- The palaeobiogeography of the *incertae sedis* genus *Ceratolithina* needs further research, especially from southern high-latitude sections, in areas around the Cauvery Basin.

- Morphometric studies on *Biscutum constans* are needed to clarify the cause of its observed increase from the Late Albian into younger sediments. As suggested in this thesis, the increase may be purely evolutionary. A size differentiation is already noted, but the precise timing of the first appearance of the large-sized morphotype is not clear at present.

- Multivariate statistical analyses, especially correspondence analysis, are recommended for the quantitative data generated in this study. Unfortunately, such studies could not be included within the scope of this work. However, the data (e.g. Gault Clay and Shatsky Rise) are amenable for such studies and could lead to further refinement of the palaeoceanographic

interpretations made here. Such studies should help to understand relationships between groups of temperature and fertility-related taxa.

- *Staurolithites* spp. continues to remain a problematic group with regards to its taxonomy. The taxon is a significant component of mid-Cretaceous assemblages. The frequent lumping of species within this group may be concealing its ecological preferences. A stringent species concept needs to be formulated for it.

- The abundance distribution of *Biscutum constans* and *Zeugrhabdotus noeliae* should be compared from upwelling sites, and other areas of high nutrient availability. This would reveal which of the two represents higher fertility conditions. *Rhagodiscus asper* should be tested for its fertility preferences and *Flabellites oblongus* for its palaeotemperature affinities.

References

Acharyya, S. K., and Lahiri, T. C., 1991. Cretaceous palaeogeography of the Indian subcontinent; a review. *Cretaceous Research*, 12, 3-26.

Applegate, J. L. & Bergen, J. A., 1989. Cretaceous calcareous nannofossil biostratigraphy of sediments recovered from the Galicia Margin, ODP Leg 103. *Proceedings of the ODP, Scientific Results*, 103, 293-348.

Applegate, J. L., Bergen, J. A., Covington, J. M. and Wise, S. W., 1989. Lower Cretaceous calcareous nannofossils from continental margin drill sites off North Carolina (DSDP Leg 93) and Portugal (ODP Leg 103): a comparison. *In*: J. A. Crux and S. E. van Heck (Eds.), *Nannofossils and their Applications*, Ellis Horwood, Chichester, 212-222.

Arthur, M. A., Brumsack, H. J., Jenkyns, H. C. & Schlanger, S. O., 1990. Stratigraphy, geochemistry and palaeoceanography of organic carbon-rich Cretaceous sequences. *In*: R. N. Ginsberg & B. Beaudoin (Eds.), *Cretaceous Resources, Events and Rhythms*, Vol. 304C, Kluwer Academic (NATO ASI Series), 75-119.

Ayyasami, K. and Banerji, R. K., 1984. Cenomanian-Turonian transition in the Cretaceous of southern India. *Bulletin of the Geological Society of Denmark*, 33, 21-30.

Backman, J. and Shackleton, N. J., 1983. Quantitative biochronology of Pliocene and early Pliestocene calcareous nannofossils from the Atlantic, Indian and Pacific Oceans. *Marine Micropaleontology*, 8, 141-170.

Barron, E. J., 1983. A warm, equable Cretaceous: the nature of the problem. *Earth-Science Reviews*, 19, 305-338.

Barron, E. J., 1987. Cretaceous plate tectonic reconstructions. *Palaeogeography, Palaeoclimatology, Palaeoecology*, 59, 3-29.

Barron, E. J. & Washington, W. M., 1985. Warm Cretaceous climates: high atmospheric CO_2 as a plausible mechanism. *In*: E. T. Sundquist & W. S. Broecker (Eds.), *The carbon cycle and atmospheric CO_2: natural variations Archean to Present, Geophysical Monograph*, Vol. 32, 546-553.

Barron, E. J., Fawcett, P. J., Pollard, D. & Thompson, S. L., 1993. Model simulations of Cretaceous climates: the role of geography and carbon dioxide. *In*: J. R. L. Allen, B. J. Hoskins, B. W. Sellwood, R. A. Spicer & P. J. Valdes (Eds.), *Palaeoclimates and their modelling with special reference to the Mesozoic Era, Philosophical Transactions of the Royal Society of London*, Series B, 341, 307-316.

Barron, E. J., Fawcett, P. J., Peterson, W. H., Pollard, D. & Thompson, S. L., 1995. A simulation of mid-Cretaceous climate. *Paleoceanography*, 10, 953-962.

Beaufort, L., 1991. Adaptation of the random settling method for quantitative studies of calcareous nannofossils. *Micropaleontology*, 37(4), 415-418.

Bellier, J. –P. and Moullade, M., 2002. Lower Cretaceous planktonic foraminiferal biostratigraphy of the western North Atlantic (ODP Leg 171B), and taxonomic clarification of key index species. *Revue de Micropaléontologie*, 45 (1), 9-26.

Benson, W. E., Sheridan, R. E. et al., 1978. *Initial Reports of the Deep Sea Drilling Project*, 44, Washington (U. S. Govt. Printing Office), 5-10.

Berger, W. H., 1979. Impact of deep-sea drilling on palaeoceanography. *In*: M. Talwani et al., (Eds.), *Deep drilling results in the Atlantic Ocean: continental margins and palaeoenvironments*, American Geophysical Union, 297-314.

Berger, W. H., Smetacek, V. S., and Wefer, G., 1989. Ocean productivity and paleoproductivity. *In:* W. H. Berger et al. (Eds.), *Productivity of the oceans: present and past*, 1-34.

Bischoff, G. and Mutterlose, J., 1998. Calcareous nannofossils of the Barremian/Aptian boundary interval in NW Europe: biostratigraphic and palaeoecologic implications of a high-resolution study. *Cretaceous Research*, 19, 635-661.

Black, M., 1971. Coccoliths of the Speeton Clay and Sutterby Marl. *Proceedings of the Yorkshire Geological Society*, 38, 381-424.

Black, M., 1972. British Lower Cretaceous Coccoliths. I-Gault Clay (Part 1) *Palaeontographical Society, London (Monograph)*, 126, 1-48, pls.1-16.

Black, M., 1973. British Lower Cretaceous Coccoliths. I-Gault Clay (Part 2). *Palaeontographical Society, London (Monograph)*, 127, 49-112, pls. 17-33.

Black, M., 1975. British Lower Cretaceous Coccoliths. I-Gault Clay (Part 3*). Palaeontographical Society, London (Monograph)*, 129, 113-142, pl. 34.

Bown, P. R., (Ed.) 1998. *Calcareous Nannofossil Biostratigraphy*, Kluwer Academic.

Bown, P. R., 2001. Calcareous nannofossils of the Gault, Upper Greensand and Glauconitic Marl (Middle Albian-Lower Cenomanian) from the BGS Selborne boreholes, Hampshire. *Proceedings of the Geologists' Association*, 112, 223-236.

Bown, P. R., *in press*. Early to mid-Cretaceous calcareous nannoplankton from the northwest Pacific Ocean (ODP Leg 198, Shatsky Rise). *Proceedings of the ODP, Scientific Results*, 198.

Bown, P. R., and Young, J. R., 1997. Mesozoic calcareous nannoplankton classification. *Journal of Nannoplankton Research*, 19, 21-36.

Bown, P. R. & Young, J. R., 1998a. Introduction. *In*: P. R. Bown (Ed.), *Calcareous Nannofossil Biostratigraphy*, Kluwer Academic, 1-15.

Bown, P. R. & Young, J. R., 1998b. Techniques. *In*: P. R. Bown (Ed.), *Calcareous Nannofossil Biostratigraphy*, Kluwer Academic, 16-28.

Bown, P. R., Rutledge, D., Crux, J. A. & Gallagher, L. T., 1998. Lower Cretaceous. *In*: P. R. Bown (Ed.), *Calcareous Nannofossil Biostratigraphy*, Kluwer Academic, 86-131.

Bown, P. R. and Concheyro, A., 2004. Lower Cretaceous calcareous nannoplankton from the Neuquén Basin, Argentina. *Marine Micropaleontology*, 52, 51-84.

Bralower, T. J., 1987. Valanginian to Aptian calcareous nannofossil stratigraphy and correlation with the upper M-sequence magnetic anomalies. *Marine Micropaleontology*, 11, 293-310.

Bralower, T. J., 1988. Calcareous nannofossil biostratigraphy and assemblages of the Cenomanian-Turonian boundary interval: implications for the origin and timing of oceanic anoxia. *Paleoceanography*, 3 (3), 275-316.

Bralower, T. J. & Thierstein, H. R., 1984. Low productivity and slow deep-water circulation in mid-Cretaceous oceans. *Geology*, 12, 614-618.

Bralower, T. J. & Thierstein, H. R., 1987. Organic carbon and metal accumulation in Holocene and mid-Cretaceous marine sediments: palaeoceangoraphic significance. *In*: J. Brooks & A. J. Fleet (Eds.), *Marine petroleum source rocks*. Special Publication of the Geological Society, 26, 345-370.

Bralower, T. J., Sliter, W. V., Arthur, M. A., Leckie, R. M., Allard, D. & Schlanger, S. O., 1993. Dysoxic/anoxic episodes in the Aptian-Albian (Early Cretaceous). *Geophysical Monograph*, 77, 5-37.

Bralower, T. J., Arthur, M. A., Leckie, R. M., Sliter, W. V., Allard, D. J. and Schlanger, S. O., 1994. Timing and palaeoceanography of oceanic dysoxia/anoxia in the late Barremian to early Aptian (Early Cretaceous), *Palaios*, 9, 335-369.

Bralower, T. J., Leckie, R. M., Sliter, W. V. and Thierstein, H. R., 1995. An integrated Cretaceous microfossil biostratigraphy. *In*: W. A. Berggren, D. V. Kent, M. -P. Aubry and J. Hardenbol (Eds.), *Geochronology Time Scales and Global Stratigraphic Correlation*, SEPM Special Publication No. 54, 65-79.

Bralower, T. J., Fullagar, P. D., Paull, C. K., Dwyer, G. S., and Leckie, R. M., 1997. Mid-Cretaceous strontium-isotope stratigraphy of deep-sea sections. *GSA Bulletin*, 109 (10), 1421-1442.

Bralower, T. J. and Bergen, J. A., 1998. Cenomanian-Santonian calcareous nannofossil biostratigraphy of a transect of cores drilled across the Western Interior Seaway. Stratigraphy and Paleoenvironments of the Cretaceous Western Interior Seaway, USA. *SEPM Concepts in Sedimentology and Paleontology* No. 6., 59-77.

Bralower, T. J., CoBabe, E., Clement, B., Sliter, W. V., Osburne, C. and Longoria, J., 1999. The record of global change in mid-Cretaceous, Barremian-Albian sections from the Sierra Madre, northeastern Mexico. *Journal of Foraminiferal Research*, 29, 418-437.

Bralower, T. J., Premoli Silva, I., and Malone, M. J. et al., 2002. *Proceedings of the ODP, Initial Reports*, 198 [CD-ROM]. Available from: Ocean Drilling Program, Texas A& M University, College Station, TX 77845-9547, USA.

Brand, L. E., 1994. Physiological ecology of marine coccolithophores. *In*: A. Winter & W. G. Siesser (Eds.), *Coccolithophores*, Cambridge University Press, 39-49.

Brass, G. W., Southam, J. R. & Peterson, W. H., 1982. Warm saline bottom water in the ancient ocean. *Nature*, 296, 620-623.

Brassell, S. C., Dumitrescu, M., the ODP Leg 198 Shipboard Scientific Party, 2004. Recognition of alkenones in a lower Aptian porcellanite from the west-central Pacific. *Organic Geochemistry*, 35, 181-188.

Bréherét, J. G., 1983. Sur des niveaux de black-shales dans l' Albien inférieur et moyen du domaine vocontien (Sud-Est de la France): étude de nannofaciès et signification des paléoenvironnements. *Bulletin du Museum National d'Histoire Naturelle*, 5C (4), 113-159.

Bréherét, J. G., Caron, M. & Delamette, M., 1986. Niveaux riches en matière organique dans l' Albien vocontien, quelques caractères du paléoenvironnement, essai d' interprétation génétique. *In*: J. G.

Bréherét (Ed.), *Les couches riches en matière organique et leurs conditions de depot.* Document du Bureau de Recherches Géologiques et Minieres, Orleans, 110, 114-191.

Bréherét, J. G., 1997. L'Aptien et l'Albien de la Fosse vocontienne (bordures au bassin): Évolution de la sédimentation et enseignements sur les événements anoxiques. *Publications de la Société Géologique du Nord*, 25, 614 pp.

Bukry, D., 1973. Low-latitude coccolith biostratigraphic zonation. *Initial Reports of the DSDP*, Vol. 15, 685-703.

Burnett, J. A., 1988. Northwest European Late Cretaceous calcareous nannofossils: biostratigraphy and selected evolutionary lineages. *Unpublished PhD thesis*, University College London.

Burnett, J. A., 1998. Upper Cretaceous. In: P. R. Bown (Ed.), *Calcareous Nannofossil Biostratigraphy*, Kluwer Academic, 132-199.

Burnett, J. A. and Whitham, F., 1999. Correlation between the nannofossil and macrofossil biostratigraphies and the lithostratigraphy of the Upper Cretaceous of NE England. *Proceedings of the Yorkshire Geological Society*, 52 (4), 371-381.

Burnett, J. A., Young, J. R. and Bown, P. R., 2000. Calcareous nannoplankton and global climate change. *In*: S. J. Culver and P. F. Rawson (Eds.), *Biotic response to global change: the last 145 million years.* The Natural History Museum, London/Cambridge University Press, Cambridge, 35-50.

Busson, G. & Noël, D., 1991. Les nannoconidés, indicateurs environnementaux des océans et mers épicontinentales du Jurassique terminal et du Crétacé inférieur. *Oceanologica Acta*, 14, 333-356.

Calvert, S. E., 1987. Oceanographic control on the accumulation of organic matter in marine sediments. *In*: J. Brooks & A. J. Fleet (Eds.), *Marine petroleum source rocks*, Special Publication of the Geological Society, 26, 137-152.

Casey, R., 1961. The stratigraphical palaeontology of the Lower Greensand. *Palaeontology*, 3, 487-621, pls. 77-84.

Cecca, F., 2002. Introduction. *In*: F. Cecca (Ed.), *Palaeobiogeography of Marine Fossil Invertebrates – Concepts and Methods.* Taylor & Francis, London, 1-11.

Cepek, P., 1981. Mesozoic calcareous nannoplankton stratigraphy of the central North Pacific (mid-Pacific Mountains and Hess Rise), DSDP Leg 62. *Initial Reports of the DSDP*, 62, 397-418.

Cepek, P. & Hay, W. W., 1969. Calcareous nannoplankton and biostratigraphic subdivision of the Upper Cretaceous. *Transactions of the Gulf Coast Association of Geological Societies*, 19, 323-336.

Cepek, P. & Hay W. W., 1970. Zonation of the Upper Cretaceous using calcareous nannoplankton. *Paläobotanik*, B, III/3-4, 333-340.

Coccioni, R., Erba, E. & Premoli Silva, I., 1992. Barremian-Aptian calcareous plankton biostratigraphy from the Gorgo Cerbara section (Marche, central Italy) and implications for plankton evolution. *Cretaceous Research*, 13, 517-537.

Covington, J. M., & Wise, S. W., 1987. Calcareous nannofossil biostratigraphy of a Lower Cretaceous deep-sea fan complex: DSDP Leg 93, Site 603, lower continental rise off Cape Hatteras. *Initial Reports of the DSDP*, 93, 617-660.

Crux, J. A., 1982.Upper Cretaceous (Cenomanian to Campanian) calcareous nannofossils. *In*: A. R. Lord (Ed.), *A Statigraphical Index of Calcareous Nannofossils*. British Micropalaeontological Society Series, Ellis Horwood, Chichester, 81-135.

Crux, J. A., 1989. Biostratigraphy and palaeogeographical applications of Lower Cretaceous nannofossils from north-western Europe. *In*: J. A. Crux and S. E. Van Heck (Eds.), *Nannofossils and their applications*. Ellis Horwood, Chichester, 143-211.

Crux, J. A. 1991. Albian calcareous nannofossils from the Gault Clay of Munday's Hill (Bedfordshire, England). *Journal of Micropalaeontology*, 10, 203-221.

Demaison, G. J. & Moore, G. T., 1980. Anoxic environments and oil source bed genesis. *AAPG Bulletin*, 64, 1179-1209.

Deres, F. & Achéritéguy, J., 1980. Biostratigraphie des Nannoconides. *Bulletin des Centres de Recherches Exploration-Production Elf-Aquitaine*, 4, 1-53.

Duncan, R. A. & Bralower, T. J., 2002. Environmental and biotic consequences of large igneous provinces. *In*: K. L. Bice et al., (Eds.), *Cretaceous Climate-Ocean Dynamics: Future Directions for IODP* [www.whoi.edu/ccod/CCOD_report.htm].

Erba, E., 1987. Mid-Cretaceous cyclic pelagic facies from the Umbria-Marche Basin: What do calcareous nannofossils suggest? *INA Newsletter*, 9, 52-53.

Erba, E., 1992a. Calcareous nannofossil distribution in pelagic rhythmic sediments (Aptian-Albian Piobbico core, Central Italy). *Rivista Italiana di Paleontologia e Stratigrafia*, 97 (3-4), 455-484.

Erba, E., 1992b. Middle Cretaceous calcareous nannofossils from the western Pacific (Leg 129): Evidence for paleoequatorial crossings. *In:* R. L. Larson, Y. Lancelot et al., *Proceedings of the ODP, Scientific Results*, 129, 189-201.

Erba, E., 1994. Nannofossils and superplumes: The early Aptian 'nannoconid crisis'. *Paleoceanography*, 9 (3), 483-501.

Erba, E., 2004. Calcareous nannofossils and Mesozoic oceanic anoxic events. *Marine Micropaleontology*, 52, 85-106.

Erba, E., Guasti, G. and Castradori, D., 1989. Calcareous nannofossils record fertility and temperature cycles: Evidence from the Albian Gault Clay Formation. *INA Newsletter*, 11, 57-58.

Erba, E. & Covington, J. M., 1992. Calcareous nannofossil biostratigraphy of Mesozoic sediments recovered from the western Pacific, Leg 129. *Proceedings of the ODP, Scientific Results*, 129, 179-187.

Erba, E., Castradori, D., Guasti, G. & Ripepe, M., 1992. Calcareous nannofossils and Milanktovitch cycles: the example of the Albian Gault Clay Formation (Southern England). *Palaeogeography, Palaeoclimatology, Palaeoecology*, 93, 47-69.

Erba, E. and Tremolada, F., 2004. Nannofossil carbonate fluxes during the Early Cretaceous: phytoplankton response to nutrification episodes, atmospheric CO_2, and anoxia. *Paleoceanography*, 19 (10.1029/2003PA000884).

Erbacher, J., Thurow, J. and Littke, R., 1996. Evolution patterns of radiolarian and organic matter variations: a new approach to identify sea-level changes in mid-Cretaceous pelagic environments. *Geology*, 24, 499-502.

Erbacher, J., Gerth, W., Schmiedl, G. & Hemleben, C., 1998. Benthic foraminiferal assemblages of late Aptian-early Albian black shale intervals in the Vocontian Basin, SE France, *Cretaceous Research*, 19, 805-826.

Erbacher, J., Hembleben, C., Huber, B. T. and Markey, M. 1999. Correlating environmental changes during Early Albian oceanic anoxic event 1B using benthic foraminiferal paleoecology. *Marine Micropaleontology*, 38, 7-28.

Erbacher, J., Huber, B. T., Norris, R. D. and Markey, M. 2001. Increased thermohaline stratification as a possible cause for an oceanic anoxic event in the Cretaceous period. *Nature*, 409, 325-327.

Eshet, Y. and Almogi-Labin, A. 1996. Calcareous nannofossils as paleoproductivity indicators in Upper Cretaceous organic-rich sequences in Israel. *Marine Micropaleontology*, 29, 37-61.

Fassell, M. L. & Bralower, T. J., 1999. Warm, equable mid-Cretaceous: Stable isotope evidence. *Geological Society of America*, Special Paper 332, 121-142.

Fisher, C. G. and Hay, W. W., 1999. Calcareous nannofossils as indicators of mid-Cretaceous paleofertility along an ocean front, U. S. Western Interior. *Geological Society of America*, Special Paper 332, 161-180.

Frakes, L. A., Francis, J. E. & Syktus, J. I., 1992. *Climate modes of the Phanerozoic*. Cambridge University Press, Cambridge, 274 pp.

Gale, A. S., 2000. The Cretaceous World. *In*: S. J. Culver and P. F. Rawson (Eds.), *Biotic response to global change: the last 145 million years.* The Natural History Museum, London/Cambridge University Press, Cambridge, 4-19.

Gale, A. S., Kennedy, W. J., Burnett, J. A., Caron, M. and Kidd, B. E., 1996. The Late Albian to Early Cenomanian succession at Mount Risou near Rosans (Drôme, SE France): an integrated study (ammonites, inoceramids, planktonic foraminifera, nannofossils, oxygen and carbon isotopes). *Cretaceous Research*, 17, 515-606.

Gale, A. S., Smith, A. B., Monks, N. E. A., Young, J. A., Howard, A., Wray, D. S. and Huggett, J. M., 2000. Marine biodiversity through the Late Cenomanian-Early Turonian: palaeoceanographic controls and sequence stratigraphic biases. *Journal of the Geological Society*, London, 157, 745-757.

Gale, A. S., Hardenbol, J., Hathway, B., Kennedy, W. J., Young, J. R., and Phansalkar, V., 2002. Global correlation of Cenomanian (Upper Cretaceous) sequences: Evidence for Milankovitch control on sea level. *Geology*, 30 (4), 291-294.

Govindan, A., 1972. Upper Cretaceous planktonic foraminifera from the Pondicherry area, south India. *Micropaleontology*, 18, 160-183.

Gradstein, F. M. & Ogg, J. G., 1996. Geological time scale for the Phanerozoic. *Episodes*, 19 (1/2), 3-5.

Gradstein, F. M., Ogg, J. G., Smith, A. G., Bleeker, W. & Lourens, L. J., 2004. A new Geologic Time Scale with special reference to Precambrian and Neogene. Episodes, 27 (2), 83-100.

Gröcke, D. R., Hesselbo, S. P. & Jenkyns, H. C., 1999. Carbon-isotope composition of Lower Cretaceous fossil wood: ocean-atmosphere chemistry and relation to sea-level change. *Geology*, 27(2), 155-158.

Gröcke, D. R., Kucera, M., Bown, P. R., Kanungo, S., MacDonald, E., Stoll, H., Lees, J. and Schmidt, D. N., 2002. Definition of the onset of OAE1b in the Proto-Atlantic. *In*: Organic-carbon burial, climate change and ocean chemistry (Mesozoic-Paleogene), *Conference Abstracts. Geological Society, London*, p. 16.

Habermann, A. and Mutterlose, J., 1999. Early Aptian black shales from NW Germany: Calcareous nannofossils and their palaeoceanographic implications. *Neues Jahrbruch für Geologie und Paläontologie Abhandlungen*, 212, 379-400.

Hancock, J. M., 1989. Sea-level changes in the British region during the Late Cretaceous. *Proceedings Geologists' Association*, 100 (4), 565-594.

Haq, B. U., Hardenbol, J. & Vail, P. R., 1987. Chronology of the fluctuating sea levels since the Triassic. *Science*, 235, 1156-1157.

Hart, M. B., Joshi, A. and Watkinson, M. P., 2001. Mid-Late Cretaceous stratigraphy of the Cauvery Basin and the development of the eastern Indian Ocean. *Journal Geological Society of India*, 58, 217-229.

Hay, W. W., 1977. Calcareous nannofossils. *In*: A. T. S. Ramsay (Ed.), *Oceanic Micropalaeontology 2*, Academic Press, London, 1055-1200.

Hay, W. W., DeConto, R. M., Wold, C. N., Wilson, K. M., Voigt, S., Schulz, M., Rossby Wold, A., Dullo, W. C., Ronov, A. B., Balukhovsky, A. N. & Söding, E., 1999. Alternative global Cretaceous palaeogeography. *In*: E. Barrera & C. C. Johnson (Eds.), *Evolution of the Cretaceous Ocean-Climate System. Geological Society of America*, Special Paper 332, 1-47.

Herrle, J. O., 2002. Paleoceanographic and paleoclimatic implications on mid-Cretaceous black shale formation in the Vocontian Basin and the Atlantic: evidence from calcareous nannofossils and stable isotopes. *Tübinger Mikropaläontologische Mitteilungen Nr. 27*, 1-115.

Herrle, J. O., 2003. Reconstructing nutricline dynamics of mid-Cretaceous oceans: evidence from calcareous nannofossils from the Niveau Paquier black shale (SE France). *Marine Micropaleontology*, 47, 307-321.

Herrle, J. O. and Mutterlose, J., 2003. Calcareous nannofossils from the Aptian-Lower Albian of southeast France: palaeoecological and biostratigraphic implications. *Cretaceous Research*, 24, 1-22.

Herrle, J. O., Pross, J., Friedrich, O. and Hemleben, C., 2003a. Short-term environmental changes in the Cretaceous Tethyan Ocean: micropaleontological evidence from the Early Albian Oceanic Anoxic Event 1b. *Terra Nova*, 15 (1), 14-19.

Herrle, J. O., Pross, J., Friedrich, O., Kößler, P. and Hemleben, C., 2003b. Forcing mechanisms for mid-Cretaceous black shale formation: evidence from the Upper Aptian and Lower Albian of the Vocontian Basin (SE France). *Palaeogeography, Palaeoclimatology, Palaeoecology*, 190, 399-426.

Hill, M. E., 1975. Selective dissolution of mid-Cretaceous (Cenomanian) calcareous nannofossils. *Micropaleontology*, 21, 227-235.

Hill, M. E., 1976. Lower Cretaceous calcareous nannofossils from Texas and Oklahoma. *Palaeontographica Abteilung B*, 156, 103-179.

Hochuli, P. A. et al., 1999. Episodes of high productivity and cooling in the early Aptian Alpine Tethys. *Geology*, 27, 657-660.

Holmes, M. A. and Watkins, D. K., 1992. Middle and Late Cretaceous history of the Indian Ocean. Synthesis of results from scientific drilling in the Indian Ocean, *Geophysical Monograph*, 70, 225-244.

Huber, B. T. & Watkins, D. K., 1992. Biogeography of Campanian-Maastrichtian calcareous plankton in the region of the Southern Ocean: paleogeographic and paleoclimatic implications. *The Antarctic paleoenvironment: a perspective on global change. Antarctic Research Series*, 56, 31-60.

Huber, B. T., Hodell, D. A. and Hamilton, C. P., 1995. Mid- to Late Cretaceous climate of the southern high latitudes: stable isotope evidence for minimal equator-to-pole thermal gradients. *Geological Society of America Bulletin*, Vol. 107, 1164-1191.

Hughes, N. F., 1975. Plant succession in the English Wealden strata. *Proceedings of the Geologists' Association*, 86 (4), 439-455.

Jafar, S. A., and Rai, J., 1989. Discovery of Albian nannoflora from type Dalmiapuram Formation, Cauvery Basin, India – paleoceanographic remarks. *Current Science*, 58 (7), 358-363.

Jahren, A. H., Arens, N. C., Sarmiento, G., Guerrero, J. & Amundson, R., 2001. Terrestrial record of methane hydrate dissociation in the Early Cretaceous. *Geology*, 29 (2), 159-162.

Jakubowksi, M., 1986. New calcareous nannofossil taxa from the Lower Cretaceous of the North Sea. *INA Newsletter*, 8, 38-42.

Jarvis, I., Carson, G. A., Cooper, M. K. E., Hart, M. B., Leary, P. N., Tocher, B. A., Horne, D. and Rosenfeld, A., 1988. Microfossil assemblages and the Cenomanian-Turonian (Late Cretaceous) Oceanic Anoxic Event. *Cretaceous Research*, 9, 3-103.

Jenkyns, H. C., 1995. Carbon-isotope stratigraphy and paleoceanographic significance of the Lower Cretaceous shallow-water carbonates of resolution Guyot, Mid-Pacific Mountains. *Proceedings of the ODP, Scientific Results*, 143, 99-104.

Jenkyns, H. C., 1999. Mesozoic anoxic events and palaeoclimate. Zentralblatt Geol. *Paläont. Teil*, 943-949.

Jenkyns, H. C., 2003. Evidence for rapid climate change in the Mesozoic-Palaeogene greenhouse world. *Philosophical Transactions of the Royal Society*, Series A 361, 1885-1916.

Jenkyns, H. C. & Wilson, P. A., 1999. Stratigraphy, paleoceanography, and evolution of Cretaceous Pacific Guyots: Relics from a Greenhouse Earth. *American Journal of Science*, 299 (5), 341-392.

Jeremiah, J., 1996. A proposed Albian to Lower Cenomanian nannofossil biozonation for England and the North Sea Basin. *Journal of Micropalaeontology*, 15, 97-129.

Jones, C. E. & Jenkyns, H. C., 2001. Seawater strontium isotopes, oceanic anoxic events, and seafloor hydrothermal activity in the Jurassic and Cretaceous. *American Journal of Science*, 301, 112-149.

Jukes-Browne, A. J. & Hill, W., 1900. The Cretaceous Rocks of Britain. 1. The Gault Clay and Upper Greensand of England. *Memoir of the Geological Survey of Great Britain*, 1-499.

Kale, A. S., and Phansalkar, V. G., 1992a. Calcareous nannofossils from the Utatur Group, Trichinopoly district, Tamil Nadu, India. *Journal of the Palaeontological Society of India*, 37, 85-102.

Kale, A. S., and Phansalkar, V. G., 1992b. Nannofossil biostratigraphy of the Utatur Group, Trichinopoly district, South India. *Memorie di Scienze Geologiche*, XLIII, 89-107.

Kale, A. S., Lotfalikani, A., and Phansalkar, V. G., 2000. Calcareous nannofossils from the Uttatur Group of Trichinopoly Cretaceous, South India. *Memoir Geological Society of India*, 46, 213-227.

Kelley, S. P., 2003. Volcanic inputs. *In*: P. Skelton (Ed.), *The Cretaceous World.* The Open University, Cambridge University Press, Cambridge, 209-248.

Kennedy, J., Gale, A. S., Bown, P. R., Caron, M., Davey, R., Gröcke, D. & Wray, D. S., 2000. Integrated stratigraphy across the Aptian-Albian boundary in the Marnes Bleues, at the Col de Pré-Guittard,

Aryanon (Drôme), and at Tartonne (Alpes-de- Haute-Provence), France: a candidate Global Boundary Stratotype Section and Boundary Point for the base of the Albian Stage. *Cretaceous Research,* 21, 591-720.

Knight, R. I., 1999. Phosphates and phosphogenesis in the Gault Clay (Albian) of the Anglo-Paris Basin. *Cretaceous Research*, 20, 507-521.

Kuhnt, W., Thurow, J., Wiedmann, J., and Herbin, J. P., 1986. Oceanic anoxic conditions around the Cenomanian/Turonian boundary and the response of the biota. *In*: E. T. Degens et al. (Eds.), *Biogeochemistry of black shales*. University of Hamburg, 205-246.

Lamolda, M. A., Gorostidi, A. and Paul, C. R. C., 1994. Quantitative estimates of calcareous nannofossil changes across the Plenus Marls (latest Cenomanian), Dover, England: implications for the generation of the Cenomanian-Turonian Boundary Event. *Cretaceous Research*, 15, 143-164.

Lamolda, M. A., Gorostidi, A., Martínez, R., López, G. and Peryt, D., 1997. Fossil occurrences in the Upper Cenomanian-Lower Turonian at Ganuza, northern Spain: an approach to Cenomanian/Turonian boundary chronostratigraphy. *Cretaceous Research*, 18, 331-353.

Larson, R. L., 1991a. Latest pulse of the Earth: evidence for a mid-Cretaceous superplume. *Geology*, 19, 547-550.

Larson, R. L., 1991b. Geological consequences of superplumes. *Geology*, 19, 963-966.

Larson, R. L., & Erba, E., 1999. Onset of the mid-Cretaceous greenhouse in the Barremian-Aptian: igneous events and the biological, sedimentary, and geochemical responses. *Paleoceanography*, 14, 663-678.

Leckie, R. M., Bralower, T. J., and Cashman, R., 2002. Oceanic anoxic events and plankton evolution: Biotic response to tectonic forcing during the mid-Cretaceous. *Paleoceanography*, 17 (3), 13-1–13-29.

Lees, J. A., 2002. Calcareous nannofossil biogeography illustrates palaeoclimate change in the Late Cretaceous Indian Ocean. *Cretaceous Research*, 23, 537-634.

Lees, J. A., Bown, P. R., Young, J. R. & Riding, J. B., 2004. Evidence for annual records of phytoplankton productivity in the Kimmeridge Clay Formation coccolith stone bands (Upper Jurassic, Dorset, UK). *Marine Micropaleontology*, 52, 29-49.

Lees, J. A. and Bown, P. R., *in press*. Upper Cretaceous calcareous nannofossil biostratigraphy, ODP Leg 198 (Shatsky Rise, northwest Pacific Ocean). *Proceedings of the ODP, Scientific Results*, 198.

Ludwig, J. A. and Reynolds, J. F., 1988. *Statistical Ecology: A Primer on Methods and Computing*, Wiley, New York, 337 pp.

Luciani, V. and Cobianchi, M., 1999. The Bonarelli Level and other black shales in the Cenomanian-Turonian of the northeastern Dolomites (Italy): calcareous nannofossil and foraminiferal data. *Cretaceous Research*, 20, 135-167.

Manivit, H., 1965. Nannofossiles calcaires de L' Albo-Aptien. *Revue de Micropaléontologie*, 8, 189-201.

Manivit, H., 1971. Nannofossiles calcaires du Crétacé francais (Aptien-Maestrichtien). Essai de Biozonation appuyée sur les stratotypes, thése doctoral, Université de Paris.

Manivit, H., Perch-Nielsen, K., Prins, B. and Verbeek, J. W., 1977. Mid Cretaceous calcareous nannofossil biostratigraphy. *Proceedings of the Koninklijke Nederlandse Akademie van Wetenschappen*, B80, 169-181.

Menegatti, A. P., Weissert, H., Brown, R., Tyson, R. V., Fairmond, P., Strasser, A., and Caron, M., 1998. High resolution $\delta^{13}C$-stratigraphy through the early Aptian 'Livello Sellii Equivalent' of the Alpine Tethys, *Paleoceanography*, 13, 530-545.

Murchey, B. L., & Jones, D. L., 1992. A mid-Permian chert event: widespread deposition of biogenic siliceous sediments in coastal, island arc and oceanic basins. *Palaeogeography, Palaeoclimatology, Palaeoecology*, 96, 161-174.

Mutterlose, J. 1989. Temperature-controlled migration of calcareous nannofloras in the north-western European Aptian. *In*: J. A. Crux and S. E. van Heck (Eds.), *Nannofossils and their Applications*, Ellis Horwood, Chichester, 122-144.

Mutterlose, J., 1991. Das Verteilungs-und Migrationmuster des kalkigen Nannoplanktons in der borealen Unterkreide (Valangin-Apt.) NW-Deutschlands. *Palaeontographica*, B221, 27-152.

Mutterlose, J., 1992a. Migration and evolution patterns of floras and faunas in marine Early Cretaceous sediments of NW Europe. *Palaeogeography, Palaeoclimatology, Palaeoecology*, 94, 261-282.

Mutterlose, J., 1992b. Biostratigraphy and palaeobiogeography of Early Cretaceous calcareous nannofossils. *Cretaceous Research*, 13, 167-189.

Mutterlose, J., 1996. The Hauterivian stage. *In*: P. F. Rawson, A. V. Dhondt, J. M. Hancock, W. J. Kennedy (Eds.), Proceedings of the Second International Symposium on Cretaceous Stage

Boundaries, *Bulletin de l'Institut Royal des Sciences Naturelles de Belgique, Sciences de la Terre Aardwetenschappen*, 66, 19-24 (supplement).

Mutterlose, J. and Ruffell, A., 1999. Milankovitch-scale palaeoclimate changes in pale-dark bedding rhythms from the Early Cretaceous (Hauterivian and Barremian) of eastern England and northern Germany. *Palaeogeography, Palaeoclimatology, Palaeoecology*, 154, 133-160.

Mutterlose, J. and Kessels, K., 2000. Early Cretaceous calcareous nannofossils from high latitudes: implications for palaeobiogeography and palaeoclimate. *Palaeogeography, Palaeoclimatology, Palaeoecology*, 160, 347-372.

Mutterlose, J., Bornemann, A., Luppold, F. W., Owen, H. G., Ruffell, A., Weiss, W. and Wray, D., 2003. The Vöhrum section (northwest Germany) and the Aptian/Albian boundary. *Cretaceous Research*, 24, 203-252.

Nagai et al., 2002. High-resolution analysis of calcareous nannofossils from OAE1 sequences exposed in SE France, 9th INA Conference, Parma 2002, Abstracts and Programme. *Journal of Nannoplankton Research*, 24 (2), p. 141.

Narayanan, V., 1977. Biozonation of the Uttatur Group, Trichinopoly, Cauvery Basin. *Journal of the Geological Society of India*, 18 (8), 415-428.

Norris, R. D., Kroon, D., Klaus, A., et al., 1998a. Site 1049. *Proceedings of the ODP, Initial Reports*, 171B, College Station, TX (Ocean Drilling Program), 47-91.

Norris, R. D., Kroon, D. and Klaus, A., et al. 1998b. Introduction. Proceedings of the ODP, Initial Reports, 171B, College Station, TX (Ocean Drilling Program), 5-10.

ODSN Plate Tectonic Reconstruction Service 2000. Based on Hay, W. W. et al., (1999). Location: www.odsn.de/odsn/services/paleomap/paleomap.html

Owen, H. G., 1971. Middle Albian stratigraphy in the Anglo-Paris Basin. *Bulletin of the British Museum (Natural History) Geology*, supplement 8, 1-164.

Owen, H. G., 1972. The Gault and its junction with the Woburn Sands in the Leighton Buzzard Area, Bedfordshire and Buckinghamshire. *Proceedings of the Geologists' Association*, 83 (3), 287-312.

Owen, H.G., 1975. The stratigraphy of the Gault and the Upper Greensand of the Weald. *Proceedings of the Geologists' Association*, 86 (4), 475-498.

Paul, C. R. C., Lamolda, M. A., Mitchell, S. F., Vaziri, M. R., Gorostidi, A. and Marshall, J. D., 1999. The Cenomanian-Turonian boundary at Eastbourne (Sussex, UK): a proposed European reference section. *Palaeogeography, Palaeoclimatology, Palaeoecology*, 150, 83-121.

Perch-Nielsen, K., 1979. Calcareous nannofossils from the Cretaceous between the North Sea and the Mediterranean. Aspekte der Kreide Europas, IUGS Series A, 6, 223-271.

Perch-Nielsen, K., 1983. Recognition of Cretaceous stage boundaries by means of calcareous nannofossils. *In*: *Symposium on Cretaceous stage boundaries*, Copenhagen, October 18-21, 1983, *Abstracts* (Eds. T. Birkelund, R. Bromley, W. K. Christensen, E. Håkansson and F. Surlyk), University of Copenhagen, 152-156.

Perch-Nielsen, K. 1985. Mesozoic calcareous nannofossils. *In*: H. M. Bolli, J. B. Saunders & K. Perch-Nielsen (Eds.), *Plankton Stratigraphy*. Cambridge University Press, Cambridge, 329-426.

Phansalkar, V. G. and Kale, A. S., 1989. Biostratigraphy of Albian-Turonian, Utatur Group from Trichinopoly District of South India. *In*: *Abstracts* (Vol. 2 of 3), *28th International Geological Congress*, Washington D. C., USA.

Poulsen, C. J., Seidov, D., Barron, E. J. and Peterson, W. H., 1998. The impact of palaeogeographic evolution on the surface oceanic circulation and the marine environment within the mid-Cretaceous Tethys. *Paleoceanography*, 13 (5), 546-559.

Poulsen, C. J., Barron, E. J., Johnson, C. C. and Fawcett, P. 1999. Links between major climatic factors and regional oceanic circulation in the mid-Cretaceous. *Geological Society of America*, Special Paper 332, 73-89.

Powell, C. McA., Roots, S. R. and Veevers, J. J., 1988. Pre-breakup continental extension in East Gondwanaland and the early opening of the eastern Indian Ocean. *Tectonophysics*, 155, 261-283.

Premoli Silva, I., Erba, E. & Tornaghi, M. E., 1989. Paleoenvironmental signals and changes in surface fertility in mid-Cretaceous C_{org}-rich pelagic facies of the Fucoid Marls (Central Italy). *Geobios*, Mémoire spécial no. 11, 225-236.

Premoli-Silva , I., Erba, E., Salvini, G., Locatelli, C. & Verga, D., 1999. Biotic changes in Cretaceous oceanic anoxic events of the Tethys. *Journal of Foraminiferal Research*, 29 (4), 352-370.

Price, F. G. H., 1874. On the Gault at Folkestone. Quarterly *Journal of the Geological Society of London*, 30, 342-366.

Price, F. G. H., 1875. On the Lower Greensand and Gault of Folkestone. *Proceedings of the Geologists' Association*, London, 4, 135-150.

Racki, G. & Cordey, F., 2000. Radiolarian palaeoecology and radiolarites: is the present the key to the past? *Earth Science Reviews*, 52, 83-120.

Rai, J., 2002. An overview of nannofossil records from India. *Journal of the Palaeontological Society of India*, 47, 1-7.

Robinson, S. A., Williams, T. & Bown, P. R., 2004. Fluctuations in biosiliceous production and the generation of Early Cretaceous oceanic anoxic events in the Pacific Ocean (Shatsky Rise, ODP Leg 198). Paleoceanography, 19 (4), PA402410.1029/2004PA001010.

Roth, P. H. 1978. Cretaceous nannoplankton biostratigraphy and oceanography of the northwestern Atlantic Ocean. *Initial reports of the DSDP*, 44, 731-760.

Roth, P. H., 1981. Mid-Cretaceous calcareous nannoplankton from the central Pacific: Implications for paleoceanography. *In*: J. Thiede, T. L. Vallier, et al., *Initial Reports of the DSDP*, 62, Washington (U. S. Govt. Printing Office), 471-489.

Roth, P. H., 1983. Jurassic and Lower Cretaceous calcareous nannofossils in the western North Atlantic (Site 534): biostratigraphy, preservation, and some observations on biogeography and palaeoceanography. *Initial Reports of the DSDP*, 76, Washington (U. S. Govt. Printing Office), 587-621.

Roth, P. H., 1986. Mesozoic palaeoceanography of the North Atlantic and Tethys Oceans. *In*: C. P. Summerhayes and N. J. Shackleton (Eds.), *North Atlantic Palaeoceanography*. Geological Society Special Publication No. 21, 299-320.

Roth, P. H., 1987. Mesozoic calcareous nannofossil evolution: relation to paleoceanographic events. *Paleoceanography*, 2, 601-611.

Roth, P. H., 1989. Ocean circulation and calcareous nannoplankton evolution during the Jurassic and Cretaceous. *Palaeogeography, Palaeoclimatology, Palaeoecology*, 74, 111-126.

Roth, P. H., 1994. Distribution of coccoliths in oceanic sediments. *In*: A. Winter and W. G. Siesser (Eds.), *Coccolithophores*, Cambridge University Press, Cambridge, 199-217.

Roth, P. H., and Berger, W. H., 1975. Distribution and dissolution of coccoliths in the South and Central Pacific. *In*: W. V. Sliter, A. W. H. Bé and W. H. Berger (Eds.), *Dissolution of Deep-Sea Carbonates*. Cushman Foundation of Foraminiferal Research, Special Publication No. 13, 87-113.

Roth, P. H., Mullin, M. M., and Berger, W. H., 1975. Coccolith sedimentation by fecal pellets: laboratory experiments and field observations. *Geological Society of America Bulletin*, 86, 1079-1084.

Roth, P. H. and Bowdler, J. L., 1981. Middle Cretaceous calcareous nannoplankton biogeography and oceanography of the Atlantic Ocean. *In*: J. E. Warme, R. G. Douglas, and E. L. Winterer (Eds.), *The Deep Sea Drilling Project: a decade of progress*. SEPM Special Publication No. 32, 517-546.

Roth, P. H. and Krumbach, K. R., 1986. Middle Cretaceous calcareous nannofossil biogeography and preservation in the Atlantic and Indian oceans: implications for palaeoceanography. *Marine Micropalaeontology*, 10, 235-266.

Rutledge, D. C., 1995. Calcareous nannofossils of the Boreal Lower Cretaceous: Applications in biostratigraphy and palaeoceanography. *Unpublished PhD thesis*, University College London.

Sastri, V. V., Raju, A. T. R., Sinha, R. N., Venkatachala, B. S. and Banerji, R. K., 1977. Biostratigraphy and evolution of the Cauvery Basin, India. *Journal of the Geological Society of India*, 18 (8), 355-377.

Sastri, V. V., Venkatachala, B. S. and Narayanan, V., 1981. The evolution of the east coast of India. *Palaeogeography, Palaeoclimatology, Palaeoecology*, 36, 23-54.

Sastry, M. V. A., Rao, B. R. J. and Mamgain, V. D., 1968. Biostratigraphic zonation of the Upper Cretaceous formations of the Trichinopoly district, south India. *Memoirs of the Geological Society of India*, 2, 10-17.

Savin, S. M., 1977. The history of the earth's surface temperature during the past 100 million years. *Annual Review of Earth and Planetary Sciences*, 5, 319-355.

Schlanger, S. O. & Jenkyns, H. C., 1976. Cretaceous anoxic events: causes and consequences. *Geologie en Mijnbouw*, 55, 179-184.

Schlanger, S. O., Jenkyns, H. C. & Premoli Silva, I., 1981. Volcanism and vertical tectonics in the Pacific basin related to global Cretaceous transgression. *Earth and Planetary Science Letters*, 52, 435-449.

Shafik, S., 1990. Late Cretaceous nannofossil biostratigraphy and biogeography of the Australian western margin. *Bureau of Mineral Resources, Geology and Geophysics*, Report 295, 1-164.

Shannon, C. E. and Weaver, W., 1949. *The Mathematical Theory of Communication*, University of Illinois Press, Champaign, IL.

Sinton, C. W. and Duncan, R. A., 1997. Potential links between ocean plateau volcanism and global ocean anoxia at the Cenomanian-Turonian boundary. *Economic Geology*, 92, 836-842.

Sissingh, W., 1977. Biostratigraphy of Cretaceous calcareous nannoplankton. *Geologie en Mijnbouw*, 56, 37-65.

Sliter, W. V., 1989. Aptian anoxia in the Pacific Basin. *Geology*, 17, 909-912.

Spath, L. F., 1923-43. A monograph of the Ammonoidea of the Gault. *Palaeontographical Society (Monograph) London*, Vol. 1 & 2, 1-787, pls. 1-72.

Stoll, H. M. & Schrag, D. P., 2001. Sr/Ca variations in Cretaceous carbonates: relation to productivity and sea-level changes. *Palaeogeography, Palaeoclimatology, Palaeoecology*, 168, 311-336.

Stover, L. E., 1966. Cretaceous coccoliths and associated nannofossils from France and the Netherlands. *Micropaleontology*, 12 (2), 133-167, pls. 1-9.

Stradner, H., 1963. New contributions to Mesozoic stratigraphy by means of nannofossils. *Proceedings of the Sixth World Petroleum Congress*, Section 1, Paper 4, 167-183.

Street, C., 1998. Palaeobiogeography of Early Cretaceous calcareous nannoplankton. *Unpublished PhD thesis*. University College London.

Street, C. and Bown, P.R., 2000. Palaeobiogeography of Early Cretaceous (Berriasian-Barremian) calcareous nannoplankton. *Marine Micropaleontology*, 39, 265-291.

Sundaram, R. and Rao, P. S., 1986. Lithostratigraphy of Cretaceous and Paleocene rocks of Tiruchirapalli district, Tamil Nadu, south India. *Records of the Geological Survey of India*, 116, 11-23.

Sundaram, R., Henderson, R. A., Ayyasami, K. and Stilwell, J. D., 2001. A lithostratigraphic revision and palaeoenvironmental assessment of the Cretaceous system exposed in the onshore Cauvery Basin, southern India. *Cretaceous Research*, 22, 743-762.

Taylor, R. J., 1978. The distribution of calcareous nannofossils in the Speeton Clay (Lower Cretaceous) of Yorkshire. *Proceedings of the Yorkshire Geological Society*, 42, 195-209.

Taylor, R. J., 1982. Lower Cretaceous (Ryazanian to Albian) calcareous nannofossils. *In*: A. R. Lord (Ed.), *A Statigraphical Index of Calcareous Nannofossils*. British Micropalaeontological Series, Ellis Horwood, Chichester, 40-80.

Tewari, A., Hart, M. B. and Watkinson, M. P., 1996a. A revised lithostratigraphic classification of the Cretaceous rocks of the Trichinopoly District, Cauvery Basin, Southeast India. *Contributions XV Indian Colloquium of Micropalaeontology and Stratigraphy*, Dehra Dun (Eds. J. Pandey, R. J. Azmi, A. Bhandari and A. Dave), 789-800.

Tewari, A., Hart, M. B. and Watkinson, M. P., 1996b. Foraminiferal recovery after the mid-Cretaceous oceanic anoxic events (OAEs) in the Cauvery Basin, southeast India. *In*: M. B. Hart (Ed.), *Biotic Recovery from Mass Extinction Events*. Geological Society Special Publication No. 102, 237-244.

Thierstein, H. R., 1971. Tentative Lower Cretaceous calcareous nannoplankton zonation. *Eclogae Geologicae Helvetiae*, 64 (3), 459-488.

Thierstein, H. R., 1973. Lower Cretaceous calcareous nannoplankton biostratigraphy. *Abhandlungen der Geologischen Bundesanstalt*, 29, 1-52.

Thierstein, H. R., 1974. Calcareous Nannoplankton – Leg 26, Deep Sea Drilling Project. *Initial Reports of the DSDP*, 26, Washington (U. S. Govt. Printing Office), 619-667.

Thierstein, H. R., 1976. Mesozoic calcareous nannoplankton biostratigraphy of marine sediments. *Marine Micropaleontology*, 1, 325-362.

Thierstein, H. R., 1980. Selective dissolution of Late Cretaceous and earliest Tertiary calcareous nannofossils: experimental evidence. *Cretaceous Research*, 2, 165-176.

Thierstein, H. R., 1981. Late Cretaceous nannoplankton and the change at the Cretaceous-Tertiary boundary. *In*: J. E. Warme, R. G. Douglas & E. L. Winterer (Eds.), *The Deep Sea Drilling Project: a decade of progress*. SEPM Special Publication No. 32, 355-394.

Thomsen, E., 1989. Seasonal variation in Boreal Early Cretaceous calcareous nannofossils. *Marine Micropaleontology*, 15, 123-152.

Tremaloda, F., 2002. Aptian to Campanian calcareous nannofossil biostratigraphy from the Bottaccione section, Gubbio, Central Italy. *Rivista Italiana di Paleontologia e Stratigrafia*, 108 (3), 441-456.

Tremaloda, F. and Erba, E., 2002. Morphometric analyses of Aptian *Assipetra infracretacea* and *Rucinolithus terebrodentarius* nannoliths: implications for taxonomy, biostratigraphy and paleoceanography. *Marine Micropaleontology*, 44, 77-92.

Tyson, R. V. and Funnel, B. M., 1987. European Cretaceous shorelines, stage by stage. *Palaeogeography, Palaeoclimatology, Palaeoecology*, 59, 69-91.

Veevers, J. J., Powell, C. McA. and Roots, D., 1991. Review of the seafloor spreading around Australia, 1. Synthesis of the pattern of spreading. *Australian Journal of Earth Sciences*, 38, 373-389.

Venkatachalapathy, R. and Ragothaman, V., 1995a. Palaeo-ecology of mid-Cretaceous foraminifera in the Cauvery Basin, east coast of India. *Journal of the Palaeontological Society of India*, 40, 9-20.

Venkatachalapathy, R. and Ragothaman, V., 1995b. A foraminiferal zonal scheme for the mid-Cretaceous sediments of the Cauvery Basin, India. *Cretaceous Research*, 16, 415-433.

Verbeek, J. W., 1977. Calcareous nannoplankton biostratigraphy of Middle and Upper Cretaceous deposits in Tunisia, southern Spain and France. *Utrecht Micropaleontological Bulletins*, 16, 1-157.

Verbeek, J. W. and Wonders, A. A. H., 1977. The position of the Cenomanian and Turonian stratotypes in planktonic biostratigraphy. *Proceedings of the Koninklijke Nederlandse Akademie van Wetenschappen*, B80, 16-19.

Watkins, D. K., 1986. Calcareous nannofossil paleoceanography of the Cretaceous Greenhorn Sea. *Geological Society of America Bulletin*, 97, 1239-1249.

Watkins, D. K., 1989. Nannoplankton productivity fluctuations and rhythmically-bedded pelagic carbonates of the Greenhorn Limestone (Upper Cretaceous). *Palaeogeography, Palaeoclimatology, Palaeoecology*, 74, 75-86.

Watkins, D. K., Wise, S. W., Pospichal, J. J. and Crux, J., 1996. Upper Cretaceous calcareous nannofossil biostratigraphy and paleoceanography of the Southern Ocean. *In*: A. Moguilevsky and R. Whatley (Eds.), University of Wales, Aberystwyth Press, 355-381.

Wei, W., 1988. A new technique for preparing quantitative nannofossil slides. *Journal of Palaeontology*, 62 (3), 472-473.

Weissert, H., 1989. C-isotope stratigraphy, a monitor of palaeoenvironmental change: a case study from the early Cretaceous. *Surveys in Geophysics*, 10, 1-61.

Weissert, H., Lini, A., Föllmi, K. B. and Kuhn, O., 1998. Correlation of Early Cretaceous carbon isotope stratigraphy and platform drowning events: a possible link? *Palaeogeography, Palaeoclimatology, Palaeoecology*, 137, 189-203.

Wignall, P. B., 1991. Model for trangressive black shales ? *Geology*, 19, 167-170.

Wignall, P. B. (Ed.), 1994. *Black Shales*. Clarendon Press, Oxford, 1-125.

Wignall, P. B., 2001. Large igneous provinces and mass extinctions. *Earth Science Reviews*, 53,1-33.

Williams, J. R., and Bralower, T. J., 1995. Nannofossil assemblages, fine fraction stable isotopes, and the paleoceanography of the Valanginian-Barremian (Early Cretaceous) North Sea Basin. *Paleoceanography*, 10 (4), 815-839.

Wilson, P. A. & Norris, R. D. 2001. Warm tropical ocean surface and global anoxia during the mid-Cretaceous period. *Nature*, 412, 425-429.

Wind, F. H., 1979. Maestrichtian-Campanian nannofloral provinces of the southern Atlantic and Indian Oceans. *In*: M. Talwani, W. W. Hay & W. B. F. Ryan (Eds.), *Deep drilling results in the Atlantic Ocean: Continental Margins and Palaeoenvironment*, Maurice Ewing Series 3, American Geophysical Union, Washington DC, 123-137.

Wind, F. H. and Cepek, P., 1979. Lower Cretaceous calcareous nannoplankton from DSDP Hole 397A (northwest African Margin). *Initial Reports of the DSDP*, 47A, Washington (U. S. Govt. Printing Office), 221-235.

Windley, D. E., 1995. Calcareous nannofossil applications in the study of cyclic sediments of the Cenomanian. *Unpublished PhD thesis*, University College London.

Winter, A. & Siesser, W. G. (Eds.), 1994. *Coccolithophores*. Cambridge University Press, Cambridge, 1-242.

Winter, A., Jordan, R. W. and Roth, P. H., 1994. Biogeography of living coccolithophores in ocean waters. *In*: A. Winter & W. G. Siesser (Eds.), *Coccolithophores*. Cambridge University Press, Cambridge, 161-177.

Winterer, E. L., Ewing, J. I., et al., 1973. *Initial Reports of the DSDP*, 17, Washington (U. S. Govt. Printing Office), 17-47.

Wise, S. W., 1983. Mesozoic and Cenozoic calcareous nannofossils recovered by DSDP Leg 71 in the Falkland Plateau region, Southwest Atlantic Ocean. *Initial Reports of the DSDP*, 71, Washington (U. S. Govt. Printing Office), 481-550.

Wise, S. R., 1988. Mesozoic-Cenozoic history of calcareous nannofossils in the region of the Southern Ocean. *Palaeogeography, Palaeoclimatology, Palaeoecology*, 67, 157-179.

Wise, S. W. and Wind, F. H., 1977. Mesozoic and Cenozoic calcareous nannofossils recovered by DSDP Leg 36 drilling on the Falkland Plateau, southwest Atlantic sector of the Southern Ocean. *Initial reports of the DSDP*, 36, Washington (U. S. Govt. Printing Office), 269-491.

Wise, S. W., Jr., Schlich, R., et al., 1992. Upper Cretaceous Nannofossils from Leg 120, Kerguelen Plateau, Southern Ocean. *Proceedings of the ODP, Scientific Results*, 120, College Station TX (Ocean Drilling Program), 343-370.

Worsley, T. R., 1971. Calcareous nannofossil zonation of Upper Jurassic and Lower Cretaceous sediments from the Western Atlantic. *In*: A. Farinacci (Ed.), Proceedings of the Second Planktonic Conference Roma, 1970. *Edizioni Tecnoscienza*, Rome, 2, 1301-1321.

Young, J. R., et al. 1997. Guidelines for coccolith and calcareous nannofossil terminology. *Palaeontology*, 40, 875-912.

Appendix 1

Chapter 4: Cauvery Basin, SE India; Chapter 8: Palaeobiogeography

The raw nannofossil data for biostratigraphy and palaeobiogeography are presented in Charts 1-8. Symbols used in the range charts are explained in Chapter 3.The chart captions are as follows:

Chart 1: Range chart for Karai Formation, Section 1 (attached in the back-pocket).

Chart 2: Range chart for Karai Formation, Section 2.

Chart 3: Presence/absence based distribution of taxa at the mid-Albian *T. orionatus* datum-level.

Chart 4: Presence/absence based distribution of taxa at the Late Albian *E. turriseiffelii* datum-level.

Chart 5: Presence/absence based distribution of taxa at the Early Cenomanian *C. kennedyi/W. britannica* datum-level.

Chart 6: Relative abundance data at the *T. orionatus* datum-level.

Chart 7: Relative abundance data at the *E. turriseiffelii* datum-level.

Chart 8: Relative abundance data at the *C. kennedyi/W. britannica* datum-level.

Karai Fm., Section 2 (at Garudamangalam)

SAMPLE (m)	PRESERVATION	ABUNDANCE	TAXON
GA 817	P	F	
GA 816	M-P	M	
GA 815	P	F	
GA 814	MISSING		
GA 813	P	F	
GA 812	M	M	
GA 811.3	G-M	M	
GA 811.2	G-M	M	
GA 811.1	M-G	L	
GA 811	M	M	
GA 810	G-M	M	
GA 89	BARREN		
GA 88	P	L	
GA 87	M-P	L	
GA 86	P	F	
GA 85	M-P	F	
GA 84	P	L	
GA 83	BARREN		
GA 82	BARREN		
GA 81	BARREN		
GAS 5	M-P	M	
GAS 4	G-M	H	
GAS 3	M-P	H	
GAS 2	M-P	H	
GAS 1	M	M	
GA 68	M-P	L	
GA 67	M	M	
GA 66	M	M	
GA 65	M	M	
GA 64	G-M	H	
GA 63	G-M	M	
GA 62	M	M	
GA 61	G-M	M	
GR 17	M	M	
GR 16	M-G	H	
GR15	M-P	M	
GR 14	M	M	
GR 13	M-P	M	
GR 12	M	M	
GR 11	M-P	M	
GR 10	M	M	
GR 9	M	M	
GR 8	M-G	H	
GR 7	M	M	
GR 6			
GR 5	M	M	
GR 4	M-P	H	
GR 3	M	M	
GR 2	G	M	
GR 1	G	M	
GM 17	M-P	L	
GM 16	M	M	
GM 15	M	L	
GM 14	M-G	M	
GM 13	M	M	
GM 12	M	L	
GM 11	M	M	
GM 10	M	M	
GM 9	M-G	M	
GM 8	M-G	M	
GM 7	M-G	M	
GM 6	M	M	
GM 5	M-G	L	
GM 4	M	M	
GM 3	M	H	
GM 2	M	M	
GM 1	M-G	M	

CHART 2

SAMPLE (m)	STAGE (NANNOFOSSIL BASED)	NANNOFOSSIL ZONE (Roth, 1978; Bralower et al.,1993, 1995)	NANNOFOSSIL ZONE (Burnett, 1998)	NANNOFOSSIL ZONE (Sissingh, 1977;Perch Nielsen, 1985)	NANNOFOSSIL EVENT
GM 1					E. turriseiffelii, G. praeobliquum, C. ehrenbergii present
GM 2			BC 27a	CC 9a	
GM 3					LO H. albiensis
GM 4					
GM 5					
GM 6					
GM 7					FO G. segmentatum (small), very rare
GM 8					FO G. theta
GM 9					
GM 10					
GM 11					
GM 12					
GM 13					
GM 14					
GM 15					
GM 16					FO G. chiastia
GM 17					
GR 1					LO G. chiastia; FO Gart. cf. G. nanum
GR 2	ALBIAN				LO W. britannica
GR 3	UPPER	NC 10A	BC 27b-c	CC 9b	LO G. theta
GR 4					G. segmentatum (regular size), consistent
GR 5					
GR 6					
GR 7					LO B. stenostaurion
GR 8					
GR 9					
GR 10					FO B. enormis
GR 11					
GR 12					
GR 13					
GR 14					
GR15					FO C. kennedyi
GR 16					
GR 17	CENOMANIAN				FO's P. cretacea, L. pseudoquadratus
GA 61	LOWER	NC 10B	UC 1-2	CC 9c	LO C. erodium
GA 62					
GA 63					LO S. glaber; Z. xenotus; FO M. decoratus
GA 64					FO L. acutus
GA 65					
GA 66			UC 2a-b		
GA 67					LO C. fiani
GA 68	CENOMANIAN				LO's Gart. cf. G. nanum, S. gausorhethium
GAS 1	UPPER				
GAS 2	MIDDLE-				
GAS 3			UC 3c-d		
GAS 4					
GAS 5		NC 11			LO C. kennedyi, G. stradneri
GA 81					
GA 82					
GA 83					
GA 84					
GA 85					FO Ahm. cf. A. octoradiata
GA 86					
GA 87			UC 3e-4	CC10	
GA 88					LO A. albianus
GA 89					
GA 810					Z. xenotus possibly reworked
GA 811		NC 12			
GA 811.1					LO R. asper
GA 811.2	hiatus				LO's H. chiastia, L. acutus
GA 811.3	hiatus				
GA 812					
GA 813	TURONIAN	(inferred)	(inferred)		
GA 814	LOWER	NC 13	UC 6a		
GA 815					
GA 816					Z. xenotus possibly reworked
GA 817					No Turonian markers

Taxa (rows of the occurrence chart):

Prediscosphaera columnata (large)
Prediscosphaera cretacea
Prediscosphaera cf. P. ponticula
Prediscosphaera spinosa
Prediscosphaera spinosa (small)
Radiolithus cf. R. planus
Radiolithus planus
Repagulum parvidentatum
Retecapsa cf. R. angustiforata
Retecapsa crenulata
Retecapsa surirella
Rhagodiscus achlyostaurion
Rhagodiscus cf. R. achlyostaurion
Rhagodiscus angustus
Rhagodiscus asper
Rhagodiscus asper (large)
Rhagodiscus gallagheri
Rhagodiscus hamptonii
Rhagodiscus infinitus
Rhagodiscus reniformis
Rhagodiscus splendens
Rotelapillus crenulatus
Seribiscutum primitivum
Sollasites horticus
Staurolithites gausorhethium
Staurolithites glaber
Staurolithites laffittei
Staurolithites mutterlosei
Staurolithites rotatus
Staurolithites laffittei s. l.
Staurolithites sp. 1 (bicyclic)
Stoverius achylosus
Tegumentum stradneri
Tetrapodorhabdus decorus
Tranolithus gabalus
Tranolithus minimus
Tranolithus orionatus
Tranolithus simplex
Tubodiscus burnettiae
Watznaueria barnesiae
Watznaueria biporta
Watznaueria britannica
Watznaueria fossacincta
Watznaueria manivitiae s. l.
Watznaueria ovata
Zeugrhabdotus bicrescenticus
Zeugrhabdotus diplogrammus
Zeugrhabdotus embergeri
Zeugrhabdotus cf. Z. embergeri (small)
Zeugrhabdotus howei
Zeugrhabdotus cf. Z. howei
Zeugrhabdotus kerguelenensis
Zeugrhabdotus noeliae
Zeugrhabdotus streetiae
Zeugrhabdotus xenotus

FO *T. orionatus* datum-level, Middle Albian

Site location with sample details	*Axopodorhabdus dietzmannii*	*Biscutum constans*	*Braarudosphaera africana*	*Braloweria boletiformis*	*Broinsonia galloisii*	*Bukrylithus ambiguus*	*Chiastozygus litterarius*	*Chiastozygus platyrhethus*	*Corollithion ? madagaskarensis*	*Corollithion protosignum*	*Corollithion signum*	*Cretarhabdus conicus*	*Cretarhabdus striatus*	*Crucibiscutum hayi*	*Cyclagelosphaera margerelii*	*Cyclagelosphaera rotaclypeata*	*Cylindralithus nudus*	*Discorhabdus ignotus*	*Eiffellithus ? hancockii*	*Eprolithus floralis*	*Flabellites oblongus*	*Gaarderella granulifera*	*Grantarhabdus coronadventis*	*Haqius circumradiatus*	*Hayesites albiensis*	*Hayesites irregularis*	*Helenea chiastia*	*Helicolithus compactus*	*Helicolithus trabeculatus*	*Hemipodorhabdus* cf. *H. gorkae*	*Laguncula dorotheae*	*Lapideacassis marlae*	*Lithraphidites carniolensis*	*Loxolithus armilla*	*Manivitella pemmatoidea*	*Manivitella fibrosa*	*Nannoconus* spp.	*Octocyclus reinhardtii*	*Percivalia fenestrata*	*Percivalia ? howardii*	*Pickelhaube furtiva*	*Placozygus* cf. *P.fibuliformis*	*Prediscosphaera columnata* (circular)	*Prediscosphaera* cf. *P. spinosa* (small)	*Radiolithus planus*	*Radiolithus* cf. *R. planus*	*Repagulum parvidentatum*
Cauvery Basin, SE India, KA 22.5	P	P			P	P	P	P	P	P	P	P	P	P	P	P		P		P	P		P	P	P		P	P	P	P	P	P	P	P	P		P	P	P	P	P	P	P	P
Col de Palluel, SE France, PG 29	P	P	P		P	P	P	P			P	P	P	P	P	P	P	P	P	P	P	P	P	P	P		P	P	P	P	P	P	P	P	P	P	P	P	P	P	P	P	P	P
Selborne, S. England, Sel2 45.5	P	P		P	P	P	P	P		P		P	P		P			P		P			P	P	P			P		P		P	P	P	P		P	P	P	P	P	P	P	P
Shatsky Rise, Pacific, ODP Leg 198, Hole 1213A, 20R	P	P			P	P	P	P	P		P	P	P		P	P	P	P	P	P	P		P	P		P	P	P			P	P	P				P	P	P	P	P	P		
Shatsky Rise, Pacific, ODP Leg 198, Hole 1214A, 9R		P				P	P	P	P	P	P	P	P		P		P	P	P	P	P		P	P		P	P	P			P	P	P	P			P	P		P				
1 site			x	x										x								x																								
2 sites																										x			x		x															
3 sites									x	x						x	x		x						x							x					x	x	x	x	x			x	x
4 sites	x				x						x				x						x					x									x										
5 sites		x				x	x	x				x	x					x		x			x	x			x		x				x	x	x					x	x		x			
Key: P=Present																																														
CHART 3																																														

Species	Cauvery Basin, KA 22.5	Col de Palluel, PG 29	Selborne, Sel2 45.5	Shatsky Rise, ODP Site 1213A, 20R	Shatsky Rise, ODP Site 1214A, 9R	1 site	2 sites	3 sites	4 sites	5 sites
Retecapsa crenulata	P	P	P	P	P					x
Retecapsa surirella	P	P	P	P	P					x
Rhagodiscus achlyostaurion	P	P	P	P	P					x
Rhagodiscus angustus	P	P	P	P	P					x
Rhagodiscus asper	P	P	P	P	P					x
Rhagodiscus gallagheri	P	P	P					x		
Rhagodiscus hamptonii	P	P	P					x		
Rhagodiscus splendens	P	P	P					x		
Rotelapillus laffittei	P	P	P	P	P					x
Seribiscutum primitivum	P	P	P					x		
Sollasites falklandensis	P					x				
Staurolithites gausorhethium	P	P	P	P	P					x
Staurolithites glaber	P	P	P					x		
Staurolithites mutterlosei	P	P		P	P				x	
Staurolithites siesseri		P		P	P				x	
Staurolithites spp.	P	P	P	P	P					x
Stoverius achylosus	P	P	P	P	P					x
Tegumentum stradneri (small/large)	P	P	P	P	P					x
Tetrapodorhabdus decorus	P	P	P	P	P					x
Tranolithus gabalus	P	P		P	P				x	
Tranolithus orionatus	P	P	P	P	P					x
Tranolithus simplex	P	P	P	P					x	
Tubodiscus burnettiae	P	P	P	P	P					x
Watznaueria barnesiae	P	P	P	P	P					x
Watznaueria biporta	P	P	P	P	P					x
Watznaueria fossacincta	P	P	P	P	P					x
Watznaueria manivitiae	P	P	P	P	P					x
Watznaueria ovata	P	P	P	P	P					x
Zeugrhabdotus diplogrammus	P	P	P	P	P					x
Zeugrhabdotus embergeri	P	P		P	P				x	
Zeugrhabdotus cf. *Z. embergeri* (small)	P	P		P	P				x	
Zeugrhabdotus howei	P	P	P	P	P					x
Zeugrhabdotus noeliae (small)	P	P	P	P	P					x
Zeugrhbdotus streetiae	P	P					x			
Zeugrhabdotus xenotus	P	P	P	P	P					x
TOTAL	74	77	56	59	55	4	10	14	14	40

Site location with sample details

FO *E. turriseiffelii* datum-level, Upper Albian

Site location with sample details	*Axopodorhabdus albianus*	*Axopodorhabdus dietzmannii*	*Biscutum constans*	*Braarudosphaera africana*	*Broinsonia galloisii*	*Bukrylithus ambiguus*	*Calciosolenia fossilis*	*Ceratolithina hamata*	*Chiastozygus litterarius*	*Chiastozygus platyrhethus*	*Chiastozygus spissus*	*Chiastozygus* spp. (small)
Cauvery Basin, SE India, KA 184.5	P	P	P		P	P	P		P	P	P	P
Col de Palluel, SE France, ColP59	P	P	P	P	P	P	P		P	P	P	P
Selborne, S. England, Sel1 54	P	P	P			P	P	P	P	P		P
Shatsky Rise, Pacific, ODP Leg 198, Hole 1213A,19R	P	P	P		P	P	P		P	P	P	
Shatsky Rise, Pacific, ODP Leg 198, Hole 1214A,8R	P	P	P		P	P			P	P	P	
1 site				x				x				
2 sites												
3 sites												x
4 sites					x		x				x	
5 sites	x	x	x			x			x	x		
Key: P=Present												
CHART 4												

Site location with sample details	*Corollithion ? madagaskarensis*	*Corollithion protosignum*	*Corollithion signum*	*Cretarhabdus conicus*	*Cretarhabdus multicavus*	*Cretarhabdus striatus*	*Cribrosphaerella ehrenbergii*	*Crucibiscutum hayi*	*Cyclagelosphaera margerelii*	*Cyclagelosphaera rotaclypeata*	*Cylindralithus nudus*	*Discorhabdus ignotus*
Cauvery Basin, SE India, KA 184.5	P		P	P		P	P	P	P		P	P
Col de Palluel, SE France, ColP59	P	P	P	P	P	P	P		P	P	P	P
Selborne, S. England, Sel1 54				P	P	P	P	?		P		P
Shatsky Rise, Pacific, ODP Leg 198, Hole 1213A,19R	P	P	P	P	P	P	P		P	P	P	P
Shatsky Rise, Pacific, ODP Leg 198, Hole 1214A,8R	P	P	P	P	P	P			P		P	P
1 site								x				
2 sites												
3 sites		x								x		
4 sites	x		x		x		x		x		x	
5 sites				x		x						x
Key: P=Present												
CHART 4												

Site location with sample details	*Eiffellithus ? hancockii*	*Eiffellithus monechiae*	*Eiffellithus turriseiffelii*	*Eprolithus floralis*	*Flabellites oblongus*	*Grantarhabdus coronadventis*	*Haqius circumradiatus*	*Hayesites albiensis*	*Hayesites irregularis*	*Helenea chiastia*	*Helicolithus compactus*	*Helicolithus trabeculatus*
Cauvery Basin, SE India, KA 184.5		P	P	P	P	P	P	P		P	P	P
Col de Palluel, SE France, ColP59	P	P	P	P	P	P	P	P		P	P	P
Selborne, S. England, Sel1 54		P	P	P		P	P	P		P	P	
Shatsky Rise, Pacific, ODP Leg 198, Hole 1213A,19R	P	P	P	P	P	P	P		P	P	P	
Shatsky Rise, Pacific, ODP Leg 198, Hole 1214A,8R	P	P	P	P	P	P	P		P	P	P	
1 site												
2 sites									x			x
3 sites	x							x				
4 sites					x							
5 sites		x	x	x		x	x			x	x	
Key: P=Present												
CHART 4												

Site location with sample details	*Hemipodorhabdus* cf. *H. gorkae*	*Laguncula dorotheae*	*Lapideacassis mariae*	*Lithraphidites carniolensis*	*Loxolithus armilla*	*Manivitella pemmatoidea*	*Manivitella fibrosa*	*Nannoconus* spp.	*Octocyclus reinhardtii*	*Owenia hillii*	*Placozygus* cf. *P.fibuliformis*
Cauvery Basin, SE India, KA 184.5	P	P	P	P	P	P	P		P		P
Col de Palluel, SE France, ColP59	P			P	P	P	P	P		P	P
Selborne, S. England, Sel1 54				P	P	P			P	P	P
Shatsky Rise, Pacific, ODP Leg 198, Hole 1213A,19R	P		P	P	P	P					P
Shatsky Rise, Pacific, ODP Leg 198, Hole 1214A,8R	P			P	P	P	P	P			P
1 site		x									
2 sites			x					x	x	x	
3 sites							x				
4 sites	x										
5 sites				x	x	x					x
Key: P=Present											
CHART 4											

Site location with sample details	Cauvery Basin, KA 184.5	Col de Palluel, ColP59	Selborne, Sel1 54	Shatsky Rise, ODP Site 1213A,19R	Shatsky Rise, ODP Site 1214A,8R	1 site	2 sites	3 sites	4 sites	5 sites
TOTAL	74	76	60	67	65	4	8	12	19	42
Prediscosphaera columnata (circular)	P	P	P	P	P					x
Prediscosphaera spinosa	P	P	P	P	P					x
Radiolithus planus	P	P	P	P	P					x
Radiolithus cf. *R. planus*	P	P	P					x		
Repagulum parvidentatum	P	P	P					x		
Retecapsa spp.				P	P		x			
Retecapsa crenulata	P	P	P	P	P					x
Retecapsa surirella	P	P	P	P	P					x
Rhagodiscus achlyostaurion	P	P	P	P	P					x
Rhagodiscus angustus	P	P	P	P	P					x
Rhagodiscus asper	P	P	P	P	P					x
Rhagodiscus hamptonii	P	P	P					x		
Rhagodiscus splendens	P	P	P					x		
Rotelapillus laffittei	P	P	P	P	P					x
Seribiscutum primitivum	P	P	P					x		
Staurolithites gausorhethium	P	P	P		P				x	
Staurolithites glaber	P	P	P	P					x	
Staurolithites mutterlosei	P	P		P	P				x	
Staurolithites spp.	P	P	P	P	P					x
Tegumentum stradneri (small/large)	P	P	P	P	P					x
Tetrapodorhabdus decorus	P		P	P	P				x	
Tranolithus gabalus	P	P		P	P				x	
Tranolithus orionatus	P	P	P	P	P					x
Tranolithus simplex	P	P	P	P	P					x
Tubodiscus burnettiae	P	P		P	P				x	
Watznaueria barnesiae	P	P	P	P	P					x
Watznaueria biporta	P	P	P	P	P					x
Watznaueria britannica	P	P		P	P				x	
Watznaueria fossacincta	P	P	P	P	P					x
Watznaueria manivitiae	P	P	P	P	P					x
Watznaueria ovata	P	P	P	P	P					x
Zeugrhabdotus diplogrammus	P	P	P	P	P					x
Zeugrhabdotus embergeri	P	P		P	P				x	
Zeugrhabdotus cf. *Z. embergeri* (small)		P		P	P			x		
Zeugrhabdotus howei	P	P	P	P	P					x
Zeugrhabdotus noeliae	P	P	P	P	P					x
Zeugrhbdotus streetiae	P		P				x			
Zeugrhabdotus xenotus	P	P	P	P	P					x

FO *C. kennedyi* /LO *W.britannica* datum-level, Lower Cenomanian

Site location with sample details	Cauvery Basin, SE India, KA 301	Mount Risou, SE France, Risou +20	Warren, Kent, S. England, Warren 7	Shatsky Rise, Pacific, ODP Leg 198, Hole 1207B, 26R	Shatsky Rise, Pacific, ODP Leg 198, Hole 1213A, 18R	1 site	2 sites	3 sites	4 sites	5 sites
Amphizygus brooksii	P	P	P					x		
Axopodorhabdus albianus	P	P	P	P	P					x
Axopodorhabdus dietzmannii	P		P	P	P				x	
Biscutum constans	P	P	P	P	P					x
Braarudosphaera africana		P	P				x			
Braarudosphaera hockwoldensis		P	P				x			
Broinsonia enormis	P	P	P					x		
Broinsonia galloisii	P	P	P	P	P					x
Broinsonia matalosa	P	P	P	P	P					x
Bukrylithus ambiguus	P	P	P	P	P					x
Calciosolenia fossilis	P	P	P					x		
Calculites anfractus			P			x				
Chiastozygus litterarius	P	P	P	P	P					x
Chiastozygus platyrhethus	P	P	P	P	P					x
Chiastozygus spissus		P	P	P				x		
Chiastozygus spp. (small)	P	P	P					x		
Corollithion kennedyi	P	P	P					x		
Corollithion ? madagaskarensis		P	P	P	P				x	
Corollithion protosignum	P	P	P					x		
Corollithion signum	P	P	P		P				x	
Cretarhabdus conicus	P	P	P	P	P					x
Cretarhabdus striatus	P	P	P	P	P					x
Cribrosphaerella ehrenbergii	P	P	P		P				x	
Crucibiscutum hayi	P	P	P					x		
Cyclagelosphaera margerelii	P	P	P	P					x	
Cyclagelosphaera rotaclypeata	P	P	P					x		
Cylindralithus nudus	P	P		P	P				x	
Discorhabdus ignotus	P	P	P	P	P					x
Eiffellithus gorkae	P	P	P					x		
Eiffellithus ? hancockii			P	P	P			x		
Eiffellithus turriseiffelii	P	P	P	P	P					x
Eprolithus floralis	P	P	P	P	P					x
Flabellites oblongus	P	P		P	P				x	
Gaarderella granulifera		P				x				
Gartnerago chiasta	P	P	P	P					x	
Gartnerago cf. *G. nanum*	P	P	P	P	P					x
Gartnerago praeobliquum	P	P	P					x		
Gartnerago theta	P	P	P					x		
Grantarhabdus coronadventis	P	P	P	P	P					x
Haqius circumradiatus	P	P	P	P	P					x
Hayesites irregularis				P	P		x			
Helenea chiastia	P	P	P	P	P					x
Helicolithus compactus	P	P	P	P					x	
Helicolithus trabeculatus	P	P	P					x		
Hemipodorhabdus cf. *H. gorkae*	P	P	P	P	P					x
Lapideacassis mariae	P	P		P	P				x	
Lithraphidites carniolensis	P	P	P	P	P					x
Loxolithus armilla	P	P	P	P	P					x
Manivitella pemmatoidea	P	P	P	P	P					x
Manivitella fibrosa	P	P	P	P					x	

Key: P= Present

CHART 5

Species	Cauvery Basin, SE India, KA 301	Mount Risou, France, Risou +20	Warren, Kent, SE England, W7	Shatsky Rise, Pacific, Hole 1207B	Shatsky Rise, Pacific, Hole 1213A	1 site	2 sites	3 sites	4 sites	5 sites
Nannoconus spp.		P	P		P			x		
Orastrum perspicuum		P	P				x			
Owenia hillii		P	P				x			
Percivalia fenestrata	P	P	P					x		
Placozygus cf. *P.fibuliformis*	P	P	P	P					x	
Prediscosphaera columnata (circular)	P	P	P	P	P					x
Prediscosphaera cretacea	P	P	P					x		
Prediscosphaera spinosa	P	P	P	P	P					x
Radiolithus planus	P	P	P	P	P					x
Radiolithus cf. *R. planus*	P	P	P					x		
Repagulum parvidentatum	P	P	P					x		
Retecapsa crenulata	P	P	P	P	P					x
Retecapsa surirella	P	P	P	P	P					x
Rhagodiscus achlyostaurion	P	P	P	P	P					x
Rhagodiscus angustus	P	P	P	P	P					x
Rhagodiscus asper	P	P	P	P	P					x
Rhagodiscus hamptonii	P	P	P					x		
Rhagodiscus cf. *R. reniformis*	P	P	P					x		
Rhagodiscus splendens	P	P	P					x		
Rotelapillus laffittei	P	P	P	P	P					x
Seribiscutum primitivum	P		P				x			
Sollasites horticus	P	P	P					x		
Staurolithites gausorhethium	P	P	P		P				x	
Staurolithites glaber	P		P	P	P				x	
Staurolithites mutterlosei	P	P		P	P				x	
Staurolithites spp.(small)	P	P	P	P	P					x
Stoverius achylosus	P	P	P	P	P					x
Tegulalithus tessellatus		P	P				x			
Tegumentum stradneri (small/large)	P	P	P	P	P					x
Tetrapodorhabdus decorus	P	P	P	P	P					x
Tranolithus gabalus		P	P	P	P				x	
Tranolithus orionatus	P	P	P	P	P					x
Tranolithus simplex	P	P	P	P	P					x
Tubodiscus burnettiae	P	P	P	P	P					x
Watznaueria barnesae	P	P	P	P	P					x
Watznaueria biporta	P	P	P	P	P					x
Watznaueria britannica	P	P	P	P	P					x
Watznaueria fossacincta	P	P	P	P	P					x
Watznaueria manivitiae	P	P	P	P	P					x
Watznaueria ovata	P	P	P	P	P					x
Zeugrhabdotus bicrescenticus	P	P	P					x		
Zeugrhabdotus diplogrammus	P	P	P	P	P					x
Zeugrhabdotus embergeri	P	P	P	P	P					x
Zeugrhabdotus cf. *Z. embergeri* (small)	P	P		P	P				x	
Zeugrhabdotus howei	P	P	P	P	P					x
Zeugrhabdotus noeliae (small)	P	P	P	P	P					x
Zeugrhabdotus xenotus	P	P	P					x		
TOTAL	84	91	90	63	61	2	7	25	17	46

Site location with sample number

FO. *T. orionatus* datum-level, Middle Albian

CHART 6

Sample details	% *Biscutum constans*	% *Discorhabdus ignotus*	% *Hayesites irregularis*	% *Helicolithus compactus*	% *Lithraphidites carniolensis*	% *Prediscosphaera* spp.	% *Repagulum parvidentatum*	% *Retecapsa crenulata*	% *Rhagodiscus* spp.	% *Staurolithites* spp.	% *Tranolithus orionatus*	% *Watznaueria barnesiae*	% *Watznaueria* sp. 1	% *Zeugrhabdotus* spp.	% Other taxa
0	15	2	0	0	3	0	6	0	6	4	0	26	0	30	8
5	17	3	2	0	13	8	0	5	5	0	2	32	11	12	7
0	19	6	0	0	10	0	0	4	2	0	0	11	2	32	7
5	7	0	0	5	4	0	6	5	5	3	0	40	0	17	6

FO *E. turriseiffelii* datum-level, Upper Albian

CHART 7

Sample details	% *Biscutum constans*	% *Discorhabdus ignotus*	% *Eiffellithus turriseiffelii*	% *Hayesites irregularis*	% *Lithraphidites carniolensis*	% *Prediscosphaera* spp.	% *Repagulum parvidentatum*	% *Retecapsa crenulata*	% *Rhagodiscus* spp.	% *Staurolithites* spp.	% *Tranolithus orionatus*	% *Watznaueria* sp. 1	% *Watznaueria barnesiae*	% *Zeugrhabdotus* spp.	% Other taxa
14	19	3	8	3	11	4	0	2	2	0	5	4	9	35	2
16	18	0	3	0	5	6	0	0	0	0	0	0	50	14	6
17	18	4	0	0	0	0	0	2	2	0	11	0	40	15	8
	17	5	2	0	7	13	2	3	2	0	7	0	25	14	3

FO *C. kennedyi*/LO of *W. britannica* datum-level, Lower Cenomanian

CHART 8

Sample details	% *Biscutum constans*	% *Cylindralithus nudus*	% Discorhabdus ignotus	% *Eiffellithus turriseiffelii*	% *Hayesites irregularis*	% *Hemipodorhabdus gorkae*	% *Lithraphidites carniolensis*	% *Owenia hillii*	% *Prediscosphaera* spp.	% *Repagulum parvidentatum*	% *Retecapsa crenulata*	% *Rhagodiscus* spp.	% *Staurolithites* spp.	% *Tegumentum stradneri*	% *Tranolithus orionatus*	% *Watznaueria barnesiae*	% *Zeugrhabdotus* spp.	% Other taxa
3	36	0	3	2	0	0	0	0	2	0	0	0	0	0	4	14	17	22
0	21	1	10	6	4	3	21	0	2	0	3	0	0	2	0	14	11	2
0	27	1	3	6	0	3	12	0	1	0	3	0	0	2	0	32	10	0
0	33	0	4	5	0	0	0	3	2	0	0	0	2	0	10	13	9	19
0	14	0	0	6	0	0	0	0	3	0	3	5	0	0	12	29	11	17

Appendix 2

Chapter 5. Gault Clay Formation, SE England

The raw nannofossil data for biostratigraphy and the geochemical data are presented in Charts 9-12. Symbols used in the range charts are explained in Chapter 3. The chart captions are as follows:

Chart 9: Range chart for the Gault Clay section.

Chart 10: Oxygen isotope and count data of selected temperature-related taxa.

Chart 11: Relative abundance data for the Gault section.

Chart 12: Comparative count-data of selected temperature-related taxa by different authors (Crux 1991; Jeremiah 1996; this study).

Gault Clay, Copt Point

CHART 9

SAMPLE NO.	REAL HEIGHT(m)	BED NUMBER (Jukes-Brown, 1900)	PRESERVATION	ABUNDANCE	TAXON
F +5	10	X	G	H	
F +4.5	9.5		VG	H	
F +4	9	top IX	G	H	
F +3.5	8.5		G	H	
F +3	8		G	H	
F +2.5	7.5		G	H	
F +2	7		G	H	
F +1.5	6.5		G	H	
F +1.4	6.4		G-M	H	
F +1.3	6.3		G	H	
F +1.2	6.2	IX	G-M	H	
F +1.1	6.1		G-M	H	
F +1	6		G	H	
F +0.9	5.9		G	H	
F +0.8	5.8		G	H	
F +0.7	5.7		G	H	
F +0.6	5.6		G-M	H	
F +0.5	5.5		G-M	H	
F +0.4	5.4		G	H	
F +0.35	5.35		G	H	
F +0.3	5.3		G	H	
F +0.2	5.2		G	H	
F +0.15	5.15		G-M	H	
F +0.1	5.1		G-M	H	
F +0.05	5.05		G	H	
F 0	5	VIII (1)	G	M	
F -0.1	4.9		G	M	
F -0.15	4.85		G	M	
F -0.2	4.8		G	M	
F -0.3	4.7		G	H	
F -0.4	4.6		G	H	
F -0.5	4.5		G	H	
F -1	4	VII	G	H	
F -1.5	3.5		G	H	
F -2	3		G	M	
F -2.5	2.5	mott. bed VI	G	H	
F -3	2	IV	G	M	
F -3.5	1.5	III	M	H	
F -4	1		G	H	
F -4.5	0.5	II	G	H	
F -5	0		G	H	

Amphizygus brooksii
Axopodorhabdus albianus
Axopodorhabdus dietzmannii
Biscutum constans
Biscutum cf. B. constans (large)
Biscutum gaultensis
Braarudosphaera africana
Braarudosphaera hockwoldensis
Braarudosphaera cf. B. primula
Braarudosphaera stenoretha
Bralowerla boletiformis
Broinsonia galloisii + B. matalosa
Bukrylithus ambiguus
Calciosolenia fossilis
Calculites percernis
Ceratolithina bicornuta
Ceratolithina cruxii
Ceratolithina hamata
Chiastozygus bifarius
Chiastozygus litterarius
Chiastozygus platyrhethus
Chiastozygus spissus
Chiastozygus synquadriperforatus
Chiastozygus cf. C. amphipons
Chiastozygus spp. (small)
Corollithion ?madagaskarensis
Corollithion protosignum
Corollithion signum
Cretarhabdus conicus
Cretarhabdus multicavus
Cretarhabdus striatus
Cribrosphaerella ehrenbergii
Crucicnbrum anglicum
Cyclagelosphaera margerelii
Cyclagelosphaera rotaclypeata
Discorhabdus ignotus
Eprolithus apertior (side view)
Eprolithus floralis
Flabellites oblongus
Gaarderella granulifera
Gartnerago cf. G. praeobliquum (small)
Grantarhabdus coronadventis
Grantarhabdus cf. G. coronadventis (small)
Haqius circumradiatus
Hayesites albiensis
Helenea chiastia
Helicolithus compactus
Helicolithus trabeculatus
Hemipodorhabdus gorkae
Laguncula dorotheae
Lapideacassis glans
Lapideacassis mariae
Lapideacassis blackii
Lithraphidites carniolensis
Loxolithus armilla
Manivitella pemmatoidea
Manivitella fibrosa
Nannoconus spp. (top view)
Octocyclus reinhardtii
Orastrum perspicuum
Owenia hilli
Percivalia fenestrata
Percivalia cf. P. hauxtonensis
Pickelhaube furtiva

SAMPLE NO.	F -5	F -4.5	F -4	F -3.5	F -3	F -2.5	F -2	F -1.5	F -1	F -0.5	F -0.4	F -0.3	F -0.2	F -0.15	F -0.1	F 0	F +0.05	F +0.1	F +0.15	F +0.2	F +0.3	F +0.35	F +0.4	F +0.5	F +0.6	F +0.7	F +0.8	F +0.9	F +1	F +1.1	F +1.2	F +1.3	F +1.4	F +1.5	F +2	F +2.5	F +3	F +3.5	F +4	F +4.5	F +5
Placozygus cf. *P.fibuliformis*							VR		VR	VR	R	R	R	R			R							R			R				VR	R	R	VR	VR	R			R	R	R
Prediscosphaera columnata	C	C	F	F	R	F	F	F	R	F	F	F	F	F	R	R	F	F	R	F	F	C	F	F	C	F	F	F	F	C	C	C	F	C	C	C	C	C	C	C	C
Prediscosphaera cf. *P. ponticula*													VR							R	VR	VR								VR	R			F	F					R	F
Prediscosphaera spinosa	VR									R	R	F	R	R	R	R		VR	R	F	F	F	R	R	R	R	R	R	R	F	F	F	F	R	C	F	R	R	F	F	F
Prediscosphaera cf. *P. spinosa* (small)										R			VR				R												R			F									
Radiolithus planus	R			VR		VR	VR		VR	R		R	R	R					R	R	F	F	R	R	R	R	?	R	R	R	R	R					R	R	VR	R	R
Radiolithus cf. *R. planus*		VR	VR	VR			VR		VR									R	F	R	F	F		R	R	R	R	F	R	R		R	F	R	R	R	R	R	R	R	
Repagulum parvidentatum	C	F	C	C	C	C	C	C	A	C	C	C	C	C	C	A	C	C	C	C	C	C	C	C	F	F	C	A	C	C	C	C	C	F	C	C	C	C	C	C	C
Retecapsa crenulata	R	R		F	F	F	F	F	F	F	F	F	F	F	F	F	C	F	F	F	F	F	F	F	F	F	F	F	F	F	F	F	F	F	F	F	F	F	F	F	F
Retecapsa surirella	F	F	F	F	F	F	F	F	F	F	F	R	R	R	F		F	F	F	F	F	F	F	F	F	F	F	F	F	F		R	F	F	C	F	F	F	F	F	F
Rhagodiscus achlyostaurion	F	C	F	F	F	F	R	R	F	F	F	F	C	F	F	C	F	C	C	F	F	C	C	C	F	F	F	C	F	C	F	C	F	C	C	C	C	C	C	C	C
Rhagodiscus cf. *R. achlyostaurion*									VR						R	VR	R	R	R			F																			
Rhagodiscus angustus	F	F	F	F	F	F	F	F	F	F	F	F	F	R	R	C	C	F	F	F	F	F	F	F	F	F	F	F	F	F	F	F	F	F	F	F	F	F	F	F	F
Rhagodiscus asper	F	F	F	F	F	F	F	C	F	F	F	F	F	F	F	C	C	C	F	F	F	F	F	F	F	F	F	F	R	C	F	F	F	R	F	F	F	F	F	F	F
Rhagodiscus gallagheri																																		R				R			
Rhagodiscus hamptonii	R	R		R		R	F	R	R	R	R	R	R	R	R	R	R	R		R	R	F	R		R	R	R	R	R	R	R	R	R	R	VR	R	R	R	R	R	R
Rhagodiscus reniformis									R								VR			VR	R	R	R	R		R	R	R	R		R			VR				R	R	R	
Rhagodiscus splendens	F	F	R	VR	R	F	R		R	F	F	F	F	R	F	F	F	F	C	R	F	F	F	F	F	F	F	F	F	F	F	F	F	F	F	F	F	F	F	F	F
Rotelapillus laffittei	F	F	F	F	F	F	F	F	F	F	F	F	F	F	F	F	F	R	F	F	F	F	F	F	F	F	F	F	F	F	F	F	F	F	C	F	F	F	F	F	F
Senbiscutum primitivum	VR	VR	VR	VR		VR		VR		R	R	R	R	R	R	F	F	F	F	F	F	F	F	F	F	F	F	F	F	F	R	R	R	R	R	R	VR	R			VR
Staurolithites angustus													?																								R	R	R	VR	R
Staurolithites gausorhethium	VR	VR	VR		R				VR	R	F	F	F	R	R	R	F	F	R	F	F	F	F	F	F	F	F	F	F	F	F	F	F	F	F	R	R	F	R	R	R
Staurolithites glaber	F	F	F	R	F	F	VR	F	R	R	F	F	R	R	VR	R	F	F	R	F	F	F	R	F	F	F	F	F	F	F	F	F	R	R	VR	VR				R	R
Staurolithites laffittei s. l.	C	C	C	C	R	R	F	F	C	F	F	F	R	R	C	R	C	C	F	F	F	C	F	R	F	R	R	F	R	F	R	F	F	R	F	F	F	R	R	R	F
Staurolithites mutterlosei							VR			?						VR	VR						VR				VR		VR												
Staurolithites cf. *S. rotatus*																																							R		R
Stoverius achylosus		F	R	VR	R	R	VR	R	VR				R					R			VR	R		R		VR	R	R	?	R	R			VR	R	R	VR	R		R	R
Stradnerlithus geometricus																																						R	R	R	R
Tegumentum stradneri	F	F	F	F	F	F	F	F	F	F	F	F	F	F	F	F	C	F	C	F	F	F	F	F	F	F	F	F	F	F	F	F	F	F	F	F	F	F	F	F	F
Tetrapodorhabdus decorus	VR	VR	VR	R	R	R		R	VR	F	R	R	R	R	R	F	F	R	F	R	R	F	R	R	R		R	F	F	R		R	R	R	R	R	VR	R	R	R	R
Tranolithus gabalus																																			R						
Tranolithus orionatus	F	F	F	R	F	F	F	C	F	F	C	F	C	F	F	F	C	F	C	F	F	F	F	F	F	F	F	F	F	C	C	C	F	C	C	C	C	C	C	C	C
Tranolithus simplex	R	R	R		R	R	R	R	R	R	R	R	R		R	R	R	R	R	VR	R	R		R	R	R	R	R	R		R			R		R			F		R
Tubodiscus burnettiae	F	F	R	R	F	F	F	F	F	F	F	F	F	F	F	F	F	F	F	F	F	F	F	F	F	F	F	F	F	C	F	F	F	F	F	F	F	F	F	F	F
Watznaueria barnesiae	C	C	C	C	C	C	C	C	C	C	C	C	C	C	C	A	A	C	A	A	A	A	A	C	C	C	A	A	C	A	A	A	C	A	A	A	A	A	C	A	A
Watznaueria biporta	F	F	R	R		R		R	R	R	F	R	R	F	R	F	F	F	F	F	F	F	F		R	R		F	R	F	F	F	F		R	R	F	F	R	R	F
Watznaueria britannica																VR	VR				VR		VR							R		VR							VR	VR	R
Watznaueria fossacincta	F	F	F	F	F	F	F	F	F	C	C	F	C	F	C	C	C	C	C	C	C	C	C	C	C	C	C	C	F	C	C	C	F	F	F	F	C	F	F	F	C
Watznaueria manivitiae s. l.	C	C	F	F	C	F	F	C	C	C	C	F	C	F	F	F	C	F	C	F	F	C	C	F	C	C	F	C	F	C	C	C	F	C	C	C	C	C	C	C	C
Watznaueria ovata	R	R	R	R	R	R	F	F	R	F	F	R	R	R	R	R	F	R	F	R	R	F	F	R	R	R	F	F		F	R	F	R	R	F	F	R	R	R	R	R
Zeugrhabdotus biperforatus				VR		VR	?			VR	VR						VR			R										VR			VR		VR			VR			
Zeugrhabdotus diplogrammus	C	C	C	C	F	F	F	F	F	F	C	F	F	R	F	C	F	F	C	F	F	F	R	F	R	F	F	F	C	F	F	F	F	R	F	F	F	F	R	F	F
Zeugrhabdotus embergeri		VR	VR		R	R	R	F	F	R	R	R	R	R	R	R	C	F	C	F	F	F	R	R	R	R	R	F	R	F	R	R		R	VR		R	R	R	R	R
Zeugrhabdotus cf. *Z. embergeri* (small)									VR														R					R	R		R			R			R				
Zeugrhabdotus howei				R	F	C	F	F	F	F	C	F	C	F	F	C	C	F	C	F	F	F	F	F	F	F	F	F	F	F	F	F		F	F	F	F	R	F	F	F
Zeugrhabdotus cf. *Z. howei*												R	F	F	F	F	F	R	F	F	F	F	F	F	F	F	F	F	F	F	F	F	R								F
Zeugrhabdotus noeliae	A	A	C	C	C	C	A	A	A	A	A	C	A	A	A	A	A	C	A	C	C	A	C	C	A	C	A	A	A	A	A	A	C	C	A	A	A	A	C	A	A
Zeugrhbdotus streetiae																															R			VR	R						
Zeugrhabdotus xenotus	F	F	F	F	F	F	F	F	F	R	F	R	F	R	R	F	R	F	R	R	R	F	R	F	R	R	F	R	F	F	F	F	F	VR	F	F		R	VR	VR	R
NANNOFOSSIL BIOEVENT	*T. orionatus* , *C. anglicum* present	LO *B. boletiformis* ; FO *C. signum*			FO *A. albianus* , *O. hilli*		FO *C. bicornuta*	FO *C. hamata*						LO *C. bicornuta*							FO *Gartnerago* cf. *praeobliquum* (small)																FO *S. angustus*				*Eiffellithus* absent, *H. albiensis* present
NF ZONE (Bown et al. 1998)			BC 24							BC 25a																		BC 25b													
NF ZONE (Jeremiah 1996)		NAL 4			NAL 5					NAL 6																NAL 7													NAL 9		
STAGE (based on nannofossil zones)									MIDDLE ALBIAN																					UPPER ALBIAN											

Gault Clay Copt Point									
Stage	% *R. parvidentatum* (this study)	*R. parvidentatum* (Crux 1991) 25 FOV	*R. parvidentatum* (Jeremiah 1996) 30 FOV	% *R. asper* (this study)	*R. asper* (Crux 1991) 25 FOV	*R. asper* (Jeremiah 1996) 30 FOV	% *T. orionatus* (this study)	*T. orionatus* (Crux 1991) 25 FOV	*T. orionatus* (Jeremiah 1996) 30 FOV
	1	8	60	2	4	6	4	69	
	2	10	39	0	5	11	2	10	70
	3	22	80	0	6	10	4	10	50
UPPER	4	8	105	0	24	35	3	8	51
ALBIAN	6	12	55	0	9	3	5	4	48
	8	37	65	0	5	12	3	17	26
	11		80	0		9	3		33
	7	37	70	0	10	4	4	14	80
MIDDLE	7	46	85	0	4	17	4	17	55
ALBIAN	6	31	50	2	12	18	5	10	21
	8	62	75	0	2	10	4	13	16
	12	62	30	1	4	5	4	8	9
CHART 12									

Gault Clay, Copt Point

CHART 11

SAMPLE NO.	REAL HEIGHT (m)	BED NO. (Jukes-Brown, 1900)	% *Biscutum constans*	% *Discorhabdus ignotus*	% *Lithraphidites carniolensis*	% *Prediscosphaera columnata*	%*Repagulum parvidentatum*	% *Retecapsa crenulata*	% *Rhagodiscus asper*	% *Seribiscutum primitivum*	% *Staurolithites* spp. (small)	% *Tranolithus orionatus*	% *Watznaueria* spp.(combined)	% *Zeugrhabdotus noeliae*	% *Zeugrhabdotus diplogrammus*	% *Zeugrhabdotus howei*	Total	Nutrient Index Herrle (2002)	Productivity Index Gale et al. (2000)	Modified Nutrient Index (this study)
F +5	10	X	21	1	5	7	3	1	1	0	5	5	20	26	0	0	95	57	2.4	71
F +4.5	9.5		21	1	8	7	3	1	0	0	2	4	17	27	0	0	91	62	2.8	74
F +4	9	top IX	15	2	6	7	2	1	1	0	1	2	16	24	0	7	84	62	2.4	72
F +3.5	8.5		27	2	6	4	2	1	1	0	2	4	20	20	0	0	89	52	2.4	71
F +3	8		25	2	5	5	3	3	0	0	6	4	27	12	0	0	92	34	1.4	59
F +2.5	7.5		26	1	8	4	3	3	0	0	2	4	19	21	0	0	91	54	2.5	72
F +2	7		22	3	5	6	4	1	0	0	1	4	18	22	0	1	87	58	2.4	72
F +1.5	6.5		30	0	3	6	2	2	0	0	2	4	23	16	0	1	89	41	2.0	67
F +1.4	6.4		26	0	2	4	2	2	0	0	2	3	19	31	0	0	90	62	3.0	75
F +1.3	6.3	IX	25	0	1	8	1	2	1	0	2	3	19	30	1	0	92	61	2.9	74
F +1.2	6.2		30	0	2	4	2	2	0	0	2	2	17	30	1	0	92	64	3.5	78
F +1.1	6.1		24	0	1	5	3	2	1	0	1	2	28	27	0	0	94	49	1.8	65
F +1.0	6		20	1	8	5	4	1	1	1	4	4	18	24	1	3	95	58	2.4	71
F +0.9	5.9		21	0	0	5	5	3	1	0	0	3	21	28	0	0	87	57	2.3	70
F +0.8	5.8		16	0	3	7	3	3	0	0	2	3	20	34	0	0	91	63	2.5	71
F +0.7	5.7		13	0	2	7	3	2	0	0	1	4	15	40	0	0	88	73	3.5	78
F +0.6	5.6		16	0	5	9	1	2	2	0	3	6	13	33	0	0	90	72	3.8	79
F +0.5	5.5		17	1	7	5	2	1	0	0	2	2	31	18	0	6	92	38	1.1	54
F+0.4	5.4		19	1	3	9	3	2	0	0	1	4	19	31	0	0	92	63	2.6	73
F+0.35	5.35		19	1	4	8	5	3	1	0	0	3	11	35	0	0	90	77	4.9	83
F+0.3	5.3		18	0	2	6	4	1	0	0	1	3	14	40	0	0	89	74	4.1	81
F+0.2	5.2		12	0	2	5	6	3	0	0	1	5	21	35	1	1	92	63	2.2	69
F+0.15	5.15		8	2	2	7	8	3	0	0	1	5	18	41	0	0	93	70	2.7	74
F+0.1	5.1		11	1	1	4	6	3	1	0	1	6	44	10	2	4	94	20	0.5	33
F+0.05	5.05		13	1	2	5	9	3	1	0	1	6	31	21	1	0	94	42	1.1	53
F 0	5	VIII (1)	11	2	6	1	11	1	0	0	3	3	33	26	0	3	90	31	0.7	44
F-0.1	4.9		13	0	1	4	7	2	0	0	2	4	36	26	0	0	95	42	1.1	52
F-0.15	4.9		14	0	6	3	9	1	0	0	2	5	25	25	1	0	93	51	1.6	62
F-0.2	4.8		22	1	3	4	7	2	0	0	2	4	16	28	0	3	93	64	3.1	76
F-0.3	4.7		14	2	5	3	6	3	0	0	1	4	17	28	1	2	89	64	2.5	72
F-0.4	4.6		13	0	5	10	8	3	0	0	2	4	16	28	1	2	92	64	2.6	72
F-0.5	4.5		18	1	9	3	12	1	1	0	2	3	22	12	1	6	92	37	1.4	58
F -1	4	VII	14	1	9	2	8	2	2	0	5	7	29	11	0	4	90	29	0.9	47
F -1.5	3.5		14	1	7	7	9	2	2	0	4	3	24	11	0	3	91	33	1.0	52
F -2	3		11	0	7	4	9	2	2	0	0	1	37	11	2	4	90	23	0.6	37
F -2.5	2.5	mott. bed VI	8	1	8	1	5	2	1	0	4	2	33	21	0	5	92	40	0.9	46
F -3	2	IV	12	1	10	1	5	1	1	0	7	5	31	14	1	3	93	33	0.8	47
F -3.5	1.5	III	25	1	3	1	5	2	1	0	10	2	22	23	1	0	96	52	2.2	69
F -4	1		22	3	5	8	2	3	1	0	4	2	22	15	2	0	89	45	1.7	65
F -4.5	0.5		21	5	5	8	3	2	0	0	5	6	21	9	0	0	85	40	1.4	63
F -5	0	II	33	2	7	6	4	1	0	0	5	4	18	9	1	0	90	38	2.3	71

Gault Clay Copt Point

Stage	% *R. parvidentatum* (this study)	*R. parvidentatum* (Crux 1991) 25 FOV	*R. parvidentatum* (Jeremiah 1996) 30 FOV	% *R. asper* (this study)	*R. asper* (Crux 1991) 25 FOV	*R. asper* (Jeremiah 1996) 30 FOV	% *T. orionatus* (this study)	*T. orionatus* (Crux 1991) 25 FOV	*T. orionatus* (Jeremiah 1996) 30 FOV
	1	8	60	2	4		6	4	69
	2	10	39	0	5	11	2	10	70
	3	22	80	0	6	10	4	10	50
UPPER	4	8	105	0	24	35	3	8	51
ALBIAN	6	12	55	0	9	3	5	4	48
	8	37	65	0	5	12	3	17	26
	11		80	0		9	3		33
	7	37	70	0	10	4	4	14	80
MIDDLE	7	46	85	0	4	17	4	17	55
ALBIAN	6	31	50	2	12	18	5	10	21
	8	62	75	0	2	10	4	13	16
	12	62	30	1	4	5	4	8	9

CHART 12

Appendix 3

Chapter 6. ODP Leg 171B, Blake Nose, western North Atlantic

The quantitative nannofossil and geochemical data are presented in Charts 13A/B and 14. The chart captions are as follows:

Chart 13A: Relative abundance and diversity data for Hole 1049C, Blake Nose section.

Chart 13B: Absolute abundance-20 fields of view count data.

Chart 14: Geochemical (oxygen and carbon isotope) and palaeotemperature data.

ODP 171B 1049C

1049C-12X Depth(mbsf)	Preservation	Preservation scale	Nannofossils / FOV	Species Richness	% *Biscutum constans*	% *Discorhabdus ignotus*	%*Lithraphidites carniolensis*	% *Nannoconus* spp.	% *Repagulum parvidentatum*	% *Rhagodiscus* spp.	% *Staurolithites* spp.	% *Watznaueria* spp.	% *Zeugrhabdotus noeliae*	Productivity Index	Nutrient Index (Herrle, 2002)	Nutrient Index (modified)	Shannon-Weiner Diversity Index	Equitability
142.00	G	100	161	62	19	2	10	0	0	3	1	20	29	2.4	61	71	2.10	0.13
142.50	G	100	107	55	17	4	9	0	0	2	1	19	38	2.9	69	76	1.84	0.11
142.72	G	100	75	50	15	9	8	0	0	4	2	9	42	6.3	85	88	1.97	0.14
142.76	G-M	75	100	55	13	10	9	0	0	5	1	13	31	3.4	76	81	2.20	0.16
142.80	G	100	150	61	20	8	12	0	0	1	1	13	33	4.1	76	82	1.93	0.11
142.84	G-M	75	56	50	16	7	15	0	0	2	0	12	33	4.1	77	82	1.98	0.15
142.88	M	50	<1	13														0.08
142.94	G	100	75	13	14	5	13	0	0.7	3	2	27	26	1.5	53	63	1.96	0.15
143.00	M	50	22	46	9	6	19	1	0	5	1	20	25	1.7	61	67	2.20	0.24
143.04	M	50	75	38	13	6	14	0	0	3	2	17	27	2.4	66	73	2.15	0.26
143.10	G	100	152	33	22	11	12	0	0	3	1	9	32	6	83	88	2.12	0.14
143.16	G	100	126	61	23	6	11	0	0	3	1	11	35	5.3	79	85	2.00	0.12
143.20	G	100	152	60	23	8	13	1	0	2	1	15	24	3.1	68	79	1.99	0.12
143.50	G-M	75	<10	61	18	5	9	0	0	4	2	22	32	2.3	63	71	1.57	0.16
143.99	M	50	>75	30	12	5	12	8	0	3	1	26	21	1.3	50	59	2.09	0.12
144.50	G	100	152	66	18	4	11	0	0	2	1	22	32	2.3	62	71	1.88	0.10
145.00	G	100	75	63	18	5	9	0	0	4	2	22	32	2.3	63	71	1.97	0.13
145.22	G-M	75	60	57	16	3	13	0	0	0	0	29	26	1.4	50	61	1.93	0.14
145.26	G-M	75	65	51	13	4	14	0	0	1	2	27	32	1.7	57	64	1.65	0.09
145.27	G	100	60	59	10	2	14	0	0	4	1	40	23	0.8	38	47	1.69	0.09
145.28	G-M	75	62	61	8	1	12	1	0	1	2	43	27	0.8	39	46	1.62	0.08
145.29	G-M	75	66	61	7	3	15	2	0	1	2	47	15	0.5	28	35	1.63	0.09
145.30	M	50	69	57	10	7	12	9	0	3	2	25	29	1.6	59	65	1.93	0.11
145.49	G	100	67	65	7	2	10	8	0	3	2	39	24	0.8	40	46	1.82	0.09
145.50	G-M	75	102	66	16	6	14	1	0	4	1	21	23	1.9	58	68	2.06	0.13
145.59	G-M	75	58	59	7	6	10	6	0	2	2	33	27	1.0	50	55	2.17	0.13
145.89	G-M	75	38	65	6	2	15	12	0	4	1	32	17	0.7	37	44	1.92	0.12
145.99	G-M	75	60	59	11	9	13	1	0	5	4	21	19	1.4	57	65	2.12	0.14
146.10	G-M	75	32	58	5	2	19	5	0	3	2	35	15	0.6	33	39	1.96	0.12
146.51	G-M	75	39	58	7	5	15	1	0	6	3	33	11	0.5	33	41	2.04	0.16
146.60	G-M	75	17	47	4	3	14	9	0	4	2	35	16	0.6	35	40	1.99	0.14
147.01	M	50	65	51	6	4	17	7	0	6	2	37	10	0.4	27	35	2.07	0.21
147.50	M	50	45	38	8	8	13	7	0	1	1	36	9	0.5	32	41	2.13	0.22
148.00	M	50	51	38	8	4	16	17	0	3	4	27	9	0.6	33	44	2.14	0.25

CHART 13A

ODP Leg 171B 1049C

1049C-12X Depth(mbsf)	Preservation	Nannofossils/20 FOV	*B. constans*/20 FOV	*D. ignotus*/20 FOV	*H. albiensis*/20 FOV	*H. irregularis*/20 FOV	*Micrantholithus spp.*/20 FOV	*Nannoconus*/20 FOV	*Watznaueria* spp./20 FOV	*Z. noeliae*/20 FOV
142.00	G	161	28	5	1	0	0	0	23	46
142.50	G	107	18	3	2	0	0	0	15	48
142.72	G	75	13	9	0	0	0	0	11	50
142.76	G-M	100	11	10	0	0	0	0	12	32
142.80	G	150	23	9	0	0	0	0	13	48
142.84	M-G	56	9	3	0	0	0	0	8	16
142.88	M	<1	0	0	0	0	0	0	0	0
142.94	G	75	15	3	0	0	0	0	28	14
143.00	M	22	8	4	0	0	0	4	25	12
143.04	M	75	6	2	0	0	0	0	18	15
143.10	G	152	17	12	1	0	0	0	26	32
143.16	G	126	29	8	1	0	0	0	19	45
143.20	G	152	37	7	0	2	0	3	28	41
143.50	G-M	<1	14	7	0	0	0	4	32	30
143.99	M	>75	9	4	0	0	0	6	28	22
144.50	VG	152	19	3	0	0	0	0	18	37
145.00	G	75	11	4	0	1	0	0	14	18
145.22	G-M	60	15	3	0	2	0	0	44	30
145.26	G-M	65	18	6	0	3	0	0	63	36
145.27	G	60	14	4	0	3	0	0	60	32
145.28	M-G	62	11	3	0	2	0	4	74	33
145.29	M-G	66	15	9	0	2	0	2	65	25
145.30	M	69	8	6	0	1	1	7	49	38
145.49	G	67	22	7	0	2	1	10	44	31
145.50	M-G	102	11	8	0	1	0	2	25	30
145.59	G-M	58	18	5	0	2	1	5	37	27
145.89	M-G	38	11	9	0	3	0	10	31	12
145.99	M-G	60	4	5	0	2	0	2	13	8
146.10	M-G	32	9	6	0	4	1	6	31	12
146.51	M-G	39	2	8	0	1	0	1	8	2
146.60	M-G	17	5	3	0	2	0	3	14	6
147.01	M	65	x	x	x	x	0	9	40	x
147.50	M	45	x	x	x	3	1	7	35	x
148.00	M	51	x	x	x	1	1	10	25	x

x: too diminutive to count because of very high density of ascidian spicules/inorganics.

CHART 13B

ODP 171B 1049C Core 12							63–150 µm						
Core	Top	Bot	Depth		Age	Age (kyr)	Sample	13C	std	18O	std	Temp	Temp
	(cm)	(cm)	(mbsf)		(kyr)	adj (10.7)			dev		dev		error
2	120	121	142.00		309.39	320.09	12X2W120-121	1.81	0.058	-1.365	0.071	16.352	0.755
3	20	21	142.50		262.51	273.21	12X3W20-21	1.33	0.056	-0.955	0.069	14.667	0.730
3	42	43	142.72		240.94	251.64	12X3W42-43	1.96	0.023	-1.902	0.081	18.627	0.856
3	46	46.5	142.76		237.02	247.72							
3	50	50.5	142.80		233.10	243.80							
3	54	54.5	142.84		229.18	239.88	OAE1b sapropel						
3	64	64.5	142.94		219.37	230.07							
3	70	70.5	143.00		213.49	224.19	NO DATA						
3	74	74.5	143.04		209.57	220.27	CARBONATE-FREE						
3	80	80.5	143.10		203.69	214.39	SEDIMENTS						
3	86	86.5	143.16		197.80	208.50							
3	90	91	143.20		193.88	204.58	12X3W90-91	2.74	0.032	-0.563	0.073	13.097	0.774
3	120	121	143.50		164.47	175.17	12X3W120-121M	2.23	0.035	-0.353	0.014	12.274	0.147
4	19	20	143.99		116.43	127.13	12X4W19-20	2.49	0.021	-0.732	0.122	13.771	1.279
4	70	71	144.50		66.43	77.13	12X4W70-71	2.09	0.039	-1.203	0.065	15.681	0.698
4	120	121	145.00		17.41	28.11	12X4W120-121	1.68	0.045	-1.186	0.059	15.611	0.629
4	142	143	145.22		-3.57	7.13	12X4W142-143	1.78	0.038	-0.295	0.097	12.048	1.019
4	146	147	145.26		-7.13	3.57	12X4W146-147	1.96	0.056	-0.983	0.089	14.782	0.943
4	147	148	145.27		-8.02	2.68	12X4W147-148	2.07	0.027	-0.343	0.087	12.235	0.924
4	148	149	145.28		-8.91	1.79	12X4W148-149	2.56	0.057	-0.463	0.073	12.704	0.772
4	149	150	145.29		-9.80	0.90	12X4W149-150	3.78	0.029	0.095	0.083	10.553	0.875
5	0	1	145.30		-10.70	0.00	12X5W0-1	3.51	0.014	0.123	0.029	10.448	0.318
5	19	20	145.49		-27.63	-16.93	12X5W19-20	3.33	0.063	0.031	0.082	10.795	0.873
5	20	21	145.50		-28.52	-17.82	12X5W20-21	3.29	0.007	0.061	0.061	10.681	0.657
5	29	30	145.59		-36.54	-25.84	12X5W29-30	3.50	0.057	0.430	0.051	9.302	0.542
5	59	60	145.89		-66.00	-55.30	12X5W59-60	3.94	0.034	0.435	0.053	9.281	0.572
5	69	70	145.99		-76.00	-65.30	12X5W69-70	3.50	0.053	0.030	0.079	10.799	0.836
5	80	81	146.10		-87.12	-76.42	12X5W80-81	3.60	0.025	0.061	0.080	10.681	0.845
5	121	122	146.51		-128.47	-117.77	12X5W121-122	3.78	0.028	0.488	0.114	9.087	1.191
5	130	131	146.60		-136.67	-125.97	12x5W130-131	4.06	0.015	0.426	0.116	9.316	1.213
6	21	22	147.01		-175.27	-164.57	12x6W21-22	4.15	0.045	0.344	0.067	9.619	0.718
6	70	71	147.50		-225.50	-214.80	12X6W70-71	4.24	0.039	0.823	0.094	7.867	0.989
6	120	121	148.00		-276.61	-265.91	12X6W120-121	4.14	0.023	0.362	0.079	9.554	0.837
CHART 14													

Appendix 4

Chapter 7. ODP Leg 198, Shatsky Rise, northwest Pacific

The quantitative nannofossil and diversity data are presented in Charts 15-23. The chart captions are as follows:

Chart 15: Relative abundance data for 198-1207B.

Chart 16: Relative abundance data for 198-1213A/B.

Chart 17: Diversity indices for 198-1207B.

Chart 18: Diversity indices for 198-1213A/B.

Chart 19: Diversity indices from the *T. orionatus* datum-level in the Karai Formation, Section 1, Cauvery Basin.

Chart 20. Diversity indices from the *E. turriseiffelii* datum-level in the Karai Formation, Section 1, Cauvery Basin.

Chart 21. Diversity indices from the Middle Albian of the Gault Clay section. Diversity indices for the Blake Nose section are presented in Chart 13.

Chart 22. Range chart for Section 1207B.

Chart 23. Range chart for Section 1213A-B.

ODP Leg 198 Hole 1207B

Sample	Preservation	Abundance	Species richness	Total count	no. of FOV's (to reach 300)	A. terebrodentarius	% A. terebrodentarius	A. dietzmannii	% A. dietzmannii	B. constans	% B. constans	B. stenostaurion	% B. stenostaurion	B. aricana	% B. africana	B. ambiguus	% B. ambiguus	Chiastozygus spissus	% Chiastozygus spissus	C. ?madagaskerensis	% C.? madagaskerensis	C.conicus	% C. conicus	C. margerelli	% C. margerelli	C. nudus	% C. nudus	D. ignotus	% D. ignotus	Eiffellithus spp.	% Eiffellithus spp.	E. ? hancockii	% E. ? hancockii	E. floralis	% E. floralis	F. oblongus	% F. oblongus	G. coronadventis	% G. coronadventis	H. circumradiatus	%H. circumradiatus	H. irregularis	% H. irregularis	H. chiastia	% H. chiastia	H. gorkae
1207B-24RCC, 373.92m	G	A	50	452	2	0	0	2	0	217	48	0	0	0	0	2	0	2	0	0	0	0	0	0	0	2	0	36	8	21	5	0	0	1	0	0	0	0	0	0	0	0	0	0	0	18
1207B-26R CC, 393.05m	M-G	A	47	303	2	0	0	0	0	82	27	0	0	0	0	1	0	0	0	0	0	0	0	0	0	2	1	10	3	18	6	0	0	0	0	0	0	0	0	0	0	0	0	0	0	8
1207B-27RCC, 402.62m	M-G	A	50	300	2	0	0	0	0	58	19	4	1	0	0	1	0	0	0	0	0	0	0	0	0	0	0	22	7	8	3	0	0	0	0	0	0	1	0	0	0	4	1	0	0	5
1207B-28R CC, 417.34m	M-G	A	45	308	2	0	0	0	0	74	24	0	0	0	0	3	1	0	0	1	0	0	0	0	0	0	0	25	8	16	5	0	0	0	0	1	0	0	0	0	0	6	2	0	0	6
1207B-29R CC, 422.12m	M-G	A	36	300	3	0	0	0	0	55	18	0	0	0	0	0	0	0	0	0	0	0	0	1	0	0	0	28	9	2	1	0	0	0	0	0	0	0	0	0	0	4	1	0	0	4
1207B-30R CC, 431.49m	M-G	A	45	306	2	0	0	0	0	34	11	0	0	0	0	0	0	0	0	0	0	0	0	0	0	0	0	44	14	0	0	0	0	3	1	0	0	0	0	0	0	14	5	0	0	2
1207B-31R CC, 440.78m	M-G	A	42	307	2	0	0	0	0	26	8	1	0	0	0	2	1	0	0	0	0	0	0	0	0	1	0	35	11	0	0	0	0	0	0	1	0	0	0	0	0	1	0	0	0	2
1207B-32R CC, 450.33m	M	A	43	304	5	0	0	0	0	21	7	0	0	1	0	0	0	0	0	0	0	0	0	0	0	0	0	19	6	0	0	0	0	0	0	0	0	0	0	0	0	9	3	1	0	8
1207B-33R CC, 460.33m	M-G	A	40	308	3	0	0	0	0	32	10	0	0	0	0	0	0	0	0	0	0	0	0	0	0	3	1	37	12	0	0	0	0	4	1	1	0	0	0	0	0	42	14	3	1	0
1207B-34R CC, 469.5m	M	A	38	302	7	0	0	0	0	15	5	0	0	0	0	0	0	0	0	0	0	0	0	0	0	3	1	14	5	0	0	0	0	0	0	1	0	0	0	0	0	24	8	3	1	0
1207B-35R CC, 478.87m	M-G	A	45	301	4	0	0	0	0	11	4	0	0	0	0	1	0	0	0	0	0	0	0	0	0	0	0	25	8	0	0	0	0	0	0	0	0	0	0	0	0	39	13	2	1	1
1207B-36R CC, 488.37m	M	A	37	301	2	0	0	3	1	2	1	0	0	0	0	0	0	0	0	0	0	0	0	2	1	5	2	11	4	0	0	0	0	0	0	2	1	1	0	1	0	1	0	0	0	0
1207B-37R CC, 498.7m	M-G	A	45	350	3	0	0	0	0	31	9	0	0	0	0	0	0	0	0	0	0	0	0	0	0	0	0	44	13	0	0	0	0	1	0	1	0	0	0	0	0	11	3	2	1	0
1207B-38R CC, 507.77m	M-G	A	43	345	3	0	0	0	0	14	4	0	0	0	0	0	0	0	0	0	0	0	0	0	0	0	0	37	11	0	0	0	0	0	0	0	0	0	0	0	0	18	5	0	0	0
1207B-39R CC, 517.27m	M	A	38	306	9	0	0	0	0	19	6	0	0	0	0	0	0	0	0	0	0	0	0	0	0	1	0	21	7	0	0	0	0	7	2	0	0	0	0	0	0	4	1	3	1	0
1207B-40R CC, 526.55m	M-G	A	45	327	2	0	0	1	0	5	2	0	0	0	0	0	0	0	0	0	0	0	0	0	0	0	0	45	14	0	0	2	1	0	0	2	1	1	0	0	0	25	8	0	0	1
1207B-41R CC, 536.25m	M	A	42	302	4	0	0	1	0	1	0	0	0	0	0	0	0	0	0	0	0	0	0	0	0	0	0	18	6	0	0	0	0	3	1	1	0	1	0	0	0	14	5	1	0	0
1207B-42R CC, 545.93m	M	A	31	314	3	1	0	0	0	2	1	0	0	0	0	0	0	0	0	0	0	0	0	0	0	0	0	42	13	0	0	0	0	1	0	0	0	0	0	0	0	31	10	0	0	0
1207B-43R CC, 557.01m	M	A	36	324	3	1	0	0	0	2	1	0	0	0	0	0	0	0	0	0	0	0	0	0	0	0	0	40	12	0	0	0	0	0	0	0	0	0	0	1	0	2	1	1	0	1
1207B-44R CC, 566.89m	M	A	32	306	2	0	0	0	0	0	0	0	0	0	0	0	0	0	0	0	0	0	0	6	2	0	0	21	7	0	0	0	0	0	0	0	0	0	0	0	0	2	1	1	0	1
1207B-45R CC, 574.89m	M	A	26	332	3	0	0	0	0	0	0	0	0	0	0	0	0	0	0	0	0	3	1	14	4	0	0	37	11	0	0	0	0	0	0	0	0	0	0	1	0	0	0	1	0	0

CHART 15

Sample	modified Nutrient Index	Nutrient Index Herrle (2002)	Productivity Index Gale et al. (2000)	% Z. xenotus	Z. xenotus	% Z. noeliae	Z. noeliae	% Z. howei	Z. howei	% Z. embergeri	Z. embergeri	% Z. diplogrammus	Z. diplogrammus	% Watznaueria spp. (combined)	Watznaueria spp. (combined)	% T. burnettiae	T. burnettiae	% T. orionatus	T. orionatus	% T. gabalus	T. gabalus	% T. coptensis	T. coptensis	% T. stradneri	T.stradneri	% S. achylosus	S. achylosus	% Staurolithites spp. (siesseri)	Staurolithites spp. (siesseri)	% R. laffittei	R. laffittei	% Rhagodiscus spp.	Rhagodiscus spp.	% R. crenulata/surirella (+rims)	R. crenulata/surirella (+rims)	% P. columnata	P. columnata	% Nannoconus spp.	Nannoconus spp.	% M. pemmatoidea	M.pemmatoidea	% L. armilla	L. armilla	% L. carniolensis	L. carniolensis	% H. gorkae
120 7B-24RCC, 373.92m	92	79	1050	0	0	0	0	1	1	0	0	2	1	6	6	0	0	2	0	0	0	0	0	1	1	0	0	0	0	0	0	1	1	3	3	0	0	2	2	0	0	0	0	6	6	4
120 7B-26R CC, 393.05m	54	26	109.4	0	0	0	0	0	0	0	0	1	0	32	32	0	0	0	0	1	1	0	0	2	2	0	0	0	0	0	0	1	1	3	3	0	0	4	4	0	0	0	0	2	2	3
120 7B-27RCC, 402.62m	45	26	65	0	0	0	0	0	0	0	0	0	0	40	40	0	0	3	1	0	0	0	0	4	4	0	0	0	0	0	0	1	1	3	3	1	1	8	8	0	0	0	0	1	1	5
120 7B-28R CC, 417.34m	55	34	97	0	0	0	0	0	0	0	0	0	0	35	35	0	0	1	1	4	4	0	0	3	3	0	0	0	0	0	0	2	2	5	5	1	1	4	4	0	0	0	0	5	5	14
120 7B-29R CC, 422.12m	46	32	66	0	0	0	0	0	0	0	0	0	0	47	47	0	0	1	1	1	2	0	0	2	2	0	0	0	0	0	0	1	1	4	4	0	0	2	2	0	0	0	0	2	2	17
120 7B-30R CC, 431.49m	45	37	51	0	0	0	0	0	0	0	0	0	0	45	45	0	0	0	0	2	2	0	0	1	1	0	0	0	0	0	0	1	1	4	4	0	0	2	2	0	0	0	0	1	1	26
120 7B-31R CC, 440.78m	43	36	50	1	1	0	0	0	0	0	0	0	0	42	42	0	0	0	0	1	1	0	0	1	1	0	0	0	0	0	0	1	1	4	4	0	0	3	3	0	0	0	0	1	1	37
120 7B-32R CC, 450.33m	32	25	35	0	0	0	0	0	0	0	0	0	0	29	29	0	0	0	0	1	1	0	0	1	1	0	0	0	0	0	0	1	1	3	3	0	0	2	2	0	0	0	0	0	0	3
120 7B-33R CC, 460.33m	52	42	66	2	1	0	0	2	1	0	0	0	0	46	46	0	0	0	0	2	1	0	0	1	1	0	0	0	0	0	0	1	1	3	3	0	0	2	2	0	0	0	0	0	0	0
120 7B-34R CC, 469.5m	20	13	15	10	3	0	0	1	0	0	0	0	0	53	53	0	0	0	0	2	1	0	0	2	1	0	0	0	0	0	0	2	1	8	4	1	1	6	3	0	0	0	0	0	0	0
120 7B-35R CC, 478.87m	35	29	28	16	5	0	0	0	0	0	0	0	0	32	32	0	0	0	0	1	1	0	0	1	1	0	0	0	0	0	0	1	1	4	4	0	0	3	3	0	0	0	0	0	0	0
120 7B-36R CC, 488.37m	43	35	50	31	10	0	0	1	1	0	0	0	0	42	42	0	0	0	0	1	1	0	0	1	1	0	0	0	0	0	0	1	1	3	3	0	0	2	2	0	0	0	0	0	0	0
120 7B-37R CC, 498.7m	59	52	92	50	14	0	0	7	2	0	0	1	0	59	59	0	0	0	0	1	1	0	0	1	1	0	0	0	0	0	0	1	1	3	3	0	0	2	2	0	0	0	0	0	0	0
120 7B-39R CC, 517.27m	38	34	37	30	10	0	0	0	0	0	0	1	0	46	45	0	0	0	0	1	1	0	0	1	1	0	0	0	0	0	0	1	1	3	3	0	0	2	2	0	0	0	0	0	0	0
120 7B-40R CC, 526.55m	35	28	37	54	17	0	0	0	0	0	0	0	0	52	52	0	0	0	0	1	1	0	0	1	1	0	0	0	0	0	0	1	1	3	3	0	0	2	2	0	0	0	0	0	0	0
120 7B-41R CC, 536.25m	53	52	66	1	0	0	0	0	0	0	0	0	0	53	53	0	0	0	0	1	1	0	0	1	1	0	0	0	0	0	0	1	1	3	3	0	0	2	2	0	0	0	0	0	0	0
120 7B-42R CC, 545.93m	36	34	21	22	7	0	0	0	0	0	0	0	0	46	46	0	0	0	0	1	1	0	0	1	1	0	0	0	0	0	0	1	1	3	3	0	0	2	2	0	0	0	0	0	0	0
120 7B-43R CC, 557.01m	28	27	15	18	6	0	0	0	0	0	0	0	0	48	48	0	0	0	0	1	1	0	0	1	1	0	0	0	0	0	0	1	1	3	3	0	0	2	2	0	0	0	0	0	0	0
120 7B-44R CC, 566.89m	14	14	4	7	2	0	0	1	0	0	0	0	0	54	54	0	0	0	0	1	1	0	0	1	1	0	0	0	0	0	0	1	1	3	3	0	0	2	2	0	0	0	0	0	0	0
120 7B-45R CC, 574.89m	18	18	3	8	2	0	0	0	0	0	0	2	0	58	58	0	0	0	0	0	0	0	0	1	1	0	0	0	0	0	0	1	1	3	3	0	0	2	2	0	0	0	0	0	0	0

ODP Leg 198 Hole 1213A-B

Sample	Preservation	Abundance	Species richness	Total count	no. of FOV's (to reach 300)
1213A 9R-CC, 76.04m	G	A	47	391	2
1213A 13R-CC, 114.83m	M-G	A	42	306	3
1213A 17R-CC, 151.52m	M=G	A	39	313	4
1213A 18R-CC, 160.45m	M-G	A	46	305	2
1213A 19R-CC, 170.13m	M-G	A	48	363	3
1213A 20R-CC, 179.61m	M	A	42	309	5
1213A 21R-CC, 189.3m	M	A	46	321	2
1213B 1R-1, 42, 190.12m	M-G	A	47	328	4
1213B 2R-1, 5, 199.34m	M-G	A	27	330	5
1213B 3R-1, 14-15, 209.04	M-G	A	43	307	5
1213B 4R-1, 48, ? 218.6,	M-G	A	28	306	6
1213B 5R-1, 2, 228.3m	M-G	A	32	306	5
1213B 6R-1, 81-84, 238.63	M-G	A	34	323	4
1213B 7R-1, 93, 248.23m	M-G	A	21	307	5
1213B 8R-1, 3, 256.83m	M-G	E	13	304	29
1213B 9R-1, 17-18, 266.57	M-G	A	32	344	3
CHART 16					

A. terebrodentarius	% A. terebrodentarius	A. albianus	% A. albianus	B. constans	% B. constans	B. ambiguus	% B. ambiguus	C. litterarius	% C. litterarius	C.? madagaskerensis	% C.? madagaskerensis	C. margerelli	% C. margerelli	C. nudus	% C.nudus	D. ignotus	% D. ignotus	Eiffellithus spp.	% Eiffellithus spp.	E. floralis	% E. floralis	F. oblongus	% F. oblongus	H. circumradiatus	%H. circumradiatus	H. irregularis	% H. irregularis	H. chiastia	% H. chiastia	H. gorkae	% H. gorkae	L carniolensis	% L.carniolensis	L. armilla	% L.armilla	M. pemmatoidea	% M. pemmatoidea	P. columnata	% P. columnata	R. crenulata/surirella (+rims)	% R. crenulata/surirella (+rims)	Rhagodiscus spp.	% Rhagodiscus spp.
0	0	7	2	80	20	0	0	3	1	0	0	0	0	4	1	10	3	27	7	8	2	1	0	0	0	1	0	0	0	0	0	41	10	1	0	1	0	21	5	18	5	1	0
0	0	0	0	106	35	1	0	1	0	0	0	0	0	2	1	27	9	12	4	2	1	0	0	1	0	1	0	0	0	1	0	33	11	0	0	2	1	3	1	8	3	2	1
0	0	0	0	68	22	0	0	1	0	0	0	0	0	3	1	11	4	6	2	1	0	0	0	0	0	0	0	0	0	1	0	42	13	1	0	1	0	0	0	8	3	2	1
0	0	0	0	63	21	1	0	0	0	0	0	0	0	3	1	30	10	18	6	0	0	0	0	0	0	0	0	0	0	11	4	65	21	0	0	1	0	2	1	9	3	1	0
0	0	0	0	55	15	2	1	0	0	0	0	0	0	0	0	36	10	7	2	0	0	0	0	0	0	0	0	0	0	8	2	89	25	0	0	1	0	7	2	10	3	9	3
0	0	0	0	16	5	0	0	0	0	0	0	0	0	0	0	17	6	0	0	0	0	0	0	1	0	15	5	0	0	32	10	22	7	0	0	2	1	6	2	16	5	2	1
0	0	0	0	31	10	0	0	1	0	0	0	0	0	5	2	7	2	0	0	6	2	1	0	0	0	29	9	4	1	1	0	95	30	3	1	1	0	4	1	14	4	7	2
0	0	0	0	31	9	2	1	2	1	0	0	0	0	5	2	8	2	0	0	11	3	1	0	0	0	12	4	1	0	6	2	44	13	0	0	1	0	0	0	10	3	9	3
0	0	0	0	1	0	0	0	2	1	0	0	0	0	5	2	1	7	2	0	0	0	2	1	2	1	0	0	2	1	4	1	65	21	0	0	1	0	0	0	5	2	1	0
0	0	0	0	23	7	0	0	0	0	0	0	0	0	2	1	25	8	0	0	2	1	1	0	2	1	32	10	3	1	4	1	22	7	0	0	1	0	6	2	16	5	2	1
0	0	1	0	0	0	0	0	0	0	0	0	0	0	0	0	2	1	0	0	1	0	1	0	0	0	19	6	1	0	0	0	33	11	0	0	0	0	4	1	16	5	2	1
0	0	0	0	1	0	0	0	0	0	0	0	0	0	3	1	12	4	0	0	0	0	0	0	0	0	18	6	1	0	0	0	96	31	0	0	0	0	0	0	8	4	1	0
0	0	0	0	1	0	0	0	0	0	0	0	0	0	3	1	0	0	0	0	0	0	0	0	0	0	15	5	3	1	0	0	90	28	0	0	0	0	0	0	13	4	1	0
0	0	0	0	0	0	0	0	0	0	0	0	0	0	0	0	4	1	0	0	1	0	0	0	2	1	7	2	12	4	0	0	75	24	0	0	0	0	0	0	11	4	2	1
0	0	0	0	0	0	0	0	0	0	0	0	0	0	0	0	0	0	0	0	2	1	0	0	0	0	0	0	0	0	0	0	73	24	0	0	0	0	0	0	1	0	5	2
1	0	0	0	0	0	0	0	0	0	0	0	0	0	0	0	0	0	0	0	1	0	0	0	0	0	0	0	2	1	0	0	0	0	0	0	0	0	0	0	0	0	0	0
4	1	0	0	0	0	0	0	0	0	0	0	0	0	0	0	0	0	0	0	0	0	0	0	0	0	0	0	0	0	0	0	0	0	0	0	0	0	0	0	0	0	0	0
2	1	0	0	0	0	0	0	0	0	0	0	0	0	0	0	0	0	0	0	0	0	0	0	0	0	0	0	0	0	0	0	0	0	0	0	0	0	0	0	0	0	0	0
29	4	0	0	0	0	0	0	0	0	0	0	0	0	0	0	0	0	0	0	0	0	0	0	0	0	0	0	0	0	0	0	0	0	0	0	0	0	0	0	0	0	0	0
3	2	0	0	0	0	0	0	0	0	0	0	0	0	0	0	0	0	0	0	0	0	0	0	0	0	0	0	0	0	0	0	0	0	0	0	0	0	0	0	0	0	0	0

Sample	modified Nutrient Index	Nutrient Index Herrle (2002)	Productivity Index Gale et al. (2000)	% Z. cf. Z. howei	Z. cf. Z. howei	% Z. noeliae	Z. noeliae	% Z. howei	Z. howei	% Z. embergeri	Z. embergeri	% Z. diplogrammus	Z. diplogrammus	% Watznaueria spp.	Watznaueria spp.	% T. burnettiae	T. burnettiae	% T. gabalus	T. gabalus	% T. coptensis	T. coptensis	% T. stradneri	T. stradneri	% S.achylosus	S. achylosus	% Staurolithites spp.	Staurolithites spp.	% R. laffittei	R. laffittei
1213A 9R-CC, 76.04m	44	19	71	0	0	5	21	0	0	1	2	2	8	35	137	0	0	0	0	0	1	0	1	0	0	0	0	0	0
1213A 13R-CC, 114.83m	66	36	160	0	0	5	15	0	0	1	2	0	1	25	77	0	0	0	0	0	1	0	10	0	0	0	0	0	0
1213A 17R-CC, 151.52m	36	9	47	0	0	1	4	2	5	0	0	1	1	14	43	0	1	0	3	0	0	0	5	0	0	0	0	0	1
1213A 18R-CC, 160.45m	75	60	229	0	0	1	4	0	1	0	0	1	2	12	45	0	0	1	1	0	0	0	2	0	0	0	0	0	4
1213A 19R-CC, 170.13m	81	76	350	0	0	0	27	0	0	0	0	1	2	1	53	0	0	0	1	0	0	0	1	0	0	0	0	0	0
1213A 20R-CC, 179.61m	26	19	21	0	0	0	13	0	0	0	0	0	1	2	39	0	1	0	1	0	0	0	2	0	0	0	0	0	7
1213A 21R-CC, 189.3m	36	17	48	0	0	0	4	0	0	1	3	0	0	1	29	94	0	0	0	0	0	0	1	0	0	0	0	0	0
1213B 1R-1, 42, 190.12m	30	19	39	0	0	0	8	0	0	0	0	0	0	2	44	145	1	2	0	0	0	0	7	0	0	0	0	0	0
1213B 2R-1, 5, 199.34m	5	5	2	0	0	0	1	0	0	0	0	0	0	1	53	175	0	0	0	0	0	0	1	0	0	0	0	0	0
1213B 3R-1, 14-15, 209.04m	37	29	38	0	0	0	8	1	4	0	1	0	2	1	39	119	0	1	0	0	0	0	2	0	0	0	0	0	7
1213B 4R-1, 48, ? 218.6.	0	0	0	0	0	0	0	0	0	0	0	0	0	0	75	229	0	0	0	0	0	0	1	0	0	0	0	0	0
1213B 5R-1, 2, 228. 3m	10	10	2	0	0	1	3	0	1	0	2	1	0	0	45	138	1	3	2	6	0	0	1	0	0	0	0	0	3
1213B 6R-1, 81-84, 238.63m	0	0	0	0	0	0	0	0	0	1	1	0	0	0	52	169	1	4	0	0	0	0	0	0	1	0	0	0	1
1213B 7R-1, 93, 248. 23m	0	0	0	0	0	0	0	0	0	0	0	0	0	0	61	187	1	2	0	0	0	0	0	0	1	0	0	0	1
1213B 8R-1, 3, 256.83m	0	0	0	0	0	0	0	0	0	0	7	2	0	0	70	212	0	0	0	0	0	0	0	0	0	0	0	0	0
1213B 9R-1, 17-18, 266.57m	0	0	0	0	0	5	0	0	1	0	0	0	0	0	39	135	0	0	0	0	0	0	0	0	0	0	0	0	1

ODP Leg 198 Hole 1207B

Sample	Preservation	Abundance	Total count	no. of FOV's (to reach 300)	% A. terebrodentarius	% A. dietzmannii	% B. constans	% B. stenostaurion	% B. africana	% B. ambiguus	% C. madagaskerensis	% C. conicus	% C. margerelli	% C. nudus	% D.ignotus	% Eiffellithus spp.	% E.? hancockii	% E. floralis	% F. oblongus	% G. coronadventis	%H. circumradiatus	% H. irregularis	% H. chiastia	% H. gorkae	% L. carniolensis	% L. armilla	% M. pemmatoidea	% Nannoconus spp.	% P. columnata	% R. crenulata/surirella (+rims)	% Rhagodiscus spp. (ang+asper+ach)	% R. laffittei	% Staurolithites spp. (siesseri mainly)	% S. achylosus	% T. stradneri	% T. coptensis	% T. gabalus	% T. orionatus	% T. burnettiae	% Watznaueria spp. (combined)	% Z. diplogrammus	% Z. embergeri
1207B-24RCC, 373.92m	G	A	452	2	0	0	48	0	0	0	0	0	0	0	8	5	0	0	0	0	0	0	0	4	6	0	0	0	1	3	1	0	0	0	1	0	0	0	0	6	1	0
1207B-26R CC, 393.05m	M-G	A	303	2	0	0	27	0	0	0	0	0	0	1	3	6	0	0	0	0	0	0	0	3	12	0	0	0	1	0	0	0	0	0	2	0	0	0	0	32	2	0
1207B-27RCC, 402.62m	M-G	A	300	2	0	0	19	1	0	0	0	0	0	0	7	3	0	0	0	0	0	1	0	2	13	0	0	0	1	1	1	0	0	0	1	0	0	0	0	40	0	0
1207B-28R CC, 417.34m	M-G	A	308	2	0	0	24	0	0	1	0	0	0	0	8	5	0	0	0	0	0	2	0	2	5	0	0	0	1	1	2	0	0	0	1	0	0	0	0	35	0	0
1207B-29R CC, 422.12m	M-G	A	300	3	0	0	18	0	0	0	0	0	0	0	9	1	0	0	0	0	0	1	0	1	6	0	0	0	1	1	1	0	0	0	0	0	0	0	0	47	1	0
1207B-30R CC, 431.49m	M-G	A	306	2	0	0	11	0	0	0	0	0	0	0	14	0	0	0	1	0	0	5	0	1	8	0	0	0	0	4	4	0	0	0	1	0	0	0	0	45	0	0
1207B-31R CC, 440.78m	M-G	A	307	2	0	0	8	0	0	1	0	0	0	0	11	0	0	0	0	0	0	5	0	1	12	0	0	0	3	4	5	0	0	0	0	0	0	0	0	42	0	0
1207B-32R CC, 450.33m	M	A	304	5	0	0	7	0	0	0	0	0	0	0	6	0	0	0	0	0	0	3	0	3	13	1	0	0	3	3	4	0	0	0	0	0	0	0	0	29	0	0
1207B-33R CC, 460.33m	M-G	A	308	3	0	0	10	0	0	0	0	0	0	1	12	0	0	0	1	0	0	14	1	0	15	0	1	0	0	3	3	0	0	0	0	0	0	0	0	49	0	0
1207B-34R CC, 469.5m	M	A	302	7	0	0	5	0	0	0	0	0	0	1	5	0	0	0	0	0	0	8	1	0	16	1	0	0	0	3	3	0	0	0	0	0	0	1	0	53	0	0
1207B-35R CC, 478.87m	M-G	A	301	4	0	0	4	0	0	0	0	0	0	0	8	0	0	0	0	0	0	13	1	0	28	0	0	0	1	4	2	2	2	0	0	0	0	1	0	32	0	0
1207B-36R CC, 488.37m	M	A	301	2	0	1	1	0	0	0	0	0	0	1	4	0	0	0	1	0	0	5	0	1	8	0	1	0	0	4	4	0	0	0	0	0	0	0	0	45	0	0
1207B-37R CC, 498.7m	M-G	A	350	3	0	0	9	0	0	0	0	0	0	0	13	0	0	0	0	0	0	3	1	0	31	0	0	0	2	2	1	1	1	0	0	0	0	1	0	57	0	2
1207B-38R CC, 507.77m	M-G	A	345	3	0	0	4	0	0	0	0	0	0	0	11	0	0	0	0	0	0	5	0	0	23	0	0	0	2	1	1	1	1	0	0	0	0	0	0	46	0	0
1207B-39R CC, 517.27m	M	A	306	9	0	0	6	0	0	0	0	0	0	0	7	0	0	0	2	0	0	1	1	0	23	0	0	0	3	1	1	0	0	0	1	0	0	0	0	43	0	0
1207B-40R CC, 526.55m	M-G	A	327	2	0	0	2	0	0	0	0	0	0	0	14	0	1	0	1	0	0	8	0	0	25	0	0	0	1	3	2	2	0	0	0	0	0	0	0	29	1	0
1207B-41R CC, 536.25m	M	A	302	4	0	0	0	0	0	0	0	0	0	0	6	0	0	0	1	0	0	5	0	0	32	0	0	0	0	1	0	2	3	0	0	0	0	0	0	38	0	0
1207B-42R CC, 545.93m	M	A	314	3	0	1	1	0	0	0	0	0	0	0	13	0	0	0	0	0	0	10	0	0	30	0	0	0	0	0	1	1	0	0	0	0	0	0	0	48	0	1
1207B-43R CC, 557.01m	M	A	324	3	0	0	1	0	0	0	0	0	0	0	12	0	0	0	0	0	0	1	0	0	23	0	0	0	0	1	1	0	1	0	0	0	0	0	0	0	0	0
1207B-44R CC, 566.89m	M	A	306	2	0	0	0	0	0	0	0	0	0	0	7	0	0	0	0	0	0	1	0	0	36	0	0	0	0	1	1	0	0	0	0	0	0	0	0	54	0	1
1207B-45R CC, 574.89m	M	A	332	3	0	0	0	0	0	0	0	0	1	4	0	11	0	0	0	0	0	0	0	0	24	0	0	0	0	1	0	0	1	0	0	0	0	0	0	58	0	1

CHART 17

% Z. howei	% Z. noeliae	% Z. spissus	% Z. xenotus	%Zeugrhabdotus. spp. (combined)	Species richness (S)	Shannon diversity (H)	Equitability (E)	Sample
0	15	0	0	16	50	1.67	0.11	1207B-24RCC, 373.92m
0	8	0	0	10	47	1.91	0.14	1207B-26R CC, 393.05m
0	7	0	0	7	50	1.83	0.12	1207B-27RCC, 402.62m
0	10	0	0	10	45	1.86	0.14	1207B-28R CC, 417.34m
0	13	0	0	14	36	1.59	0.14	1207B-29R CC, 422.12m
1	12	0	0	13	45	2.02	0.17	1207B-30R CC, 431.49m
0	13	0	0	13	42	1.78	0.14	1207B-31R CC, 440.78m
0	10	0	0	10	43	1.78	0.14	1207B-32R CC, 450.33m
1	9	0	0	10	40	2.11	0.21	1207B-33R CC, 460.33m
1	3	0	0	4	38	1.70	0.14	1207B-34R CC, 469.5m
0	5	0	0	5	45	1.89	0.15	1207B-35R CC, 478.87m
0	2	0	0	4	37	1.55	0.13	1207B-36R CC, 488.37m
2	14	0	0	17	45	1.96	0.16	1207B-37R CC, 498.7m
0	13	0	0	13	43	1.65	0.12	1207B-38R CC, 507.77m
0	10	0	0	10	38	1.70	0.14	1207B-39R CC, 517.27m
0	17	0	0	17	45	1.90	0.15	1207B-40R CC, 526.55m
0	0	0	0	0	42	1.53	0.11	1207B-41R CC, 536.25m
0	7	0	0	7	31	1.55	0.15	1207B-42R CC, 545.93m
0	6	0	0	7	36	1.51	0.13	1207B-43R CC, 557.01m
0	2	0	0	2	32	1.18	0.10	1207B-44R CC, 566.89m
0	2	0	0	3	26	1.25	0.13	1207B-45R CC, 574.89m

ODP Leg 198 Hole 1213A-B

Sample	Preservation	Abundance	Total count	no. of FOV's (to reach 300)	% A. terebrodentarius	% A. albianus	% B. constans	% B. ambiguus	% C. litterarius	% C. madagaskerensis	% C. margerelli	% C. nudus	% D. ignotus	% Eiffellithus spp.	% E. floralis	% F. oblongus	%H. circumradiatus	% H. irregularis	% H. chiastia	% H. gorkae	% L. carniolensis	% L. armilla	% M. pemmatoidea	% P.columnata	% R. crenulata/surirella (+rims)	% Rhagodiscus spp.	% R. laffittei	% Staurolithites spp.	% S.achylosus	% T. stradneri	% T. coptensis	% T. gabalus	% T. burnettiae	% Watznaueria spp. (combined)	% Z. diplogrammus	% Z. embergeri	% Z. howei	% Z. noeliae	% Z. cf. Z. howei	% Zeugrhabdotus spp. (combined	Species richness (S)	Shannon's diversity (H)	Equitability (E)
1213A 9R-CC, 76.04m	G	A	391	2	0	2	20	0	0	1	3	7	2	0	0	0	10	0	5	5	0	0	35	2	1	0	5	0	8	47	1.99	0.16
1213A 13R-CC, 114.83m	M-G	A	306	3	0	0	35	0	1	0	1	9	4	1	0	0	11	0	1	1	0	0	25	0	1	0	5	0	6	42	1.91	0.16
1213A 17R-CC, 151.52m	M-G	A	313	4	0	0	22	0	0	0	0	4	2	0	0	0	13	0	0	3	1	0	49	0	2	1	0	0	3	39	1.52	0.12
1213A 18R-CC, 160.45m	M-G	A	305	2	0	0	21	0	0	0	1	10	6	0	0	0	21	0	0	3	0	0	14	0	0	0	11	0	11	46	2.11	0.18
1213A 19R-CC, 170.13m	M-G	A	363	3	0	15	1	0	0	0	0	10	2	0	0	0	25	0	2	1	0	0	12	1	0	0	27	0	28	48	1.98	0.15
1213A 20R-CC, 179.61m	M	A	309	5	0	5	0	0	0	0	0	6	0	1	0	0	0	5	0	2	1	0	42	0	0	0	4	0	4	42	1.89	0.16
1213A 21R-CC, 189.3m	M	A	321	2	0	0	10	0	0	0	2	2	0	2	0	0	30	1	0	2	1	0	29	0	1	0	4	0	5	46	1.92	0.15
1213B 1R-1, 42, 190.12m	M-G	A	328	4	0	0	9	1	1	0	2	2	0	3	0	0	13	0	2	3	1	0	44	0	0	0	8	0	8	47	2.03	0.16
1213B 2R-1, 5, 199.34m	M-G	A	330	5	0	0	0	0	0	0	1	2	0	1	1	0	15	0	0	2	1	0	53	0	0	1	1	0	2	27	1.43	0.15
1213B 3R-1, 14-15, 209.04m	M-G	A	307	5	0	7	0	0	0	0	1	8	0	1	0	1	7	0	0	2	1	2	39	1	0	1	8	0	10	43	2.14	0.20
1213B 4R-1, 48, ? 218.6	M-G	A	306	6	0	0	0	0	0	0	0	0	0	1	0	0	11	0	0	5	1	2	75	0	0	0	0	0	0	28	0.92	0.09
1213B 5R-1, 2, 228.3m	M-G	A	306	5	1	0	0	0	0	0	1	4	0	0	0	0	31	0	2	2	1	0	45	0	1	1	1	0	3	32	1.58	0.15
1213B 6R-1, 81-84, 238.63m	M-G	A	323	4	0	0	0	0	0	0	1	0	0	0	1	0	28	0	4	4	0	0	52	0	0	0	1	0	4	34	1.33	0.11
1213B 7R-1, 93, 248.23m	M-G	A	307	5	2	0	0	0	0	0	0	1	0	0	0	1	24	0	0	0	0	0	61	0	0	0	0	0	0	21	1.15	0.15
1213B 8R-1, 3, 256.83m	M-G	C	304	29	1	0	0	0	0	0	0	0	0	0	1	0	24	0	0	0	0	0	70	0	2	0	0	0	2	13	0.84	0.18
1213B 9R-1, 17-18, 266.57m	M-G	A	344	3	1	0	0	0	0	0	0	0	0	0	0	0	47	0	0	1	0	0	39	0	0	0	0	1	1	32	1.23	0.11

CHART 18

Cauvery Basin, Karai Formation Section 1

CHART 19

Sample details	KA 22.5 (FO *T. orionatus*)	KA 18	KA 27
% *Biscutum constans*	15	4	14
% *Broinsonia galloisii*	0	0	1
% *Chiastozygus litterarius*	1	0	1
% *Discorhabdus ignotus*	2	2	1
% *Hayesites albiensis*	1	0	1
% *Helenea chiastia*	1	0	0
% *Loxolithus armilla*	0	1	1
% *Lithraphidites carniolensis*	3	0	1
% Manivitella pemmatoidea	0	1	0
% *Prediscosphaera* spp.	0	1	1
% *Repagulum parvidentatum*	6	5	15
% *Retecapsa crenulata*	1	1	0
% *Rhagodiscus* spp.	6	3	9
% *Rotelapillus laffittei*	0	0	1
% *Staurolithites glaber*	1	0	0
% *Staurolithites laffittei*	2	1	0
% *Staurolithites* spp.	1	0	1
% *Tegumentum stradneri*	1	0	0
% *Tranolithus orionatus*	1	0	2
% *Tubodiscus burnettiae*	1	0	0
% *Watznaueria barnesiae*	26	44	22
% *Zeugrhabdotus diplogrammus*	2	3	1
% *Zeugrhabdotus embergeri*	1	3	0
% *Zeugrhabdotus noeliae*	28	20	23
Shannon's Diversity	2.1	1.6	2.0
Species richness	69	29	60
Equitability	0.1	0.2	0.1

Cauvery Basin Karai Formation Section 1

CHART 20

Sample details	KA 184.5 (FO *E. turriseiffelii*)	KA 180	KA 189
% *A. albianus*	0	3	0
% *B. constans*	14	7	5
% *B. ambiguus*	0	0	1
% *C. platyrhethus*	0	0	1
% *C. madagaskarensis*	1	0	0
% *D. ignotus*	1	1	1
% *E. turriseiffelii*	1	0	0
% *G. coronadventis*	1	0	0
% *H. trabeculatus*	0	0	1
% *L. armilla*	1	1	0
% *L. carniolensis*	1	0	0
% *M. pemmatoidea*	1	0	0
% *P. fibuliformis*	2	1	0
% *Prediscosphaera* spp.	7	10	5
% *R. parvidentatum*	1	4	0
% *R. crenulata*	4	5	2
% *Rhagodiscus* spp.	2	6	0
% *Staurolithites* spp.	0	1	1
% *T. orionatus*	5	12	6
% *T. stradneri*	1	0	0
% *W. barnesiae*	29	24	55
% *Z. diplogrammus*	3	0	1
% *Z. embergeri*	0	1	0
% *Z. howei*	3	0	4
% *Z. noeliae*	18	21	12
Shannon's Diversity	2.2	2.1	1.5
Species richness	61	67	43
Equitability	0.1	0.1	0.1

Gault Clay, Copt Point

CHART 21

SAMPLE NO.	REAL HEIGHT (m)	% *A. albianus*	% *B. constans*	%*B. matalosa*	% *B. ambiguus*	% *C. litterarius*	% *C. fossilis*	%*C. madagaskarensis*	% *C. protosignum*	% *C. anglicum*	% *D. ignotus*	%*E. floralis*	% *H. albiensis*	% *H. compactus*	% *H. gorkae*	% *L. carniolensis*	%*L. armilla*	% *M. pemmatoidea*	% *Prediscosphaera* spp.	% *R. planus*	%*R. parvidentatum*	% *R. crenulata*	% *Rhagodiscus* spp.	% *R. laffittei*	% *S. glaber*	% *Staurolithites* spp. (small)	% *T. stradneri*	% *T. orionatus*	% *T. burnettiae*	% *Watznaueria* spp.	% *Z. diplogrammus*	% *Z. embergeri*	% *Z. howei*	% *Z. noeliae*	% *Z. xenotus*	Shannon's Diversity	Equitability	Species Richness	
F 0	5	0	11	0	0	0	0	0	0	1	2	0	0	1	0	2	1	0	1	0	7	3	4	0	0	2	1	6	0	1	0	18	0	2.07	0.12	66	
F-0.1	4.9	0	13	0	0	0	0	0	0	0	0	0	0	1	0	1	1	1	1	0	7	2	2	0	0	2	0	4	1	1	0	26	0	1.80	0.09	68	
F-0.15	4.85	0	14	0	1	0	1	0	0	0	0	0	0	0	0	1	0	0	3	0	9	2	5	0	0	2	1	5	1	25	1	0	0	28	0	2.11	0.14	61	
F-0.2	4.8	0	22	0	1	0	1	0	0	0	1	0	0	0	0	3	0	0	4	0	7	2	2	1	0	2	0	4	1	16	1	0	0	28	0	2.15	0.13	66	
F-0.3	4.7	1	14	0	1	0	0	0	0	0	2	0	0	0	0	5	0	2	3	0	6	3	3	1	0	1	0	5	0	17	1	0	0	28	0	2.29	0.16	62	
F-0.4	4.6	0	13	0	1	0	0	0	0	0	0	1	0	0	0	5	0	1	10	0	8	3	4	0	0	2	0	4	0	16	1	0	2	28	0	2.20	0.16	57	
F -0.5	4.5	0	15	0	0	1	0	0	0	0	1	1	0	1	0	3	0	0	8	0	10	3	3	0	0	1	1	3	0	29	0	0	3	27	0	2.27	0.16	60	MIDDLE
F-1	4	1	14	0	0	1	0	0	0	0	1	1	0	0	0	9	1	0	2	0	8	2	5	1	0	5	2	3	0	24	0	4	4	11	2	2.34	0.15	70	ALBIAN
F-1.5	3.5	0	14	0	0	0	0	0	0	0	1	0	0	0	0	10	1	0	7	0	9	2	3	2	0	4	0	7	0	37	2	1	4	11	0	2.36	0.18	59	
F-2	3	1	11	0	0	1	0	0	0	0	0	1	0	0	0	7	0	0	4	0	9	2	3	1	0	0	0	1	0	0	0	1	0	0	0	2.05	0.14	55	
F-2.5	2.5	0	8	0	0	0	0	0	0	0	1	0	0	0	1	8	1	0	8	0	5	2	6	1	0	4	0	2	0	33	0	5	4	21	0	2.08	0.13	60	
F-3	2	0	12	0	1	0	0	0	0	0	0	0	0	0	0	10	0	1	10	0	8	3	6	1	0	2	0	4	0	16	1	0	2	28	0	2.21	0.19	48	
F-3.5	1.5	0	25	0	0	0	0	0	0	1	1	0	0	0	0	3	0	0	3	0	7	2	5	0	0	1	0	3	1	17	1	0	2	28	0	2.01	0.15	50	
F-4	1	0	22	1	0	0	0	1	0	0	3	1	0	0	0	5	0	0	4	0	9	2	6	0	0	1	0	6	0	22	2	0	0	15	1	2.28	0.17	57	
F-4.5	0.5	0	21	0	0	1	0	0	0	0	5	1	0	0	0	5	3	1	8	0	3	2	8	0	0	5	0	6	0	21	0	0	0	9	1	2.37	0.17	61	
F -5	0	0	33	0	1	0	0	0	1	0	2	0	0	0	0	7	1	0	6	0	4	1	1	1	1	5	0	4	1	18	1	0	0	9	1	2.19	0.16	55	

CHART 22

1207B

SAMPLE	24R-CC	26R-CC	27R-CC	28R-CC	29R-CC	30R-CC	31R-CC	32R-CC	33R-CC	34R-CC	35R-CC	36R-CC	37R-CC	38R-CC	39R-CC	40R-CC	41R-CC	42R-CC	43R-CC	44R-CC	45R-CC
Depth (mbsf)	373.92	393.1	402.6	417.3	422.1	431.5	440.8	450.3	460.3	469.5	478.9	488.4	498.7	507.8	517.3	526.6	536.3	545.9	557	566.9	574.9
PRESERVATION	M-G	M	M-G	M-G	M-G	M-G	M-G	M	M-G	M	M-G	M	M-G	M-G	M	M-G	M	M	M	M	M
ABUNDANCE	A	A	A	A	A	A	A	A	A	A	A	A	A	A	A	A	A	A	A	A	A
TAXON																					
Assipetra infracretacea																				?	
Assipetra terebrodentarius																F	R	R	R	R	F
Axopodorhabdus albianus	C	R			?																
Axopodorhabdus dietzmannii	R	R	F		F		R	R	R	R	F	F	C	F	R	F	F	R	F	R	R
Biscutum constans	A	A	A	A	A	A	A	C	A	C	C	C	A	C	C	C	F	C	F	F	C
Biscutum cf. *B. constans* (large)	F	C	C	C	C																
Braarudosphaera hockwoldensis								VR													
Broinsonia galloisii			VR					VR													
Broinsonia stenostaurion			F	R	R	F	F														
Bukrylithus ambiguus	C	F	F	C	F	R	F	C	F	F	F	F	F	F							R
Calciosolenia fossilis																					
calcispheres											VR						VR				
Chiastozygus litterarius	R	F	R	R	C	R	R	F	R												
Chiastozygus platyrhethus		R		R		R													VR		
Chiastozygus spissus	F																				
Corollithion signum	R																				
Cretarhabdus conicus			R			R	R		R				R	R		R	R		C	C	F
Cretarhabdus cf. *C. conicus*																			F	F	
Cretarhabdus striatus				R	R	R							R	R	R						
Cribrosphaerella ehrenbergii	F																				
Cyclagelosphaera margerelii		VR						R												C	C
Cylindralithus nudus	F	F	F	F	F	F	F	F	C	C	C	C	F	F	F	F	R				
Cylindralithus cf. *C. nudus*			R		R	R	R	R	F	F	F	F									
Discorhabdus ignotus	C	C	C	C	C	A	C	A	C	A	A	C	A	A	C	A	C	A	A	A	C
Eiffellithus hancockii							R		F				F	R	R	C				R	
Eiffellithus monechiae			F	F	C																
Eiffellithus turriseiffelii	C	C	C	C																	
Eprolithus floralis	F				R	F	R	R	R	R	R	F	F	R	C	C	C	C	R		
Flabellites oblongus	F	R	R	F		C	F	R	C	F	F	F	C	F	R	F	F	F	F	F	
Gartnerago cf. *G. theta*	R																				
Grantarhabdus coronadventis	F	R	R	R		R					R	F	R	F		F					
Haqius circumradiatus						F	R	F	F	R	F	F	R		R		R	R	F	R	F
Hayesites irregularis		VR	F	F	F	C	F	F	A	C	A	F	C	C	F	A	F	A	F	F	
Hayesites cf. *H. albiensis*			F			F			C												
Helenea chiastia						R		R	C	C	F	R	C	C	F	F	F	F	F	F	F
Helicolithus compactus			VR																		
Helicolithus trabeculatus											R										
Hemipodorhabdus gorkae	C	C	C	C	C	C	C	C	F	F	F	F	F		F	F	F	F	F	F	
Lapideacassis mariae						R															
Lithraphidites carniolensis	F	C	C	C	C	A	A	C	A	C	A	A	A	A	C	A	A	A	A	F	
Loxolithus armilla	F	R	F	R	F	R	F	F	F	R											
Manivitella pemmatoidea	C	F	R	R	R	F	F	R	F	F	R			R	R	R	R			F	
Manivitella fibrosa					R			R		F	F	R	F	R		R	F		F		
Nannoconus truitii Group														VR			R				
Nannoconus (top view)																	R				
Pickelhaube furtiva														R			VR	VR	VR		
Prediscosphaera columnata	C	C	C	F	C	C	C	R	R	F	R	?	?								
Prediscosphaera columnata (subcircular)										F	F	R	F	VR							
Prediscosphaera cf. *P. spinosa* (small)	C	VR	VR																		
Radiolithus planus		VR														VR	VR				
Retecapsa angustiforata																					R
Retecapsa crenulata	C	F	F	F	F	C	F	F	F	F					R	F	F			R	F

SAMPLE	45R-CC	44R-CC	43R-CC	42R-CC	41R-CC	40R-CC	39R-CC	38R-CC	37R-CC	36R-CC	35R-CC	34R-CC	33R-CC	32R-CC	31R-CC	30R-CC	29R-CC	28R-CC	27R-CC	26R-CC	24R-CC
Retecapsa surirella		F	R	R					F			?R	?R	R	R				R		R
retecapsid rims										C	F	F	F	F							
Rhagodiscus achlyostaurion				?VR	VR					VR	R	F	C	C	C	C	C	C	C	C	F
Rhagodiscus angustus						F	R	F	C	R	C	F	C	C	C	C	C	F	F	F	C
Rhagodiscus asper	C	C	C	F	F	A	F	C	C	F	F	F	C	F	F	C	F	C	R	R	R
Rhagodiscus gallagheri			F	R		F	F	F	F	F											
Rhagodiscus reniformis																					VR
Rotelapillus laffittei	F	F	C	F	C	C	R	C	C	F	C	C		F	C	R	F	R	F	R	F
Staurolithites gausorhethium																					R
Staurolithites glaber								VR											R		C
Staurolithites mutterlosei	VR	F	R	R	R	F	R	R	F		R	VR	R	R	R						
Staurolithites spp. (small, bicyclic)			F			F		R							R	R	R	R	R		
Stoverius achylosus					R	C			VR		R	VR	R		R		VR				
Tegumentum stradneri	VR	VR	R		F	F	R	F	F	F	F	F	C	F	F	C	F	C	C	F	C
Tetrapodorhabdus coptensis	VR		VR	VR	VR		R	R	F	R	F			R	F	R		F	F	F	C
Tranolithus gabalus	R		R	F	R	F	R	F	C	F	R	F	F	F	F	F	F	F	R	VR	VR
Tranolithus orionatus															VR	C	F	F	C	R	F
Tubodiscus burnettiae	F		R		R	F		R	F											R	R
Watznaueria barnesiae	A	A	A	A	A	A	C	A	A	A	A	A	A	A	A	A	A	A	A	A	A
Watznaueria britannica			R	R	R	R	F		R			R	F			R				VR	
Watznaueria fossacincta														R							
Watznaueria sp. 1	R	F	F	C	F	C		F	C	C	F	F		R		C	F	C		F	F
Zeugrhabdotus diplogrammus				VR	R	F	R	R	F	R	R	R	F	R	R	R	C	C	F	C	C
Zeugrhabdotus embergeri	C	F	C	F	R	F	R	F	F	F	F	F	F	R	VR	F	R	R		F	F
Zeugrhabdotus cf. *Z. embergeri* (small)													R		R	F			F	F	F
Zeugrhabdotus howei	R	R	R	R	F	C	R	C	C	F	F	C	C	F	F	C	F	F	F	C	C
Zeugrhabdotus noeliae	C	C	C	A	C	A	C	A	A	C	C	C	C	C	A	C	A	A	A	A	A
Zeugrhabdotus scutula	F	F																			
Zeugrhabdotus xenotus	?R	?R				F	F		R				?R		R		R	VR			
NANNOFOSSIL ZONE	NC5d-e	NC6			NC7						NC8a-b				8c-9a		NC9b		NC10a		UC1-2
STAGE	BARREMIAN				APTIAN									ALBIAN							CENOMANIAN

CHART 23 — 1213A-B

SAMPLE	Depth (mbsf)	PRESERVATION	ABUNDANCE	TAXON
1213A-9R-CC	76.04	G	A	
13R-CC	114.8	M-G	A	
17R-CC	151.5	M-G	A	
18R-CC	160.5	M-G	A	
19R-CC	170.1	M-G	A	
20R-CC	179.6	M	A	
21R-CC	189.3	M	A	
1213B-1R-CC	190.1	M-G	A	
2R-CC	199.3	M-G	A	
3R-CC	209.4	M-G	A	
4R-CC	218.6	M-G	A	
5R-CC	228.3	M-G	A	
6R-CC	238.6	M-G	A	
7R-CC	248.2	M-G	A	
8R-CC	256.8	M-G	C	
9R-CC	266.6	M-G	A	
				Assipetra infracretacea
				Assipetra terebrodentarius
				Axopodorhabdus albianus
				Axopodorhabdus dietzmannii
				Biscutum constans
				Biscutum cf. *B. constans* (large)
				Braarudosphaera africana
				Broinsonia cenomanicus
				Broinsonia enormis
				Broinsonia galloisii
				Broinsonia signata
				Broinsonia stenostaurion
				Bukrylithus ambiguus
				Calciosolenia fossilis
				calcispheres
				Chiastozygus litterarius
				Chiastozygus platyrhethus
				Corollithion ? madagaskerensis
				Corollithion signum
				Cretarhabdus conicus
				Cretarhabdus striatus
				Cribrosphaerella ehrenbergii
				Cyclagelosphaera margerelii
				Cylindralithus nudus
				Cylindralithus cf. *C. nudus*
				Discorhabdus ignotus
				Eiffellithus hancockii
				Eiffellithus monechiae
				Eiffellithus turriseiffelii
				Eprolithus floralis
				Flabellites oblongus
				Gartnerago cf. *G. nanum*
				Grantarhabdus coronadventis
				Haqius circumradiatus
				Hayesites irregularis
				Hayesites cf. *H. albiensis*
				Helenea chiastia
				Helicolithus compactus
				Hemipodorhabdus gorkae
				Lapideacassis mariae
				Lithraphidites carniolensis
				Loxolithus armilla
				loxoliths (large)
				Manivitella pemmatoidea
				Manivitella fibrosa
				Nannoconus (top view)
				Percivalia fenestrata
				Pickelhaube furtiva
				Prediscosphaera columnata
				Prediscosphaera columnata (large)
				Prediscosphaera spinosa
				Radiolithus planus

	1213A-9R-CC	13R-CC	17R-CC	18R-CC	19R-CC	20R-CC	21R-CC	1213B-1R-CC	2R-CC	3R-CC	4R-CC	5R-CC	6R-CC	7R-CC	8R-CC	9R-CC
Retecapsa crenulata	F	F	C	F	F	F	F	F	R	F		R		R		
Retecapsa surirella			R		R		R	F	VR	F	R					R
retecapsid rims					F	F	C	C		C	F		F			C
Rhagodiscus achlyostaurion	F	C	F	C	C	C	C	C		VR						
Rhagodiscus angustus	F	F	R	F	C	F	F	C		F		VR				
Rhagodiscus asper	F	R		F	F	F	F	F	R	F	R	R	R	R		F
Rhagodiscus asper (large)					R			VR	VR	R	F	F	F	R		F
Rotelapillus laffittei	F	R		R	A	F	F	F	R	C	R	C	C	F		C
Staurolithites gausorhethium		VR										R				
Staurolithites glaber		F			F											
Staurolithites mutterlosei				R	R	R	F	R		F		R				
Staurolithites siesseri							R	R			F	C	F		?	
Staurolithites spp. (small, bicyclic)					R	R		F								
Stoverius achylosus					F			R		F		VR				
Tegumentum stradneri	C	C	F	C	C	C	C	C	R	C		R	R			R
Tetrapodorhabdus coptensis	F	F	R	F	C	F	F			R						
Tranolithus gabalus		R	F	F	F	F	F	F	R	R		F	R			
Tranolithus orionatus	C	F	R	F	R	VR										
Tubodiscus burnettiae	F	R	R			R	R	F	F	F		F	F	F		F
Watznaueria barnesiae	A	A	A	A	A	A	A	A	A	A	A	A	A	C	C	A
Watznaueria britannica				VR	R	F	R	R	R	R	R	R	F		R	
Watznaueria fossacincta	A	F	F	A	F	F	C	F	A	F	A	A	A	C	C	A
Watznaueria sp. 1																
Zeugrhabdotus diplogrammus	C	C	F	C	F	F	F	F	R	R	R	R				
Zeugrhabdotus embergeri	C	F	F	R	R	F	F	R	F	R	R	F	F	F	F	C
Zeugrhabdotus cf. *Z. embergeri* (small)	F		R	R		F										
Zeugrhabdotus howei	C	C	F	F	F	C	C	C	F	C	F	F	R			
Zeugrhabdotus noeliae	C	C	F	C	C	C	C	C	F	F						
Zeugrhabdotus scutula																C
Zeugrhabdotus xenotus		?R				?R										
NANNOFOSSIL ZONE	UC2	UC1		NC10a		NC8c-9				NC8a-b				NC7		NC6
STAGE		CENOMANIAN					ALBIAN								APTIAN	
SAMPLE	1213A-9R-CC	13R-CC	17R-CC	18R-CC	19R-CC	20R-CC	21R-CC	1213B-1R-CC	2R-CC	3R-CC	4R-CC	5R-CC	6R-CC	7R-CC	8R-CC	9R-CC